

Drivers of plant nutrient acquisition and allocation strategies and their influence
on plant responses to environmental change

by

Evan A. Perkowski, B.S.

A Dissertation

In

Biological Sciences

Submitted to the Graduate Faculty
of Texas Tech University in
Partial Fulfillment of
the Requirements for
the Degree of

DOCTOR OF PHILOSOPHY

Approved

Nicholas G. Smith, Ph.D.
Chair of Committee

Aimée T. Classen, Ph.D.

Natasja van Gestel, Ph.D.

Lindsey C. Slaughter, Ph.D.

Dylan W. Schwilk, Ph.D.

Mark Sheridan, Ph.D.
Dean of the Graduate School

May 2023

Copyright 2023, Evan A. Perkowski

Acknowledgements

This dissertation was made possible by the mentorship, collaboration, and friendship of many people. I am so thankful to be surrounded by such supportive and helpful mentors, peers, and friends that have made navigating through graduate school and finishing this dissertation an enjoyable experience. Specifically, I am thankful for the mentorship of my advisor and committee chair, Dr. Nick Smith, who provided invaluable insight and tools that have helped shape me into the plant ecophysiologicalist I claim to be today. I am also indebted to my committee members, Drs. Aimée Classen, Natasja van Gestel, Dylan Schwilk, and Lindsey Slaughter, for useful feedback, support, and encouragement as I planned and implemented experiments.

I am also thankful for past and present members of the EcoHealth lab for encouragement, support, and extracurricular activities that made time inside and outside the lab enjoyable and memorable. Particular thanks go to Dr. Lizz Waring, Dr. Xiulin Gao, Helen Scott, and Risa McNellis, Billi Jean Petermann, and the late Dr. Kris Petterson, all of whom provided friendship and useful advice as I navigated my first year. I am especially thankful for the mentorship and friendship of Dr. Lizz Waring, as our weekly coffee chats were instrumental for helping me feel welcome in Lubbock and acclimate to life as a graduate student. I am also grateful for the friendship of Billi Jean Petermann and the late Dr. Kris Petterson for their encouragement and willingness to discuss microbial symbioses over coffee on Saturday mornings.

Additional thanks go out to Isa Beltran, Snehanjana Chatterjee, Jeff Chi-

eppa, Peter Eludini, Zinny Ezekannagha, Hannah German, Eve Gray, Monika Kelley, Azaj Mahmud, Jorge Ochoa, Brad Posch, Avery Schoenherr, Christine Vanginault, and Jose Villeda for help with experiments or for lending an ear over puzzling results. I am also thankful for collaborators Dr. Christy Goodale and Dave Frey, who provided insight for the second experimental chapter.

I would like to thank my undergraduate advisor, Dr. Janice Krumm, for continued mentorship and friendship and for insightful advice about navigating graduate school, but most of all for helping me realize my career aspirations and pushing me to pursue this endeavor. Additional thanks go out to my family, particularly my parents, partner, and dog for continued support and distractions outside the lab. The experiments included here would not have been possible without their emotional and monetary support.

This work was made possible from funding by the NSF, USDA, Braun and Gresham, PLLC., and was a contribution to the LEMONTREE (Land Ecosystem Models based On New Theory, obseRvations and ExperimEnts) project. The LEMONTREE project is funded through the generosity of Eric and Wendy Schmidt by recommendation of the Schmidt Futures programme and the Imperial College initiative on Grand Challenges in Ecosystems and the Environment. This work was also funded by graduate student research awards from Texas Tech University and the Botanical Society of America.

I have inevitably missed thanking folks that were instrumental to the completion of these experiments and contributed to my development as a plant eco-physiologist. Please know that I am grateful and appreciative of our interactions.

Table of Contents

Acknowledgements	ii
Abstract	viii
List of Tables	x
List of Figures	xiv
1. Introduction	1
2. Root mass carbon costs to acquire nitrogen are determined by nitrogen and light availability in two species with different nitrogen acquisition strategies	7
2.1 Introduction	7
2.2 Methods	11
2.2.1 <i>Experiment setup</i>	11
2.2.2 <i>Plant measurements and calculations</i>	12
2.2.3 <i>Statistical analyses</i>	13
2.3 Results	15
2.3.1 <i>Carbon costs to acquire nitrogen</i>	15
2.3.2 <i>Whole plant nitrogen biomass</i>	18
2.3.3 <i>Root carbon biomass</i>	20
2.3.4 <i>Root nodule biomass</i>	22
2.4 Discussion	26
3. Soil nitrogen availability modifies leaf nitrogen economies in mature temperate deciduous forests: a direct test of photosynthetic least-cost theory	34
3.1 Introduction	34
3.2 Methods	38
3.2.1 <i>Study site description</i>	38
3.2.2 <i>Experimental design</i>	39
3.2.3 <i>Leaf gas exchange and trait measurements</i>	39
3.2.4 <i>Response curve fitting and parameter estimation</i>	42

3.2.5 <i>Tradeoffs between nitrogen and water use</i>	44
3.2.6 <i>Soil nitrogen availability and pH</i>	44
3.2.7 <i>Statistical analyses</i>	46
3.3 Results	48
3.3.1 <i>Leaf nitrogen content</i>	48
3.3.2 <i>Net photosynthesis and leaf biochemistry</i>	51
3.3.3 <i>Tradeoffs between nitrogen and water use</i>	54
3.4 Discussion	57
4. The relative cost of resource use for photosynthesis drives variance in leaf nitrogen content across a climate and soil resource availability gradient	64
4.1 Introduction	64
4.2 Methods	70
4.2.1 <i>Site descriptions and sampling methodology</i>	70
4.2.2 <i>Site climate data</i>	70
4.2.3 <i>Site edaphic characteristics</i>	71
4.2.4 <i>Leaf trait measurements</i>	73
4.2.5 <i>Plant functional group assignments</i>	78
4.2.6 <i>Data analysis</i>	78
4.3 Results	82
4.3.1 <i>Cost to acquire nitrogen relative to water</i>	82
4.3.2 <i>Leaf $C_i:C_a$</i>	85
4.3.3 <i>Leaf nitrogen content</i>	88
4.3.4 <i>Piecewise structural equation model</i>	92
4.4 Discussion	95
5. Optimal resource investment to photosynthetic capacity maximizes nutrient allocation to whole plant growth under elevated CO₂	103
5.1 Introduction	103
5.2 Methods	108

5.2.1	<i>Seed treatments and experimental design</i>	108
5.2.2	<i>Growth chamber conditions</i>	109
5.2.3	<i>Leaf gas exchange measurements</i>	111
5.2.4	<i>Leaf trait measurements</i>	112
5.2.5	<i>Response curve fitting and parameter estimation</i>	114
5.2.6	<i>Stomatal limitation</i>	114
5.2.7	<i>Proportion of leaf nitrogen allocated to photosynthesis and structure</i>	115
5.2.8	<i>Whole plant traits</i>	117
5.2.9	<i>Statistical analyses</i>	119
5.3	Results	121
5.3.1	<i>Leaf nitrogen and chlorophyll content</i>	121
5.3.2	<i>Leaf biochemistry and stomatal conductance</i>	125
5.3.3	<i>Leaf nitrogen allocation</i>	129
5.3.4	<i>Whole plant traits</i>	133
5.3.5	<i>Nitrogen fixation</i>	137
5.4	Discussion	141
6.	Conclusions	150
References		160
Appendices		188
A:	Supplemental material for “Root mass carbon costs to acquire nitrogen are determined by nitrogen and light availability in two species with different nitrogen acquisition strategies”	188
B:	Supplemental material for “Soil nitrogen availability modifies leaf nitrogen economies in mature temperate deciduous forests: a direct test of photosynthetic least-cost theory”	192
C:	Supplemental material for “The relative cost of resource use for photosynthesis drives variance in leaf nitrogen content across a climate and soil resource availability gradient”	197

D: Supplemental material for “Optimal resource investment to photosynthetic capacity maximizes nutrient allocation to whole plant growth under elevated CO ₂ ”	203
---	-----

Abstract

Photosynthesis is the largest carbon flux between the atmosphere and terrestrial biosphere and is constrained by ecosystem biogeochemical cycles. Terrestrial biosphere models exhibit strong divergence in simulated carbon and nitrogen fluxes under future environmental conditions. Divergence across model products may be due to the high sensitivity of terrestrial biosphere models to the formulation of photosynthetic processes, coupled with uncertainty in the photosynthetic acclimation response to changing aboveground and belowground environments. Photosynthetic least-cost theory provides a promising framework for understanding such photosynthetic responses to changing environments; however, empirical tests of the theory are rare, limiting our ability to assess whether the theory is suitable for implementing in future iterations of terrestrial biosphere model products.

Here, I present four experiments designed to test assumptions of photosynthetic least-cost theory. Experiment chapters are flanked by a general introduction chapter and general conclusion chapter. The first experimental chapter quantifies structural carbon costs to acquire nitrogen in *Glycine max* and *Gossypium hirsutum* grown under four nitrogen fertilization levels and four light availability levels in a full factorial greenhouse experiment. I find that carbon costs to acquire nitrogen in both species increase with increasing light availability and decrease with increasing fertilization, though responses to fertilization in *G. max* were markedly less than *G. hirsutum*. The second experimental chapter quantifies leaf nitrogen and photosynthetic traits in upper canopy leaves of deciduous trees growing in a 9-year nitrogen-by-sulfur field manipulation experiment. I find

evidence for nitrogen-water use tradeoffs with increasing soil nitrogen availability, evidenced through a negative relationship between leaf nitrogen content and ratio of leaf intercellular CO₂ concentration to atmospheric CO₂ concentration (leaf $C_i:C_a$) and stronger increase in leaf nitrogen content with increasing soil nitrogen availability than leaf $C_i:C_a$. The third experiment investigates variance in leaf nitrogen content across a climate and soil resource availability gradient in Texan grasslands, showing that effects of soil resource availability and climate on leaf nitrogen content are driven by changes in leaf $C_i:C_a$. Finally, the fourth experiment quantifies leaf and whole plant acclimation responses in *G. max* grown under two atmospheric CO₂ levels, with and without inoculation with *Bradyrhizobium japonicum*, and across one of nine nitrogen fertilization treatments in a full factorial growth chamber experiment. I find that photosynthetic responses to CO₂ were independent of soil nitrogen fertilization and inoculation treatment, though the positive effect of elevated CO₂ on total leaf area and total biomass was stronger with increasing fertilization and in inoculated pots under low fertilization.

Experiments included in this dissertation provide consistent support for patterns expected from photosynthetic least-cost theory. The use of multiple experimental approaches allowed me to examine mechanisms driving patterns expected from the theory and investigate whether these patterns occur in the field across environmental gradients. Findings from these chapters challenge common paradigms in plant ecophysiology, providing empirical evidence suggesting that including photosynthetic least-cost frameworks in terrestrial biosphere models may improve longstanding divergence in simulated carbon fluxes across terrestrial biosphere model products.

List of Tables

2.1 Analysis of variance results exploring species-specific effects of light availability, nitrogen fertilization, and their interactions on carbon costs to acquire nitrogen, whole-plant nitrogen biomass, and root carbon biomass	16
2.2 Analysis of variance results exploring effects of light availability, nitrogen fertilization, and their interactions on <i>G. max</i> root nodule biomass and the ratio of root nodule biomass to root biomass	23
2.3 Slopes of the regression line describing the relationship between each dependent variable and nitrogen fertilization at each light level	24
3.1 Effects of soil nitrogen availability, soil pH, and species on leaf nitrogen content per unit leaf area, leaf nitrogen content per unit leaf mass, and leaf mass per unit leaf area	49
3.2 Effects of soil nitrogen availability, soil pH, species, and N_{area} on net photosynthesis, the maximum rate of Rubisco carboxylation, the maximum rate of RuBP regeneration, and the ratio of the maximum rate of RuBP regeneration to the maximum rate of Rubisco carboxylation	52
3.3 Effects of soil nitrogen availability, soil pH, species, and N_{area} on χ , photosynthetic nitrogen use efficiency, leaf nitrogen content per unit χ , and maximum Rubisco carboxylation rate per unit χ	55

4.1	Site locality information, sampling year, 2006-2020 mean annual precipitation, mean annual temperature, and water holding capacity	76
4.2	Effects of soil moisture, soil nitrogen availability, and plant functional group on β	83
4.3	Effects of soil moisture, soil nitrogen availability, and plant functional group on leaf $C_i:C_a$	86
4.4	Effects of soil moisture, soil nitrogen availability, plant functional group, and leaf $C_i:C_a$ on leaf nitrogen content per unit leaf area, leaf nitrogen content per unit leaf biomass, and leaf biomass per unit leaf area	90
4.5	Structural equation model results investigating direct effects of climatic and soil resource availability on leaf nitrogen content	93
5.1	Effects of soil nitrogen fertilization, inoculation, and CO ₂ treatments on leaf nitrogen content per unit leaf area, leaf nitrogen content per unit leaf mass, leaf mass per unit leaf area, and chlorophyll content per unit leaf area	123
5.2	Effects of soil nitrogen fertilization, inoculation, and CO ₂ on the maximum rate of Rubisco carboxylation, the maximum rate of RuBP regeneration, dark respiration, the ratio of the maximum rate of RuBP regeneration to the maximum rate of Rubisco carboxylation, stomatal conductance, and stomatal limitation	127

5.3	Effects of soil nitrogen fertilization, inoculation, and CO ₂ on the fraction of leaf nitrogen allocated to Rubisco, bioenergetics, light harvesting proteins, photosynthesis, and structure	131
5.4	Effects of CO ₂ , fertilization, and inoculation on total leaf area, whole plant biomass, carbon costs to acquire nitrogen, belowground carbon biomass, and whole plant nitrogen biomass	135
5.5	Effects of CO ₂ , fertilization, and inoculation on root nodule biomass, plant investments in symbiotic nitrogen fixation, and percent nitrogen fixed from the atmosphere	139
A1	Summary table containing volumes of compounds used to create modified Hoagland's solutions for each soil nitrogen fertilization treatment	188
A2	Analysis of variance results exploring species-specific effects of light availability, nitrogen fertilization, and their interactions on the ratio of whole plant biomass to pot volume	189
A3	Slopes of the regression line describing the relationship between each dependent variable and nitrogen fertilization at each light level	190
B1	Sample sizes of each species, abbreviated by their USDA NRCS PLANTS database code, within each plot at each site	192
B2	Analysis of variance results exploring the linear effect of leaf temperature on net photosynthesis rate and stomatal conductance measured at 400 μmol mol ⁻¹ CO ₂	193

B3	Second order log-polynomial regression coefficients that described the effect of leaf temperature on net photosynthesis and stomatal conductance measured at $400 \mu\text{mol mol}^{-1} \text{CO}_2$	194
B4	Mean, standard error, and 95% confidence interval ranges of soil nitrogen availability estimates across all measured plots	195
C1	List of sampled species and their plant functional group assignment	199
C2	Model selection results for soil moisture and vapor pressure deficit	201
D1	Summary table containing volumes of compounds used to create modified Hoagland's solutions for each soil nitrogen fertilization treatment	203
D2	Summary of the daily growth chamber program	204
D3	Effects of CO_2 , fertilization, and inoculation on whole plant biomass: pot volume	205

List of Figures

2.1 Effects of shade cover and nitrogen fertilization on plant carbon costs to acquire nitrogen in <i>G. hirsutum</i> and <i>G. max</i>	17
2.2 Effects of shade cover and nitrogen fertilization on whole-plant nitrogen biomass in <i>G. hirsutum</i> and <i>G. max</i>	19
2.3 Effects of shade cover and nitrogen fertilization on root carbon biomass in <i>G. hirsutum</i> and <i>G. max</i>	21
2.4 Effects of shade cover and nitrogen fertilization on root nodule biomass and the ratio of root nodule biomass to root biomass in <i>G. max</i>	25
3.1 Relationships between soil nitrogen availability and species on leaf nitrogen allocation	50
3.2 Effects of soil nitrogen availability, species, and leaf nitrogen content on net photosynthesis, maximum Rubisco carboxylation rate, and maximum RuBP regeneration rate	53
3.3 Effects of soil nitrogen availability, species, and leaf nitrogen content on tradeoffs between nitrogen and water use	56
4.1 Site locations along 2006-2020 mean annual precipitation and mean annual temperature gradients in Texas, USA.	77
4.2 Effects of soil nitrogen availability and soil moisture on the cost of acquiring and using nitrogen relative to water	84

4.3 Effects of 4-day mean vapor pressure deficit, 3-day soil moisture (per water holding capacity), and soil nitrogen availability on leaf $C_i:C_a$	87
4.4 Effects of leaf $C_i:C_a$, soil nitrogen availability, and soil moisture on leaf nitrogen content per unit leaf area, leaf nitrogen content per unit leaf biomass, and leaf mass per area.	91
4.5 Structural equation model results exploring drivers of leaf nitrogen content	94
5.1 Effects of CO ₂ , fertilization, and inoculation on leaf nitrogen per unit leaf area, leaf nitrogen content, leaf mass per unit leaf area, and chlorophyll content per unit leaf area	124
5.2 Effects of CO ₂ , fertilization, and inoculation on maximum rate of Rubisco carboxylation, the maximum rate of RuBP regeneration, and the ratio of the maximum rate of RuBP regeneration to the maximum rate of Rubisco carboxylation leaf mass per unit leaf area, dark respiration, stomatal conductance, and stomatal limitation .	128
5.3 Effects of CO ₂ , fertilization, and inoculation on the relative fraction of leaf nitrogen allocated to photosynthesis and the fraction of leaf nitrogen allocated to structure	132
5.4 Effects of CO ₂ , fertilization, and inoculation on total leaf area, total biomass, and structural carbon costs to acquire nitrogen	136

5.5 Effects of CO ₂ , fertilization, and inoculation on nodule biomass, nodule biomass: root biomass, and percent nitrogen fixed from the atmosphere	140
A1 Effects of shade cover and nitrogen fertilization on the ratio of plant biomass to rooting volume in <i>G. hirsutum</i> and <i>G. max</i>	191
B1 Effects of leaf temperature on net photosynthesis rate and stomatal conductance values when measured at 400 μmol mol ⁻¹ CO ₂	196
C1 Model selection results exploring relevant timescales for soil moisture and vapor pressure deficit	202
D1 Relationships between area-based leaf nitrogen content, mass-based leaf nitrogen content, and leaf mass per unit leaf area measured on the focal leaf used to generate CO ₂ response curves and leaf nitrogen content measured on the leaf used for chlorophyll extractions	206
D2 Effects of CO ₂ , fertilization, and inoculation on the ratio of whole plant biomass to pot volume	207

Chapter 1

Introduction

Photosynthesis represents the largest carbon flux between the atmosphere and biosphere, and is regulated by complex ecosystem biogeochemical cycles (Hungate et al. 2003; IPCC 2021). As a result, the inclusion of robust, empirically tested representations of photosynthetic processes is critical in order for terrestrial biosphere models to accurately and reliably simulate carbon and nutrient fluxes between the atmosphere and terrestrial biosphere (Oreskes et al. 1994; Smith and Dukes 2013; Prentice et al. 2015; Wieder et al. 2015). Despite evidence that the inclusion of coupled carbon and nutrient cycles can reduce model uncertainty, widespread divergence in predicted carbon and nutrient fluxes is still apparent across model products (Friedlingstein et al. 2014; Arora et al. 2020; Davies-Barnard et al. 2020). Divergence in predicted carbon and nutrient fluxes across terrestrial biosphere models may be due to an incomplete understanding of how plants acclimate to changing environments (Smith and Dukes 2013; Davies-Barnard et al. 2020), as terrestrial biosphere models are sensitive to the formulation of photosynthetic processes (Bonan et al. 2011; Ziehn et al. 2011; Booth et al. 2012; Smith et al. 2016; Smith et al. 2017; Rogers et al. 2017).

Many terrestrial biosphere models predict leaf-level photosynthesis through linear relationships between area-based leaf nitrogen content and the maximum rate of Ribulose-1,5-bisphosphate carboxylase/oxygenase (“Rubisco”), following the idea that large fractions of leaf nitrogen content are allocated to the construction and maintenance of Rubisco and other photosynthetic enzymes (Evans 1989).

The inclusion of coupled carbon and nutrient cycles in terrestrial biosphere models (Shi et al. 2016; Braghieri et al. 2022) allows leaf nitrogen content to be predicted by soil nitrogen availability, causing models to predict photosynthetic processes indirectly through changes in soil nitrogen availability (Smith et al. 2014; Lawrence et al. 2019). While these patterns are commonly observed in ecosystems globally (Brix 1971; Evans 1989; Firn et al. 2019; Liang et al. 2020), this formulation does not allow terrestrial biosphere models to predict photosynthetic acclimation responses to changing environments (Smith and Dukes 2013; Rogers et al. 2017; Harrison et al. 2021) and suggests that constant leaf nitrogen-photosynthesis relationships are ubiquitous across ecosystems.

Photosynthetic least-cost theory (Prentice et al. 2014; Wang et al. 2017; Smith et al. 2019; Paillassa et al. 2020; Scott and Smith 2022; Harrison et al. 2021) provides a framework for predicting leaf and whole plant responses to environmental change. The theory, which unifies optimal coordination (Chen et al. 1993; Maire et al. 2012) and least-cost (Wright et al. 2003) theories, posits that plants acclimate to changing aboveground environments by allocating nutrients and water to photosynthetic leaf tissue such that net photosynthesis rates are equally co-limited by the maximum rate of Rubisco carboxylation and the maximum rate of Ribulose-1,5-bisphosphate (RuBP) regeneration (Chen et al. 1993; Maire et al. 2012). The theory predicts that optimized photosynthesis rates are achieved at the lowest summed cost of nutrient and water use (Prentice et al. 2014). Importantly, costs of nutrient use and costs of water use are substitutable, where plants may maintain optimal photosynthesis rates by sacrificing inefficient use of a relatively more abundant (and less costly) resource for more efficient use

of a relatively less abundant (and more costly) resource (Wright et al. 2003).

While photosynthetic least-cost theory predicts that the lowest summed cost of nutrient and water use should remain constant in a given aboveground growing environment, changes in soil resource availability may alter the ratio of the cost to use nutrients relative to the cost to use water (i.e., β). For example, plants may respond to increasing soil nitrogen availability by reducing the cost of acquiring nitrogen, reducing β , and causing plants growing under high soil nitrogen availability to have similar optimal photosynthesis rates achieved with increased leaf nitrogen allocation and decreased stomatal conductance and therefore decreased nitrogen use efficiency and increased water use efficiency. In contrast, plants may respond to increasing soil moisture by reducing the cost of using water, increasing β , and causing plants growing under high soil moisture to have similar optimal photosynthesis rates achieved with reduced leaf nitrogen allocation and increased stomatal conductance and therefore increased nitrogen use efficiency and decreased water use efficiency.

Optimality models that use patterns expected from photosynthetic least-cost theory have been developed for both C₃ (Wang et al. 2017; Smith et al. 2019; Stocker et al. 2020) and more recently for C₄ species (Scott and Smith 2022). Such models agree with patterns observed across environmental gradients (Smith et al. 2019; Stocker et al. 2020; Paillassa et al. 2020; Querejeta et al. 2022; Westerband et al. 2023), and are capable of reconciling dynamic leaf nitrogen-photosynthesis relationships and acclimation responses to elevated CO₂, temperature, light availability, and vapor pressure deficit (Dong et al. 2017; Dong et al. 2020; Smith and Keenan 2020; Luo et al. 2021; Peng et al. 2021; Dong et al. 2022; Dong

et al. 2022; Querejeta et al. 2022; Westerband et al. 2023). However, current versions of optimality models that invoke patterns expected from photosynthetic least-cost theory hold β constant across growing environments. As growing evidence suggests that costs of nutrient use are plastic across resource availability and climatic gradients in species with different nutrient acquisition strategies (Fisher et al. 2010; Brzostek et al. 2014; Terrer et al. 2018; Allen et al. 2020), one might expect that β should dynamically change across environments and in species with different nutrient acquisition strategies.

Patterns expected from photosynthetic least-cost theory have recently been supported across broad environmental gradients. Despite this, a limited number of studies have investigated how β varies across edaphic and climatic gradients and how variance in β might scale to influence leaf nutrient-water use tradeoffs (Lavergne et al. 2020; Paillassa et al. 2020). Furthermore, no previous study has investigated whether β varies in species with different nutrient acquisition strategies or if changes in β due to changes in edaphic characteristics scale to influence leaf or whole plant responses to changing environments. The lack of such studies provided motivation for the experimental chapters included in this dissertation and are important toward considering frameworks for improving the method by which optimality models simulate photosynthetic processes.

In this dissertation, I use a combination of greenhouse, field manipulation, environmental gradient, and growth chamber experiments to quantify leaf and whole plant acclimation responses across various climatic and edaphic conditions and species representing different nutrient acquisition strategies. Together, these experiments evaluate patterns expected from photosynthetic least-cost theory and

test mechanisms predicted to drive responses expected from theory. The empirical data collected in these experiments provide important information needed to refine existing optimality models that include photosynthetic least-cost frameworks, and could help determine whether such models are suitable for implementing in next-generation terrestrial biosphere models. While theory suggests that plants acclimate across environments by minimizing the summed cost of nutrients relative to water, I chose to isolate effects of soil nitrogen availability on costs of nitrogen acquisition relative to water for the sake of brevity. I acknowledge that patterns expected from theory may be modified by other nutrients (e.g., phosphorus) or other edaphic characteristics (Smith et al. 2019; Paillassa et al. 2020; Westerband et al. 2023), and, though not included here, should also be investigated.

In the first experimental chapter, I re-analyze data from a greenhouse experiment that grew *Glycine max* and *Gossypium hirsutum* seedlings under full-factorial combinations of four light treatments and four fertilization treatments to examine effects of nitrogen and light availability on structural carbon costs to acquire nitrogen. In the second experimental chapter, I measure leaf physiological traits in the upper canopy of mature trees growing in a 9-year nitrogen-by-pH field manipulation experiment to assess whether changes in soil nitrogen availability or soil pH modify nitrogen-water use tradeoffs expected from photosynthetic least-cost theory. I then investigate primary drivers of leaf nitrogen content across a precipitation and soil nitrogen availability gradient in Texan grasslands in the third experimental chapter. In the fourth experimental chapter, I use growth chambers to quantify leaf and whole plant acclimation responses to CO₂ in *Glycine max* grown across a soil nitrogen fertilization gradient. I also manipulate nutrient

acquisition strategy by controlling whether *Glycine max* seedlings were able to form associations with symbiotic nitrogen-fixing bacteria.

Across experiments, I find consistent support for patterns expected from photosynthetic least-cost theory, showing that shifts in edaphic characteristics predictably alter β , and that changes in β facilitate changes in leaf nitrogen-water use tradeoffs and leaf nitrogen-photosynthesis relationships. I also show that costs of nitrogen acquisition vary in species with different nitrogen acquisition strategies. Finally, I show strong evidence suggesting that photosynthetic acclimation responses to CO₂ are decoupled from soil nitrogen availability and inoculation with symbiotic nitrogen-fixing bacteria. It is my hope that these experiments will encourage future iterations of optimality models that adopt photosynthetic least-cost frameworks to consider frameworks for implementing dynamic β values across soil resource availability gradients and in species with different nutrient acquisition strategies.

The four experimental chapters included in this dissertation are presented either as previously published journal articles or as manuscript drafts currently in preparation for journal submission. Specifically, the first experimental chapter was published in *Journal of Experimental Botany* in 2021 and the second chapter is currently in review, while the third and fourth chapters are each in preparation for journal submission. The dissertation concludes with a sixth chapter that summarizes experiment findings, briefly synthesizes common themes observed across experiments, and provides some suggestions for future experimentation.

Chapter 2

Root mass carbon costs to acquire nitrogen are determined by nitrogen and light availability in two species with different nitrogen acquisition strategies

Perkowski EA, EF Waring, NG Smith, "Root mass carbon costs to acquire nitrogen are determined by nitrogen and light availability in two species with different nitrogen acquisition strategies", *Journal of Experimental Botany*, 2021, Volume 72, Issue 15, Pages 5766-5776, by permission of Oxford University Press

2.1 Introduction

Carbon and nitrogen cycles are tightly coupled in terrestrial ecosystems. This tight coupling influences photosynthesis (Walker et al. 2014; Rogers et al. 2017), net primary productivity (LeBauer and Treseder 2008; Thomas et al. 2013), decomposition (Cornwell et al. 2008; Bonan et al. 2013; Sulman et al. 2019), and plant resource competition (Gill and Finzi 2016; Xu-Ri and Prentice 2017). Terrestrial biosphere models are beginning to include connected carbon and nitrogen cycles to improve the realism of their simulations (Fisher et al. 2010; Brzostek et al. 2014; Wieder et al. 2015; Shi et al. 2016; Zhu et al. 2019). Simulations from these models indicate that coupling carbon and nitrogen cycles can influence future biosphere-atmosphere feedbacks under global change, such as elevated carbon dioxide or nitrogen deposition (Thornton et al. 2007; Goll et al. 2012; Wieder et al. 2015; Wieder et al. 2019). Nonetheless, there are still limitations in our quantitative understanding of connected carbon and nitrogen dynamics (Thomas et al. 2015; Meyerholt et al. 2016; Rogers et al. 2017; Exbrayat et al. 2018; Shi et al. 2019), forcing models to make potentially unreliable assumptions.

Plant nitrogen acquisition is a process in terrestrial ecosystems by which

carbon and nitrogen are tightly coupled (Vitousek and Howarth 1991; Delaire et al. 2005; Brzostek et al. 2014). Plants must allocate carbon belowground to produce and maintain root systems or exchange with symbiotic soil microbes in order to acquire nitrogen (Högberg et al. 2008; Högberg et al. 2010). Thus, plants have an inherent carbon cost associated with acquiring nitrogen, which can include both direct energetic costs associated with nitrogen acquisition and indirect structural costs associated with allocation (Gutschick 1981; Rastetter et al. 2001; Vitousek et al. 2002; Menge et al. 2008). Model simulations (Fisher et al. 2010; Brzostek et al. 2014; Shi et al. 2016; Allen et al. 2020) and meta-analyses (Terrer et al. 2018) suggest that these carbon costs vary between species, particularly those with different nitrogen acquisition strategies. For example, simulations using iterations of the Fixation and Uptake of Nitrogen (FUN) model indicate that species that acquire nitrogen from non-symbiotic active uptake pathways (e.g., mass flow) generally have larger carbon costs to acquire nitrogen than species that acquire nitrogen through symbiotic associations with nitrogen-fixing bacteria (Brzostek et al. 2014; Allen et al. 2020).

Carbon costs to acquire nitrogen likely vary in response to changes in soil nitrogen availability. For example, if the primary mode of nitrogen acquisition is through non-symbiotic active uptake, then nitrogen availability could decrease carbon costs to acquire nitrogen as a result of increased per-root nitrogen uptake (Franklin et al. 2009; Wang et al. 2018). However, if the primary mode of nitrogen acquisition is through symbiotic active uptake, then nitrogen availability may incur additional carbon costs to acquire nitrogen if it causes microbial symbionts to shift toward parasitism along the parasitism–mutualism continuum

(Johnson et al. 1997; Hoek et al. 2016; Friel and Friesen 2019) or if it reduces the nitrogen acquisition capacity of a microbial symbiont (van Diepen et al. 2007; Soudzilovskaia et al. 2015; Muñoz et al. 2016). Species may respond to shifts in soil nitrogen availability by switching their primary mode of nitrogen acquisition to a strategy with lower carbon costs to acquire nitrogen in order to maximize the magnitude of nitrogen acquired from a belowground carbon investment and outcompete other individuals for soil resources (Rastetter et al. 2001; Menge et al. 2008).

Environmental conditions that affect plant nitrogen demand (e.g., CO₂, light availability) could also affect plant carbon costs to acquire nitrogen. For example, an increase in plant nitrogen demand could increase carbon costs to acquire nitrogen if this increases the carbon that must be allocated belowground to acquire a proportional amount of nitrogen (Kulmatiski et al. 2017; Noyce et al. 2019). This could be driven by a temporary state of diminishing return associated with investing carbon toward building and maintaining structures that are necessary to support enhanced nitrogen uptake, such as fine roots (Matamala and Schlesinger 2000; Norby et al. 2004; Arndal et al. 2018), mycorrhizal hyphae (Saleh et al. 2020), or root nodules (Parvin et al. 2020). Alternatively, if the environmental factor that increases plant nitrogen demand causes nitrogen to become more limiting in the system (e.g. atmospheric CO₂) (Luo et al. 2004; LeBauer and Treseder 2008; Vitousek et al. 2010; Liang et al. 2016), species might switch their primary mode of nitrogen acquisition to a strategy with lower relative carbon costs to acquire nitrogen in order to gain a competitive advantage over species with either different or more limited modes of nitrogen acquisition

(Ainsworth and Long 2005; Taylor and Menge 2018).

Using a plant economics approach, I examined the influence of plant nitrogen demand and soil nitrogen availability on plant carbon costs to acquire nitrogen. This was done by growing a species capable of forming associations with nitrogen-fixing bacteria (*Glycine max* L. (Merr)) and a species not capable of forming these associations (*Gossypium hirsutum* L.) under four levels of light availability (plant nitrogen demand proxy) and four levels of soil nitrogen fertilization (soil nitrogen availability proxy) in a full-factorial, controlled greenhouse experiment. These species are commonly used in regional west Texan cropping systems and have fast growth rates, but differ in growth form (*G. hirsutum* is a perennial woody species, *G. max* is an annual herbaceous species). Species were selected as a hypothesis generation exercise to determine whether effects of fertilization and light availability on carbon costs to acquire nitrogen were directionally similar between species, though this selection does limit my ability to deduce mechanisms that drive species differences across treatment combinations.

I used this experimental design to test the following hypotheses:

1. An increase in plant nitrogen demand due to increasing light availability will increase carbon costs to acquire nitrogen through a proportionally larger increase in belowground carbon than whole-plant nitrogen acquisition. This will be the result of an increased investment of carbon toward belowground structures that support enhanced nitrogen uptake, but at a lower nitrogen return.
2. An increase in soil nitrogen availability will decrease carbon costs to acquire nitrogen as a result of increased per root nitrogen uptake in *G. hirsutum*.

However, soil nitrogen availability will not affect carbon costs to acquire nitrogen in *G. max* because of the already high return of nitrogen supplied through nitrogen fixation.

2.2 Methods

2.2.1 *Experiment setup*

Gossypium hirsutum and *G. max*. were planted in individual 3 liter pots (NS-300; Nursery Supplies, Orange, CA, USA) containing a 3:1 mix of unfertilized potting mix (Sungro Sunshine Mix #2, Agawam, MA, USA) to native soil extracted from an agricultural field most recently planted with *G. max* at the USDA-ARS Laboratory in Lubbock, TX, USA (33.59°N , -101.90°W). The field soil was classified as Amarillo fine sandy loam (75% sand, 10% silt, 15% clay). Upon planting, all *G. max* pots were inoculated with *Bradyrhizobium japonicum* (Verdesian N-DureTM Soybean, Cary, NC, USA) to stimulate root nodulation. Individuals of both species were grown under similar, unshaded, ambient greenhouse conditions for 2 weeks to germinate and begin vegetative growth.

Three blocks were set up in the greenhouse, each containing four light treatments created using shade cloth that reduced incoming radiation by either 0 (full sun), 30, 50, or 80%. Two weeks post-germination, individuals were randomly placed in the four light treatments in each block. Individuals received one of four nitrogen fertilization doses as 100mL of a modified Hoagland solution (Hoagland and Arnon 1950) equivalent to either 0, 70, 210, or 630 ppm N twice per week within each light treatment. Nitrogen fertilization doses were received as topical agents to the soil surface. Each Hoagland solution was modified to keep concen-

trations of other macro- and micronutrients equivalent (Table A1). Plants were routinely well watered to eliminate water stress.

2.2.2 Plant measurements and calculations

Each individual was harvested after 5 weeks of treatment, and biomass was separated by organ type (leaves, stems, and roots). Nodules on *G. max* roots were also harvested. Except for the 0% shade cover and 630 ppm N treatment combination, all treatment combinations in both species had lower average dry biomass:pot volume ratios than the 1:1 ratio recommended by Poorter et al. (2012) to minimize the likelihood of pot volume-induced growth limitation (Table A2, A3; Fig. A1).

All harvested material was dried, weighed, and ground by organ type. Carbon and nitrogen content (g g^{-1}) was determined by subsampling from ground and homogenized biomass of each organ type using an elemental analyzer (Costech 4010; Costech, Inc., Valencia, CA, USA). I scaled these values to total leaf, stem, and root carbon and nitrogen biomass (g) by multiplying dry biomass of each organ type by carbon or nitrogen content of each corresponding organ type. Whole plant nitrogen biomass (g) was calculated as the sum of total leaf (g), stem (g), and root (g) nitrogen biomass. Root nodule carbon biomass was not included in the calculation of root carbon biomass; however, relative plant investment toward root or root nodule standing stock was estimated as the ratio of root biomass to root nodule biomass (g g^{-1}), following similar metrics to those adopted by Dovrat et al. (2018) and Dovrat et al. (2020).

Carbon costs to acquire nitrogen (N_{cost} ; gC gN^{-1}) were estimated as the ratio of total root carbon biomass (C_{bg} ; gC) to whole-plant nitrogen biomass

(N_{wp} ; gN). This calculation quantifies the relationship between carbon spent on nitrogen acquisition and whole plant nitrogen acquisition by using root carbon biomass as a proxy for estimating the magnitude of carbon allocated toward nitrogen acquisition. This calculation therefore assumes that the magnitude of root carbon standing stock is proportional to carbon transferred to root nodules or mycorrhizae, or lost through root exudation or turnover. The assumption has been supported in species that associate with ectomycorrhizal fungi (Hobbie 2006; Hobbie and Hobbie 2008), but is less clear in species that acquire nitrogen through non-symbiotic active uptake or symbiotic nitrogen fixation. It is also unclear whether relationships between root carbon standing stock and carbon transfer to root nodules are similar in magnitude to carbon lost through exudation or when allocated toward other active uptake pathways. Thus, because of the way measurements were calculated, proximal values of carbon costs to acquire nitrogen are underestimates.

2.2.3 *Statistical analyses*

I explored the effects of light and nitrogen availability on carbon costs to acquire nitrogen using separate linear mixed-effects models for each species. Models included shade cover, nitrogen fertilization, and interactions between shade cover and nitrogen fertilization as continuous fixed effects, and also included block as a random intercept term. Three separate models for each species were built with this independent variable structure for three different dependent variables: (i) carbon costs to acquire nitrogen (gC gN^{-1}); (ii) whole plant nitrogen biomass (denominator of carbon cost to acquire nitrogen; gN); and (iii) belowground car-

bon biomass (numerator of carbon cost to acquire nitrogen; gC). I constructed two additional models for *G. max* with the same model structure described above to investigate the effects of light availability and nitrogen fertilization on root nodule biomass (g) and the ratio of root nodule biomass to root biomass (unitless).

I used Shapiro–Wilk tests of normality to determine whether species specific linear mixed-effects model residuals followed a normal distribution. Zero models satisfied residual normality assumptions when models were fit using untransformed data (Shapiro–Wilk: $p<0.05$ in all cases). I attempted to satisfy residual normality assumptions by first fitting models using dependent variables that were natural-log transformed. If residual normality assumptions were still not met (Shapiro–Wilk: $p<0.05$), then models were fit using dependent variables that were square root transformed. All residual normality assumptions were satisfied when models were fit with either a natural-log or square root transformation (Shapiro–Wilk: $p>0.05$ in all cases). Specifically, I natural-log transformed *G. hirsutum* carbon costs to acquire nitrogen and *G. hirsutum* whole-plant nitrogen biomass. I also square root transformed *G. max* carbon costs to acquire nitrogen, *G. max* whole-plant nitrogen biomass, root carbon biomass in both species, *G. max* root nodule biomass, and the *G. max* ratio of root nodule biomass to root biomass. I used the ‘lmer’ function in the ‘lme4’ R package (Bates et al. 2015) to fit each model and the ‘Anova’ function in the ‘car’ R package (Fox and Weisberg 2019) to calculate Wald’s χ^2 to determine the significance ($\alpha=0.05$) of each fixed effect coefficient. Finally, I used the ‘emmeans’ R package (Lenth et al. 2019) to conduct post-hoc comparisons of our treatment combinations using Tukey’s tests. Degrees of freedom for all Tukey’s tests were approximated using the Ken-

ward–Roger approach (Kenward and Roger 1997). All analyses and plots were conducted in R version 4.0.1 (R Core Team 2021).

2.3 Results

2.3.1 Carbon costs to acquire nitrogen

Carbon costs to acquire nitrogen in *G. hirsutum* increased with increasing light availability ($p<0.001$; Table 2.1; Fig. 2.1) and decreased with increasing nitrogen fertilization ($p<0.001$; Table 2.1; Fig. 2.1). There was no interaction between light availability and nitrogen fertilization ($p=0.486$, Table 2.1; Fig. 2.1).

Carbon costs to acquire nitrogen in *G. max* also increased with increasing light availability ($p<0.001$, Table 2.1; Fig. 2.1) and decreased with increasing nitrogen fertilization ($p<0.001$; Table 2.1; Fig. 2.1). There was no interaction between light availability and nitrogen fertilization ($p=0.261$, Table 2.1; Fig. 2.1).

Table 2.1. Analysis of variance results exploring species-specific effects of light availability, nitrogen fertilization, and their interactions on carbon costs to acquire nitrogen (N_{cost} ; gC gN $^{-1}$), whole plant nitrogen biomass (N_{wp} ; gN), and root carbon biomass (C_{bg} ; gC)

	N_{cost}			N_{wp}			C_{bg}			
	df	Coefficient	χ^2	p	Coefficient	χ^2	p	Coefficient	χ^2	p
<i>G. hirsutum</i>										
Intercept		1.594	-	-	-3.232	-	-	0.432	-	-
Light (L)	1	$-1.09 * 10^{-2}$	56.494	<0.001	$-6.41 * 10^{-3}$	91.275	<0.001	$-2.62 * 10^{-3}$	169.608	<0.001
Nitrogen (N)	1	$-1.34 * 10^{-3}$	54.925	<0.001	$1.83 * 10^{-3}$	118.784	<0.001	$1.15 * 10^{-4}$	2.901	<i>0.089</i>
L*N	1	$3.88 * 10^{-6}$	0.485	0.486	$-1.34 * 10^{-5}$	10.721	0.001	$-1.67 * 10^{-6}$	3.140	<i>0.076</i>
<i>G. max</i>										
Intercept		1.877	-	-	0.239	-	-	0.438	-	-
Light (L)	1	$-7.67 * 10^{-3}$	174.156	<0.001	$-6.72 * 10^{-4}$	39.799	<0.001	$-2.55 * 10^{-3}$	194.548	<0.001
Nitrogen (N)	1	$-2.35 * 10^{-4}$	21.948	<0.001	$1.55 * 10^{-4}$	70.771	<0.001	$2.52 * 10^{-4}$	19.458	<0.001
L*N	1	$-2.89 * 10^{-6}$	1.262	0.261	$-6.32 * 10^{-7}$	1.435	0.231	$-3.16 * 10^{-6}$	10.803	0.001

*Significance determined using Wald's χ^2 tests ($p=0.05$). P -values less than 0.05 are in bold and p -values between 0.05 and 0.1 are italicized. Negative coefficients for light treatments indicate a positive effect of increasing light availability on all response variables, as light availability is treated as percent shade cover in all linear mixed-effects models.

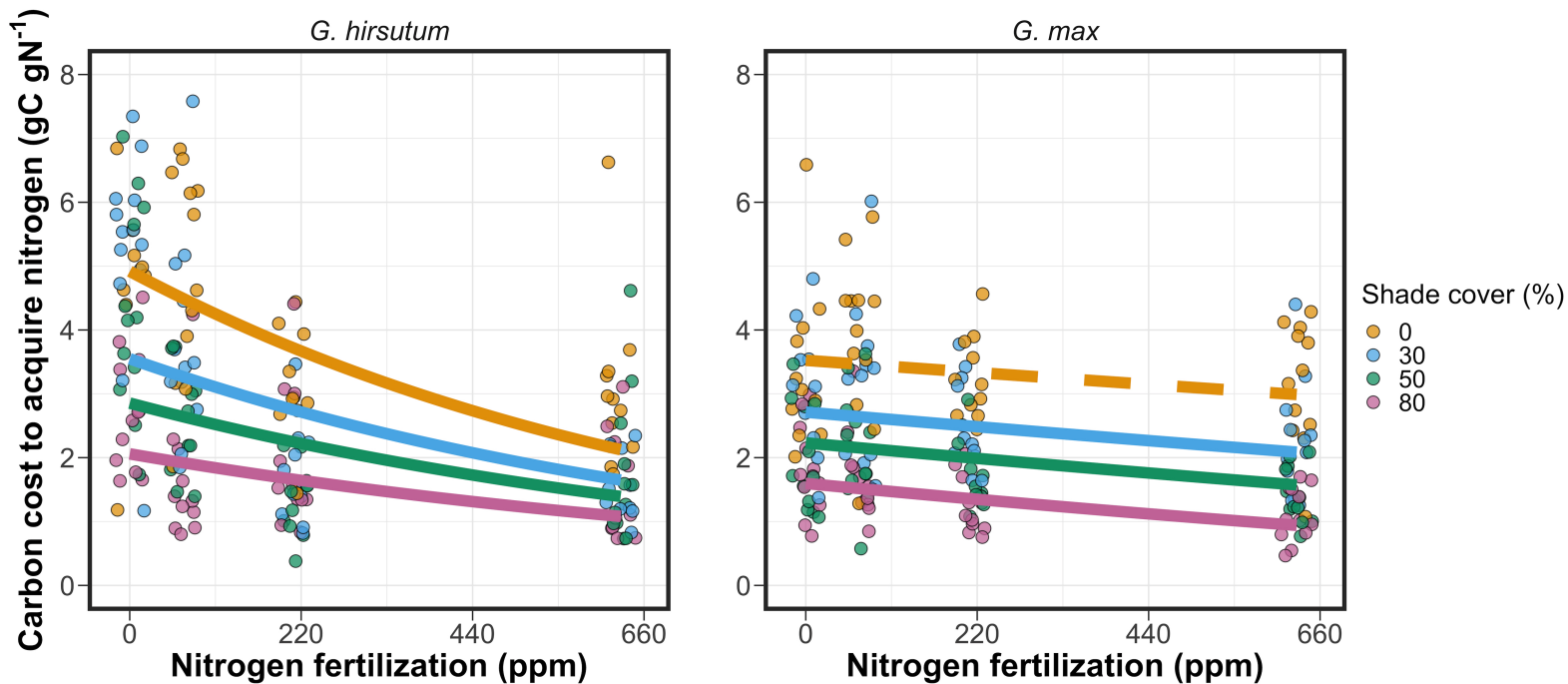


Figure 2.1. Effects of shade cover and nitrogen fertilization on plant carbon costs to acquire nitrogen in *G. hirsutum* (left panel) and *G. max* (right panel). Nitrogen fertilization treatments are represented on the x-axis. Shade cover treatments are represented through colored points and trendlines. Trendlines were created by back-transforming predicted marginal mean values across the range in x-axis values using the ‘emmeans’ function in the ‘emmeans’ R package (Lenth et al. 2019). Specifically, carbon costs to acquire nitrogen were natural-log transformed for *G. hirsutum* and square root transformed in *G. max*. Points are jittered across the x-axis for visibility. Yellow points and trendlines represent the 0% shade cover treatment, blue points and trendlines represent the 30% shade cover treatment, green points and trendlines represent the 50% shade cover treatment, and purple points and trendlines represent the 80% shade cover treatment. Solid trendlines indicate slopes that are significantly different from zero (Tukey: $p < 0.05$), while dashed trendlines indicate slopes that are not statistically different from zero.

2.3.2 Whole plant nitrogen biomass

Whole plant nitrogen biomass in *G. hirsutum* was driven by an interaction between light availability and nitrogen fertilization ($p=0.001$; Table 2.1; Fig. 2.2). This interaction indicated a greater stimulation of whole-plant nitrogen biomass by nitrogen fertilization as light levels increased (Table 2.1; Fig. 2.2).

Whole plant nitrogen biomass in *G. max* increased with increasing light availability ($p<0.001$) and nitrogen fertilization ($p<0.001$), with no interaction between light availability and nitrogen fertilization ($p=0.231$; Table 2.1; Fig. 2.2).

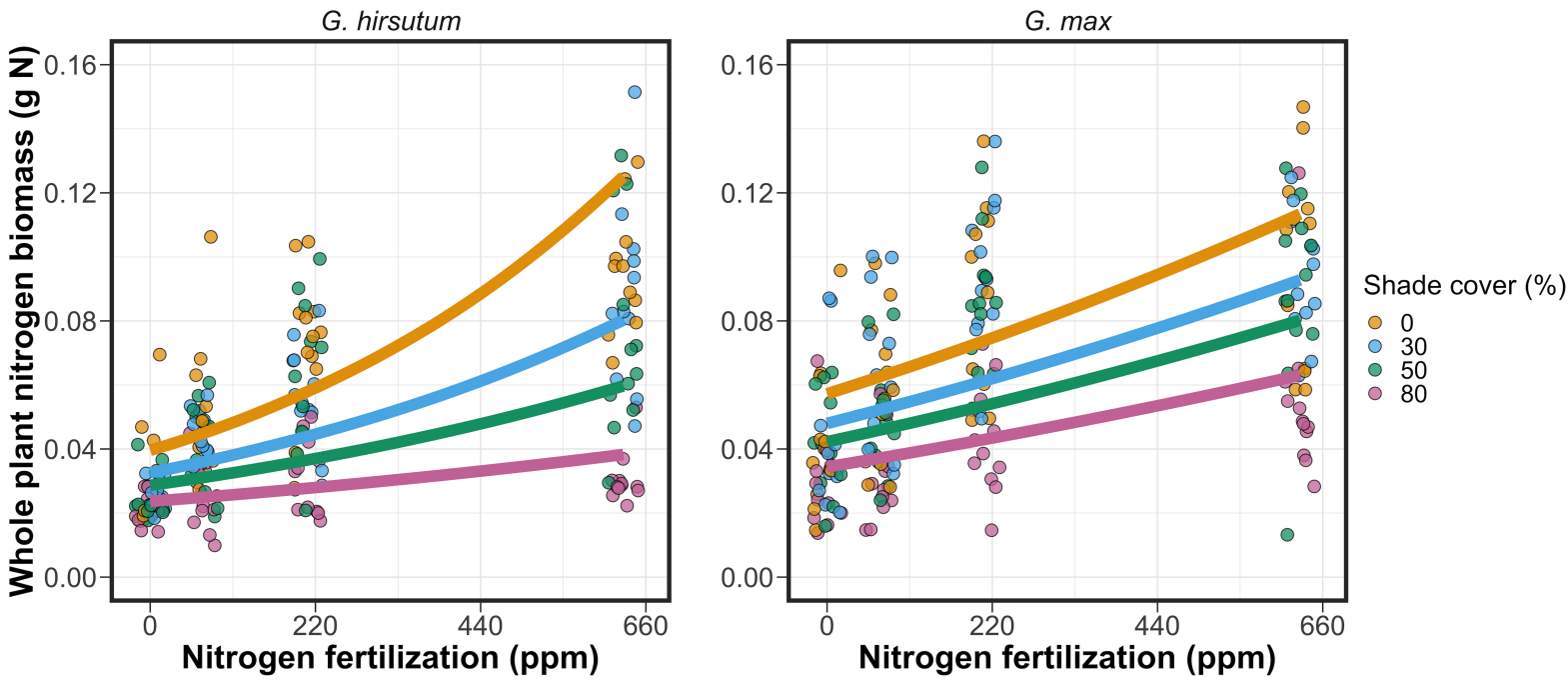


Figure 2.2. Effects of shade cover and nitrogen fertilization on whole-plant nitrogen biomass in *G. hirsutum* (left panel) and *G. max* (right panel). Whole-plant nitrogen biomass is the denominator of the carbon cost to acquire nitrogen calculation. Nitrogen fertilization treatments are represented on the x-axis. Shade cover treatments are represented through colored points and trendlines. Trendlines were created by back-transforming predicted marginal mean values across the range in x-axis values using the ‘*emmeans*’ function in the ‘*emmeans*’ R package (Lenth et al. 2019). Specifically, whole plant nitrogen biomass was natural-log transformed for *G. hirsutum* and square root transformed in *G. max*. Points are jittered across the x-axis for visibility. Points and trendlines are as explained in Fig. 2.1. Solid trendlines indicate slopes that are significantly different from zero (Tukey: $p < 0.05$), while dashed trendlines indicate slopes that are not statistically different from zero.

2.3.3 Root carbon biomass

Root carbon biomass in *G. hirsutum* significantly increased with increasing light availability ($p<0.001$; Table 2.1; Fig. 2.3) and marginally increased with nitrogen fertilization ($p=0.089$; Table 2.1; Fig. 2.3). There was also a marginal interaction between light availability and nitrogen fertilization ($p=0.076$; Table 2.1), driven by an increase in the positive response of root carbon biomass to increasing nitrogen fertilization as light availability increased (Table 2.3). This pattern resulted in significantly positive trends between root carbon biomass and nitrogen fertilization in the two highest light treatments (Tukey: $p<0.05$ in both cases; Table 2.3; Fig. 2.3) and no effect of nitrogen fertilization in the two lowest light treatments (Tukey: $p>0.05$ in both cases; Table 2.3; Fig. 2.3).

There was an interaction between light availability and nitrogen fertilization on root carbon biomass in *G. max* ($p=0.001$; Table 2.1; Fig. 2.3). Post-hoc analyses indicated that the positive effects of nitrogen fertilization on *G. max* root carbon biomass increased with increasing light availability (Table 2.3; Fig. 2.3). There were also positive individual effects of increasing nitrogen fertilization ($p<0.001$; Table 2.3) and light availability ($p<0.001$; Table 2.3) on *G. max* root carbon biomass (Table 2.1; Fig. 2.3).

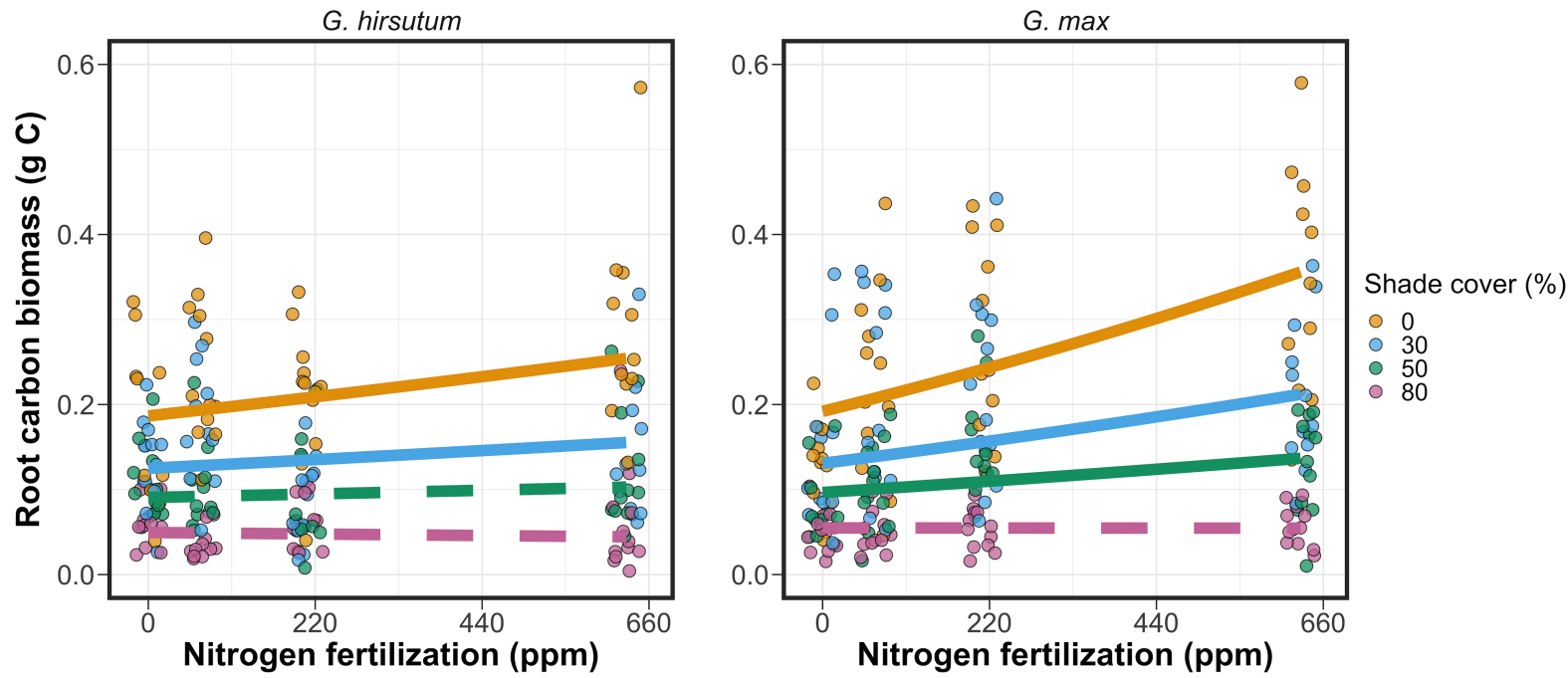


Figure 2.3. Effects of shade cover and nitrogen fertilization on root carbon biomass in *G. hirsutum* (left panel) and *G. max* (right panel). Root carbon biomass is the numerator of the carbon cost to acquire nitrogen calculation. Nitrogen fertilization treatments are represented on the x-axis. Shade cover treatments are represented through colored points and trendlines. Trendlines were created by back-transforming predicted marginal mean values across the range in x-axis values using the ‘emmeans’ function in the ‘emmeans’ R package (Lenth et al. 2019). Specifically, root carbon biomass was square root transformed for both species. Points are jittered across the x-axis for visibility. Colored points and trendlines are as explained in Fig. 2.1. Solid trendlines indicate slopes that are significantly different from zero (Tukey: $p < 0.05$), while dashed trendlines indicate slopes that are not statistically different from zero.

2.3.4 Root nodule biomass

Root nodule biomass in *G. max* increased with increasing light availability ($p<0.001$; Table 2.2; Fig. 2.4a) and decreased with increasing nitrogen fertilization ($p<0.001$; Table 2.2; Fig. 2.4a). There was no interaction between nitrogen fertilization and light availability ($p=0.133$; Table 2.2; Fig. 2.4a). The ratio of root nodule biomass to root biomass did not change in response to light availability ($p=0.481$; Table 2.2; Fig. 2.4b) but decreased with increasing nitrogen fertilization ($p<0.001$; Table 2.2; Fig. 2.4b). There was no interaction between nitrogen fertilization and light availability on the ratio of root nodule biomass to root biomass ($p=0.621$; Table 2.2; Fig. 2.4b).

Table 2.2. Analysis of variance results exploring effects of light availability, nitrogen fertilization, and their interactions on *G. max* root nodule biomass (g) and the ratio of root nodule biomass to root biomass (g g⁻¹)*

	Nodule biomass			Nodule biomass: root biomass			<i>p</i>
	df	Coefficient	χ^2	<i>p</i>	Coefficient	χ^2	
(Intercept)		$3.02 * 10^{-1}$	-	-	$4.48 * 10^{-1}$	-	-
Light (L)	1	$-1.81 * 10^{-3}$	72.964	<0.001	$-8.76 * 10^{-5}$	0.496	0.481
Nitrogen (N)	1	$-2.83 * 10^{-4}$	115.377	<0.001	$-5.09 * 10^{-4}$	156.476	<0.001
L*N	1	$1.14 * 10^{-6}$	2.226	0.133	$-7.30 * 10^{-7}$	0.244	0.621

*Significance determined using Wald's χ^2 tests ($\alpha=0.05$). *P*-values less than 0.05 are in bold. Negative coefficients for light treatments indicate a positive effect of increasing light availability on all response variables, as light availability is treated as percent shade cover in all linear mixed-effects models. Root nodule biomass and nodule biomass: root biomass models were only constructed for *G. max* because *G. hirsutum* was not inoculated with *B. japonicum* and is not capable of forming root nodules.

Table 2.3. Slopes of the regression line describing the relationship between each dependent variable and nitrogen fertilization at each light level*

Shade cover	Carbon cost to acquire nitrogen	Whole plant nitrogen biomass	Belowground carbon biomass	Root nodule biomass	Nodule biomass: root biomass
<i>G. hirsutum</i>					
0%	$-1.34 * 10^{-3a}$	$1.83 * 10^{-3a}$	$1.15 * 10^{-4b}$	-	-
30%	$-1.22 * 10^{-3a}$	$1.43 * 10^{-3a}$	$1.17 * 10^{-4b}$	-	-
50%	$-1.14 * 10^{-3a}$	$1.17 * 10^{-3a}$	$3.12 * 10^{-5b}$	-	-
80%	$-1.02 * 10^{-3a}$	$7.66 * 10^{-4a}$	$-1.89 * 10^{-6b}$	-	-
<i>G. max</i>					
0%	$-2.35 * 10^{-4b}$	$1.55 * 10^{-5b}$	$2.51 * 10^{-4b}$	$-2.83 * 10^{-4b}$	$-5.09 * 10^{-4b}$
30%	$-3.22 * 10^{-4b}$	$1.35 * 10^{-5b}$	$1.57 * 10^{-4b}$	$-2.49 * 10^{-4b}$	$-5.31 * 10^{-4b}$
50%	$-3.80 * 10^{-4b}$	$1.23 * 10^{-5b}$	$9.37 * 10^{-5b}$	$-2.26 * 10^{-4b}$	$-5.45 * 10^{-4b}$
80%	$-4.66 * 10^{-4b}$	$1.04 * 10^{-5b}$	$-9.95 * 10^{-7b}$	$-1.92 * 10^{-4b}$	$-5.67 * 10^{-4b}$

* Slopes represent estimated marginal mean slopes from linear mixed-effects models described in the Methods. Slopes were calculated using the ‘emmeans’ R package (Lenth et al. 2019). Superscripts indicate slopes fit to natural-log (^a) or square root (^b) transformed data. Slopes statistically different from zero (Tukey: $p < 0.05$) are indicated in bold. Marginally significant slopes (Tukey: $0.05 < p < 0.1$) are italicized.

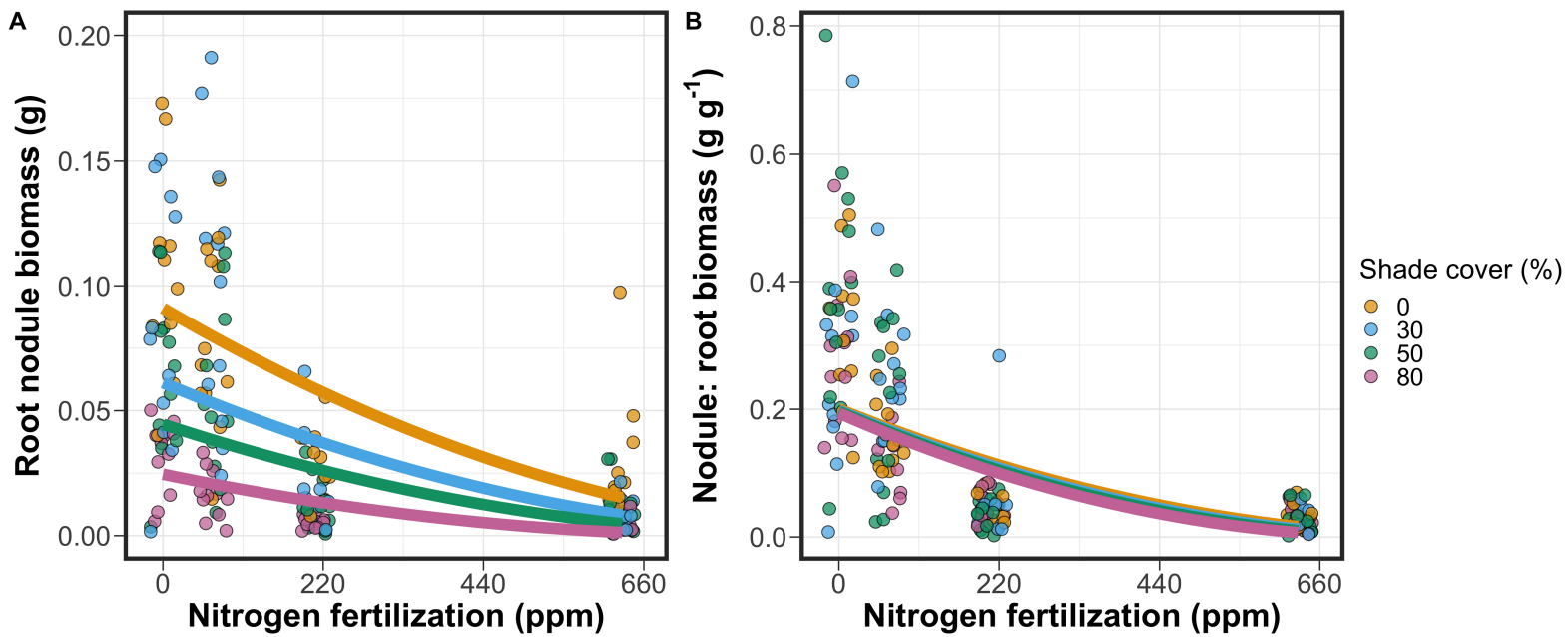


Figure 2.4. Effects of shade cover and nitrogen fertilization on root nodule biomass (A) and the ratio of root nodule biomass to root biomass (B) in *G. max*. Nitrogen fertilization treatments are represented on the x-axis. Shade cover treatments are represented through colored points and trendlines. Trendlines were created by back-transforming predicted marginal mean values across the range in x-axis values using the ‘emmeans’ function in the ‘emmeans’ R package (Lenth et al. 2019). Specifically, root nodule biomass and the ratio of root nodule biomass to root biomass were each square root transformed. Points are jittered across the x-axis for visibility. Colored points and trendlines are as explained in Fig. 2.1. Solid trendlines indicate slopes that are significantly different from zero (Tukey: $p < 0.05$), while dashed trendlines indicate slopes that are not statistically different from zero.

2.4 Discussion

In this chapter, I determined the effects of light availability and soil nitrogen fertilization on root mass carbon costs to acquire nitrogen in *G. hirsutum* and *G. max*. In support of my hypotheses, I found that carbon costs to acquire nitrogen generally increased with increasing light availability and decreased with increasing soil nitrogen fertilization in both species. These findings suggest that carbon costs to acquire nitrogen are determined by factors that influence plant nitrogen demand and soil nitrogen availability. In contrast to my second hypothesis, root nodulation data suggested that *G. max* and *G. hirsutum* achieved similar directional carbon cost responses to nitrogen fertilization despite a likely shift in *G. max* allocation from nodulation to root biomass along the nitrogen fertilization gradient.

Both *G. max* and *G. hirsutum* experienced an increase in carbon costs to acquire nitrogen due to increasing light availability. These patterns were driven by a larger increase in root carbon biomass than whole-plant nitrogen biomass. Increases in root carbon biomass due to factors that increase plant nitrogen demand are a commonly observed pattern, as carbon allocated belowground provides substrate needed to produce and maintain structures that satisfy aboveground plant nitrogen demand (Nadelhoffer and Raich 1992; Giardina et al. 2005; Raich et al. 2014). Findings suggest that plants allocate relatively more carbon for acquiring nitrogen when demand increases over short temporal scales, which may cause a temporary state of diminishing return due to asynchrony between belowground carbon and whole-plant nitrogen responses to plant nitrogen demand (Kulmatiski et al. 2017; Noyce et al. 2019). These responses might be attributed to a temporal lag associated with producing structures that enhance nitrogen acquisition. For

example, fine roots (Matamala and Schlesinger 2000; Norby et al. 2004; Arndal et al. 2018) and root nodules (Parvin et al. 2020) take time to build and first require the construction of coarse roots. Thus, full nitrogen returns from these investments may not occur immediately (Kayler et al. 2010; Kayler et al. 2017), and may vary by species acquisition strategy. I speculate that increases in nitrogen acquisition from a given carbon investment may occur beyond the 5-week scope of this experiment. A similar study conducted over a longer temporal scale would address this.

Increasing soil nitrogen fertilization generally decreased carbon costs to acquire nitrogen in both species. These patterns were driven by a larger increase in whole-plant nitrogen biomass than root carbon biomass. In *G. hirsutum*, reductions in carbon costs to acquire nitrogen may have been due to an increase in per-root nitrogen uptake, allowing individuals to maximize the amount of nitrogen acquired from a belowground carbon investment. Interestingly, increased soil nitrogen fertilization increased whole-plant nitrogen biomass in *G. max* despite reductions in root nodule biomass that likely reduced the nitrogen-fixing capacity of *G. max* (Andersen et al. 2005; Muñoz et al. 2016). While reductions in root nodulation due to increased soil nitrogen availability are commonly observed (Gibson and Harper 1985; Fujikake et al. 2003), root nodulation responses were observed in tandem with increased root carbon biomass, implying that *G. max* shifted relative carbon allocation from nitrogen fixation to soil nitrogen acquisition (Markham and Zekveld 2007; Dovrat et al. 2020). This was likely because there was a reduction in the carbon cost advantage of acquiring fixed nitrogen relative to soil nitrogen, and suggests that species capable of associating with symbiotic

nitrogen-fixing bacteria shift their relative nitrogen acquisition pathway to optimize nitrogen uptake (Rastetter et al. 2001). Future studies should investigate these patterns with a larger quantity of phylogenetically related species, or different varieties of a single species that differ in their ability to form associations with symbiotic nitrogen-fixing bacteria to more directly test the impact of nitrogen fixation on the patterns observed in this study.

Carbon costs to acquire nitrogen are subsumed in the general discussion of economic analogies to plant resource uptake (Bloom et al. 1985; Rastetter et al. 2001; Vitousek et al. 2002; Phillips et al. 2013; Terrer et al. 2018; Henneron et al. 2020). Despite this, terrestrial biosphere models rarely include costs of nitrogen acquisition to predict plant nitrogen uptake. There is currently one plant resource uptake model, the Fixation and Uptake of Nitrogen model (FUN), that quantitatively predicts carbon costs to acquire nitrogen within a framework for predicting plant nitrogen uptake for different nitrogen acquisition strategies (Fisher et al. 2010; Brzostek et al. 2014). Iterations of FUN are currently coupled to two terrestrial biosphere models: the Community Land Model 5.0 and the Joint UK Land Environment Simulator (Clark et al. 2011; Shi et al. 2016; Lawrence et al. 2019). Recent work suggests that coupling FUN to CLM 5.0 caused a large overprediction of plant nitrogen uptake associated with nitrogen fixation (Davies-Barnard et al. 2020) compared to other terrestrial biosphere model products. Thus, empirical data from manipulative experiments that explicitly quantify carbon costs to acquire nitrogen in species capable of associating with nitrogen-fixing bacteria across different environmental contexts is an important step toward identifying potential biases in models such as FUN.

These findings support the FUN formulation of carbon costs to acquire nitrogen in response to soil nitrogen availability. FUN calculates carbon costs to acquire nitrogen based on the sum of carbon costs to acquire nitrogen via nitrogen fixation, mycorrhizal active uptake, non-mycorrhizal active uptake, and retranslocation (Fisher et al. 2010; Brzostek et al. 2014). Carbon costs to acquire nitrogen via mycorrhizal or non-mycorrhizal active uptake pathways are derived as a function of nitrogen availability, root biomass, and two parameterized values based on nitrogen acquisition strategy (Brzostek et al. 2014). Due to this, FUN simulates a net decrease in carbon costs to acquire nitrogen with increasing nitrogen availability for mycorrhizal and non-mycorrhizal active uptake pathways, assuming constant root biomass. This was a pattern I observed in *G. hirsutum* regardless of light availability. In contrast, FUN would not simulate a net change in carbon costs to acquire nitrogen via nitrogen fixation due to nitrogen availability. This is because carbon costs to acquire nitrogen via nitrogen fixation are derived from a well established function of soil temperature, which is independent of soil nitrogen availability (Houlton et al. 2008; Fisher et al. 2010). I observed a net reduction in carbon costs to acquire nitrogen in *G. max*, except when individuals were grown under 0% shade cover. While a net reduction of carbon costs in response to nitrogen fertilization runs counter to nitrogen fixation carbon costs simulated by FUN, these patterns were likely because *G. max* individuals switched their primary mode of nitrogen acquisition from symbiotic nitrogen fixation to a non-symbiotic active uptake pathway.

The metric used in this study to determine carbon costs to acquire nitrogen has several limitations. Most notably, this metric uses root carbon biomass

as a proxy for estimating the amount of carbon spent on nitrogen acquisition. Although it is true that most carbon allocated belowground has at least an indirect structural role in acquiring soil resources, it remains unclear whether this assumption holds true for species that acquire nitrogen via symbiotic nitrogen fixation. I also cannot quantify carbon lost through root exudates or root turnover, which may increase due to factors that increase plant nitrogen demand (Tingey et al. 2000; Phillips et al. 2011), and can increase the magnitude of available nitrogen from soil organic matter through priming effects on soil microbial communities (Uselman et al. 2000; Bengtson et al. 2012). It is also not clear whether these assumptions hold under all environmental conditions, such as those that shift belowground carbon allocation toward a different mode of nitrogen acquisition (Taylor and Menge 2018; Friel and Friesen 2019) or between species with different acquisition strategies. In this study, increasing soil nitrogen fertilization increased carbon investment to roots relative to carbon transferred to root nodules. By assuming that carbon allocated to root carbon was proportional to carbon allocated to root nodules across all treatment combinations, these observed responses to soil nitrogen fertilization were likely to be overestimated in *G. max*. I encourage future research to quantify these carbon fates independently.

Carbon costs to acquire nitrogen decreased with increasing fertilization more strongly in *G. hirsutum* than *G. max*, a pattern that may have been driven by decreased investment to symbiotic nitrogen-fixing bacteria with increasing fertilization in *G. max*. However, species differed by more than just acquisition strategy, as *G. hirsutum* is a woody perennial species and *G. max* is a herbaceous annual species. Therefore, assigning causality to the stronger reduction

in costs of nitrogen acquisition in *G. hirsutum* is a challenge, and only provides anecdotal evidence that such patterns are generalizable across species. As previously mentioned, future experiments should attempt to measure such responses across a wider range of phylogenetically similar species or in a single species while explicitly controlling the source of nitrogen uptake.

Researchers conducting pot experiments must carefully choose pot volume to minimize the likelihood of growth limitations induced by pot volume (Poorter et al. 2012). Poorter et al. (2012) indicate that researchers are likely to avoid growth limitations associated with pot volume if measurements are collected when the plant biomass:pot volume ratio is less than 1 g L^{-1} . In this experiment, all treatment combinations in both species had biomass:pot volume ratios less than 1 g L^{-1} except for *G. max* and *G. hirsutum* that were grown under 0% shade cover and had received 630 ppm N. Specifically, *G. max* and *G. hirsutum* had average respective biomass:pot volume ratios of $1.24 \pm 0.07 \text{ g L}^{-1}$ and $1.34 \pm 0.13 \text{ g L}^{-1}$, when grown under 0% shade cover and received 630 ppm N (Table A2, A3; Fig. A1). If growth in this treatment combination was limited by pot volume, then individuals may have had larger carbon costs to acquire nitrogen than would be expected if they were grown in larger pots. This pot volume induced growth limitation could cause a reduction in per-root nitrogen uptake associated with more densely packed roots, which could reduce the positive effect of nitrogen fertilization on whole-plant nitrogen biomass relative to root carbon biomass (Poorter et al. 2012).

Pot size may have limited plant growth, which provides a possible explanation for the marginally insignificant effect of increasing nitrogen fertilization on

G. max carbon costs to acquire nitrogen when grown under 0% shade cover. This is because the regression line describing the relationship between carbon costs to acquire nitrogen and nitrogen fertilization in *G. max* grown under 0% shade cover would have flattened if growth limitation had caused larger than expected carbon costs to acquire nitrogen in the 0% shade cover, 630 ppm N treatment combination. This may have been exacerbated by the fact that *G. max* likely shifted relative carbon allocation from nitrogen fixation to soil nitrogen acquisition, which could have increased the negative effect of more densely packed roots on nitrogen uptake. These patterns could have also occurred in *G. hirsutum* grown under 0% shade cover; however, there was no change in the effect of nitrogen fertilization on *G. hirsutum* carbon costs to acquire nitrogen grown under 0% shade cover relative to other shade cover treatments. Regardless, the possibility of growth limitation due to pot volume suggests that effects of increasing nitrogen fertilization on carbon costs to acquire nitrogen in both species grown under 0% shade cover could have been underestimated. Follow-up studies using a similar experimental design with a larger pot volume would be necessary in order to determine whether these patterns were impacted by pot volume-induced growth limitation.

In conclusion, this chapter provides empirical evidence that carbon costs to acquire nitrogen are influenced by light availability and soil nitrogen fertilization in a species capable of acquiring nitrogen via symbiotic nitrogen fixation and a species not capable of forming such associations. We show that carbon costs to acquire nitrogen generally increase with increasing light availability and decrease with increasing nitrogen fertilization. This chapter provides important empirical data needed to evaluate the formulation of carbon costs to acquire nitrogen in

terrestrial biosphere models, particularly carbon costs to acquire nitrogen that are associated with symbiotic nitrogen fixation. Findings broadly support the general formulation of these carbon costs in the FUN biogeochemical model in response to shifts in nitrogen availability. However, there is a need for future studies to explicitly quantify carbon costs to acquire nitrogen under different environmental contexts, over longer temporal scales, and using larger selections of phylogenetically related species. In addition, I suggest that future studies minimize the limitations associated with the metric used here by explicitly measuring belowground carbon fates independently.

Chapter 3

Soil nitrogen availability modifies leaf nitrogen economies in mature temperate deciduous forests: a direct test of photosynthetic least-cost theory

3.1 Introduction

Photosynthesis represents the largest carbon flux between the atmosphere and land surface (IPCC 2021), and plays a central role in biogeochemical cycling at multiple spatial and temporal scales (Vitousek and Howarth 1991; LeBauer and Treseder 2008; Kaiser et al. 2015; Wieder et al. 2015). Therefore, carbon and energy fluxes simulated by terrestrial biosphere models are sensitive to the formulation of photosynthetic processes (Ziehn et al. 2011; Bonan et al. 2011; Booth et al. 2012; Smith et al. 2016; Smith et al. 2017) and must be represented using robust, empirically tested processes (Prentice et al. 2015; Wieder et al. 2019). Current formulations of photosynthesis vary across terrestrial biosphere models (Smith and Dukes 2013; Rogers et al. 2017), which causes variation in modeled ecosystem processes (Knorr 2000; Knorr and Heimann 2001; Bonan et al. 2011; Friedlingstein et al. 2014) and casts uncertainty on the ability of these models to accurately predict terrestrial ecosystem responses and feedbacks to global change (Zaehle et al. 2005; Schaefer et al. 2012; Davies-Barnard et al. 2020).

Terrestrial biosphere models commonly represent C₃ photosynthesis through variants of the Farquhar et al. (1980) biochemical model (Smith and Dukes 2013; Rogers 2014; Rogers et al. 2017). This well-tested photosynthesis model estimates leaf-level carbon assimilation, or photosynthetic capacity, as a function of the maximum rate of Ribulose-1,5-bisphosphate carboxylase-oxygenase (Ru-

bisco) carboxylation (V_{cmax}) and the maximum rate of Ribulose-1,5-bisphosphate (RuBP) regeneration (J_{max}) (Farquhar et al. 1980). Many terrestrial biosphere models predict these model inputs through plant functional group specific linear relationships between leaf nutrient content and V_{cmax} (Smith and Dukes 2013; Rogers 2014; Rogers et al. 2017) under the tenet that a large fraction of leaf nutrients, and nitrogen in particular, are partitioned toward building and maintaining enzymes that support photosynthetic capacity, such as Rubisco (Brix 1971; Gulmon and Chu 1981; Evans 1989; Kattge et al. 2009; Walker et al. 2014). Terrestrial biosphere models predict leaf nutrient content from soil nutrient availability based on the assumption that increasing soil nutrients generally increases leaf nutrients (Firn et al. 2019; Li et al. 2020; Liang et al. 2020) which, in the case of nitrogen, often corresponds with an increase in photosynthetic processes (Li et al. 2020; Liang et al. 2020).

Recent work calls the generality of relationships between soil nutrient availability, leaf nutrient content, and photosynthetic capacity into question, suggesting instead that leaf nutrients and photosynthetic capacity are better predicted as an integrated product of aboveground climate, leaf traits, and soil nutrient availability, rather than soil nutrient availability alone (Dong et al. 2017; Dong et al. 2020; Dong et al. 2022; Firn et al. 2019; Smith et al. 2019; Peng et al. 2021). It has been reasoned that this result is because plants allocate added nutrients to growth and storage rather than alterations in leaf chemistry (Smith et al. 2019), perhaps as a result of nutrient limitation of primary productivity (LeBauer and Treseder 2008; Fay et al. 2015). Additionally, recent work suggests that relationships between leaf nutrient content and photosynthesis vary across environments,

and that the proportion of leaf nutrient content allocated to photosynthetic tissue varies over space and time with plant acclimation and adaptation responses to light availability, vapor pressure deficit, soil pH, soil nutrient availability, and environmental factors that influence leaf mass per area (Pons and Pearcy 1994; Niinemets and Tenhunen 1997; Evans and Poorter 2001; Hikosaka and Shigeno 2009; Ghimire et al. 2017; Onoda et al. 2017; Luo et al. 2021). The use of linear relationships between leaf nutrient content and V_{cmax} to predict photosynthetic capacity, as commonly used in terrestrial biosphere models (Rogers 2014), is not capable of detecting such responses.

Photosynthetic least-cost theory provides an alternative framework for understanding relationships between soil nutrient availability, leaf nutrient content, and photosynthetic capacity (Harrison et al. 2021). Using a two-input microeconomics approach (Wright et al. 2003), the theory posits that plants acclimate to a given environment by optimizing leaf photosynthesis rates at the lowest summed cost of using nutrients and water (Prentice et al. 2014; Wang et al. 2017; Smith et al. 2019; Paillassa et al. 2020). Across resource availability gradients, the theory predicts that optimal photosynthetic rates can be achieved by trading less efficient use of a more abundant (or less costly) resource to acquire for more efficient use of a less abundant (or more costly) resource to acquire. For example, an increase in soil nutrient availability should reduce the cost of acquiring and using nutrients (Bae et al. 2015; Eastman et al. 2021; Perkowski et al. 2021), which could increase leaf nutrient investments in photosynthetic proteins to allow similar photosynthetic rates to be achieved with greater nutrient use (reduced nutrient use efficiency) and reduced water use (greater water use efficiency). The

theory suggests similar tradeoffs in response to increasing soil pH (Paillassa et al. 2020), specifically, that increasing soil pH should reduce the cost of acquiring soil nutrients due to an increase in plant-available nutrient concentration (Paillassa et al. 2020; Dong et al. 2022). The theory is also capable of reconciling dynamic leaf nutrient-photosynthesis relationships at global scales (Luo et al. 2021).

Patterns expected from photosynthetic least-cost theory have recently received empirical support both in global environmental gradient (Smith et al. 2019; Paillassa et al. 2020; Luo et al. 2021; Querejeta et al. 2022; Westerband et al. 2023) and local manipulative invasion (Bialic-Murphy et al. 2021) studies. However, nutrient addition experiments that directly examine nutrient-water use tradeoffs expected from the theory are rare (but see Guerrieri et al. 2011), and only global gradient studies testing the theory have considered soil pH in their analyses. Therefore, empirical data collected from nutrient addition and soil pH manipulation experiments are critical to test mechanisms driving responses predicted by the theory.

In this study, I measured leaf responses to soil nitrogen availability in five deciduous tree species growing in the upper canopy of mature closed canopy temperate forests in the northeastern United States. Soil nitrogen availability and pH were manipulated through a nitrogen-by-pH field manipulation experiment with treatments applied since 2011, eight years prior to measurement. Two different soil nitrogen treatments were applied to increase nitrogen availability with opposing effects on soil pH. An additional nitrogen-free acidifying treatment was applied to decrease soil pH. I hypothesized that increased soil nitrogen availability would enable plants to create more photosynthetic enzymes per leaf, allowing similar

photosynthetic rates achieved with reduced stomatal conductance and increased leaf nitrogen content allocated to photosynthetic leaf tissue. I expected that this response would be driven by a reduction in the cost of acquiring nitrogen, which would cause trees to sacrifice efficient nitrogen use to enable more efficient use of other limiting resources (i.e., water). Finally, I hypothesized similar leaf responses to increasing soil pH.

3.2 Methods

3.2.1 *Study site description*

I conducted this study in summer 2019 at three stands located within a 20-km radius of Ithaca, NY, USA (42.444°N , 76.502°W). All stands contain mature, closed-canopy forests dominated by deciduous tree species. Stands contained abundant sugar maple (*Acer saccharum* Marshall), American beech (*Fagus grandifolia* Ehrh.), and white ash (*Fraxinus americana* L.), accounting for 43%, 15%, and 17% of the total aboveground biomass across the three stands, respectively, with less frequent red maple (*Acer rubrum* L.; 9% of total aboveground biomass) and red oak occurrences (*Quercus rubra* L.; 10% of total aboveground biomass). Soils at each site were broadly classified as a channery silt loam Inceptisols using the USDA NRCS Web Soil Survey data product (Soil Survey Staff 2022). Between 2006 and 2020, study sites averaged 972 mm of precipitation per year and had an average temperature of 7.9°C per a weather station located near the Cornell University campus (42.449°N , 76.449°W) part of the NOAA NCEI Global Historical Climatology Network (Menne et al. 2012).

3.2.2 *Experimental design*

Four 40 m x 40 m plots were set up at each site in 2009, each with an additional 10 m buffer along plot perimeters (60 m x 60 m total). The plots were set up as a nitrogen-by-pH field manipulation experiment, with one each of four treatments at each site. Two nitrogen treatments were applied, both at 50 kg N ha⁻¹ yr⁻¹, as either sodium nitrate (NaNO₃) to raise soil pH, or ammonium sulfate ((NH₄)₂SO₄) to acidify; an elemental sulfur treatment was selected to acidify without nitrogen, applied at the same rate of S addition from the ammonium sulfate plot (57 kg S ha⁻¹ yr⁻¹); and control plots received no additions. All amendments were added in pelletized form using hand-held fertilizer spreaders to both the main plots and buffers. Amendments were divided into three equal doses distributed across the growing season from 2011-2017 and added as a single dose from 2018 onward. During 2019, plots were fertilized during the week of May 20.

3.2.3 *Leaf gas exchange and trait measurements*

I sampled one leaf each from 6 to 10 individuals per plot between June 25 and July 12, 2019 for gas exchange measurements (Table B1), between one and two months after fertilization. Leaves were collected from deciduous broadleaf trees represented across all sites and plots and were replicated in efforts to mimic the species abundance of each plot at each site. I attempted to collect leaves from the upper canopy to reduce differential shading effects on leaf physiology. Leaves were accessed by pulling down small branches using an arborist's slingshot and weighted beanbag attached to a throw line. Branches were immediately recut under deionized water and remained submerged to reduce stomatal closure and

avoid xylem embolism, as done in Smith and Dukes (2018), until gas exchange data were collected.

Randomly selected leaves with little to no visible external damage were attached to a Li-COR LI-6800 (Li-COR Bioscience, Lincoln, Nebraska, USA) portable photosynthesis machine to measure net photosynthesis (A_{net} ; $\mu\text{mol m}^{-2} \text{s}^{-1}$), stomatal conductance (g_{sw} ; $\text{mol m}^{-2} \text{s}^{-1}$), and intercellular CO_2 concentration (C_i ; $\mu\text{mol mol}^{-1}$) at different reference CO_2 concentrations (C_a ; $\mu\text{mol mol}^{-1}$) concentrations (i.e., an A_{net}/C_i curve) under saturating light conditions ($2,000 \mu\text{mol m}^{-2} \text{s}^{-1}$). Reference CO_2 concentrations followed the sequence: 400, 300, 200, 100, 50, 400, 400, 600, 800, 1000, 1200, 1500, and 2000 $\mu\text{mol mol}^{-1} \text{CO}_2$. Leaf temperatures were not controlled in the cuvette and ranged from 21.8 °C to 31.7 °C (mean \pm SD: 27.2 \pm 2.2 °C). A linear and second order log-polynomial regression suggested no effect of temperature on stomatal conductance measured at 400 $\mu\text{mol mol}^{-1} \text{CO}_2$ or net photosynthesis measured at 400 $\mu\text{mol mol}^{-1} \text{CO}_2$ (Table B2, B3; Fig. B1). All A_{net}/C_i curves were generated within one hour of branch severance.

Leaf morphological and chemical traits were collected on the same leaf used to generate each A_{net}/C_i curve. Images of each leaf were taken using a flat-bed scanner to determine fresh leaf area using the ‘LeafArea’ R package (Katabuchi 2015), which automates leaf area calculations using ImageJ software (Schneider et al. 2012). Each leaf was dried at 65°C for at least 48 hours, weighed, and ground using a Retsch MM200 ball mill grinder (Verder Scientific, Inc., Newtown, PA, USA) until homogenized. Leaf mass per unit leaf area (M_{area} , g m^{-2}) was calculated as the ratio of dry leaf biomass to fresh leaf area. Using a subsample

of ground and homogenized leaf biomass, leaf nitrogen content (N_{mass} ; gN g⁻¹) and leaf $\delta^{13}\text{C}$ (‰, relative to Vienna Pee Dee Belemnite international reference standard) were measured at the Cornell Stable Isotope Lab with an elemental analyzer (NC 2500, CE Instruments, Wigan, UK) interfaced to an isotope ratio mass spectrometer (Delta V Isotope Ratio Mass Spectrometer, ThermoFisher Scientific, Waltham, MA, USA). Leaf nitrogen content per unit leaf area (N_{area} ; gN m⁻²) was calculated by multiplying N_{mass} by M_{area} .

I used leaf $\delta^{13}\text{C}$ values to estimate χ (unitless), which is an isotope-derived estimate of the leaf $C_i:C_a$ ratio. While intercellular and atmospheric CO₂ concentrations were directly measured during each A_{net}/C_i curve, deriving χ from $\delta^{13}\text{C}$ provides a more integrative estimate of the leaf $C_i:C_a$ over an individual leaf's lifespan and minimizes any effect of recent branch severance on our measurements. I derived χ following the approach of Farquhar et al. (1989) described in Cernusak et al. (2013):

$$\chi = \frac{\Delta^{13}\text{C} - a}{b - a} \quad (3.1)$$

where $\Delta^{13}\text{C}$ represents the relative difference between leaf $\delta^{13}\text{C}$ (‰) and air $\delta^{13}\text{C}$ (‰), and is calculated from the following equation:

$$\Delta^{13}\text{C} = \frac{\delta^{13}\text{C}_{\text{air}} - \delta^{13}\text{C}_{\text{leaf}}}{1 + \delta^{13}\text{C}_{\text{leaf}}} \quad (3.2)$$

where $\delta^{13}\text{C}_{\text{air}}$ is assumed to be -8‰ (Keeling et al. 1979; Farquhar et al. 1989), a represents the fractionation between ¹²C and ¹³C due to diffusion in air, assumed to be 4.4‰, and b represents the fractionation caused by Rubisco carboxylation, assumed to be 27‰ (Farquhar et al. 1989).

3.2.4 Response curve fitting and parameter estimation

I fit A_{net}/C_i curves of each individual using the ‘fitaci’ function in the ‘planteophys’ R package (Duursma 2015). This function estimates the maximum rate of Rubisco carboxylation (V_{cmax} ; $\mu\text{mol m}^{-2} \text{s}^{-1}$) and maximum rate of electron transport for RuBP regeneration (J_{max} ; $\mu\text{mol m}^{-2} \text{s}^{-1}$) based on the Farquhar, von Caemmerer, and Berry biochemical model of C₃ photosynthesis (Farquhar et al. 1980). For each curve fit, I included triose phosphate utilization (TPU) limitation to avoid underestimating J_{max} (Gregory et al. 2021). Curves were visually examined to confirm the likely presence of TPU limitation.

I determined Michaelis-Menten coefficients for Rubisco affinity to CO₂ (K_c ; $\mu\text{mol mol}^{-1}$) and O₂ (K_o ; $\mu\text{mol mol}^{-1}$), and the CO₂ compensation point (Γ^* ; $\mu\text{mol mol}^{-1}$) using leaf temperature and equations described in Medlyn et al. (2002) and derived in Bernacchi et al. (2001). Specifically, K_c and K_o were calculated as:

$$K_c = 404.9 * \exp^{\frac{79430(T_k - 298)}{298RT_k}} \quad (3.3)$$

and

$$K_o = 278.4 * \exp^{\frac{36380(T_k - 298)}{298RT_k}} \quad (3.4)$$

while Γ^* was calculated as:

$$\Gamma^* = 42.75 * \exp^{\frac{37830(T_k - 298)}{298RT_k}} \quad (3.5)$$

In all three equations, T_k is the leaf temperature (in Kelvin) during each A_{net}/C_i curve and R is the universal gas constant (8.314 J mol⁻¹ K⁻¹).

I standardized V_{cmax} and J_{max} estimates to 25 °C using a modified Arrhenius equation (Kattge and Knorr 2007):

$$k_{25} = \frac{k_{\text{obs}}}{e^{\frac{H_a(T_{\text{obs}} - T_{\text{ref}})}{T_{\text{ref}} R T_{\text{obs}}}} * \frac{1 + e^{\frac{T_{\text{ref}} \Delta S - H_d}{T_{\text{obs}}}}}{1 + e^{\frac{T_{\text{obs}} \Delta S - H_d}{T_{\text{obs}}}}}} \quad (3.6)$$

k_{25} represents the standardized V_{cmax} or J_{max} rate at 25°C, k_{obs} represents the V_{cmax} or J_{max} estimate at the average leaf temperature measured inside the cuvette during the A_{net}/C_i curve. H_a is the activation energy of V_{cmax} (71,513 J mol⁻¹) Kattge and Knorr (2007) or J_{max} (49,884 J mol⁻¹) (Kattge and Knorr 2007). H_d represents the deactivation energy of both V_{cmax} and J_{max} (200,000 J mol⁻¹) (Medlyn et al. 2002), and R represents the universal gas constant (8.314 J mol⁻¹ K⁻¹). T_{ref} represents the standardized temperature of 298.15 K (25°C) and T_{obs} represents the mean leaf temperature (in K) during each A_{net}/C_i curve. ΔS is an entropy term that (Kattge and Knorr 2007) derived as a linear relationship with average growing season temperature (T_g ; °C), where:

$$\Delta S_{v_{\text{cmax}}} = -1.07 T_g + 668.39 \quad (3.7)$$

and

$$\Delta S_{j_{\text{max}}} = -0.75 T_g + 659.70 \quad (3.8)$$

I estimated T_g in Equations 3.7 and 3.8 based on mean daily (24-hour) air temperature of the 30 days leading up to the day of each sample collection using the same weather station reported in the site description. I used $V_{\text{cmax}25}$ and $J_{\text{max}25}$ estimates to calculate the ratio of $J_{\text{max}25}$ to $V_{\text{cmax}25}$ ($J_{\text{max}25}:V_{\text{cmax}25}$; unitless).

3.2.5 *Tradeoffs between nitrogen and water use*

Photosynthetic nitrogen use efficiency (PNUE; $\mu\text{mol CO}_2 \text{ mol}^{-1} \text{ N s}^{-1}$) was calculated by dividing A_{net} by N_{area} , first converting N_{area} to mol N m^{-2} using the molar mass of nitrogen (14 g mol^{-1}). I used χ as an indicator of water use efficiency, which exploratory analyses suggest had similar responses to soil nitrogen availability and pH as intrinsic water use efficiency measured from gas exchange ($A_{\text{net}}/g_{\text{sw}}$). Tradeoffs between nitrogen and water use were determined by calculating the ratio of N_{area} to χ ($N_{\text{area}}:\chi$; gN m^{-2}) and V_{cmax25} to χ ($V_{\text{cmax25}}:\chi$; $\mu\text{mol m}^{-2} \text{ s}^{-1}$). This approach is similar to tradeoff calculations in which nitrogen-water use tradeoffs are measured as the ratio of N_{area} or V_{cmax25} to g_{sw} (Paillassa et al. 2020; Bialic-Murphy et al. 2021). In this chapter, I quantify these relationships using χ in lieu of g_{sw} because g_{sw} rapidly changes with environmental conditions and therefore may have been altered by recent tree branch severance and/or placement in the cuvette.

3.2.6 *Soil nitrogen availability and pH*

To characterize soil nitrogen availability at the time of leaf gas exchange measurements, I used mixed bed resin bags to quantify mobile ammonium-N and nitrate-N concentrations in each plot. Lycra mesh bags were filled with 5 g of Dowex® Marathon MR-3 hydrogen and hydroxide form resin (MilliporeSigma, Burlington, MA USA) and sealed with a zip tie. Each bag was activated by soaking in 0.5 M HCl for 20 minutes, then in 2 M NaCl until pH of the saline solution stabilized, as described in Allison et al. (2008). Five resin bags were inserted about 10 cm below the soil surface at each plot on June 25, 2019: one near each

of the four plot corners and one near the plot center. All resin bags were collected 24 days later on July 19, 2019 and were frozen until extracted.

Prior to anion and cation extraction, each resin bag was rinsed with ultrapure water (MilliQ IQ 7000; Millipore Sigma, Burlington, MA) to remove any surface soil residues. Anions and cations were extracted from surface-cleaned resin bags by individually soaking and shaking each bag in 100 mL of a 0.1 M HCl/2.0 M NaCl matrix for one hour. Using a microplate reader (Biotek Synergy H1; Biotek Instruments, Winooski, VT USA), I quantified nitrate-N concentrations spectrophotometrically at 540 nm with the end product of a single reagent vanadium (III) chloride reaction (Doane and Horwáth 2003), and ammonium-N concentrations quantified at 650 nm with the end product of a modified phenol-hypochlorite reaction (Weatherburn 1967; Rhine et al. 1998). Both the single reagent vanadium (III) chloride and modified phenol-hypochlorite methodologies are well established for determining nitrate-N and ammonium-N concentrations in resin bag extracts (Arnone 1997; Allison et al. 2008). I used a series of negative and positive controls throughout each well plate to verify the accuracy and precision of measurements, assaying each resin bag extract and control in triplicate. Soil nitrogen availability was estimated as the sum of the nitrate-N and ammonium-N concentration in each resin bag, normalized per gram of resin and duration in the field ($\mu\text{g N g}^{-1} \text{ resin d}^{-1}$), then subsequently averaged across all resin bags in a plot for a plot-level mean.

Soil pH was measured on 0-10 cm mineral soil samples collected prior to fertilization in 2019. Near each of the four plot corners, three 5.5 cm diameter soil cores were collected after first removing the forest floor where present. Each set

of three cores was placed in a plastic bag, and later composited by hand mixing and sieved to 4 mm. Soil pH was determined for a 1:2 soil:water slurry (10 g field-moist soil to 20 mL DI water) of each sample using an Accumet AB15 pH meter with flushable junction probe (Fisher Scientific; Hampton, NH, USA), and was estimated at the plot level as the mean soil pH within each plot.

3.2.7 Statistical analyses

I built two separate series of linear mixed-effects models to explore effects of soil nitrogen availability, soil pH, species, and leaf nitrogen content on leaf physiological traits. In the first series of linear mixed-effects models, I explored the effect of soil nitrogen availability, soil pH, and species on leaf nitrogen content, leaf photosynthesis, stomatal conductance, and nitrogen-water use tradeoffs. Models included plot-level soil nitrogen availability and plot-level soil pH as continuous fixed effects, species as a categorical fixed effect, and site as a categorical random intercept term. Interaction terms between fixed effects were not included due to the small number of experimental plots. I built a series of separate models with this independent variable structure to quantify individual effects of soil nitrogen availability, soil pH, and species on N_{area} , M_{area} , N_{mass} , A_{net} , V_{cmax25} , J_{max25} , $J_{\text{max25}}:V_{\text{cmax25}}$, χ , PNUE, $N_{\text{area}}:\chi$, and $V_{\text{cmax25}}:\chi$.

A second series of linear mixed-effects models were built to investigate relationships between leaf nitrogen content and photosynthetic parameters. Statistical models included N_{area} as a single continuous fixed effect with species and site designated as individual random intercept terms. I used this independent variable structure to quantify individual effects of leaf nitrogen content on A_{net} ,

V_{cmax25} , J_{max25} , $J_{\text{max25}}:V_{\text{cmax25}}$, and χ .

For all linear mixed-effects models, I used Shapiro-Wilk tests of normality to determine whether linear mixed-effects models satisfied residual normality assumptions. If residual normality assumptions were not met, then models were fit using dependent variables that were natural log transformed. If residual normality assumptions were still not met (Shapiro-Wilk: $p < 0.05$), then models were fit using dependent variables that were square root transformed. All residual normality assumptions for both sets of models that did not originally satisfy residual normality assumptions were met with either a natural log or square root data transformation (Shapiro-Wilk: $p > 0.05$ in all cases).

In the first series of models, models for N_{area} , M_{area} , N_{mass} , V_{cmax25} , J_{max25} , χ , $N_{\text{area}}:\chi$, and $V_{\text{cmax25}}:\chi$ satisfied residual normality assumptions without data transformations (Shapiro-Wilk: $p > 0.05$ in all cases). The model for $J_{\text{max25}}:V_{\text{cmax25}}$ satisfied residual normality assumptions with a natural log data transformation, while models for A_{net} and PNUE each satisfied residual normality assumptions with square root data transformations. In the second series of models, models for V_{cmax25} , J_{max25} , χ , and $V_{\text{cmax25}}:\chi$ satisfied residual normality assumptions without data transformations (Shapiro-Wilk: $p > 0.05$ in all cases). The model for $J_{\text{max25}}:V_{\text{cmax25}}$ required a natural log data transformation and the model for A_{net} required a square root data transformation (Shapiro-Wilk: $p > 0.05$ in both cases).

In all models, I used the ‘lmer’ function in the ‘lme4’ R package (Bates et al. 2015) to fit each model and the ‘Anova’ function in the ‘car’ R package (Fox and Weisberg 2019) to calculate Type II Wald’s χ^2 and determine the significance level ($\alpha=0.05$) of each fixed effect coefficient. Finally, I used the ‘emmeans’ R

package (Lenth et al. 2019) to conduct post-hoc comparisons using Tukey's tests, where degrees of freedom were approximated using the Kenward-Roger approach (Kenward and Roger 1997). All analyses and plots were conducted in R version 4.1.1 (R Core Team 2021). All figure regression lines and associated 95% confidence interval error bars were plotted using predictions generated across the soil nitrogen availability gradient using the ‘emmeans’ R package (Lenth et al. 2019).

3.3 Results

3.3.1 Leaf nitrogen content

Increasing soil nitrogen availability generally increased N_{area} (Table 3.1; Fig. 3.1a). This pattern was driven by an increase in N_{mass} (Table 3.1; Fig. 3.1c) and a marginal increase in M_{area} (Table 3.1; Fig. 3.1e) with increasing soil nitrogen availability. There was no effect of soil pH on N_{area} , N_{mass} , or M_{area} (Table 3.1); however, I also observed strong differences in N_{area} (Fig. 3.1b), N_{mass} (Fig. 3.1d), and M_{area} (Fig. 3.1e) between species (Table 3.1).

Table 3.1. Effects of soil nitrogen availability, soil pH, and species on leaf nitrogen content per unit leaf area (N_{area} ; gN m⁻²), leaf nitrogen content per unit leaf mass (N_{mass} ; gN g⁻¹), and leaf mass per unit leaf area (M_{area} ; g m⁻²)*

	N_{area}			N_{mass}			M_{area}			
	df	Coefficient	χ^2	p	Coefficient	χ^2	p	Coefficient	χ^2	p
Intercept	-	$9.03 * 10^{-1}$	-	-	$1.68 * 10^{+0}$	-	-	$4.60 * 10^{+1}$	-	-
Soil N	1	$1.68 * 10^{-2}$	11.990	0.001	$1.25 * 10^{-2}$	6.902	0.009	$4.87 * 10^{-1}$	4.143	0.042
Soil pH	1	$9.28 * 10^{-2}$	0.836	0.361	$8.08 * 10^{-2}$	0.663	0.415	$4.05 * 10^{+0}$	0.653	0.419
Species	4	-	72.128	<0.001	-	35.074	<0.001	-	29.869	<0.001

*Significance determined using Type II Wald χ^2 tests ($\alpha=0.05$). P-values<0.05 are in bold.

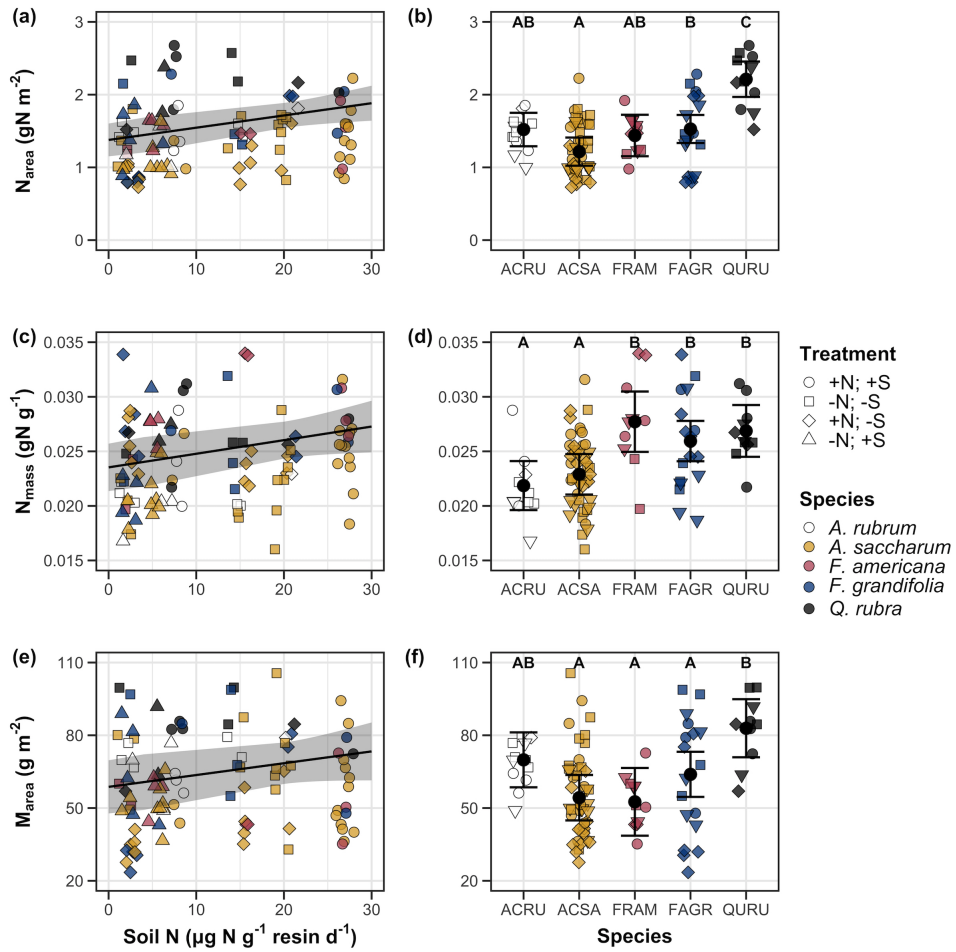


Figure 3.1. Effects of soil nitrogen availability and species on N_{area} (a-b), N_{mass} (c-d), and M_{area} (e-f). Soil nitrogen availability and species are represented on the x-axis of the leaf and right panel columns, respectively. Species are represented as colored points and treatment plots are represented as shaped points, jittered across the x-axis for visibility. In the right column, species are abbreviated through their NRCS PLANTS Database symbol (USDA NRCS 2022): ACRU represents *A. rubrum*, ASCA represents *A. saccharum*, FRAM represents *F. americana*, FAGR represents *F. grandifolia*, and QURU represents *Q. rubrum*. Trendlines indicate the regression line that describes the relationship between soil nitrogen availability and each response variable and are only included when the regression line slope is different from zero ($p < 0.05$). Solid black points in the right column represent marginal means for each species and error bars represent the upper and lower 95% confidence intervals predicted from each mixed-effect model. Compact lettering in the right column indicate Tukey post-hoc comparisons where $p < 0.05$.

3.3.2 Net photosynthesis and leaf biochemistry

Increasing soil nitrogen availability generally had no effect on A_{net} , V_{cmax25} , J_{max25} , or $J_{\text{max25}} \cdot V_{\text{cmax25}}$ (Table 3.2, Figs. 3.2a, 3.2d, 3.2g). I observed strong species effects on all measured leaf photosynthetic traits (Table 3.2; Figs. 3.2b, 3.2e, 3.2h). Increasing soil pH had a marginal negative effect on A_{net} , but had no effect on V_{cmax25} , J_{max25} , or $J_{\text{max25}} \cdot V_{\text{cmax25}}$ (Table 3.2). There was a weak positive effect of increasing N_{area} on A_{net} (Fig. 3.2c), but quite strong positive effects of increasing N_{area} on V_{cmax25} and J_{max25} (Table 3.2; Fig. 3.2f and 3.2i).

Table 3.2. Effects of soil nitrogen availability, soil pH, species, and N_{area} on net photosynthesis (A_{net} ; $\mu\text{mol m}^{-2} \text{s}^{-1}$), the maximum rate of Rubisco carboxylation (V_{cmax25} ; $\mu\text{mol m}^{-2} \text{s}^{-1}$), the maximum rate of RuBP regeneration (J_{max25} ; $\mu\text{mol m}^{-2} \text{s}^{-1}$), and the ratio of the maximum rate of RuBP regeneration to the maximum rate of Rubisco carboxylation ($J_{\text{max25}}:V_{\text{cmax25}}$; unitless)*

	A_{net}			V_{cmax25}			J_{max25}			
	df	Coefficient	χ^2	p	Coefficient	χ^2	p	Coefficient	χ^2	p
(Intercept)	-	$3.29 * 10^{+0\text{b}}$	-	-	$6.38 * 10^{+1}$	-	-	$1.12 * 10^{+2}$	-	-
Soil N	1	$-1.23 * 10^{-3\text{b}}$	1.798	0.180	$-3.84 * 10^{-1}$	1.745	0.187	$-6.70 * 10^{-1}$	2.172	0.141
Soil pH	1	$-3.09 * 10^{-1\text{b}}$	3.312	0.069	$-4.91 * 10^{+0}$	0.655	0.418	$-8.18 * 10^{+0}$	0.742	0.389
Species	4	-	11.838	0.019	-	31.748	<0.001	-	27.291	<0.001
(N_{area} int.)	-	$6.59 * 10^{-1\text{b}}$	-	-	$1.45 * 10^{-1}$	-	-	$2.86 * 10^{+1}$	-	-
N_{area}	4	$3.13 * 10^{-1\text{b}}$	4.790	0.029	$2.43 * 10^{+1}$	22.616	<0.001	$4.04 * 10^{+1}$	28.259	<0.001

	$J_{\text{max25}}:V_{\text{cmax25}}$			
	df	Coefficient	χ^2	p
(Intercept)	-	$6.59 * 10^{-1\text{a}}$	-	-
Soil N	1	$7.04 * 10^{-4\text{a}}$	0.088	0.767
Soil pH	1	$-7.84 * 10^{-3\text{a}}$	0.025	0.874
Species	4	-	12.745	0.013
(N_{area} int.)	-	$6.69 * 10^{-1\text{a}}$	-	-
N_{area}	4	$-4.69 * 10^{-2\text{a}}$	1.142	0.285

*Significance determined using Type II Wald χ^2 tests ($\alpha=0.05$). P-values less than 0.05 are in bold, while p-values between 0.05 and 0.1 are italicized. Superscript letters indicate model coefficients fit to natural-log ^(a) or square-root ^(b) transformed data. Relationships between N_{area} and each response variable were fit using the second series of bivariate mixed-effects models, so model coefficients and results are independent of model coefficients and results reported for relationships between soil nitrogen, soil pH, and species for each response variable.

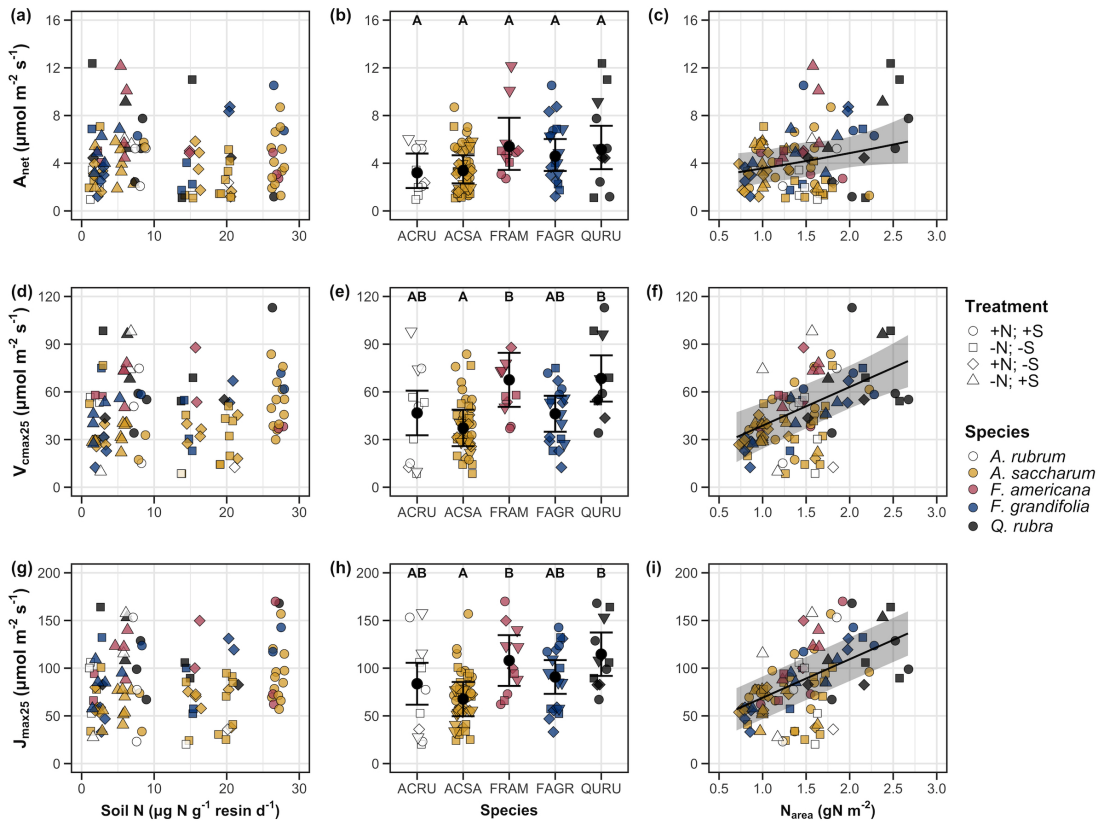


Figure 3.2. Effects of soil nitrogen availability (left column), species (middle column), and N_{area} (right column) on net photosynthesis (a-c), maximum RuBisco carboxylation rate (d-f), and maximum RuBP regeneration rate (g-i). Soil nitrogen availability, species, and N_{area} are respectively represented on the x-axis in the left, middle, and right columns. Species abbreviations and position along the x-axis in the middle column of panels, colored points, shapes, and trendlines are as explained in Figure 3.1.

3.3.3 *Tradeoffs between nitrogen and water use*

Although soil nitrogen availability did not affect χ (Table 3.3; Fig. 3.3a), increasing soil nitrogen availability decreased PNUE (Table 3.3; Fig. 3.3d) and increased the ratio of $N_{\text{area}}:\chi$ (Table 3.3; Fig. 3.3f). Specifically, this response yielded a 26% reduction in PNUE and 37% stimulation in $N_{\text{area}}:\chi$ across the soil nitrogen availability gradient. There was no apparent effect of soil nitrogen availability on $V_{\text{cmax25}}:\chi$ (Table 3.3; Fig. 3.3h). Increasing soil pH had a weak marginal negative effect on PNUE, but did not influence χ , $N_{\text{area}}:\chi$, or $V_{\text{cmax25}}:\chi$ (Table 3.3). I observed differences in χ (Fig. 3.3b), PNUE (Fig. 3.3e), $N_{\text{area}}:\chi$ (Fig. 3.3g), and $V_{\text{cmax25}}:\chi$ (Fig. 3.3i) between species (Table 3.3). Finally, increasing N_{area} had a strong negative effect on χ (Table 3.3; Fig. 3.3c) and a strong positive effect on $V_{\text{cmax25}}:\chi$ (Table 3.3; Fig. 3.3j).

Table 3.3. Effects of soil nitrogen availability, soil pH, species, and N_{area} on χ (unitless), photosynthetic nitrogen use efficiency (PNUE; $\mu\text{mol CO}_2 \text{ mol}^{-1} \text{ N s}^{-1}$), leaf nitrogen content per unit χ ($N_{\text{area}}:\chi$; gN m^{-2}), and maximum Rubisco carboxylation rate per unit χ ($V_{\text{cmax25}}:\chi$; $\mu\text{mol m}^{-2} \text{ s}^{-1}$)^{*}

	χ		PNUE				$N_{\text{area}}:\chi$			
	df	Coefficient	χ^2	p	Coefficient	χ^2	p	Coefficient	χ^2	p
(Intercept)	-	$8.12 * 10^{-1}$	-	-	$9.57 * 10^{+0}$ ^b	-	-	$9.19 * 10^{-1}$	-	-
Soil N	1	$-1.14 * 10^{-3}$	1.698	0.193	$-6.63 * 10^{-2}$ ^b	6.396	0.011	$2.60 * 10^{-2}$	9.533	0.002
Soil pH	1	$-1.91 * 10^{-2}$	1.087	0.297	$-9.25 * 10^{-1}$ ^b	2.843	<i>0.092</i>	$2.03 * 10^{-1}$	1.321	0.250
Species	4	-	18.843	0.001	-	13.454	0.009	-	52.983	<0.001
(N_{area} int.)	-	$8.93 * 10^{-1}$	-	-	-	-	-	-	-	-
N_{area}	1	$-1.11 * 10^{-1}$	80.606	<0.001	-	-	-	-	-	-

	$V_{\text{cmax25}}:\chi$			
	df	Coefficient	χ^2	p
(Intercept)	-	$7.20 * 10^{+1}$	-	-
Soil N	1	$3.99 * 10^{-1}$	0.963	0.326
Soil pH	1	$-3.12 * 10^{+0}$	0.138	0.711
Species	4	-	31.450	<0.001
(N_{area} int.)	-	$1.18 * 10^{+1}$	-	-
N_{area}	4	$3.87 * 10^{+1}$	32.797	<0.001

*Significance determined using Type II Wald χ^2 tests ($\alpha = 0.05$). P -values less than 0.05 are in bold, while p -values between 0.05 and 0.1 are italicized. Superscript letters indicate model coefficients fit to natural-log (^a) or square-root (^b) transformed data. Relationships between N_{area} and each response variable were fit using the second series of bivariate mixed-effects models, so model coefficients and results are independent of model coefficients and results reported for relationships between soil nitrogen, soil pH, and species for each response variable.

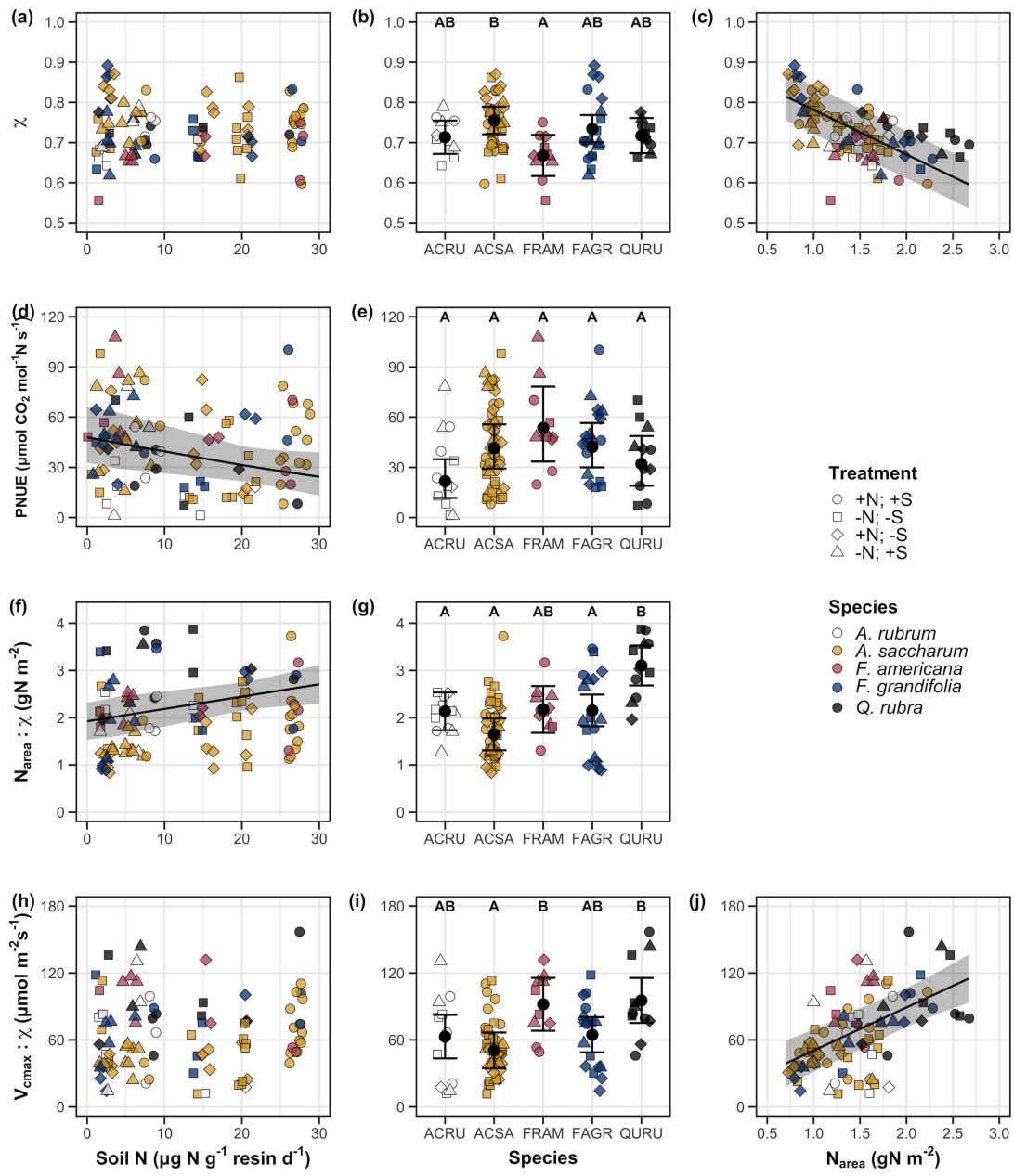


Figure 3.3. Effects of soil nitrogen availability (left column), species (middle column), and N_{area} (right column) on χ (a-c), photosynthetic nitrogen use efficiency (d-e), N_{area} per χ (f-g), and maximum Rubisco carboxylation rate per χ (h-j). Soil nitrogen availability, species, and N_{area} are represented on the x-axis in the left, middle, and right columns, respectively. Species abbreviations and position along the x-axis in the middle column, colored points, shapes, trendlines, error bars, and compact lettering are as explained in Figure 3.1.

3.4 Discussion

Photosynthetic least-cost theory provides an explanation for understanding relationships between soil nutrient availability, leaf nutrient allocation, and photosynthetic capacity. The theory suggests that plants acclimate to a given environment by optimizing leaf photosynthesis rates at the lowest summed cost of using nutrients and water (Prentice et al. 2014; Wang et al. 2017; Smith et al. 2019; Paillassa et al. 2020). The theory predicts that an increase in soil nutrient availability should allow similar photosynthesis rates to be achieved with increased leaf nutrient content and photosynthetic capacity (i.e., V_{cmax25} and J_{max25}) at reduced leaf $C_i:C_a$ (χ), resulting in an increase in water use efficiency, decrease in nutrient use efficiency, and increase in both leaf nutrient content and photosynthetic capacity per unit χ . The theory predicts similar leaf responses to increasing soil pH under acidic conditions due to reduced costs of acquiring nutrients with increasing soil pH (Wang et al. 2017; Paillassa et al. 2020; Dong et al. 2020).

Supporting the theory, increasing soil nitrogen availability was associated with increased leaf nitrogen content, a pattern that reduced photosynthetic nitrogen use efficiency and increased leaf nitrogen content per unit χ . Increasing soil nitrogen coincided with slight decreases in χ and increases in V_{cmax25} and J_{max25} ($p<0.2$, Table 3.2). The positive trend between soil nitrogen availability and photosynthetic capacity was supported by the concurrent strong increase in leaf nitrogen content with increasing soil nitrogen availability, which resulted in no change in the proportion of leaf nitrogen content allocated to photosynthesis across the soil nitrogen availability gradient. Additionally, leaf nitrogen content exhibited a strong negative correlation with χ indicative of nitrogen-water use

tradeoffs at the leaf level. Responses tended to vary more due to soil nitrogen availability than soil pH. Overall, these findings are consistent with the nutrient-water use tradeoffs predicted from theory.

Supporting expected least-cost outcomes and past environmental gradient studies (Dong et al. 2017; Paillassa et al. 2020), increasing soil nitrogen availability was associated with increased leaf nitrogen content. Soil nitrogen availability had smaller impacts on net photosynthesis and χ , reducing PNUE and increasing leaf nitrogen content per unit χ , as expected from theory. Photosynthetic least-cost theory suggests that reductions in PNUE should be driven by increased proportions of leaf nitrogen allocated to photosynthetic tissue, a pattern that should allow plants to achieve optimal photosynthetic rates with greater photosynthetic capacity to make more efficient use of available light. Contrasting theory predictions, I found no effect of soil nitrogen availability on photosynthetic capacity. However, photosynthetic capacity did tend to increase with increasing soil nitrogen availability ($p<0.20$; Table 3.2) resulting in no effect of soil nitrogen availability on the relative fraction of leaf nitrogen allocated to photosynthesis, Rubisco, or bioenergetics. These lines of evidence support the idea that trees use additional nitrogen to support increased leaf nitrogen allocation toward photosynthetic tissue and enhance photosynthetic capacity (Wright et al. 2003).

Soil nitrogen availability had a stronger effect on leaf nitrogen than photosynthetic capacity, suggesting that additional plant nitrogen uptake due to increased soil nitrogen availability was being used to support non-photosynthetic nitrogen pools, possibly structural tissue or stress-induced amino acid and polyamine synthesis (Minocha et al. 2000; Onoda et al. 2004; Bubier et al. 2011).

This pattern is supported by the weak positive effect of increasing soil nitrogen availability on leaf mass per unit leaf area, suggesting that increasing soil nitrogen availability allowed plants to increase nitrogen investment to leaf structural tissue, perhaps as a mechanism to increase leaf longevity in deciduous leaves with finite growing seasons (Wright et al. 2004; Reich 2014; Wang et al. 2023).

Opposing patterns expected from least-cost theory, increasing soil nitrogen availability had a null effect on χ . Despite this, I observed a strong negative effect of increasing N_{area} on χ , consistent with the nitrogen-water use tradeoffs expected from theory. The null response of χ to increasing soil nitrogen availability may have been due to a lack of water limitation in the system, given that the area received approximately 20% more precipitation (1167 mm) during the 12-month period leading up to our measurement period than normally expected (972 mm). However, droughts can and do occur in temperate forests of the northeastern United States (Sweet et al. 2017), so the observed increase in leaf nitrogen content with increasing soil nitrogen availability could be a strategy that allows trees to hedge bets against drier than normal growing seasons (Onoda et al. 2004; Onoda et al. 2017; Hallik et al. 2009). As suggested in Paillassa et al. (2020) and more recently by Querejeta et al. (2022), negative effects of soil nitrogen availability on χ may increase with increasing aridity. This strategy would be especially advantageous if it allows individuals growing in arid regions to maintain carbon assimilation rates with reduced water loss. Future work should attempt to quantify interactive roles of climate and soil nitrogen availability on nitrogen-water use tradeoffs, which could be done using coordinated and multifactor nutrient (Borer et al. 2014) and water (Knapp et al. 2017) manipulation experiments

across broad climatic gradients.

While the primary purpose of this study was to examine the role of soil nitrogen availability on nitrogen-water use tradeoffs, this experiment manipulated both soil nitrogen and pH, thus providing an opportunity to isolate these variables. Previous correlational studies along environmental gradients have identified soil pH as an important factor that can modify tradeoffs between nutrient and water use (Smith et al. 2019; Paillassa et al. 2020; Westerband et al. 2023) and the proportion of leaf nitrogen allocated to photosynthesis (Luo et al. 2021). Such studies implied that these patterns may be driven by reduced costs of acquiring nutrients with increasing pH, which may be exacerbated in acidic soils.

Consistent with theory (Wright et al. 2003; Prentice et al. 2014), results indicate that PNUE was negatively associated with increasing soil pH. However, there was no effect of soil pH on leaf nitrogen content, χ , or leaf nitrogen content per unit χ , most likely because the experimental nitrogen additions increased soil nitrogen supply while both increasing (sodium nitrate) and decreasing (ammonium sulfate) soil pH. These results suggest that soil pH did not play a major role in modifying expected photosynthetic least-cost theory patterns, contrasting findings from Paillassa et al. (2020) and other gradient studies that note positive effects of increasing soil pH on leaf nitrogen content, Rubisco carboxylation, and χ (Viet et al. 2013; Cornwell et al. 2018; Luo et al. 2021). Instead, null responses to soil pH show that leaf photosynthetic parameters depend more on soil nitrogen availability than pH per se, and that inferences from gradient studies might be confounding covariation between nitrogen availability and soil acidity.

Species identity generally explained a larger amount of variation in mea-

sured leaf traits than soil nitrogen availability or soil pH. Interspecific variation is an important factor to consider when deducing mechanisms that drive photosynthetic least-cost theory, particularly for species that form distinct mycorrhizal associations or have different photosynthetic pathways, growth forms, or leaf habit (Espelta et al. 2005; Adams et al. 2016; Bialic-Murphy et al. 2021; Scott and Smith 2022). The need to consider species may also be important when comparing nutrient-water use tradeoffs in early and late successional species, or in species with different resource economic strategies (Abrams and Mostoller 1995; Ellsworth and Reich 1996; Wright et al. 2004; Reich 2014; Onoda et al. 2017; Ziegler et al. 2020). The previous dissertation chapter notes species-specific carbon cost to acquire nitrogen responses to soil nitrogen availability, a pattern that was either driven by differences in the dominant mode of nitrogen acquisition or growth form and duration.

A strength of the study design and sampling effort is that it controls for many species differences that should modify nitrogen-water use tradeoffs expected from theory. All tree species measured in this study shared the leaf habit of deciduous broadleaves, were growing in forests of similar successional stage, but differed in mycorrhizal association and consequent resource economic strategies. As stands tended to be dominated by trees that associate with arbuscular mycorrhizae (*Fraxinus* and both *Acer* species made up roughly 70% of total above-ground biomass across stands), ecosystem biogeochemical cycle dynamics may be more closely aligned to the inorganic nutrient economy proposed in Phillips et al. (2013), which may promote stronger nitrogen-water use tradeoffs in tree species that associate with arbuscular mycorrhizae. This result was not observed here,

as photosynthetic properties varied as much within as across the two mycorrhizal associations represented.

In the field, soil nutrient availability is heterogeneous across time and space (Table B4). Unaccounted within-plot heterogeneity may have contributed to the low amount of variation explained by soil nitrogen availability in statistical models, as resin bags are a coarse surrogate for soil nitrogen availability. Despite this, I still observed evidence for nutrient-water use tradeoffs, suggesting that observed responses reported here may underestimate the net effect of soil nitrogen availability on such tradeoffs. While I urge caution in the interpretation of these results, they do provide a promising baseline for future studies investigating patterns expected from photosynthetic least-cost theory at finer spatiotemporal resolutions.

The general stronger relationship between leaf nitrogen content and photosynthetic parameters versus between leaf nitrogen content and soil nitrogen availability suggests that leaf nitrogen content is more directly tied to photosynthesis than soil nitrogen availability. While this could be due to the high spatiotemporal heterogeneity of soil nitrogen availability, principles from photosynthetic least-cost theory suggest that leaf nitrogen content is the downstream product of leaf nutrient demand to build and maintain photosynthetic machinery, which is set by aboveground environmental conditions such as light availability, CO₂, temperature, or vapor pressure deficit (Smith et al. 2019; Paillassa et al. 2020; Peng et al. 2021; Westerband et al. 2023). The stronger relationship between leaf nitrogen and photosynthetic parameters, paired with the strong negative relationship between leaf nitrogen and χ , could indicate a stronger effect of climate

on leaf nitrogen-photosynthesis relationships than soil resource availability. However, the short distance between plots and across sites limit my ability to test this hypothesis.

Variation in soil pH affected least cost responses less than variations in soil nitrogen availability, in part because experimental treatments directly increased soil nitrogen and affected soil pH in opposite directions. While soil pH has been shown to drive nitrogen-water tradeoffs in global gradient analyses (Viet et al. 2013; Paillassa et al. 2020), these responses may be due to covariations between soil pH and nutrient cycling rather than a role of pH per se. The direct manipulations of soil pH and soil nitrogen availability in this study partly disentangle these factors and show that variation in nitrogen availability matters more for least-cost tradeoffs than pH alone.

Increasing soil nitrogen availability generally increased leaf nitrogen content (both area- and mass-based) but did not significantly influence net photosynthesis or χ , leading to a reduction in PNUE and an increase in leaf nitrogen per unit χ with increasing soil nitrogen availability. Despite null effects of soil nitrogen availability on χ , I observed a strong negative relationship between leaf nitrogen content and χ . These results provide empirical support for nutrient-water use tradeoffs expected from photosynthetic least-cost theory, but suggest that all tenets of the theory may not hold in every environment. Findings reported here experimentally test previous work suggesting that leaf nitrogen-water economies vary across gradients of soil nutrient availability and pH, and show that variations in nutrient availability matter more for predicting leaf photosynthetic traits than soil pH.

Chapter 4

The relative cost of resource use for photosynthesis drives variance in leaf nitrogen content across a climate and soil resource availability gradient

4.1 Introduction

Terrestrial biosphere models, which comprise the land surface component of Earth system models, are sensitive to the formulation of photosynthetic processes (Knorr and Heimann 2001; Ziehn et al. 2011; Booth et al. 2012; Walker et al. 2021). This is because photosynthesis is the largest carbon flux between the atmosphere and terrestrial biosphere (IPCC 2021), and is constrained by ecosystem nutrient and water cycles (Hungate et al. 2003; LeBauer and Treseder 2008; Fay et al. 2015). Many terrestrial biosphere models parameterize photosynthetic capacity through plant functional group specific empirical linear relationships between area-based leaf nitrogen content (N_{area}) and the maximum carboxylation rate of Ribulose-1,5-bisphosphate carboxylase/oxygenase (V_{cmax}) (Kattge et al. 2009; Rogers 2014; Rogers et al. 2017). Models are beginning to include connected carbon-nitrogen cycles (Wieder et al. 2015; Shi et al. 2016; Davies-Barnard et al. 2020; Braghieri et al. 2022), which allows models to predict leaf photosynthesis directly through changes in N_{area} and indirectly through changes in soil nitrogen availability (e.g., LPJ-GUESS, CLM5.0) (Smith et al. 2014; Lawrence et al. 2019). Despite recent model developments, open questions remain regarding the generality of ecological relationships between soil nitrogen availability, leaf nitrogen content, and leaf photosynthesis across edaphic and climatic gradients.

Empirical support for positive relationships between soil nitrogen availabil-

ity and N_{area} is abundant (Firn et al. 2019; Liang et al. 2020), and is a result often attributed to the high nitrogen cost of building and maintaining Rubisco (Evans 1989; Evans and Seemann 1989; Onoda et al. 2004; Walker et al. 2014; Onoda et al. 2017; Dong et al. 2020). Such patterns imply that positive relationships between soil nitrogen availability and N_{area} should increase net photosynthesis by increasing nutrient allocation to photosynthetic enzyme construction and maintenance. This integrated N_{area} -photosynthesis response to soil nitrogen availability has been observed both in manipulative experiments and across environmental gradients (Field and Mooney 1986; Evans 1989; Walker et al. 2014; Li et al. 2020), and is thought to be driven by ecosystem nitrogen limitation, which limits primary productivity globally (LeBauer and Treseder 2008; Fay et al. 2015). However, recent studies note variable N_{area} -photosynthesis relationships across edaphic and climatic gradients (Liang et al. 2020; Luo et al. 2021) and that aboveground growing conditions (e.g., light availability, temperature, vapor pressure deficit) or species identity traits (e.g., photosynthetic pathway, dominant mode of nutrient acquisition) may be more important for explaining variance in N_{area} and photosynthetic capacity across environmental gradients (Adams et al. 2016; Dong et al. 2017; Smith et al. 2019; Dong et al. 2020; Peng et al. 2021; Dong et al. 2022; Westerband et al. 2023).

Photosynthetic least-cost theory provides a possible mechanism to explain variance in N_{area} across environmental gradients (Wright et al. 2003; Prentice et al. 2014; Paillassa et al. 2020; Harrison et al. 2021). The theory predicts that plants acclimate to environments by optimizing photosynthetic assimilation rates at the lowest summed cost of nitrogen and water use (Wright et al. 2003; Prentice

et al. 2014). In a given environment, nitrogen and water use can be substituted for each other to maintain the lowest summed cost of resource use, which alters the cost of acquiring and using nitrogen relative to water, a ratio herein referred to as β . All else equal, the theory predicts that increasing soil nitrogen availability should decrease β , resulting in optimal photosynthetic rates achieved with greater N_{area} at decreased stomatal conductance and reduced leaf $C_i:C_a$ (Wright et al. 2003; Prentice et al. 2014; Paillassa et al. 2020). Alternatively, increasing soil moisture should reduce costs of water acquisition and use, therefore increasing β (Lavergne et al. 2020), stomatal conductance, and leaf $C_i:C_a$, resulting in optimal photosynthetic rates achieved with decreased N_{area} . The theory also predicts nitrogen-water use tradeoffs in response to climatic factors, suggesting that the optimal response to increased vapor pressure deficit should be a reduction in stomatal conductance and leaf $C_i:C_a$ that is counterbalanced by an increase in N_{area} to support the greater photosynthetic capacity needed to maintain photosynthesis rates at decreased conductance (Grossiord et al. 2020; Dong et al. 2020; López et al. 2021; Westerband et al. 2023).

Leaf nitrogen allocation responses to changing climates or soil resource availability may depend on species' dominant mode of nutrient acquisition. For example, species that form associations with symbiotic nitrogen-fixing bacteria (referred as "N-fixing species" from this point forward) should, in theory, have access to less finite nitrogen supply than species not capable of forming such associations (referred as "non-fixing species" from this point forward), which may result in decreased β values in N-fixing species than non-fixing species. In support of this, a greenhouse experiment showed that N-fixing species had anecdotally

lower costs of nitrogen acquisition compared to a non-fixing species, though the study was limited to deduce the mechanism driving this response (Perkowski et al. 2021). Reduced β values could be an explanation for why N-fixing species commonly have greater leaf nitrogen content than non-fixing species (Adams et al. 2016; Dong et al. 2017).

Similarly, leaf nitrogen allocation patterns across environmental gradients may be dependent on photosynthetic pathway. Reduced leaf $C_l:C_a$ values in C₄ species suggests that C₄ species should have reduced β values compared to C₃ species (Scott and Smith 2022), a pattern that could be the result of increased costs associated with water acquisition and use or reduced costs of nitrogen acquisition and use relative to C₃ species. Theory predicts that this response in C₄ species will cause C₄ species to have higher leaf nitrogen content on average compared to C₃ species, though several studies document decreased leaf nitrogen content in C₄ species (Schmitt and Edwards 1981; Sage and Pearcy 1987; Ghannoum et al. 2011). No study to date has directly quantified β in C₄ species aside from the initial parameterization of β in an optimality model for C₄ species (Scott and Smith 2022) using a global dataset of leaf $\delta^{13}\text{C}$ values (Cornwell et al. 2018).

While photosynthetic least-cost theory provides a unified framework for understanding integrated effects of climate and soil resource availability on N_{area} , empirical tests of the theory are sparse. Previous work shows that increasing soil nitrogen availability decreases costs of acquiring nutrients (Bae et al. 2015; Perkowski et al. 2021; Lu et al. 2022), which can induce predictable nutrient-water use tradeoffs expected from the theory across broad environmental gradients (Paillassa et al. 2020; Querejeta et al. 2022; Westerband et al. 2023) and in

manipulation experiments (Bialic-Murphy et al. 2021). Additionally, increasing vapor pressure deficit has been shown to have a positive effect on N_{area} , which is commonly associated with reduced leaf $C_i:C_a$ (Dong et al. 2017; Dong et al. 2020; Firn et al. 2019; López et al. 2021).

Despite evidence for patterns expected from photosynthetic least-cost theory, studies have been restricted to exploring these patterns in C₃ species and, while variance in N_{area} across environmental gradients has been shown to be driven by strong negative relationships with leaf $C_i:C_a$ (Dong et al. 2017; Paillassa et al. 2020; Westerband et al. 2023), no study has explicitly investigated effects of soil resource availability or species identity on N_{area} using β as a direct predictor of leaf $C_i:C_a$. Furthermore, as N_{area} can be broken down into its component parts, leaf mass per area (M_{area} ; g m⁻²) and mass-based leaf nitrogen content (N_{mass} ; gN g⁻¹) components (Dong et al. 2017), no study has investigated which component of N_{area} drives the hypothesized response of N_{area} to leaf $C_i:C_a$. The lack of such studies limit our ability to assess whether changes in N_{area} across environmental gradients are driven by changes in leaf morphology (i.e. M_{area}), leaf stoichiometry (i.e. N_{mass}), or both.

In this study, I measured N_{area} , N_{mass} , M_{area} , leaf $\delta^{13}\text{C}$ -derived estimates of leaf $C_i:C_a$, and β in 504 individuals spanning 52 species scattered across 24 grassland sites in Texas, USA. The state of Texas contains a diverse climatic gradient, indicated by 2006-2020 mean annual precipitation totals ranging from 204 to 1803 mm and 2006-2020 mean annual temperature ranging from 11.8° to 24.6°C within state boundaries (Fig. 4.1). Variability in soil nitrogen availability and soil moisture was expected across sites, owing to differences in soil texture

and aboveground climate that would drive differential rates of water retention and nitrogen transformations to plant-available nitrogen substrate. I leveraged the expected climatic and soil resource variability across sites to test the following hypotheses:

1. Increasing soil nitrogen availability will decrease β through a reduction in costs of nitrogen acquisition and use, while increasing soil moisture will increase β through a reduction in costs of water acquisition and use. N-fixing species were expected to have lower β values than non-fixing species as a result of having reduced costs of nitrogen acquisition. C₄ species were also expected to have lower β values due to reduced stomatal conductance and greater water use efficiency than C₃ species.
2. Leaf $C_i:C_a$ will be positively related to β , a pattern that will result in a negative indirect effect of increasing soil nitrogen availability on leaf $C_i:C_a$, a positive indirect effect of increasing soil moisture on leaf $C_i:C_a$, and reduced leaf $C_i:C_a$ in both N-fixing species and C₄ species. I expected that leaf $C_i:C_a$ would be negatively related to vapor pressure deficit due to stomatal closure.
3. N_{area} will be negatively related to leaf $C_i:C_a$, resulting in an indirect positive and negative effect of increasing soil nitrogen availability and soil moisture, respectively, on N_{area} , and larger N_{area} values in N-fixing species. While theory predicts that reduced β values in C₄ species should yield larger N_{area} in C₄ species, I expected that C₄ species would have decreased N_{area} than C₃ species due to greater nitrogen use efficiency in C₄ species. Finally, I expected that reductions in leaf $C_i:C_a$ with increasing vapor pressure deficit would increase N_{area} .

4.2 Methods

4.2.1 *Site descriptions and sampling methodology*

Leaf and soil samples were collected from 24 open canopy grassland sites scattered across central and eastern Texas in summer 2020 and summer 2021 (Fig. 4.1). Twelve sites were visited between June and July 2020 and 14 sites (11 unique from 2020) were visited between May and June 2021 (Table 4.1). Sites were chosen to maximize precipitation and edaphic variability across sites (Table 4.1). No site with personally communicated or anecdotal evidence of grazing or disturbance (e.g., mowing, feral hog activity, etc.) was used. Leaf material was collected from three individuals each of the five most abundant species at random locations at each site, only selecting species that were broadly classified as graminoid or forb/herb growth habits per the USDA PLANTS database (USDA NRCS 2022). All collected leaves were fully expanded with no visible herbivory or other external damage and also free from shading by nearby shrubs or trees. Five soil samples were collected from 0-15 cm below the soil surface at each site near the leaf collection sample locations. Soil samples were mixed together to create one composite soil sample per site.

4.2.2 *Site climate data*

I used the Parameter elevation Regressions on Independent Slopes Model (PRISM) (Daly et al. 2008) climate product to access gridded daily temperature and precipitation data for the coterminous United States at a 4-km grid resolution between January 1, 2006 and July 31, 2021 (PRISM Climate Group, Oregon State University, <https://prism.oregonstate.edu>, data created 4 Feb 2014, accessed 24 Mar

2022). Mean daily air temperature, mean daily vapor pressure deficit, and total daily precipitation data were extracted from the grid cell that contained the latitude and longitude of each property using the ‘extract’ function in the ‘terra’ R package (Hijmans et al. 2022). PRISM data were used in lieu of local weather station data because several rural sites did not have a local weather station present within a 20-km radius of the site. Daily site climate data were used to estimate mean annual precipitation and mean annual temperature for each site between 2006 and 2020 (Table 4.1). I calculated total precipitation and mean daily vapor pressure deficit for the prior 1, 2, 3, 4, 5, 6, 7, 8, 9, 10, 15, 20, 25, 30, 60, and 90 days leading up to each site visit. Temperature was not included in any analysis due to the close range in mean annual temperature between sites (mean \pm SD: $19.8\pm0.9^{\circ}\text{C}$; Table 4.1).

4.2.3 *Site edaphic characteristics*

Composted soil samples were sent to the Texas A&M Soil, Water and Forage Laboratory to quantify soil nitrate concentration ($\text{NO}_3\text{-N}$; ppm). Soil $\text{NO}_3\text{-N}$ was determined by extracting composite soil samples in 1 M KCl, measuring absorbance values of extracts at 520 nm using the end product of a $\text{NO}_3\text{-N}$ to $\text{NO}_2\text{-N}$ cadmium reduction reaction (Kachurina et al. 2000; Keeney and Nelson 1983). Soil texture data from 0-15 cm below the soil surface were accessed using the SoilGrids2.0 data product (Poggio et al. 2021) through the ‘fetchSoilGrids’ function in the ‘soilDB’ R package (Beaudette et al. 2022). I used SoilGrids2.0 to access soil texture data in lieu of analyses using the composite soil sample due to a lack of soil material from some sites after sending samples for soil $\text{NO}_3\text{-N}$.

Soil moisture was estimated using the ‘Simple Process-Led Algorithms for Simulating Habitats’ model (SPLASH) (Davis et al. 2017). This model, derived from the STASH model (Cramer and Prentice 1988), initiates a bucket model using Priestley-Taylor equations (Priestley and Taylor 1972) to calculate daily soil moisture (W_n ; mm) as a function of the previous day’s soil moisture (W_{n-1} ; mm), daily precipitation (P_n ; mm), condensation (C_n ; mm), actual evapotranspiration (E_n^a ; mm), and runoff (RO; mm):

$$W_n = W_{n-1} + P_n + C_n - E_n^a - RO \quad (4.1)$$

Models were initiated by equilibrating the previous day’s soil moisture using successive model iterations with daily mean air temperature, daily precipitation total, the number of daily sunlight hours, and latitude as model inputs (Davis et al. 2017). Daily sunlight hours were estimated for each day at each site using the ‘getSunlightTimes’ function in the ‘suncalc’ R package, which estimated sunrise and sunset times of each property using date and site coordinates (Thieurmel and Elmarhraoui 2019). Water holding capacity (mm), or bucket size, was estimated as a function of soil texture using pedotransfer equations explained in Saxton and Rawls (2006), as done in Stocker et al. (2020) and Bloomfield et al. (2023). A summary of these equations is included in Appendix C.1.

Daily soil moisture outputs from the SPLASH model for each site were used to calculate mean daily soil moisture for the prior 1, 2, 3, 4, 5, 6, 7, 8, 9, 10, 15, 20, 25, 30, 60, and 90 days leading up to each site visit. Mean daily soil moisture values were then expressed as a fraction of water holding capacity to normalize across sites with different bucket depths, as done in Stocker et al.

(2018). Site water holding capacity values are referenced in Table 4.1.

4.2.4 Leaf trait measurements

Images of each leaf were taken immediately following each site visit using a flatbed scanner. Fresh leaf area was determined from each image using the ‘LeafArea’ R package (Katabuchi 2015), which automates leaf area calculations using ImageJ software (Schneider et al. 2012). Each leaf was dried at 65°C for at least 48 hours to a constant mass, weighed, and manually ground in a mortar and pestle until homogenized. Leaf mass per area (M_{area} ; g m⁻²) was calculated as the ratio of dry leaf biomass to fresh leaf area. Subsamples of dried and homogenized leaf tissue were used to measure leaf nitrogen content (N_{mass} ; gN g⁻¹) through elemental combustion analysis (Costech-4010, Costech Instruments, Valencia, CA). Leaf nitrogen content per unit leaf area (N_{area} ; gN m⁻²) was calculated as the product of N_{mass} and M_{area} .

Subsamples of dried and homogenized leaf tissue were sent to the University of California-Davis Stable Isotope Facility to determine leaf $\delta^{13}\text{C}$. Leaf $\delta^{13}\text{C}$ values were determined using an elemental analyzer (PDZ Europa ANCA-GSL; Sercon Ltd., Chestshire, UK) interfaced to an isotope ratio mass spectrometer (PDZ Europa 20-20 Isotope Ratio Mass Spectrometer, Sercon Ltd., Chestshire, UK). I used leaf $\delta^{13}\text{C}$ values (‰; relative to Vienna Pee Dee Belemnite international reference standard) to estimate the ratio of intercellular (C_i) to extracellular (C_a) CO₂ ratio (leaf $C_i:C_a$; unitless) following the approach of Farquhar et al. (1989)

described in Cernusak et al. (2013). Specifically, I derived leaf $C_i:C_a$ as:

$$C_i : C_a = \frac{\Delta^{13}C - a}{b - a} \quad (4.2)$$

where $\Delta^{13}C$ represents the relative difference between leaf $\delta^{13}\text{C}$ (\textperthousand) and air $\delta^{13}\text{C}$ (\textperthousand), calculated as:

$$\Delta^{13}C = \frac{\delta^{13}C_{air} - \delta^{13}C_{leaf}}{1 + \delta^{13}C_{leaf}} \quad (4.3)$$

$\delta^{13}C_{air}$ was assumed to be $-8\text{\textperthousand}$ (Keeling et al. 1979; Farquhar et al. 1989). The parameter a represents the fractionation between ^{12}C and ^{13}C due to diffusion in air, assumed to be $4.4\text{\textperthousand}$, while b represents the fractionation caused by Rubisco carboxylation, assumed to be $27\text{\textperthousand}$ (Farquhar et al. 1989). For C₄ species, b in Eqn. 4.2 was set to $6.3\text{\textperthousand}$, and was derived from:

$$b = c + (d \cdot \phi) \quad (4.4)$$

Where c was set to $-5.7\text{\textperthousand}$ and d was set to $30\text{\textperthousand}$ (Farquhar et al. 1989). ϕ , which is the bundle sheath leakiness term, was set to 0.4. All leaf $C_i:C_a$ values less than 0.1 and greater than 0.95 were assumed to be incorrect and removed from the analysis.

I derived the unit cost of resource use (β) using leaf $C_i:C_a$ and site climate data using equations first described in Prentice et al. (2014) and simplified in Lavergne et al. (2020):

$$\beta = 1.6\eta^*VPD \frac{\chi - (\frac{\Gamma^*}{C_a})^2}{(1 - \chi)^2(K_m + \Gamma^*)} \quad (4.5)$$

where η^* is the viscosity of water relative to 25°C, calculated using elevation and mean air temperature of the seven days leading up to each site visit following equations in Huber et al. (2009). VPD (Pa) was set to the mean vapor pressure deficit of the seven days leading up to each site visit, C_a represents atmospheric CO₂ concentration, arbitrarily set to 420 $\mu\text{mol mol}^{-1}$ CO₂. C_a was converted to partial pressure (Pa) and corrected by site elevation. K_m (Pa) is the Michaelis-Menten coefficient for Rubisco affinity to CO₂ and O₂, calculated as:

$$K_m = K_c \cdot \left(1 + \frac{O_i}{K_o}\right) \quad (4.6)$$

where K_c (Pa) and K_o (Pa) are the Michaelis-Menten coefficients for Rubisco affinity to CO₂ and O₂, respectively, and O_i is the intercellular O₂ concentration. Γ^* (Pa) is the CO₂ compensation point in the absence of dark respiration. K_c , K_o , and Γ^* were determined using equations described in Medlyn et al. (2002) and derived in Bernacchi et al. (2001), invoking an elevation correction for atmospheric pressure as explained in Stocker et al. (2020).

Table 4.1. Site locality information, sampling year, 2006-2020 mean annual precipitation (MAP; mm), mean annual temperature (MAT; °C), and water holding capacity (WHC; mm)*

Site	Latitude	Longitude	Sampling year	MAP	MAT	WHC
Edwards_2019_17	29.95	-100.36	2020	563.5	19.0	224.7
Uvalde_2020_02	29.59	-100.09	2020, 2021	648.5	19.5	224.7
Menard_2020_01	30.91	-99.59	2020	641.9	18.3	220.2
Kerr_2020_03	30.06	-99.34	2021	672.4	18.3	237.5
Bandera_2020_03	29.85	-99.30	2021	789.4	18.8	235.1
Sansaba_2020_01	31.29	-98.62	2020	733.0	18.8	234.3
Comal_2020_21	29.79	-98.43	2020	878.5	19.9	220.7
Blanco_2019_16	29.99	-98.43	2020	833.0	19.2	222.2
Bexar_2019_13	29.24	-98.43	2020	759.3	21.5	206.0
Burnet_2020_14	30.84	-98.34	2021	763.3	19.5	217.8
Comal_2020_19	30.01	-98.32	2021	845.0	19.3	220.4
Hays_2020_54	29.96	-98.17	2021	861.3	20.0	225.6
Burnet_2020_12	30.82	-98.06	2021	815.1	19.4	245.3
Williamson_2019_09	30.71	-97.86	2020	867.7	19.7	270.2
Williamson_2019_10	30.54	-97.77	2020	819.5	19.9	239.8
Bell_2021_08	31.06	-97.55	2021	937.3	19.6	232.3
Fayette_2021_12	29.86	-97.21	2021	985.7	20.4	165.6
Fayette_2019_04	30.09	-96.78	2020	1017.4	20.6	226.9
Fayette_2020_09	29.86	-96.71	2021	1002.7	20.8	187.6
Washington_2020_08	30.28	-96.41	2021	1077.4	20.4	203.9
Austin_2020_03	29.78	-96.24	2021	1108.7	20.6	253.0
Brazos_2020_16	30.93	-96.23	2021	1078.0	20.1	202.2
Brazos_2020_18	30.52	-96.21	2020, 2021	1099.4	20.4	233.5
Harris_2020_03	29.88	-95.31	2020, 2021	1492.0	21.6	265.6

* Rows are arranged by longitude to visualize precipitation variability across sites

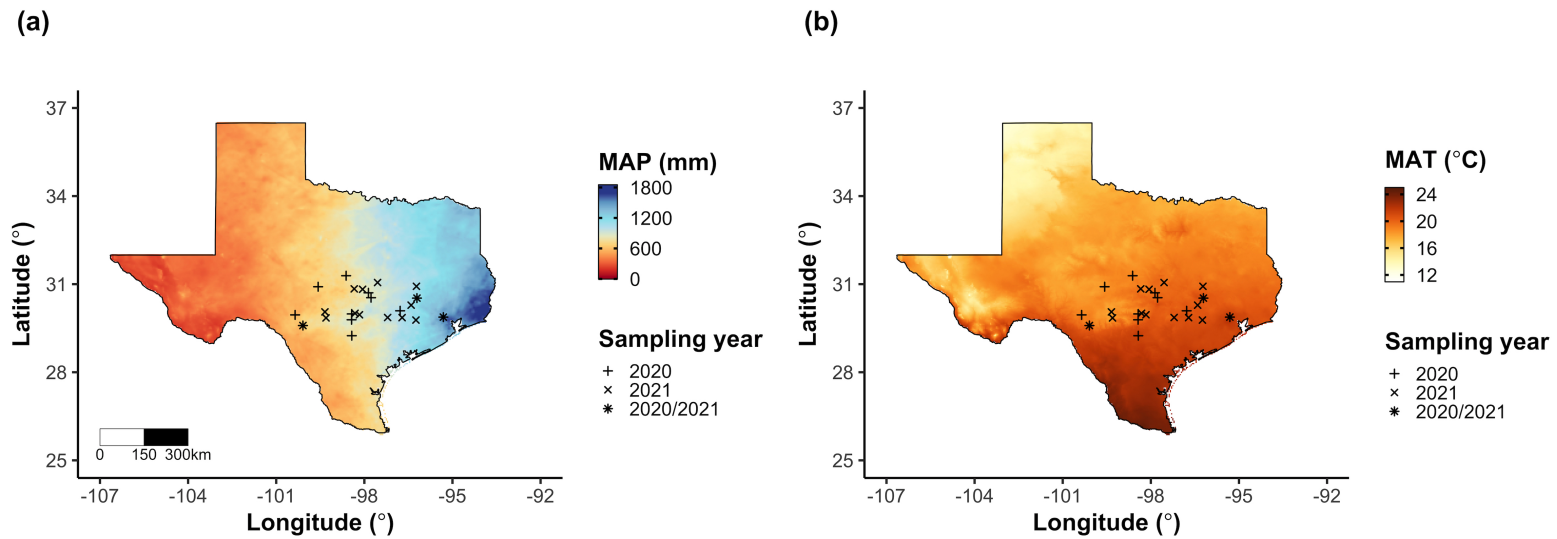


Figure 4.1. Site locations along 2006-2020 mean annual precipitation (a) and mean annual temperature (b) gradients in Texas, USA. Precipitation and temperature data were plotted using PRISM data at a 4-km grid resolution and are masked to include only grid cells that occur within the Texas state boundary of the United States. In both panels, addition signs refer to sites visited in 2020, multiplication signs to sites visited in 2021, and asterisks to sites visited in 2020 and 2021. The scale bar in (a) also applies to (b).

4.2.5 Plant functional group assignments

Plant functional groups were assigned to each species and used as the primary descriptor of species identity. Specifically, plant functional groups were assigned based on photosynthetic pathway (C_3 , C_4) and ability to form associations with symbiotic nitrogen-fixing bacteria (N-fixer, non-fixer). The ability to form associations with symbiotic nitrogen-fixing bacteria was assigned based on whether species were in the *Fabaceae* family, and photosynthetic pathway of each species was determined from past literature and confirmed through leaf $\delta^{13}\text{C}$ values. I chose these plant functional groups based on *a priori* hypotheses regarding the functional role of nitrogen fixation and photosynthetic pathway on the sensitivity of plant nitrogen uptake and leaf nitrogen allocation to soil nitrogen availability and aboveground growing conditions. These plant functional group classifications resulted in three distinct plant functional groups within the dataset: C_3 N-fixers ($n=53$), C_3 non-fixers ($n=334$), and C_4 non-fixers ($n=117$).

4.2.6 Data analysis

All analyses and plotting were conducted in R version 4.1.1 (R Core Team 2021). I constructed a series of separate linear mixed-effects models to investigate environmental drivers of β , leaf $C_i:C_a$, N_{area} , N_{mass} , and M_{area} , followed by a path analysis using a piecewise structural equation model to investigate direct and indirect effects of climate and soil resource availability on N_{area} .

To explore environmental drivers of β , I built a linear mixed-effects model that included soil moisture, soil nitrogen availability, and plant functional group as fixed effect coefficients. Species were designated as a random intercept term.

Interaction coefficients between all possible combinations of the three fixed effect coefficients were also included. β was natural log transformed to linearize data. I used an information-theoretic model selection approach to determine whether 90-, 60-, 30-, 20-, 15-, 10-, 9-, 8-, 7-, 6-, 5-, 4-, 3-, 2-, or 1-day mean daily soil moisture conferred the best model fit for β . To do this, I constructed 16 separate linear mixed-effects models where log-transformed β was included as the response variable and each soil moisture time step was separately included as a single continuous fixed effect. Species were included as a random intercept term for all models. I used corrected Akaike Information Criterion (AICc) to select the soil moisture timescale that conferred the best model fit, indicated by the model with the lowest AICc score (Table C2; Fig. C1).

To explore environmental drivers of leaf $C_i:C_a$, I constructed a second linear mixed effects model that included vapor pressure deficit, soil moisture, soil nitrogen availability, and plant functional group as fixed effect coefficients. Two-way interactions between plant functional group and vapor pressure deficit, soil nitrogen availability, or soil moisture were included as additional fixed effect coefficients, in addition to a three-way interaction between soil moisture, soil nitrogen availability, and plant functional group. Species were included as a random intercept term. I used an information-theoretic model selection approach to determine whether 90-, 60-, 30-, 20-, 15-, 10-, 9-, 8-, 7-, 6-, 5-, 4-, 3-, 2-, or 1-day mean daily vapor pressure deficit conferred the best model fit for leaf $C_i:C_a$ using the same approach explained above for the soil moisture effect on β . The soil moisture timescale was set to the same timescale that conferred the best fit for β .

To explore environmental drivers of N_{area} , N_{mass} , and M_{area} , I constructed

a linear mixed effects model for each trait, including leaf $C_i:C_a$, soil nitrogen availability, soil moisture, and plant functional group as fixed effect coefficients for each model. Two-way interactions between plant functional group and β , leaf $C_i:C_a$, soil nitrogen availability, or soil moisture were included as additional fixed effect coefficients, in addition to a three-way interaction between soil nitrogen availability, soil moisture, and plant functional group. Species were included as a random intercept term, with the soil moisture timescale set to the same timescale that conferred the best fit for β .

In all linear mixed-effects models explained above, including those to select relevant timescales, I used the ‘lmer’ function in the ‘lme4’ R package (Bates et al. 2015) to fit each model and the ‘Anova’ function in the ‘car’ R package (Fox and Weisberg 2019) to calculate Type II Wald’s χ^2 and determine the significance level ($\alpha=0.05$) of each fixed effect coefficient. I used the ‘emmeans’ R package (Lenth et al. 2019) to conduct post-hoc comparisons using Tukey’s tests, where degrees of freedom were approximated using the Kenward-Roger approach (Kenward and Roger 1997). Trendlines and error ribbons for all plots were drawn using a series of ‘emmeans’ outputs across the range in plotted x-axis values.

Finally, I conducted a path analysis using a piecewise structural equation model to examine direct and indirect pathways that determined variance in N_{area} . Seven separate linear mixed effects models were loaded into the piecewise structural equation model. Models were constructed per *a priori* hypotheses following patterns expected from photosynthetic least-cost theory. The first model regressed N_{area} against N_{mass} and M_{area} . The second model regressed M_{area} against leaf $C_i:C_a$ and soil nitrogen availability. The third model regressed N_{mass} against

leaf $C_i:C_a$ and M_{area} (Dong et al. 2017; Dong et al. 2020). The fourth model regressed leaf $C_i:C_a$ against β and vapor pressure deficit. The fifth model regressed β against soil nitrogen availability, soil moisture, ability to associate with symbiotic nitrogen-fixing bacteria, and photosynthetic pathway. The sixth model regressed soil nitrogen availability against soil moisture, while a seventh model regressed soil moisture against percent clay. All models included the relevant timescale selected in the individual linear mixed effect models explained above. Models included species as a random intercept term, were built using the ‘lme’ function in the ‘nlme’ R package (Pinheiro et al. 2022), and subsequently loaded into the piecewise structural equation model using the ‘psem’ function in the ‘piecewiseSEM’ R package (Lefcheck 2016).

4.3 Results

4.3.1 *Cost to acquire nitrogen relative to water*

Model selection indicated that 3-day mean soil moisture conferred the best model fit for β (AICc=1870.10, RMSE=1.4135; Table C2; Fig. C1). An interaction between soil nitrogen availability and plant functional group ($p=0.005$; Table 4.2) indicated that a negative effect of increasing soil nitrogen availability on β was driven by a negative effect of increasing soil nitrogen on β in C₄ non-fixers (Tukey: $p<0.001$) and marginal negative effect in C₃ non-fixers (Tukey: $p=0.100$), with no effect of soil nitrogen availability on β in C₃ N-fixers (Tukey: $p=0.147$; Table 4.2; Fig. 4.2a). A second interaction between soil moisture and plant functional group ($p<0.001$; Table 4.2) indicated that a negative effect of increasing soil moisture on β ($p=0.002$) was driven by C₄ non-fixers and null effects of soil moisture on β in C₃ non-fixers (Tukey: $p=0.852$) or C₃ N-fixers (Tukey: $p=0.650$; Table 4.2; Fig. 4.2b). A functional group effect ($p<0.001$; Table 4.2) indicated that C₄ non-fixers had lower β than both C₃ N-fixers and C₃ non-fixers (Tukey: $p<0.001$ in both cases), while β in C₃ N-fixers did not differ from C₃ non-fixers (Tukey: $p=0.628$).

Table 4.2. Effects of soil moisture, soil nitrogen availability, and plant functional group on β (unitless)*

	df	Coefficient	χ^2	p
Intercept	-	$3.37 * 10^{+0}$	-	-
Soil moisture (SM_3)	1	$2.07 * 10^{-1}$	9.254	0.002
Soil N (N)	1	$-1.67 * 10^{-2}$	14.547	<0.001
PFT	2	-	408.426	<0.001
SM_3*N	1	$-4.03 * 10^{-3}$	0.134	0.714
SM_3*PFT	2	-	36.746	<0.001
$N*PFT$	2	-	10.485	0.005
$SM_3*N*PFT$	2	-	1.324	0.516

*Significance determined using Type II Wald χ^2 tests ($\alpha=0.05$). P-values<0.05 are in bold. Model coefficients are expressed on the natural-log scale and are only included for continuous fixed effects. Key: df=degrees of freedom; χ^2 =Wald Type II chi-square test statistic

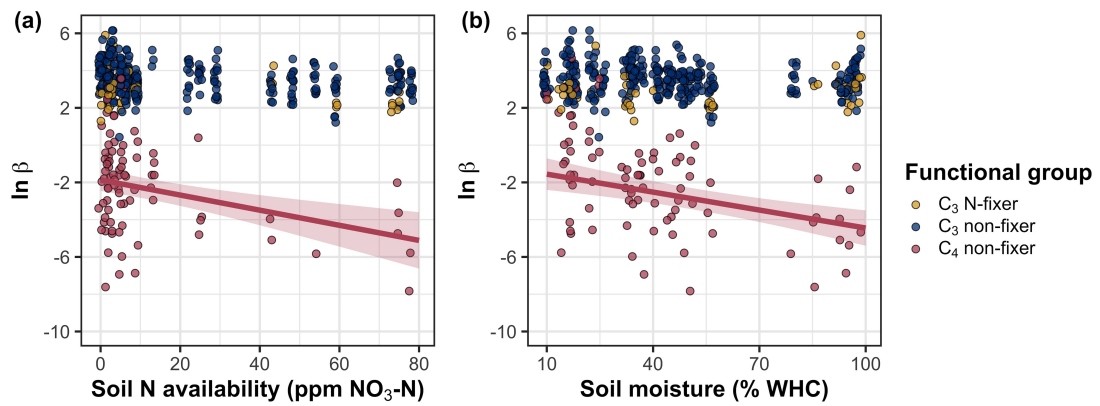


Figure 4.2. Effects of soil nitrogen availability (a) and soil moisture (b) on the cost of acquiring and using nitrogen relative to water (β ; unitless). Soil nitrogen availability is represented on the x-axis in (a), soil moisture is represented on the x-axis in (b) as a percent of site water holding capacity, and natural-log transformed β is represented on the y-axis for both panels. Yellow points represent C₃ N-fixers, blue points represent C₃ non-fixers, and red points represent C₄ non-fixers. Points are jittered along the x-axis for visibility. Colored trendlines note bivariate relationships within plant functional groups and are only included when the regression line slope is different from zero ($p<0.05$). Error ribbons represent the upper and lower 95% confidence interval range.

4.3.2 Leaf $C_i:C_a$

Model selection indicated that 4-day mean vapor pressure deficit conferred the best model fit for leaf $C_i:C_a$ (AICc=-867.19; RMSE=0.0725; Table C2; Fig. C1). An interaction between vapor pressure deficit and plant functional group ($p=0.034$; Table 4.3) revealed that the negative effect of increasing vapor pressure deficit on leaf $C_i:C_a$ ($p<0.001$; Table 4.3) was driven by C_3 non-fixers (Tukey: $p<0.001$) and C_3 N-fixers (Tukey: $p=0.040$; Table 4.3; Fig. 4.3a). An additional interaction between soil nitrogen availability and plant functional group ($p=0.005$; Table 4.3) indicated a negative effect of increasing soil nitrogen availability on leaf $C_i:C_a$ in C_4 non-fixers (Tukey: $p=0.007$), with no effect in C_3 non-fixers (Tukey: $p=0.660$) or C_3 N-fixers (Tukey: $p=0.231$; Fig. 4.3c). There was no effect of soil moisture on leaf $C_i:C_a$ (Table 4.3; Fig. 4.3b). A plant functional group effect ($p<0.001$; Table 4.3) indicated that C_4 non-fixers had lower leaf $C_i:C_a$ than C_3 N-fixers and C_3 non-fixers (Tukey: $p<0.001$ in both cases), with no difference between C_3 N-fixers and C_3 non-fixers (Tukey: $p=0.866$).

Table 4.3. Effects of soil moisture, soil nitrogen availability, and plant functional group on leaf $C_i:C_a$ (unitless)*

	df	Coefficient	χ^2	<i>p</i>
Intercept	-	$1.08 * 10^{+0}$	-	-
Vapor pressure deficit (VPD_4)	1	$-2.59 * 10^{-1}$	14.042	<0.001
Soil moisture (SM_3)	1	$-3.26 * 10^{-3}$	1.398	0.237
Soil N (N)	1	$-1.40 * 10^{-3}$	0.708	0.400
PFT	2	-	451.106	<0.001
SM_3*N	1	$1.47 * 10^{-3}$	0.318	0.573
VPD_4*N	2	-	6.737	0.034
SM_3*N	2	-	3.890	0.143
$N*N$	2	-	10.622	0.005
$SM_{90}*N*N$	2	-	0.409	0.815

*Significance determined using Type II Wald χ^2 tests ($\alpha=0.05$). *P*-values less than 0.05 are in bold and *p*-values where $0.05 < p < 0.1$ are italicized. Leaf $C_i:C_a$ was not transformed prior to model fitting, so model coefficients are reported on the response scale. Model coefficients are only included for continuous fixed effects. Key: df=degrees of freedom; χ^2 =Wald Type II chi-square test statistic

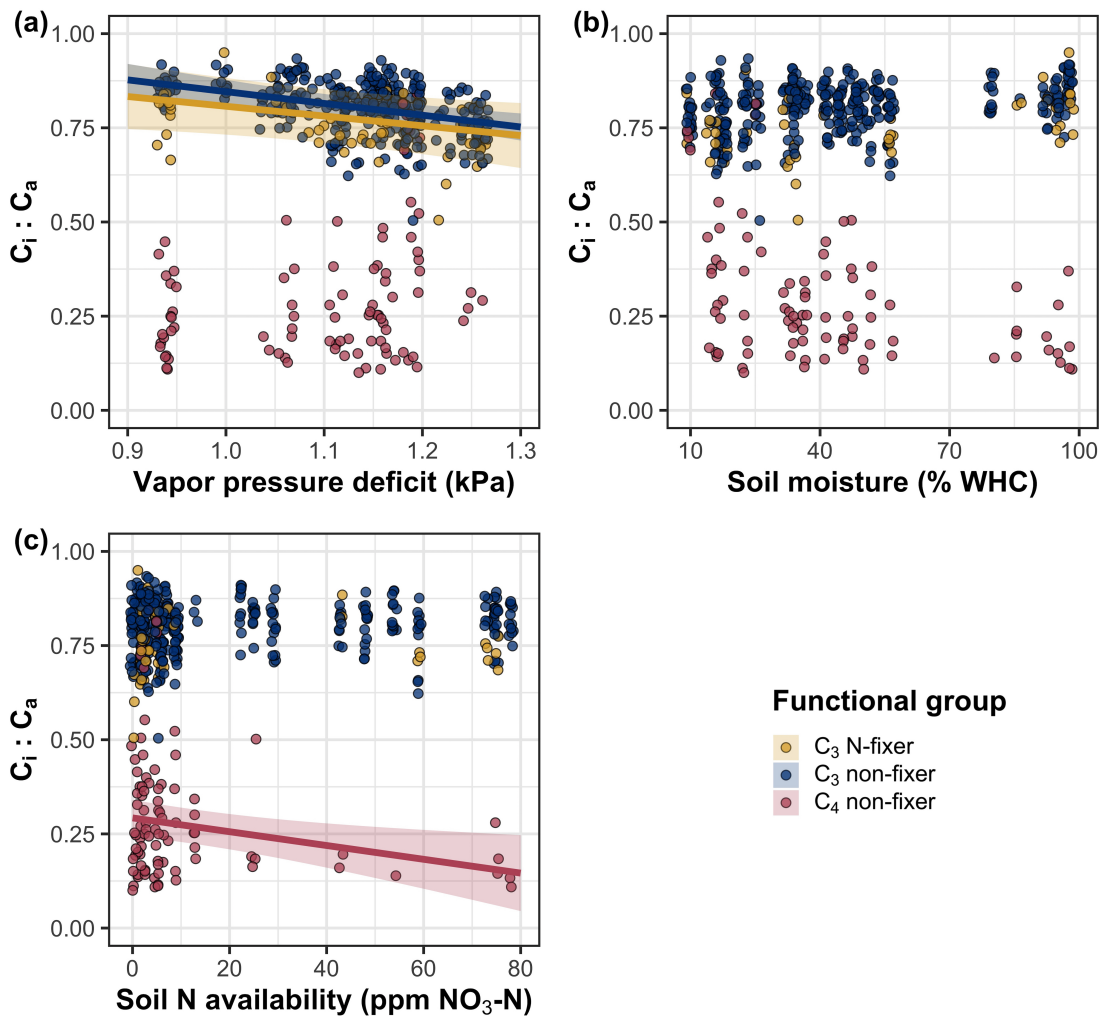


Figure 4.3. Effects of 4-day mean vapor pressure deficit (a), 3-day soil moisture (per water holding capacity; b), and soil nitrogen availability (c) on leaf $C_i:C_a$. Shading and trendlines are as explained in Figure 4.2. Points are jittered for visibility. Variably colored trendlines are only included if there is an interaction between the x-axis and plant functional group, where solid trendlines indicate slopes that are different from zero ($p < 0.05$). Error ribbons represent the upper and lower 95% confidence intervals of each fitted trendline.

4.3.3 Leaf nitrogen content

An interaction between leaf $C_i:C_a$ and plant functional group ($p<0.001$; Table 4.4) revealed that the negative effect of increasing leaf $C_i:C_a$ on N_{area} ($p=0.003$; Table 4.4) was driven by negative effects of increasing leaf $C_i:C_a$ on N_{area} in C₃ non-fixers (Tukey: $p<0.001$) and marginal negative effect in C₃ N-fixers (Tukey: $p=0.089$; Fig. 4.4a). An interaction between soil nitrogen availability and soil moisture ($p=0.019$; Table 4.4) indicated that the positive effect of increasing soil nitrogen availability on N_{area} ($p=0.046$; Table 4.4; Fig. 4.4d) declined with increasing soil moisture despite no individual effect of soil moisture on N_{area} ($p=0.858$; Table 4.4; Fig. 4.4g). Specifically, there was at least a marginal positive effect of increasing soil nitrogen availability on N_{area} when soil moisture was between 10% and 60% of water holding capacity (Tukey: $p<0.1$ in all cases), with no effect of soil nitrogen availability on N_{area} when soil moisture was greater than 65% of water holding capacity (Tukey: $p>0.1$ in all cases). Finally, a plant functional group effect ($p<0.001$; Table 4.4) indicated that C₄ non-fixers had lower N_{area} compared to C₃ N-fixers (Tukey: $p<0.001$) and C₃ non-fixers (Tukey: $p=0.011$), while C₃ N-fixers had lower N_{area} compared to C₃ non-fixers (Tukey: $p=0.020$).

Leaf $C_i:C_a$ had no effect on N_{mass} ($p=0.943$; Table 4.4; Fig. 4.4b), though a marginal interaction between leaf $C_i:C_a$ and plant functional group ($p=0.065$; Table 4.4) indicated a marginal negative effect of increasing leaf $C_i:C_a$ in C₃ non-fixers (Tukey: $p=0.094$). An interaction between soil nitrogen availability and soil moisture ($p<0.001$; Table 4.4) revealed that the positive effect of increasing soil nitrogen availability ($p<0.001$; Table 4.4; Fig. 4.4e) declined with increasing soil moisture. Specifically, this interaction indicated that the positive effect of

increasing soil nitrogen availability on N_{mass} was only apparent when soil moisture was equal to or less than 70% of water holding capacity (Tukey: $p<0.05$ in all cases). Increasing soil moisture also generally increased N_{mass} ($p<0.001$; Table 4.4; Fig. 4.4h). A plant functional group effect ($p<0.001$; Table 4.4) indicated that C₄ non-fixers had lower N_{mass} compared to C₃ N-fixers (Tukey: $p=0.006$) and C₃ non-fixers (Tukey: $p=0.026$ in both cases), while N_{mass} did not differ between C₃ N-fixers and C₃ non-fixers (Tukey: $p=0.293$).

An interaction between leaf $C_i:C_a$ and plant functional group ($p<0.001$; Table 4.4) revealed that the negative effect of increasing leaf $C_i:C_a$ on M_{area} ($p=0.002$; Table 4.4) was driven by negative effects of increasing leaf $C_i:C_a$ on M_{area} in C₃ N-fixers (Tukey: $p<0.001$) and C₃ non-fixers (Tukey: $p=0.004$; Fig. 4.4c). An interaction between soil nitrogen availability and plant functional group ($p=0.028$; Table 4.4) indicated that the negative effect of increasing soil nitrogen availability on M_{area} ($p<0.001$; Table 4.4) was driven by negative effects of increasing soil nitrogen availability on M_{area} in C₄ non-fixers (Tukey: $p=0.009$) and C₃ non-fixers (Tukey: $p<0.001$; Fig. 4.4f). A third interaction between soil nitrogen availability and soil moisture ($p<0.001$; Table 4.4) indicated that the negative effect of increasing soil nitrogen availability on M_{area} ($p<0.001$; Table 4.4) diminished with increasing soil moisture due to a negative individual effect of increasing soil moisture on M_{area} ($p=0.006$; Table 4.4; Fig. 4.4i). This interaction indicated that the negative effect of increasing soil nitrogen availability on M_{area} was only apparent when soil moisture was equal to or less than 65% of water holding capacity (Tukey: $p<0.05$ in all cases). Increasing soil moisture generally

Table 4.4. Effects of soil moisture, soil nitrogen availability, plant functional group, and leaf $C_i:C_a$ on leaf nitrogen content per unit leaf area (N_{area} ; gN m $^{-2}$), leaf nitrogen content per unit leaf biomass (N_{mass} ; gN g $^{-1}$), and leaf biomass per unit leaf area (M_{area} ; g m $^{-2}$)

	N_{area}			N_{mass}			M_{area}			
	df	Coefficient	χ^2	p	Coefficient	χ^2	p	Coefficient	χ^2	p
(Intercept)	-	$1.96 * 10^{+0}$	-	-	$1.772 * 10^{-1}$	-	-	$6.42 * 10^{+0}$	-	-
$C_i:C_a$	1	$-1.31 * 10^{+0}$	4.387	0.036	$8.05 * 10^{-1}$	0.005	0.943	$-2.21 * 10^{+0}$	9.673	0.002
Soil N (N)	1	$1.18 * 10^{-2}$	3.972	0.046	$1.35 * 10^{-2}$	49.093	<0.001	$-1.59 * 10^{-3}$	24.314	<0.001
Soil moisture (SM ₃)	1	$3.79 * 10^{-1}$	0.032	0.858	$5.07 * 10^{-1}$	11.443	<0.001	$-9.92 * 10^{-2}$	7.649	0.006
PFT	1	-	43.761	<0.001	-	19.758	<0.001	-	10.168	0.006
SM ₃ *N	1	$-1.27 * 10^{-2}$	5.521	0.019	$-1.80 * 10^{-2}$	44.013	<0.001	$4.79 * 10^{-3}$	14.195	<0.001
$C_i:C_a$ *PFT	1	-	17.302	<0.001	-	5.471	0.065	-	13.974	<0.001
N*PFT	1	-	1.540	0.463	-	1.047	0.592	-	7.182	0.028
SM ₃ *PFT	1	-	1.113	0.573	-	2.004	0.367	-	3.785	0.151
SM ₃ *N*PFT	1	-	0.632	0.729	-	0.895	0.639	-	0.913	0.634

*Significance determined using Type II Wald χ^2 tests ($\alpha=0.05$). P -values less than 0.05 are in bold and p -values where $0.05 < p < 0.1$ are italicized. Coefficients are reported on the natural-log scale for all traits and are only included for continuous fixed effects. Key: df=degrees of freedom; χ^2 =Wald Type II chi-square test statistic

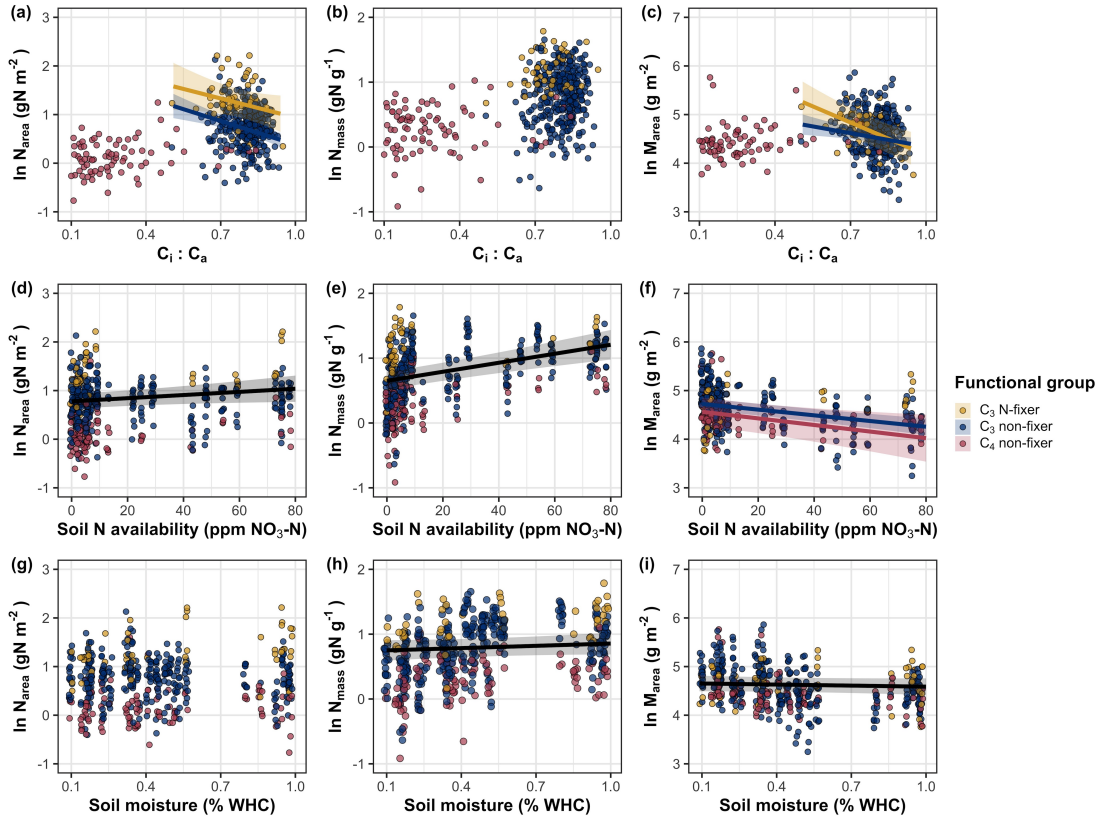


Figure 4.4. Effects of leaf $C_i:C_a$ (a-c), soil nitrogen availability (d-f), and soil moisture (g-i) on leaf nitrogen content per unit leaf area (a, d, g), leaf nitrogen content per unit leaf biomass (b, e, h), and leaf mass per area (c, f, i). Yellow points and trendlines indicate C_3 N-fixers, blue points and trendlines indicate C_3 non-fixers, and red points and trendlines indicate C_4 non-fixers. Points are jittered for visibility. Variably colored trendlines are only included if there is an interaction between plant functional group and the x-axis. Black solid trendlines denote bivariate slopes that are different from zero ($p < 0.05$) where there is no apparent interaction between plant functional group and the x-axis.

4.3.4 Piecewise structural equation model

The piecewise structural equation model explained 89%, 56%, 58%, 93%, and 28% of variance in N_{area} , N_{mass} , M_{area} , leaf $C_i:C_a$, and β , respectively (Table 4.5; Fig. 4.5). Increasing N_{mass} and M_{area} were each positively related to N_{area} ($p<0.001$ in both cases; Table 4.5; Fig. 4.5). N_{mass} increased with increasing soil nitrogen availability ($p<0.001$; Table 4.5) and leaf $C_i:C_a$ ($p=0.001$; Table 4.5), and was generally larger in N-fixing species ($p<0.001$; Table 4.5), but was negatively related to increasing M_{area} ($p<0.001$; Table 4.5). M_{area} decreased with increasing leaf $C_i:C_a$ ($p=0.019$ in both cases; Table 4.5) and soil nitrogen availability ($p<0.001$; Table 4.5). Leaf $C_i:C_a$ declined with increasing vapor pressure deficit, but was positively related to β ($p<0.001$ in both cases; Table 4.5). β decreased with increasing soil nitrogen availability ($p=0.001$; Table 4.5) and was greater in C₃ species ($p<0.001$; Table 4.5), but did not change with soil moisture ($p=0.915$; Table 4.5) or with ability to acquire nitrogen via symbiotic nitrogen fixation ($p=0.306$; Table 4.5). Finally, soil nitrogen availability was positively associated with increasing soil moisture ($p<0.001$; Table 4.5; Fig. 4.5), while soil moisture was negatively related to percent clay ($p<0.001$; Table 4.5; Fig. 4.5).

Table 4.5. Structural equation model results investigating direct effects of climatic and soil resource availability on leaf nitrogen content (N_{area} ; g m⁻²)*

Predictor	Coefficient	<i>p</i>
N_{area} ($R^2_c=0.89$)		
M_{area}	0.713	<0.001
N_{mass}	0.787	<0.001
N_{mass} ($R^2_c=0.56$)		
Leaf $C_i:C_a$	0.207	0.001
M_{area}	-0.240	<0.001
Soil N	0.242	<0.001
N-fixing ability	0.335	<0.001
M_{area} ($R^2_c=0.58$)		
Leaf $C_i:C_a$	-0.187	0.019
Soil N	-0.209	<0.001
Leaf $C_i:C_a$ ($R^2_c=0.93$)		
β	0.154	<0.001
VPD ₄	-0.082	<0.001
β ($R^2_c=0.28$)		
Soil N	-0.161	0.001
SM ₃	-0.006	0.915
Photo. pathway	0.417	<0.001
N-fixing ability	-0.082	0.306
Soil N ($R^2_c=0.41$)		
SM ₃	-0.409	<0.001
Soil moisture ($R^2_c=0.51$)		
% clay	-0.433	<0.001

*Coefficients are standardized across the structural equation model. *P*-values less than 0.05 are noted in bold. Positive coefficients for photosynthetic pathway indicate generally larger values in C₃ species, while positive coefficients for N-fixing ability indicate generally larger values in N-fixing species. Key: df=degrees of freedom; χ^2 =Wald Type II chi-square test statistic; R^2_c =conditional R² value; N_{mass} =leaf nitrogen content per unit leaf biomass (gN g⁻¹); M_{area} =leaf mass per unit leaf biomass (g m⁻²); β =cost of acquiring nitrogen relative to water (unitless); VPD₄=4-day mean vapor pressure deficit (kPa); SM₉₀=90-day mean soil moisture (mm)

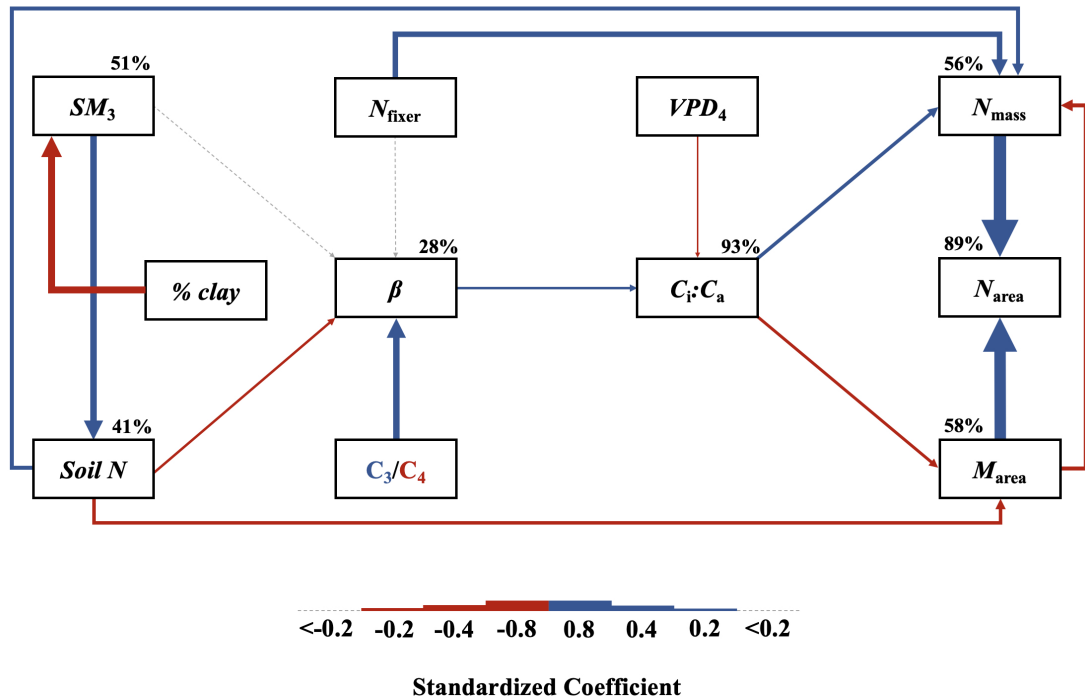


Figure 4.5. Structural equation model results exploring drivers of leaf nitrogen content. Boxes indicate measured edaphic factors, climatic factors, and leaf traits. Solid arrows indicate bivariate relationships where $p < 0.05$, while dashed arrows indicate relationships where $p > 0.05$. Positive model coefficients are indicated through blue arrows, negative model coefficients are indicated through red arrows, and insignificant coefficients are indicated through gray dashed arrows. Arrow thickness scales with the standardized model coefficient of each bivariate relationship. A positive coefficient for photosynthetic pathway indicates larger values in C_3 species, while a positive coefficient for N_{fixer} indicates larger values in N-fixing species. Standardized model coefficients and associated p -values are reported in Table 4.5, with conditional R^2 values for each response variable reported on the top right of each box.

4.4 Discussion

In this study, direct and indirect effects of edaphic and climatic characteristics on N_{area} and components of N_{area} (N_{mass} and M_{area}) were quantified in 504 individuals spanning across a soil resource availability and climate gradient in Texas, USA. Consistent patterns emerged in support of those expected from photosynthetic least-cost theory, a result driven by a strong direct negative relationship between leaf $C_i:C_a$ and N_{area} mediated through changes in M_{area} . In further support of patterns expected from theory, increasing soil nitrogen availability had a negative effect on β , resulting in an indirect stimulation in N_{area} mediated through a positive relationship between β and $C_i:C_a$. Increasing vapor pressure deficit also indirectly increased N_{area} through a direct negative effect of increasing vapor pressure deficit on leaf $C_i:C_a$, following hypotheses and patterns expected from theory. Interestingly, a positive association between soil moisture and N_{area} was driven by covariance between soil moisture and soil nitrogen availability and was not associated with a direct effect of soil moisture on β . Overall, results provide strong and consistent support for patterns expected from photosynthetic least-cost theory, showing that both soil resource availability and climate drive variance in N_{area} through changes in leaf $C_i:C_a$.

The negative response of N_{area} to increasing leaf $C_i:C_a$ is consistent with previous environmental gradient (Dong et al. 2017; Querejeta et al. 2022) and manipulation experiments (3.3c), showing strong support for the nitrogen-water use tradeoffs expected from photosynthetic least cost theory (Wright et al. 2003; Prentice et al. 2014). Negative effects of increasing leaf $C_i:C_a$ on N_{area} were driven by negative effect of increasing leaf $C_i:C_a$ on M_{area} coupled with a weak positive

effect of increasing leaf $C_i:C_a$ on N_{mass} , suggesting that changes in N_{area} across the environmental gradient were driven more strongly by changes in leaf morphology than leaf chemistry. Interestingly, the negative relationship between M_{area} and N_{mass} suggested that stimulations in N_{mass} were often associated with larger, thinner leaves (i.e., lower M_{area}). These results are consistent with patterns reported from previous studies indicating that variance in N_{area} is driven by changes in M_{area} across environmental gradients, and that part of this response is due to negative covariance between M_{area} and N_{mass} (Dong et al. 2017; Dong et al. 2020). Negative covariance between M_{area} and N_{mass} could be a response associated with tradeoffs between leaf longevity and leaf productivity (Wright et al. 2004; Dong et al. 2017; Dong et al. 2022; Querejeta et al. 2022; Wang et al. 2023).

The negative relationship between leaf $C_i:C_a$ and M_{area} could be indicative of tradeoffs between leaf longevity and leaf productivity. Tradeoffs between leaf longevity and leaf productivity are commonly observed and are included in a continuum of coordinated leaf traits that position individuals along a fast- or slow-growing leaf economics spectrum (Wright et al. 2003; Onoda et al. 2004; Reich 2014; Onoda et al. 2017; Wang et al. 2023). Negative relationships between leaf $C_i:C_a$ and M_{area} indicate that increased stomatal conductance and reduced water use efficiency were associated with thinner, larger leaves (i.e., lower M_{area}). Combined with the negative covariance between M_{area} and N_{mass} mentioned above, these responses may have allowed individuals to maximize light interception and productivity by exploiting high light environments at the expense of increased water loss and decreased water-use efficiency. This strategy may be especially advantageous for fast-growing species in open canopy systems. In this study, C₃

N-fixers and C₃ non-fixers dominated the dataset (77% of total sampling effort), of which 23% (17% of total sampling effort) were classified as annual species with short growing seasons. We observed no effect of leaf $C_i:C_a$ on N_{area} or M_{area} in C₄ non-fixers, which made up 23% of the sampling effort and were generally classified as warm season graminoid species with slower growth rates and longer growing seasons. These patterns indicate that stronger tradeoffs between nitrogen and water use may be more apparent in fast-growing species with high demand for building and maintaining productive leaf tissues.

The structural equation model indicated multiple pathways where increasing soil nitrogen availability increased N_{area} . First, N_{area} increased with increasing soil nitrogen availability due to larger positive direct effects of increasing soil nitrogen availability on N_{mass} than the corresponding negative direct effect of increasing soil nitrogen availability on M_{area} . These patterns corroborate those observed in the individual linear mixed effect models. Second, soil nitrogen availability increased N_{area} indirectly through reductions in β , which increased leaf $C_i:C_a$ and stimulated N_{area} through a stronger negative effect of increasing leaf $C_i:C_a$ on M_{area} than corresponding positive effect of increasing leaf $C_i:C_a$ on N_{mass} . Reductions in β with increasing soil nitrogen availability were likely driven by reductions in the cost of acquiring and using nitrogen, following patterns observed in previous experiments (Bae et al. 2015; Eastman et al. 2021; Perkowski et al. 2021; Lu et al. 2022). These pathways indicate that soil nitrogen availability can have direct positive effects on N_{area} by increasing leaf nitrogen concentration, following previous work (Firn et al. 2019; Liang et al. 2020), or can alternatively have indirect positive effects on N_{area} through changes in leaf morphology associated

with a reduction in the cost of acquiring nitrogen, following patterns expected from photosynthetic least-cost theory. Results reported here indicate that photosynthetic least-cost frameworks are capable of detecting predictable variance in N_{area} and tradeoffs between nitrogen and water use across soil nitrogen availability gradients.

Increasing soil moisture had a positive effect on N_{area} , though this response was associated with a null effect of soil moisture on β . These results contrast patterns expected from theory, where increasing soil moisture is expected to indirectly decrease N_{area} through an increase in β due to a reduction in costs associated with water acquisition and use (Wright et al. 2003; Prentice et al. 2014; Lavergne et al. 2020). Interestingly, structural equation model results revealed a strong positive association between soil moisture and soil nitrogen availability, indicating an indirect positive effect of increasing soil moisture on N_{area} mediated by the negative effect of increasing soil nitrogen availability on β . In Texan grasslands, productivity and nutrient uptake are often co-limited by precipitation and nutrient availability (Yahdjian et al. 2011; Wang et al. 2017). Thus, increasing soil moisture may have facilitated more favorable and productive environments for soil microbial communities (Reichman et al. 1966; Stark and Firestone 1995; Paul et al. 2003), or alternatively greater plant nitrogen uptake rates that may have been associated with greater nitrogen mobility in soil solution (Alam 1999; Dijkstra and Cheng 2008). As discussed above, the positive indirect response of N_{area} to increasing soil nitrogen availability mediated through reductions in β follow patterns expected from theory.

In support of hypotheses and patterns expected from theory, increasing

vapor pressure deficit indirectly increased N_{area} , mediated through the negative effect of increasing vapor pressure deficit on leaf $C_i:C_a$. These responses are consistent with previous work noting strong reductions in stomatal conductance with increasing vapor pressure deficit (Oren et al. 1999; Novick et al. 2016; Sulman et al. 2016; Grossiord et al. 2020; López et al. 2021), a response that allows plants to minimize water loss as a result of high atmospheric water demand. Results also support findings from previous experiments across environmental gradients, where increasing vapor pressure deficit generally increases N_{area} at lower stomatal conductance across environmental gradients (Dong et al. 2017; Dong et al. 2022; Paillassa et al. 2020; Westerband et al. 2023). The increase in N_{area} with increasing vapor pressure deficit could allow plants to maximize photosynthetic capacity under reduced stomatal conductance (Dong et al. 2022), though this pattern contrasts previous work suggesting that long-term increases in vapor pressure deficit are associated with increased plant mortality, reduced net primary productivity, and perhaps reductions in net photosynthesis rates over time due to prolonged stomatal closure (Eamus et al. 2013; Yuan et al. 2019; Grossiord et al. 2020). Importantly, such negative effects of increasing vapor pressure deficit often occur along much broader timescales compared to the timescale used here. Responses observed here suggest that variance in N_{area} across environmental gradients is a deterministic acclimation response to changing aboveground climate, allowing plants to satisfy demand to build and maintain photosynthetic enzymes and optimize photosynthetic processes by maximizing resource use efficiency (Paillassa et al. 2020; Peng et al. 2021; Dong et al. 2022; Westerband et al. 2023).

N-fixing species had greater N_{area} values on average compared to non-fixing

species, a pattern driven by a stronger stimulation in N_{mass} in N-fixing species coupled with no change in M_{area} between species with different N-fixation ability. There was no evidence to suggest that N-fixing species had different β or leaf $C_i:C_a$ values compared to non-fixing species across the environmental gradient. These results follow patterns from previous environmental gradient experiments that investigate variance in leaf nitrogen allocation in N-fixing species (Adams et al. 2016; Dong et al. 2017; Dong et al. 2020), and that increases in N_{mass} and N_{area} in N-fixing species are not necessarily correlated to increases in water use efficiency or reductions in leaf $C_i:C_a$ (Adams et al. 2016). While results are consistent with results from previous environmental gradient experiments, they do not support hypotheses presented here or patterns expected from theory, which predicts that stimulations in N_{area} by N-fixing species should be driven by a reduction in β relative to non-fixing species, and that this response should decrease stomatal conductance and leaf $C_i:C_a$.

C_4 species had reduced β , leaf $C_i:C_a$, and N_{area} than C_3 species. Reduced β and leaf $C_i:C_a$ values in C_4 species follow hypotheses listed above, a pattern that could be the result of either reduced costs of nitrogen acquisition and use, increased costs of water acquisition and use, or both (Wright et al. 2003; Prentice et al. 2014). Results also indicate that β in C_4 non-fixers was unresponsive to changes in soil nitrogen availability despite an apparent negative effect of increasing soil nitrogen availability on β in C_3 N-fixers and C_3 non-fixers. Combined with a general null response of β to soil moisture regardless of plant functional group, these patterns imply that reduced β values in C_4 species may be the result of lower costs of nitrogen acquisition and use relative to C_3 species. While lower β values in

C_4 species provides a possible explanation for why C_4 species often have lower leaf $C_i:C_a$ and greater water use efficiency, theory predicts that this response should cause C_4 species to have greater N_{area} values compared to C_3 species, though C_4 species commonly exhibit lower N_{area} and higher nitrogen use efficiency than C_3 species (Schmitt and Edwards 1981; Sage and Pearcy 1987; Ghannoum et al. 2011). Lowered costs of nitrogen acquisition and use in C_4 species could be driven by more efficient Rubisco carboxylation efficiency in C_4 species associated with CO₂ concentrating mechanisms that eliminate photorespiration (Ghannoum et al. 2011), which could reduce or eliminate the need to sacrifice inefficient nitrogen use for efficient water use to achieve optimal photosynthesis rates.

Optimality models for both C_3 and C_4 species have been developed using principles from photosynthetic least-cost theory (Prentice et al. 2014; Wang et al. 2017; Smith et al. 2019; Stocker et al. 2020; Scott and Smith 2022). In both C_3 and C_4 model variants, β values are held constant using global datasets of leaf δ¹³C (Wang et al. 2017; Cornwell et al. 2018). Specifically, the C_3 optimality model initially assumed a constant β value of 240 (Wang et al. 2017), later corrected to 146 (Stocker et al. 2020), while the C_4 optimality model assumes a constant β value of 166 (Scott and Smith 2022). These results, which build on findings from Paillassa et al. (2020) and Lavergne et al. (2020), demonstrate high variability in calculated β values across the environmental gradient. Specifically, β values in C_3 species ranged from 1.5 to 469.4 (mean: 47.2; median: 31.6; standard deviation: 54.2), while ranged from less than 0.1 to 35.5 in C_4 species (mean: 2.2; median: 0.1; standard deviation: 6.2). Mean β values in both C_3 and C_4 species were consistently lower than values currently implemented in optimality

models, though this was likely the result of increased water limitation across sites relative to global averages. Regardless, the high degree of β variability across this environmental gradient, together with findings from Lavergne et al. (2020) and Paillassa et al. (2020), suggests that the use of constant β values may contribute to erroneous errors when conducting optimality model simulations. Results from this experiment build on suggestions from Wang et al. (2017), suggesting that future photosynthetic least-cost optimality model developments should consider adopting frameworks for dynamically calculating β .

To summarize, variability in N_{area} across an environmental gradient in Texan grasslands was driven by indirect effects of climate and soil resource availability mediated by changes in β and leaf $C_i:C_a$. Results from this experiment provide strong and consistent support for patterns expected from photosynthetic least-cost theory, demonstrating that negative relationships between $C_i:C_a$ and N_{area} unify expected effects of climatic and edaphic characteristics on N_{area} across environmental gradients. Results reported here also demonstrate a need to consider the dynamic nature of the relative cost of nitrogen versus water uptake (β) across environmental gradients in optimality models that leverage principles of photosynthetic least-cost theory.

Chapter 5

Optimal resource investment to photosynthetic capacity maximizes nutrient allocation to whole plant growth under elevated CO₂

5.1 Introduction

Terrestrial ecosystems are regulated by complex carbon and nitrogen cycles. As a result, terrestrial biosphere models, which are beginning to include coupled carbon and nitrogen cycles (Shi et al. 2016; Davies-Barnard et al. 2020; Braghieri et al. 2022), must accurately represent these cycles under different environmental scenarios to reliably simulate carbon and nitrogen atmosphere-biosphere fluxes (Hungate et al. 2003; Prentice et al. 2015). While the inclusion of coupled carbon and nitrogen cycles tends to reduce model uncertainty (Arora et al. 2020), large uncertainty in role of soil nitrogen availability and nitrogen acquisition strategy on leaf and whole plant acclimation responses to CO₂ remains (Smith and Dukes 2013; Terrer et al. 2018; Smith and Keenan 2020). This source of uncertainty likely contributes to the widespread divergence in future carbon and nitrogen flux simulations across terrestrial biosphere models (Friedlingstein et al. 2014; Zaehle et al. 2014; Meyerholt et al. 2020).

Plants grown under elevated CO₂ generally have less leaf nitrogen content than those grown under ambient CO₂, a response that often corresponds with reductions in photosynthetic capacity and stomatal conductance at the leaf-level and biomass stimulation over time at the whole plant level (Curtis 1996; Drake et al. 1997; Ainsworth et al. 2002; Makino 2003; Morgan et al. 2004; Ainsworth and Long 2005; Ainsworth and Rogers 2007; Smith and Dukes 2013; Poorter et al. 2022). As net primary productivity is generally limited by nitrogen availability

(Vitousek and Howarth 1991; LeBauer and Treseder 2008; Fay et al. 2015), and soil nitrogen availability is often positively correlated with leaf nitrogen content and photosynthetic capacity (Field and Mooney 1986; Evans and Seemann 1989; Evans 1989; Walker et al. 2014; Firn et al. 2019; Liang et al. 2020), some have hypothesized that leaf and whole plant acclimation responses to CO₂ are constrained by soil nitrogen availability.

The progressive nitrogen limitation hypothesis predicts that elevated CO₂ will increase plant nitrogen demand, which will increase plant nitrogen uptake and progressively deplete soil nitrogen if soil nitrogen supply does not exceed plant nitrogen demand (Luo et al. 2004). The hypothesis predicts that this response should result in strong acute stimulations in whole plant growth and primary productivity that diminish over time as nitrogen becomes more limiting. Assuming a positive relationship between soil nitrogen availability, leaf nitrogen content, and photosynthetic capacity, this hypothesis also implies that progressive reductions in soil nitrogen availability should be the mechanism that drives the reduction in leaf nitrogen content and photosynthetic capacity under elevated CO₂. The progressive nitrogen limitation hypothesis has received some support from free air CO₂ enrichment experiments (Reich et al. 2006; Norby et al. 2010), although is not consistently observed across experiments (Finzi et al. 2006; Moore et al. 2006; Liang et al. 2016).

While possible that progressive nitrogen limitation may determine leaf and whole plant acclimation responses to CO₂, growing evidence indicates that leaf nitrogen content and photosynthetic capacity are more strongly determined through aboveground growing conditions than by soil resource availability (Dong et al.

2017; Dong et al. 2020; Dong et al. 2022; Smith et al. 2019; Smith and Keenan 2020; Paillassa et al. 2020; Peng et al. 2021; Querejeta et al. 2022; Westerband et al. 2023), and satellite-derived chlorophyll fluorescence data indicate that increasing atmospheric CO₂ may decrease leaf and canopy demand for nitrogen (Dong et al. 2022). Together, results from these studies suggest that the reduction in leaf nitrogen content and photosynthetic capacity due to increasing CO₂ may not be as tightly linked to progressive nitrogen limitation as previously hypothesized.

A unification of optimal coordination and least-cost theories predicts that leaves acclimate to elevated CO₂ by reducing nitrogen allocation to Ribulose-1,5-bisphosphate (RuBP) carboxylase/oxygenase (Rubisco) to optimize resource use efficiencies at the leaf level, which allows for greater resource allocation to whole plant growth (Drake et al. 1997; Wright et al. 2003; Prentice et al. 2014; Smith et al. 2019). The theory predicts that the reduction in nitrogen allocation to Rubisco results in a stronger reduction in the maximum rate of Rubisco carboxylation (V_{cmax}) than the maximum rate of RuBP regeneration (J_{max}), which maximizes photosynthetic efficiency by allowing net photosynthesis rates to be equally co-limited by Rubisco carboxylation and RuBP regeneration (Chen et al. 1993; Maire et al. 2012). This acclimation response allows plants to make more efficient use of available light while avoiding overinvestment in Rubisco, which has high nitrogen and energetic costs of building and maintaining (Evans 1989; Evans and Clarke 2019). Instead, additional acquired resources not needed to optimize leaf photosynthesis may be allocated to the maintenance of structures that support whole plant growth (e.g., total leaf area, whole plant biomass, etc.) or to

allocation processes not related to leaf photosynthesis or growth, such as plant defense mechanisms. Regardless, optimized resource allocation at the leaf level should allow for greater resource allocation to whole plant growth. The theory indicates that leaf acclimation responses to CO₂ should be independent of changes in soil nitrogen availability. While this leaf acclimation response maximizes nitrogen allocation to structures that support whole plant growth, the theory suggests that the positive effect of elevated CO₂ on whole plant growth may be further stimulated by soil nitrogen availability through reductions in the cost of acquiring nitrogen (Bae et al. 2015; Perkowski et al. 2021; Lu et al. 2022).

Plants acquire nitrogen by allocating photosynthetically derived carbon belowground in exchange for nitrogen through different nitrogen acquisition strategies. These nitrogen acquisition strategies can include direct uptake pathways such as mass flow or diffusion (Barber 1962), symbioses with mycorrhizal fungi or symbiotic nitrogen-fixing bacteria (Vance and Heichel 1991; Marschner and Dell 1994; Smith and Read 2008; Udvardi and Poole 2013), or through the release of root exudates that prime free-living soil microbial communities (Phillips et al. 2011; Wen et al. 2022). Plants cannot acquire nitrogen without first allocating carbon belowground, which implies an inherent carbon cost to the plant for acquiring nitrogen regardless of nitrogen acquisition strategy. Carbon costs to acquire nitrogen often vary in species with different nitrogen acquisition strategies and are dependent on external environmental factors such as atmospheric CO₂, light availability, and soil nitrogen availability (Brzostek et al. 2014; Terrer et al. 2016; Terrer et al. 2018; Allen et al. 2020; Perkowski et al. 2021; Lu et al. 2022). These patterns suggest that acquisition strategy may at least partially determine the net

effect of soil nitrogen availability on leaf and whole plant acclimation responses to elevated CO₂.

A recent meta-analysis using data across 20 grassland and forest CO₂ enrichment experiments suggested that species which acquire nitrogen from symbiotic nitrogen-fixing bacteria had reduced costs of nitrogen acquisition under elevated CO₂ (Terrer et al. 2018). Though these analyses included data from two experimental sites, findings from this meta-analysis indicated that reduced costs of nitrogen acquisition in species that form associations with symbiotic nitrogen-fixing bacteria under elevated CO₂ may drive stronger increases in whole plant growth and reductions in V_{cmax} than species that associate with arbuscular mycorrhizal fungi (Smith and Keenan 2020), which generally have greater costs of nitrogen acquisition under elevated CO₂ (Terrer et al. 2018). However, plant investments in symbiotic nitrogen fixation generally decline with increasing nitrogen availability (Dovrat et al. 2018; Perkowski et al. 2021), a response that has been previously inferred to driven by a shift to direct uptake pathways as costs of direct uptake decrease (Rastetter et al. 2001; Perkowski et al. 2021). Thus, effects of symbiotic nitrogen fixation on plant acclimation responses to CO₂ should decline with increasing soil nitrogen availability, although manipulative experiments that directly test these patterns are rare.

Here, I conducted a 7-week growth chamber experiment using *Glycine max* L. (Merr.) to examine the effects of soil nitrogen fertilization and inoculation with symbiotic nitrogen-fixing bacteria on leaf and whole plant acclimation responses to elevated CO₂. Following patterns expected from theory, I hypothesized that individual leaves should respond to elevated CO₂ by decreasing V_{cmax} more strongly

than J_{\max} , allowing leaf photosynthesis to approach optimal coordination. I expected this response to correspond with a stronger reduction in leaf nitrogen content than $V_{c\max}$ and J_{\max} , which would increase the fraction of leaf nitrogen content allocated to photosynthesis under elevated CO₂. At the whole-plant level, I hypothesized that plants would respond to elevated CO₂ by increasing whole plant growth and productivity, a response that would be driven by an increase in total leaf area and total biomass. I predicted that leaf responses to elevated CO₂ would be independent of soil nitrogen fertilization and inoculation with symbiotic nitrogen-fixing bacteria. However, I expected that increasing fertilization would increase the positive effect of elevated CO₂ on total leaf area and aboveground biomass due to a stronger reduction in the cost of acquiring nitrogen under elevated CO₂ with increasing fertilization. Finally, I expected stronger increases in whole plant growth under elevated CO₂ in inoculated pots, but expected that this effect would only be apparent under low fertilization due to a reduction in root nodulation with increasing fertilization.

5.2 Methods

5.2.1 Seed treatments and experimental design

Glycine max L. (Merr) seeds were planted in 144 6-liter surface sterilized pots (NS-600, Nursery Supplies, Orange, CA, USA) containing a steam-sterilized 70:30 v:v mix of *Sphagnum* peat moss (Premier Horticulture, Quakertown, PA, USA) to sand (Pavestone, subsidiary of Quikrete Companies, Atlanta, GA, USA). Before planting, all *G. max* seeds were surface sterilized in 2% sodium hypochlorite for 3 minutes, followed by three separate 3-minute washes with ultrapure water (MilliQ

7000; MilliporeSigma, Burlington, MA USA). A subset of surface sterilized seeds were inoculated with *Bradyrhizobium japonicum* (Verdesian N-DureTM Soybean, Cary, NC, USA) in a slurry following manufacturer recommendations (3.12 g inoculant and 241 g deionized water per 1 kg seed).

Seventy-two pots were randomly planted with surface-sterilized seeds inoculated with *B. japonicum*, while the remaining 72 pots were planted with surface-sterilized uninoculated seeds. Thirty-six pots within each inoculation treatment were randomly placed in one of two atmospheric CO₂ treatments (ambient and 1000 $\mu\text{mol mol}^{-1}$ CO₂). Pots within each unique inoculation-by-CO₂ treatment combination randomly received one of nine soil nitrogen fertilization treatments equivalent to 0, 35, 70, 105, 140, 210, 280, 350, or 630 ppm N. Nitrogen fertilization treatments were created using a modified Hoagland solution (Hoagland and Arnon 1950) designed to keep concentrations of other macronutrients and micronutrients equivalent across treatments (Table D1). Pots received the same fertilization treatment throughout the entire duration experiment, which were applied twice per week in 150 mL doses as topical agents to the soil surface. This experimental design yielded a fully factorial experiment with four replicates per unique fertilization-by-inoculation-by-CO₂ combination.

5.2.2 Growth chamber conditions

Upon experiment initiation, pots were randomly placed in one of six Percival LED-41L2 growth chambers (Percival Scientific Inc., Perry, IA, USA) over two experimental iterations due to chamber space limitation. Two iterations were conducted such that one iteration included all elevated CO₂ pots and the second

iteration included all ambient CO₂ pots. Mean (\pm SD) CO₂ concentrations across chambers throughout the experiment were $439 \pm 5 \mu\text{mol mol}^{-1}$ CO₂ for the ambient CO₂ treatment and $989 \pm 4 \mu\text{mol mol}^{-1}$ CO₂ for the elevated CO₂ treatment.

Daytime growing conditions were simulated using a 16-hour photoperiod, with incoming light radiation set to chamber maximum (mean \pm SD: $1240 \pm 32 \mu\text{mol m}^{-2} \text{ s}^{-1}$ across chambers), air temperature set to 25°C, and relative humidity set to 50%. The remaining 8 hours simulated nighttime growing conditions, with incoming light radiation set to 0 $\mu\text{mol m}^{-2} \text{ s}^{-1}$, chamber temperature set to 17°C, and relative humidity set to 50%. Transitions between daytime and nighttime growing conditions were simulated by ramping incoming light radiation in 45-minute increments and temperature in 90-minute increments over a 3-hour period (Table D2).

Including the two, 3-hour ramping periods, pots grew under average (\pm SD) daytime light intensity of $1049 \pm 27 \mu\text{mol m}^{-2} \text{ s}^{-1}$. In the elevated CO₂ iteration, pots grew under $24.0 \pm 0.2^\circ\text{C}$ during the day, $16.4 \pm 0.8^\circ\text{C}$ during the night, and $51.6 \pm 0.4\%$ relative humidity. In the ambient CO₂ iteration, pots grew under $23.9 \pm 0.2^\circ\text{C}$ during the day, $16.0 \pm 1.4^\circ\text{C}$ during the night, and $50.3 \pm 0.2\%$ relative humidity. I accounted for any climatic differences across the six chambers by shuffling the same group of pots daily throughout the growth chambers. This process was done by iteratively moving the group of pots on the top rack of a chamber to the bottom rack of the same chamber, while simultaneously moving the group of pots on the bottom rack of a chamber to the top rack of the adjacent chamber. I moved pots within and across chambers daily throughout the course of each experiment iteration.

5.2.3 Leaf gas exchange measurements

Gas exchange measurements were collected for all individuals on the seventh week of development. All gas exchange measurements were collected on the center leaf of the most recent fully expanded trifoliate leaf set. Specifically, I measured net photosynthesis (A_{net} ; $\mu\text{mol m}^{-2} \text{s}^{-1}$), stomatal conductance (g_{sw} ; $\text{mol m}^{-2} \text{s}^{-1}$), and intercellular CO_2 (C_i ; $\mu\text{mol mol}^{-1}$) concentrations across a range of atmospheric CO_2 concentrations (i.e., an A_{net}/C_i curve) using the Dynamic Assimilation TechniqueTM. The Dynamic Assimilation TechniqueTM has been shown to correspond well with traditional steady-state CO_2 response curves in *G. max* (Saathoff and Welles 2021). A_{net}/C_i curves were generated along a reference CO_2 ramp down from $420 \mu\text{mol mol}^{-1} \text{CO}_2$ to $20 \mu\text{mol mol}^{-1} \text{CO}_2$, followed by a ramp up from $420 \mu\text{mol mol}^{-1} \text{CO}_2$ to $1620 \mu\text{mol mol}^{-1} \text{CO}_2$ after a 90-second wait period at $420 \mu\text{mol mol}^{-1} \text{CO}_2$. The ramp rate for each curve was set to $200 \mu\text{mol mol}^{-1} \text{min}^{-1}$, logging every five seconds, which generated 96 data points per response curve. All A_{net}/C_i curves were generated after A_{net} and g_{sw} stabilized in a LI-6800 cuvette set to a 500 mol s^{-1} , 10,000 rpm mixing fan speed, 1.5 kPa vapor pressure deficit, 25°C leaf temperature, $2000 \mu\text{mol m}^{-2} \text{s}^{-1}$ incoming light radiation, and initial reference CO_2 set to $420 \mu\text{mol mol}^{-1} \text{CO}_2$.

With the same focal leaf used to generate A_{net}/C_i curves, I measured dark respiration (R_{d25} ; $\mu\text{mol m}^{-2} \text{s}^{-1}$) following at least a 30-minute darkness period. Measurements were collected on a 5-second log interval for 60 seconds after stabilizing in a LI-6800 cuvette set to a 500 mol s^{-1} , 10,000 rpm mixing fan speed, 1.5 kPa vapor pressure deficit, 25°C leaf temperature, and $420 \mu\text{mol mol}^{-1}$ reference CO_2 concentration (for both CO_2 concentrations), with incoming light radiation

set to $0 \text{ } \mu\text{mol m}^{-2} \text{ s}^{-1}$. A single dark respiration value was determined for each focal leaf by calculating the mean dark respiration value (i.e. the absolute value of A_{net} during the logging period) across the logging interval.

5.2.4 Leaf trait measurements

The focal leaf used to generate A_{net}/C_i curves and dark respiration was harvested immediately following gas exchange measurements. Images of each focal leaf were curated using a flat-bed scanner to determine wet leaf area using the ‘LeafArea’ R package (Katabuchi 2015), which automates leaf area calculations using ImageJ software (Schneider et al. 2012). Each leaf was dried at 65°C for at least 48 hours, and subsequently weighed and ground until homogenized. Leaf mass per area (M_{area} ; g m^{-2}) was calculated as the ratio of dry leaf biomass to fresh leaf area. Using subsamples of ground and homogenized leaf tissue, I measured leaf nitrogen content (N_{mass} ; gN g^{-1}) through elemental combustion analysis (Costech-4010, Costech, Inc., Valencia, CA, USA). Leaf nitrogen content per unit leaf area (N_{area} ; gN m^{-2}) was calculated by multiplying N_{mass} and M_{area} . Subsamples of ground and homogenized leaf tissue were also sent to the UC-Davis Stable Isotope Facility to quantify leaf $\delta^{15}\text{N}$, later used to estimate the fraction of leaf nitrogen derived from the atmosphere.

I extracted chlorophyll content from a second leaf in the same trifoliolate leaf set as the focal leaf used to generate A_{net}/C_i curves. Prior to chlorophyll extraction, I used a cork borer to punch between 3 and 5 0.6 cm^2 disks from the leaf. Separate images of each punched leaf and set of leaf disks were curated using a flat-bed scanner to determine wet leaf area, quantified using the ‘LeafArea’ R

package (Katabuchi 2015). The punched leaf was dried and weighed after at least 65°C in the drying oven to determine M_{area} of the chlorophyll leaf.

Leaf disks were shuttled into a test tube containing 10mL dimethyl sulfoxide, vortexed, and incubated at 65°C for 120 minutes (Barnes et al. 1992). Incubated test tubes were vortexed again before loaded in 150 μL triplicate aliquots to a 96-well plate. Dimethyl sulfoxide was also loaded in a 150 μL triplicate aliquot as a blank. Absorbance measurements at 649.1 nm ($A_{649.1}$) and 665.1 nm ($A_{665.1}$) were read in each well using a plate reader (Biotek Synergy H1; Biotek Instruments, Winooski, VT USA) (Wellburn 1994), with triplicates subsequently averaged and corrected by the mean of the blank absorbance value. Blank-corrected absorbance values were used to estimate Chl_a ($\mu\text{g mL}^{-1}$) and Chl_b ($\mu\text{g mL}^{-1}$) following equations from Wellburn (1994):

$$Chl_a = 12.47A_{665.1} - 3.62A_{649.1} \quad (5.1)$$

and

$$Chl_b = 25.06A_{665.1} - 6.50A_{649.1} \quad (5.2)$$

Chl_a and Chl_b were converted to mmol mL^{-1} using the molar mass of chlorophyll a (893.51 g mol^{-1}) and the molar mass of chlorophyll b (907.47 g mol^{-1}), then added together to calculate total chlorophyll content in the dimethyl sulfoxide extractant (mmol mL^{-1}). Total chlorophyll content was multiplied by the volume of the dimethyl sulfoxide extractant (10 mL) and converted to area-based chlorophyll content by dividing by the total area of the leaf disks (Chl_{area} ; mmol m^{-2}). Mass-based chlorophyll content (Chl_{mass} ; mmol g^{-1}) was calculated by dividing Chl_{area}

by the leaf mass per area of the punched leaf.

5.2.5 Response curve fitting and parameter estimation

I fit A_{net}/C_i curves of each individual using the ‘fitaci’ function in the ‘plantecophys’ R package (Duursma 2015). This function estimates the maximum rate of Rubisco carboxylation (V_{cmax} ; $\mu\text{mol m}^{-2} \text{s}^{-1}$) and maximum rate of electron transport for RuBP regeneration (J_{max} ; $\mu\text{mol m}^{-2} \text{s}^{-1}$) based on the Farquhar biochemical model of C₃ photosynthesis (Farquhar et al. 1980). Triose phosphate utilization (TPU) limitation was included in all curve fits, and all curve fits included measured dark respiration values. As A_{net}/C_i curves were generated using a common leaf temperature, curves were fit using Michaelis-Menten coefficients for Rubisco affinity to CO₂ (K_c ; $\mu\text{mol mol}^{-1}$) and O₂ (K_o ; $\mu\text{mol mol}^{-1}$), and the CO₂ compensation point (Γ^* ; $\mu\text{mol mol}^{-1}$) reported in Bernacchi et al. (2001). Specifically, K_c was set to 404.9 $\mu\text{mol mol}^{-1}$, K_o was set to 278.4 $\mu\text{mol mol}^{-1}$, and Γ^* was set to 42.75 $\mu\text{mol mol}^{-1}$. All curve fits were visually examined for goodness-of-fit. The use of a common leaf temperature across curves and dark respiration measurements eliminated the need to temperature standardize rate estimates. For clarity, I reference V_{cmax} , J_{max} , and R_d estimates throughout the rest of the chapter as V_{cmax25} , J_{max25} , and R_{d25} .

5.2.6 Stomatal limitation

I quantified the extent by which stomatal conductance limited photosynthesis (l; unitless) following equations originally described in Farquhar and Sharkey (1982).

Stomatal limitation was calculated as:

$$l = 1 - \frac{A_{net}}{A_{mod}} \quad (5.3)$$

where A_{mod} represents the photosynthetic rate where $C_i=C_a$. A_{mod} was calculated as:

$$A_{mod} = V_{cmax25} - \frac{420 - \Gamma^*}{420 + K_m} - R_{d25} \quad (5.4)$$

K_m is the Michaelis-Menten coefficient for Rubisco-limited photosynthesis, calculated as:

$$K_m = K_c \cdot \left(1 + \frac{O_i}{K_o}\right) \quad (5.5)$$

where O_i refers to leaf intercellular O_2 concentrations, set to $210 \mu\text{mol mol}^{-1}$.

5.2.7 Proportion of leaf nitrogen allocated to photosynthesis and structure

I used equations from Niinemets and Tenhunen (1997) to estimate the proportion of leaf nitrogen content allocated to Rubisco, bioenergetics, and light harvesting proteins. The proportion of leaf nitrogen allocated to Rubisco ($\rho_{rubisco}$; gN gN^{-1}) was calculated as a function of V_{cmax25} and N_{area} :

$$\rho_{rubisco} = \frac{V_{cmax25} N_r}{V_{cr} N_{area}} \quad (5.6)$$

where N_r is the amount of nitrogen in Rubisco, set to $0.16 \text{ gN (gN in Rubisco)}^{-1}$ and V_{cr} is the maximum rate of RuBP carboxylation per unit Rubisco protein, set to $20.5 \mu\text{mol CO}_2 (\text{g Rubisco})^{-1}$. The proportion of leaf nitrogen allocated to bioenergetics (ρ_{bioe} ; gN gN^{-1}) was similarly calculated as a function of J_{max25} and

N_{area} :

$$\rho_{\text{bioe}} = \frac{J_{\text{max}25} N_b}{J_{\text{mc}} N_{\text{area}}} \quad (5.7)$$

where N_b is the amount of nitrogen in cytochrome f, set to 0.12407 gN ($\mu\text{mol cytochrome f}$) $^{-1}$ assuming a constant 1:1:1.2 cytochrome f: ferredoxin NADP reductase: coupling factor molar ratio (Evans and Seemann 1989; Niinemets and Tenhunen 1997), and J_{mc} is the capacity of electron transport per cytochrome f, set to 156 $\mu\text{mol electron}$ ($\mu\text{mol cytochrome f}$) $^{-1}\text{s}^{-1}$.

The proportion of leaf nitrogen allocated to light harvesting proteins (ρ_{light} ; gN gN $^{-1}$) was calculated as a function of Chl_{mass} and N_{mass} :

$$\rho_{\text{light}} = \frac{Chl_{\text{mass}}}{N_{\text{mass}} c_b} \quad (5.8)$$

where c_b is the stoichiometry of the light-harvesting chlorophyll complexes of photosystem II, set to 2.75 mmol chlorophyll (gN in chlorophyll) $^{-1}$. I used the N_{mass} value of the focal leaf used to generate A_{net}/C_i curves instead of the leaf used to extract chlorophyll content, as the two leaves are from the same trifoliolate leaf set and are therefore highly correlated (Figure D1).

The proportion of leaf nitrogen content allocated to photosynthetic tissue (ρ_{photo} ; gN gN $^{-1}$) was estimated as the sum of ρ_{rubisco} , ρ_{bioe} , and ρ_{light} . Finally, the proportion of leaf nitrogen content allocated to structural tissue ($\rho_{\text{structure}}$; gN gN $^{-1}$) was estimated as:

$$\rho_{\text{structure}} = \frac{N_{\text{cw}}}{N_{\text{area}}} \quad (5.9)$$

where N_{cw} is the leaf nitrogen content allocated to cell walls (gN m $^{-2}$), calculated

as a function of M_{area} using an empirical equation from Onoda et al. (2017):

$$N_{cw} = 0.000355 * M_{area}^{1.39} \quad (5.10)$$

5.2.8 Whole plant traits

Seven weeks after experiment initiation and immediately following gas exchange measurements, I harvested all experimental individuals and separated biomass of each experimental individual into major organ types (leaves, stems, roots, and nodules when present). Fresh leaf area of all harvested leaves was measured using an LI-3100C (Li-COR Biosciences, Lincoln, Nebraska, USA). Total fresh leaf area (cm^2) was calculated as the sum of all leaf areas, including the focal leaf used to collect gas exchange data and the focal leaf used to extract chlorophyll content. All harvested material was dried in an oven set to 65°C for at least 48 hours, weighed, and ground to homogeneity. Leaves and nodules were manually ground with a mortar and pestle, while stems and roots were ground using a Wiley mill (E3300 Mini Mill; Eberbach Corp., MI, USA). Total dry biomass (g) was calculated as the sum of dry leaf (including focal leaf for both the A_{net}/C_i curve and leaf used to extract chlorophyll content), stem, root, and root nodule biomass. I quantified carbon and nitrogen content of each respective organ type through elemental combustion (Costech-4010, Costech, Inc., Valencia, CA, USA) using subsamples of ground and homogenized organ tissue.

Following the approach explained in the first experimental chapter, I calculated structural carbon costs to acquire nitrogen as the ratio of total belowground carbon biomass to whole plant nitrogen biomass (N_{cost} ; gC gN^{-1}). Belowground

carbon biomass (C_{bg} ; gC) was calculated as the sum of root carbon biomass and root nodule carbon biomass. Root carbon biomass and root nodule carbon biomass was calculated as the product of the organ biomass and the respective organ carbon content. Whole plant nitrogen biomass (N_{wp} ; gN) was similarly calculated as the sum of total leaf, stem, root, and root nodule nitrogen biomass, including the focal leaf used for A_{net}/C_i curve and chlorophyll extractions. Leaf, stem, root, and root nodule nitrogen biomass was calculated as the product of the organ biomass and the respective organ nitrogen content. This calculation only quantifies plant structural carbon costs to acquire nitrogen and does not include any additional costs of nitrogen acquisition associated with respiration, root exudation, or root turnover. An explicit explanation of the limitations for interpreting this calculation can be found in Perkowski et al. (2021) and Terrer et al. (2018).

Finally, plant investments in nitrogen fixation were calculated as the ratio of root nodule biomass to root biomass, where increasing values indicate an increase in plant investments to nitrogen fixation (Dovrat et al. 2018; Dovrat et al. 2020; Perkowski et al. 2021). I also calculated the percent of leaf nitrogen acquired from the atmosphere (% N_{dfa} ; %) using leaf $\delta^{15}\text{N}$ and the following equation from Andrews et al. (2011):

$$\%N_{dfa} = \frac{\delta^{15}\text{N}_{reference} - \delta^{15}\text{N}_{sample}}{\delta^{15}\text{N}_{reference} - B} * 100 \quad (5.11)$$

where $\delta^{15}\text{N}_{reference}$ refers to a reference plant that exclusively acquires nitrogen via direct uptake, $\delta^{15}\text{N}_{sample}$ refers to an individual's leaf $\delta^{15}\text{N}$, and B refers to individuals that are entirely reliant on nitrogen fixation. Within each unique nitrogen

fertilization treatment-by-CO₂ treatment combination, I calculated the mean leaf δ¹⁵N for individuals growing in the non-inoculated treatment for δ¹⁵N_{reference}. Any individuals with visual confirmation of root nodule formation were omitted from the calculation of δ¹⁵N_{reference}. Following recommendations from Andrews et al. (2011) I calculated B within each CO₂ treatment using the mean leaf δ¹⁵N of inoculated individuals that received 0 ppm N. I did not calculate B within each unique soil nitrogen-by-CO₂ treatment combination, as previous studies suggest decreased reliance on nitrogen fixation with increasing soil nitrogen availability (Perkowski et al. 2021).

5.2.9 Statistical analyses

Uninoculated pots that had substantial root nodule formation (nodule biomass: root biomass values greater than 0.05 g g⁻¹) were removed from all analyses, as pots were assumed to have been colonized by symbiotic nitrogen-fixing bacteria from outside sources. This decision resulted in the removal of sixteen pots from analyses: two pots in the elevated CO₂ treatment that received 35 ppm N, three pots in the elevated CO₂ treatment that received 70 ppm N, one pot in the elevated CO₂ treatment that received 210 ppm N, two pots in the elevated CO₂ treatment that received 280 ppm N, two pots in the ambient CO₂ treatment that received 0 ppm N, three pots in the ambient CO₂ treatment that received 70 ppm N, two pots in the ambient CO₂ treatment that received 105 ppm N, and one pot in the ambient CO₂ treatment that received 280 ppm N.

I built a series of linear mixed effects models to investigate the impacts of CO₂ concentration, soil nitrogen fertilization, and inoculation with *B. japonicum*

on *G. max* gas exchange, tradeoffs between nitrogen and water use, whole plant growth, and investment in nitrogen fixation. All models included CO₂ treatment as a categorical fixed effect, inoculation treatment as a categorical fixed effect, soil nitrogen fertilization as a continuous fixed effect, with interaction terms between all three fixed effects. All models also accounted for climatic differences between chambers across experiment iterations by including a random intercept term that nested starting chamber rack by CO₂ treatment. Models with this independent variable structure were created for each of the following dependent variables: N_{area} , M_{area} , N_{mass} , Chl_{area} , V_{cmax25} , J_{max25} , $J_{\text{max25}}:V_{\text{cmax25}}$, R_{d25} , g_{sw} , stomatal limitation, ρ_{rubisco} , ρ_{bioe} , ρ_{light} , ρ_{photo} , $\rho_{\text{structure}}$, total biomass, total leaf area, N_{cost} , C_{bg} , N_{wp} , nodule biomass, the ratio of nodule biomass to root biomass, and $\%N_{\text{dfa}}$.

I used Shapiro-Wilk tests of normality to determine whether linear mixed effects models satisfied residual normality assumptions. If residual normality assumptions were not met (Shapiro-Wilk: $p < 0.05$), then models were fit using dependent variables that were natural log transformed. If residual normality assumptions were still not met (Shapiro-Wilk: $p < 0.05$), then models were fit using dependent variables that were square root transformed. All residual normality assumptions that did not originally satisfy residual normality assumptions were met with either a natural log or square root data transformation (Shapiro-Wilk: $p > 0.05$ in all cases). Specifically, models for N_{area} , N_{mass} , Chl_{area} , V_{cmax25} , J_{max25} , $J_{\text{max25}}:V_{\text{cmax25}}$, R_{d25} , g_{sw} , stomatal limitation, ρ_{rubisco} , ρ_{bioe} , ρ_{light} , ρ_{photo} , total leaf area, N_{cost} satisfied residual normality assumptions without data transformation. Models for M_{area} , $\rho_{\text{structure}}$, C_{bg} , and total biomass satisfied residual normality as-

sumptions with a natural log data transformation, while models for N_{wp} , nodule biomass, nodule biomass: root biomass, and $\%N_{dfa}$ satisfied residual normality assumptions with a square root data transformation.

In all statistical models, I used the ‘lmer’ function in the ‘lme4’ R package (Bates et al. 2015) to fit each model and the ‘Anova’ function in the ‘car’ R package (Fox and Weisberg 2019) to calculate Type II Wald’s χ^2 and determine the significance ($\alpha=0.05$) of each fixed effect coefficient. I used the ‘emmeans’ R package (Lenth et al. 2019) to conduct post-hoc comparisons using Tukey’s tests, where degrees of freedom were approximated using the Kenward-Roger approach (Kenward and Roger 1997). All analyses and plots were conducted in R version 4.2.0 (R Core Team 2021).

5.3 Results

5.3.1 Leaf nitrogen and chlorophyll content

Elevated CO₂ reduced N_{area} , N_{mass} , and Chl_{area} by 29%, 50%, and 31%, respectively, and increased M_{area} by 44% ($p<0.001$ in all cases; Table 5.1). An interaction between fertilization and CO₂ (CO₂-by-fertilization interaction: $p_{N_{area}}=0.017$, $p_{N_{mass}}<0.001$, $p_{Chl_{area}}=0.083$; Table 5.1) indicated that the positive effect of increasing fertilization on N_{area} , N_{mass} , and Chl_{area} ($p<0.001$ in all cases; Table 5.1) was stronger under ambient CO₂ (Tukey _{N_{area}} : $p=0.026$; Tukey _{N_{mass}} : $p<0.001$; Tukey _{Chl_{area}} : $p=0.065$; Table 5.1; Figs. 5.1a, 5.1b, 5.1d). An interaction between fertilization and CO₂ on M_{area} (CO₂-by-fertilization interaction: $p=0.006$; Table 5.1) indicated that the positive effect of increasing fertilization on M_{area} was stronger under elevated CO₂ (Tukey: $p=0.009$; Fig. 5.1c). Overall, interactions

between fertilization and CO₂ resulted in stronger reductions in N_{area} , N_{mass} , and Chl_{area} , and a stronger stimulation in M_{area} under elevated CO₂ with increasing fertilization.

An interaction between inoculation and CO₂ on N_{area} (CO₂-by-inoculation interaction: $p=0.030$; Table 5.1) indicated that the positive effect of inoculation on N_{area} ($p<0.001$; Table 5.1) was stronger under elevated CO₂ (45% increase; Tukey: $p<0.001$) than under ambient CO₂ (18% increase; Tukey: $p<0.001$), a result that increased the reduction in N_{area} in inoculated pots under elevated CO₂. Inoculation treatment did not modify the reduction in N_{mass} (CO₂-by-inoculation interaction: $p=0.148$; Table 5.1) and Chl_{area} ($p = 0.147$; Table 5.1) or the stimulation in M_{area} ($p=0.866$; Table 5.1) under elevated CO₂. However, interactions between fertilization and inoculation on N_{area} , N_{mass} , M_{area} , and Chl_{area} (fertilization-by-inoculation interaction: $p_{N_{\text{area}}}<0.001$, $p_{N_{\text{mass}}}=0.001$, $p_{M_{\text{area}}}=0.025$, $p_{Chl_{\text{area}}}=0.083$; Table 5.1) indicated that the positive effect of increasing fertilization on each trait was stronger in uninoculated pots (Tukey _{N_{area}} : $p<0.001$; Tukey _{N_{mass}} : $p=0.001$; Tukey _{M_{area}} : $p=0.031$; Tukey _{Chl_{area}} : $p<0.001$; Figs. 5.1a-d).

Table 5.1. Effects of soil nitrogen fertilization, inoculation, and CO₂ treatments on leaf nitrogen content per unit leaf area (N_{area} ; gN m⁻²), leaf nitrogen content per unit leaf mass (N_{mass} , gN g⁻¹), leaf mass per unit leaf area (M_{area} ; g m⁻²), and chlorophyll content per unit leaf area (Chl_{area} ; mmol m⁻²)^{*}

N_{area}			N_{mass}			$M_{\text{area}}^{\text{a}}$				
df	Coefficient	χ^2	p	Coefficient	χ^2	p	Coefficient	χ^2	p	
(Intercept)	-	$1.10 * 10^{+0}$	-	-	$3.05 * 10^{-2}$	-	-	$3.64 * 10^{+0}$	-	
CO ₂	1	$-5.67 * 10^{-1}$	155.908	<0.001	$-1.80 * 10^{-2}$	272.362	<0.001	$3.04 * 10^{-1}$	151.319	<0.001
Inoculation (I)	1	$6.21 * 10^{-1}$	86.029	<0.001	$7.54 * 10^{-3}$	15.576	<0.001	$1.81 * 10^{-1}$	19.158	<0.001
Fertilization (N)	1	$3.06 * 10^{-3}$	316.408	<0.001	$5.78 * 10^{-5}$	106.659	<0.001	$3.10 * 10^{-4}$	21.440	<0.001
CO ₂ *I	1	$2.63 * 10^{-1}$	4.729	0.030	$3.96 * 10^{-3}$	2.025	0.155	$-3.37 * 10^{-2}$	0.029	0.866
CO ₂ *N	1	$-3.68 * 10^{-4}$	5.723	0.017	$-2.85 * 10^{-5}$	22.542	<0.001	$2.80 * 10^{-4}$	7.619	0.006
I*N	1	$-1.36 * 10^{-3}$	43.381	<0.001	$-2.00 * 10^{-5}$	11.137	0.001	$-3.36 * 10^{-4}$	5.022	0.025
CO ₂ *I*N	1	$-3.23 * 10^{-4}$	0.489	0.484	$-2.59 * 10^{-6}$	0.041	0.839	$1.15 * 10^{-4}$	0.208	0.649
Chl_{area}										
df	Coefficient	χ^2	p							
(Intercept)	-	$2.13 * 10^{-2}$	-	-						
CO ₂	1	$-1.33 * 10^{-2}$	69.233	<0.001						
Inoculation (I)	1	$1.24 * 10^{-1}$	136.341	<0.001						
Fertilization (N)	1	$3.35 * 10^{-4}$	163.111	<0.001						
CO ₂ *I	1	$-3.18 * 10^{-2}$	2.102	0.147						
CO ₂ *N	1	$-8.79 * 10^{-5}$	2.999	0.083						
I*N	1	$-2.65 * 10^{-4}$	75.769	<0.001						
CO ₂ *I*N	1	$7.68 * 10^{-5}$	2.144	0.147						

*Significance determined using Type II Wald χ^2 tests ($\alpha=0.05$). P-values less than 0.05 are in bold, while p-values between 0.05 and 0.1 are italicized. A superscript “a” is included after trait labels to indicate if models were fit with natural log transformed response variables. Key: df=degrees of freedom, χ^2 =Wald Type II chi-square test statistic.

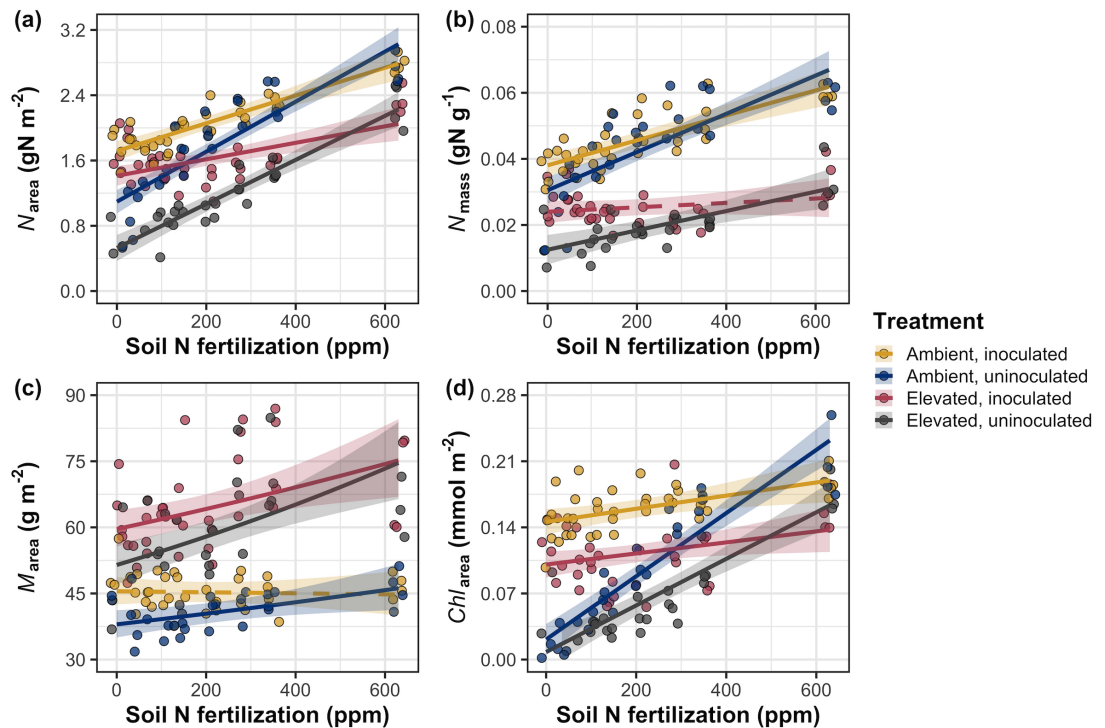


Figure 5.1. Effects of CO_2 , fertilization, and inoculation on leaf nitrogen per unit leaf area (a), leaf nitrogen content (b), leaf mass per unit leaf area (c), and chlorophyll content per unit leaf area (d). Soil nitrogen fertilization is represented on the x-axis in all panels. Yellow points and trendlines indicate inoculated individuals grown under ambient CO_2 , blue points and trendlines indicate uninoculated individuals grown under ambient CO_2 , red points and trendlines indicate inoculated individuals grown under elevated CO_2 , and gray points indicate uninoculated individuals grown under elevated CO_2 . Solid trendlines indicate regression slopes that are different from zero ($p < 0.05$), while dashed trendlines indicate slopes that are not distinguishable from zero ($p > 0.05$).

5.3.2 Leaf biochemistry and stomatal conductance

Elevated CO₂ reduced V_{cmax25} ($p<0.001$; Table 5.2) and J_{max25} ($p=0.014$; Table 5.2) by 16% and 10%, respectively, but did not influence R_{d25} ($p=0.613$; Table 5.2; Fig. 5.2d). A relatively stronger reduction in V_{cmax25} than J_{max25} resulted in an 8% increase in $J_{max25}:V_{cmax25}$ under elevated CO₂ ($p<0.001$; Table 5.2). The negative effect of CO₂ on V_{cmax25} and J_{max25} was not modified across the fertilization gradient (CO₂-by-fertilization interaction: $p=0.185$ and $p=0.389$ for V_{cmax25} and J_{max25} , respectively; Table 5.2; Figs. 5.2a, 5.2b) or between inoculation treatments (CO₂-by-inoculation interaction: $p=0.799$ and $p=0.714$ for V_{cmax25} and J_{max25} , respectively; Table 5.2). However, a strong interaction between fertilization and inoculation (fertilization-by-inoculation interaction: $p\leq0.001$ in all cases; Table 5.2) indicated that the positive effect of increasing fertilization on V_{cmax25} ($p<0.001$; Table 5.2), J_{max25} ($p<0.001$; Table 5.2), and R_{d25} ($p=0.015$; Table 5.2) was only observed in uninoculated pots (Tukey: $p\leq0.001$ in all cases; Figs. 5.2a, 5.2b). A stronger positive effect of increasing fertilization on V_{cmax25} than J_{max25} resulted in a reduction in $J_{max25}:V_{cmax25}$ with increasing fertilization ($p<0.001$; Table 5.2), though this pattern was only observed in uninoculated pots (fertilization-by-inoculation interaction: $p=0.002$; Table 5.2; Fig. 5.2c).

Elevated CO₂ reduced stomatal conductance by 20% ($p<0.001$; Table 5.2; Fig. 5.2e), but this pattern did not influence stomatal limitation of photosynthesis ($p=0.355$; Table 5.2; Fig. 5.2f). As with V_{cmax25} and J_{max25} , the reduction in stomatal conductance under elevated CO₂ was not modified across the fertilization gradient (CO₂-by-fertilization interaction: $p=0.141$; Table 5.2) or between inoculation treatments (CO₂-by-inoculation interaction: $p=0.179$; Table 5.2). Fer-

tilization did not modify the null effect of CO₂ on stomatal limitation (CO₂-by-fertilization interaction: $p=0.554$; Table 5.2). An interaction between CO₂ and inoculation (CO₂-by-inoculation interaction: $p=0.043$; Table 5.2) indicated that inoculation increased stomatal limitation under ambient CO₂ (Tukey: $p=0.021$), but not under elevated CO₂ (Tukey: $p>0.999$). An additional interaction between inoculation and fertilization on stomatal conductance (fertilization-by-inoculation interaction: $p<0.001$; Table 5.2) indicated that increasing fertilization increased stomatal conductance in uninoculated pots (Tukey: $p=0.003$) but decreased stomatal conductance in inoculated pots (Tukey: $p=0.021$). The similar in magnitude, but opposite direction, trend in the effect of increasing fertilization on stomatal conductance between inoculation treatments likely drove a null response of stomatal conductance to increasing fertilization ($p=0.642$; Table 5.2).

Table 5.2. Effects of soil nitrogen fertilization, inoculation, and CO₂ on the maximum rate of Rubisco carboxylation ($V_{\text{cmax}25}$; $\mu\text{mol m}^{-2} \text{s}^{-1}$), the maximum rate of RuBP regeneration ($J_{\text{max}25}$; $\mu\text{mol m}^{-2} \text{s}^{-1}$), dark respiration ($R_{\text{d}25}$; $\mu\text{mol m}^{-2} \text{s}^{-1}$), the ratio of the maximum rate of RuBP regeneration to the maximum rate of Rubisco carboxylation ($J_{\text{max}25}:V_{\text{cmax}25}$; unitless), stomatal conductance (g_{sw} ; $\text{mol m}^{-2} \text{s}^{-1}$), and stomatal limitation (unitless)*

	$V_{\text{cmax}25}$			$J_{\text{max}25}$			$R_{\text{d}25}$			
	df	Coefficient	χ^2	p	Coefficient	χ^2	p	Coefficient	χ^2	p
(Intercept)	-	$4.36 * 10^{+1}$	-	-	$8.30 * 10^{+1}$	-	-	$1.69 * 10^{+0}$	-	-
CO ₂	1	$-7.05 * 10^{+0}$	18.039	<0.001	$-9.11 * 10^{+0}$	6.042	0.014	$4.53 * 10^{-1}$	0.256	0.613
Inoculation (I)	1	$5.87 * 10^{+1}$	98.579	<0.001	$9.62 * 10^{+1}$	85.064	<0.001	$1.04 * 10^{+0}$	3.094	0.079
Fertilization (N)	1	$1.32 * 10^{-1}$	37.053	<0.001	$2.09 * 10^{-1}$	25.356	<0.001	$2.86 * 10^{-3}$	5.965	0.015
CO ₂ *I	1	$-4.65 * 10^{+0}$	0.065	0.799	$7.84 * 10^{-1}$	0.667	0.414	$-5.71 * 10^{-1}$	2.563	0.109
CO ₂ *N	1	$-3.58 * 10^{-2}$	1.758	0.185	$-4.33 * 10^{-2}$	0.742	0.389	$-1.55 * 10^{-3}$	2.675	0.102
I*N	1	$-1.35 * 10^{-1}$	60.394	<0.001	$-2.30 * 10^{-1}$	57.410	<0.001	$-2.84 * 10^{-3}$	12.083	0.001
CO ₂ *I*N	1	$2.73 * 10^{-2}$	0.748	0.387	$3.46 * 10^{-2}$	0.377	0.539	$7.21 * 10^{-4}$	0.244	0.622

127

	$J_{\text{max}25}:V_{\text{cmax}25}$			g_{sw}			Stomatal limitation			
	df	Coefficient	χ^2	p	Coefficient	χ^2	p	Coefficient	χ^2	p
(Intercept)	-	$1.92 * 10^{+0}$	-	-	$1.95 * 10^{-1}$	-	-	$2.12 * 10^{-1}$	-	-
CO ₂	1	$5.71 * 10^{-2}$	92.010	<0.001	$-6.23 * 10^{-2}$	9.718	0.002	$3.91 * 10^{-2}$	0.856	0.355
Inoculation (I)	1	$-1.79 * 10^{-1}$	27.768	<0.001	$1.30 * 10^{-1}$	22.351	<0.001	$7.87 * 10^{-2}$	4.582	0.032
Fertilization (N)	1	$-4.61 * 10^{-4}$	28.147	<0.001	$2.50 * 10^{-4}$	0.066	0.797	$2.60 * 10^{-4}$	32.218	<0.001
CO ₂ *I	1	$8.94 * 10^{-2}$	2.916	0.088	$6.69 * 10^{-2}$	1.810	0.179	$-7.84 * 10^{-2}$	4.093	0.043
CO ₂ *N	1	$2.35 * 10^{-4}$	3.210	0.073	$-8.50 * 10^{-5}$	2.165	0.141	$-1.24 * 10^{-4}$	0.350	0.554
I*N	1	$3.27 * 10^{-4}$	9.607	0.002	$-3.09 * 10^{-4}$	14.696	<0.001	$-1.67 * 10^{-4}$	2.547	0.110
CO ₂ *I*N	1	$-1.66 * 10^{-4}$	1.102	0.294	$-8.89 * 10^{-5}$	0.234	0.629	$1.67 * 10^{-4}$	2.231	0.135

*Significance determined using Type II Wald χ^2 tests ($\alpha=0.05$). P-values less than 0.05 are in bold, while p-values between 0.05 and 0.1 are italicized. Key: df=degrees of freedom; χ^2 =Wald Type II chi-square test statistic.

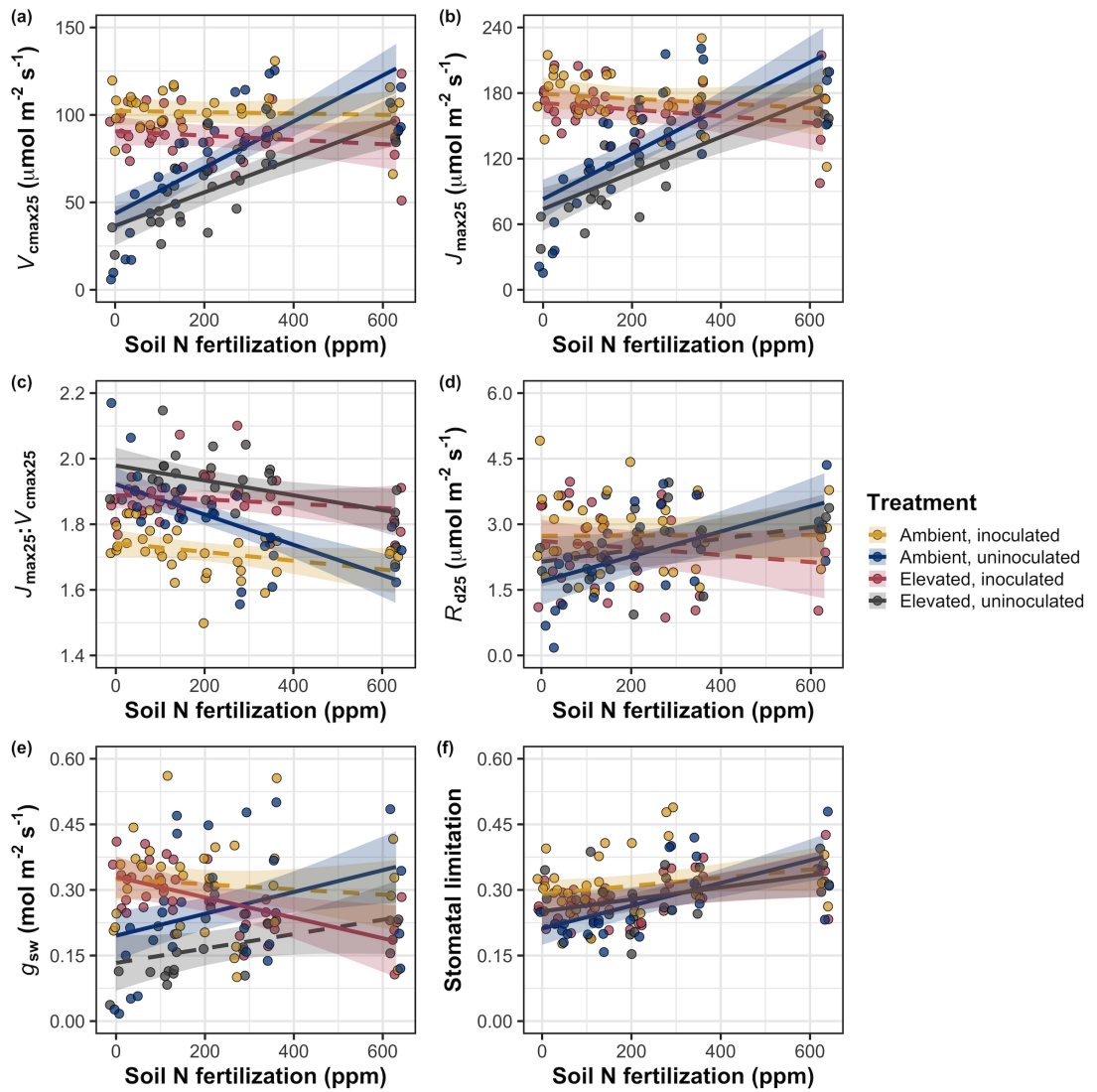


Figure 5.2. Effects of CO_2 , fertilization, and inoculation on maximum rate of Rubisco carboxylation (a), the maximum rate of RuBP regeneration (b), and the ratio of the maximum rate of RuBP regeneration to the maximum rate of Rubisco carboxylation leaf mass per unit leaf area (c), dark respiration (d), stomatal conductance (e), and stomatal limitation (f). Soil nitrogen fertilization is represented on the x-axis in all panels. Colored points and trendlines are as explained in Figure 5.1.

5.3.3 Leaf nitrogen allocation

A relatively stronger reduction in N_{area} than V_{cmax25} or J_{max25} under elevated CO₂ resulted in an 20% and 29% respective increase in ρ_{rubisco} and ρ_{bioe} ($p<0.001$ in both cases; Table 5.3). There was no effect of CO₂ on ρ_{light} ($p=0.700$; Table 5.3), but the increase in ρ_{rubisco} and ρ_{bioe} resulted in 21% greater ρ_{photo} under elevated CO₂ ($p<0.001$; Table 5.3; Fig. 5.3a). Effects of CO₂ on ρ_{rubisco} , ρ_{bioe} , and ρ_{photo} were not modified across the fertilization gradient (CO₂-by-fertilization interaction: $p_{\text{rubisco}}=0.269$, $p_{\text{bioe}}=0.298$, $p_{\text{photo}}=0.281$; Table 5.3). A marginal interaction between inoculation and CO₂ on ρ_{rubisco} and ρ_{photo} (CO₂-by-inoculation interaction: $p_{\text{rubisco}}=0.057$, $p_{\text{photo}}=0.055$; Table 5.3) indicated that the positive effect of inoculation on ρ_{rubisco} and ρ_{photo} ($p<0.001$ in both cases; Table 5.3) was only apparent under ambient CO₂ (Tukey: $p<0.001$ in both cases). Inoculation did not modify the positive effect of elevated CO₂ on ρ_{bioe} (CO₂-by-inoculation interaction: $p=0.122$; Table 5.3) or the null effect of CO₂ on ρ_{bioe} (CO₂-by-inoculation interaction: $p=0.298$; Table 5.3). An interaction between fertilization and inoculation on ρ_{rubisco} , ρ_{bioe} , and ρ_{photo} (fertilization-by-inoculation interaction: $p<0.001$ in all cases; Table 5.3) indicated that the negative effect of increasing fertilization on each trait ($p<0.001$ in all cases; Table 5.3) was only observed in inoculated pots (Tukey: $p<0.001$ in all cases). An additional interaction between fertilization and inoculation on ρ_{light} (fertilization-by-inoculation interaction: $p<0.001$; Table 5.3) indicated a negative effect of increasing fertilization on ρ_{light} in inoculated pots (Tukey: $p=0.041$), but a positive effect of increasing fertilization in uninoculated pots (Tukey: $p<0.001$).

Greater M_{area} under elevated CO₂ resulted in an 133% increase in $\rho_{\text{structure}}$

($p<0.001$; Table 5.3; Fig 5.3b). An interaction between fertilization and CO₂ (CO₂-by-fertilization interaction: $p=0.039$; Table 5.3) indicated that the negative effect of increasing fertilization ($p<0.001$; Table 5.3) on $\rho_{\text{structure}}$ was marginally larger under ambient CO₂ (Tukey: $p=0.055$). A marginal interaction between inoculation and CO₂ (CO₂-by-inoculation interaction: $p=0.057$; Table 5.3) indicated that the positive effect of inoculation on $\rho_{\text{structure}}$ ($p<0.001$; Table 5.3) was only observed under elevated CO₂ (Tukey: $p<0.001$), with no apparent inoculation effect observed under ambient CO₂ (Tukey: $p=0.513$). Finally, an interaction between fertilization and inoculation (fertilization-by-inoculation interaction: $p<0.001$; Table 5.3) indicated that, while increasing fertilization generally increased $\rho_{\text{structure}}$ ($p<0.001$; Table 5.3), this response was larger in uninoculated pots (Tukey: $p=0.001$; Fig. 5.3b).

Table 5.3. Effects of soil nitrogen fertilization, inoculation, and CO₂ on the fraction of leaf nitrogen allocated to Rubisco (ρ_{rubisco} ; gN gN⁻¹), bioenergetics (ρ_{bioe} ; gN gN⁻¹), light harvesting proteins (ρ_{light} ; gN gN⁻¹), photosynthesis (ρ_{photo} ; gN gN⁻¹), and structure ($\rho_{\text{structure}}$; gN gN⁻¹)*

	ρ_{rubisco}			ρ_{bioe}			ρ_{light}			
	df	Coefficient	χ^2	p	Coefficient	χ^2	p	Coefficient	χ^2	p
(Intercept)	-	$2.70 * 10^{-1}$	-	-	$5.26 * 10^{-2}$	-	-	$8.48 * 10^{-3}$	-	-
CO ₂	1	$1.42 * 10^{-1}$	23.510	<0.001	$3.00 * 10^{-2}$	53.899	<0.001	$2.03 * 10^{-3}$	0.149	0.700
Inoculation (I)	1	$1.83 * 10^{-1}$	23.475	<0.001	$2.80 * 10^{-2}$	13.860	<0.001	$2.04 * 10^{-2}$	147.234	<0.001
Fertilization (N)	1	$1.35 * 10^{-4}$	16.609	<0.001	$1.22 * 10^{-5}$	26.827	<0.001	$3.22 * 10^{-5}$	19.378	<0.001
CO ₂ *I	1	$-1.07 * 10^{-1}$	3.629	0.057	$-1.67 * 10^{-2}$	2.390	0.122	$-5.33 * 10^{-3}$	0.684	0.408
CO ₂ *N	1	$-2.16 * 10^{-4}$	1.223	0.269	$-3.59 * 10^{-5}$	1.085	0.298	$-7.01 * 10^{-6}$	0.351	0.553
I*N	1	$-4.26 * 10^{-4}$	20.045	<0.001	$-6.87 * 10^{-5}$	15.458	<0.001	$-4.37 * 10^{-5}$	64.042	<0.001
CO ₂ *I*N	1	$2.50 * 10^{-4}$	3.327	0.068	$4.08 * 10^{-5}$	2.651	0.103	$1.74 * 10^{-5}$	3.735	0.053

	ρ_{photo}			$\rho_{\text{structure}}^a$			
	df	Coefficient	χ^2	p	Coefficient	χ^2	p
(Intercept)	-	$3.32 * 10^{-1}$	-	-	$-2.93 * 10^{+0}$	-	-
CO ₂	1	$1.81 * 10^{-1}$	27.651	<0.001	$8.77 * 10^{-1}$	229.571	<0.001
Inoculation (I)	1	$2.31 * 10^{-1}$	26.238	<0.001	$-2.55 * 10^{-1}$	13.872	<0.001
Fertilization (N)	1	$1.76 * 10^{-4}$	15.899	<0.001	$-1.51 * 10^{-3}$	38.128	<0.001
CO ₂ *I	1	$-1.36 * 10^{-1}$	3.671	0.055	$-2.99 * 10^{-1}$	3.622	0.057
CO ₂ *N	1	$-2.72 * 10^{-4}$	1.163	0.281	$3.14 * 10^{-4}$	4.266	0.039
I*N	1	$-5.37 * 10^{-4}$	21.355	<0.001	$7.00 * 10^{-4}$	11.025	0.001
CO ₂ *I*N	1	$3.29 * 10^{-4}$	4.009	0.045	$4.52 * 10^{-4}$	0.669	0.413

*Significance determined using Type II Wald χ^2 tests ($\alpha=0.05$). P-values less than 0.05 are in bold, while p-values between 0.05 and 0.1 are italicized. A superscript “a” is included after trait labels to indicate if models were fit with natural log transformed response variable. Key: df=degrees of freedom; χ^2 =Wald Type II chi-square test statistic.

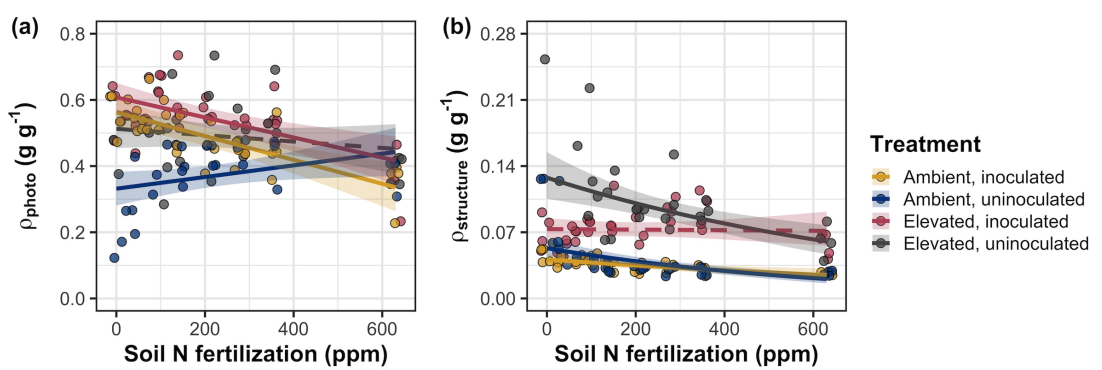


Figure 5.3. Effects of CO_2 , fertilization, and inoculation on the relative fraction of leaf nitrogen allocated to photosynthesis (a) and the fraction of leaf nitrogen allocated to structure (b). Soil nitrogen fertilization is represented on the x-axis in both panels. Colored points and trendlines are as explained in Figure 5.1.

5.3.4 Whole plant traits

Total leaf area and total biomass were 51% and 102% greater under elevated CO₂, respectively ($p<0.001$ in both cases; Table 5.4). The increase in total leaf area and total biomass under elevated CO₂ was enhanced by increasing fertilization (CO₂-by-fertilization interaction: $p<0.001$ in both cases; Table 5.4; Figs. 5.4a, 5.4b) but was not modified across inoculation treatments (CO₂-by-inoculation interaction: $p_{total_leaf_area}=0.151$, $p_{total_biomass}=0.472$; Table 5.4). The positive effect of increasing fertilization on total leaf area and total biomass was modified by inoculation treatment (fertilization-by-inoculation interaction: $p<0.001$ in both cases; Table 5.4), indicating a stronger positive effect of increasing fertilization in uninoculated pots (Tukey: $p_{total_leaf_area}=0.002$, $p_{total_biomass}=0.001$, Figs. 5.4a, 5.4b).

A 62% increase in N_{cost} under elevated CO₂ was modified through a strong three-way interaction between CO₂, fertilization, and inoculation (CO₂-by-inoculation-by-fertilization interaction: $p<0.001$; Table 5.4; Fig. 5.4). This interaction revealed a general negative effect of increasing fertilization on N_{cost} ($p<0.001$; Table 5.4) that was observed in all treatment combinations (Tukey: $p<0.001$ in all cases) except for inoculated pots grown under elevated CO₂ (Tukey: $p=0.779$; Fig. 5.4c). This response also resulted in stronger negative effects of increasing fertilization on N_{cost} in uninoculated pots grown under elevated CO₂ than uninoculated pots grown under ambient CO₂ (Tukey: $p=0.001$) and inoculated pots grown under either ambient CO₂ (Tukey: $p<0.001$) or elevated CO₂ (Tukey: $p<0.001$), while uninoculated pots grown under ambient CO₂ had stronger negative effects of increasing fertilization on N_{cost} than inoculated pots grown under elevated CO₂.

(Tukey: $p=0.002$), but not inoculated pots grown under ambient CO₂ (Tukey: $p=0.216$; Fig. 5.4). The reduction in N_{cost} with increasing fertilization and in uninoculated pots were driven by a stronger positive effect of increasing fertilization on N_{wp} (denominator of N_{cost}) than C_{bg} (numerator of N_{cost}), while the increase in N_{cost} under elevated CO₂ was driven by a stronger positive effect of elevated CO₂ on C_{bg} than N_{wp} (Table 5.4).

Table 5.4. Effects of CO₂, fertilization, and inoculation on total leaf area (cm²), whole plant biomass (g), carbon costs to acquire nitrogen (N_{cost} ; gC gN⁻¹), belowground carbon biomass (C_{bg} ; gC), and whole plant nitrogen biomass (N_{wp} ; gN)^{*}

Total leaf area				Total biomass ^b				N_{cost}				
	df	Coefficient	χ^2		df	Coefficient	χ^2		df	Coefficient	χ^2	p
(Intercept)	-	$8.78 * 10^{+1}$	-	-	-	$9.96 * 10^{-1}$	-	-	-	$8.67 * 10^{+0}$	-	-
CO ₂	1	$3.36 * 10^{+1}$	69.291	<0.001	1	$5.07 * 10^{-1}$	131.477	<0.001	1	$8.75 * 10^{+0}$	88.189	<0.001
Inoculation (I)	1	$1.88 * 10^{+2}$	35.715	<0.001	1	$7.96 * 10^{-1}$	34.264	<0.001	1	$-1.68 * 10^{+0}$	136.343	<0.001
Fertilization (N)	1	$9.35 * 10^{-1}$	274.199	<0.001	1	$3.14 * 10^{-3}$	269.046	<0.001	1	$-8.50 * 10^{-3}$	80.501	<0.001
CO ₂ *I	1	$6.44 * 10^{+1}$	2.064	0.151	1	$-7.69 * 10^{-2}$	0.518	0.472	1	$-8.38 * 10^{+0}$	85.237	<0.001
CO ₂ *N	1	$5.05 * 10^{-1}$	18.655	<0.001	1	$1.61 * 10^{-3}$	16.877	<0.001	1	$-9.17 * 10^{-3}$	1.050	0.306
I*N	1	$-3.84 * 10^{-1}$	10.804	0.001	1	$-1.45 * 10^{-3}$	15.779	<0.001	1	$4.20 * 10^{-3}$	46.489	<0.001
CO ₂ *I*N	1	$-2.97 * 10^{-3}$	<0.001	0.990	1	$-1.14 * 10^{-4}$	0.023	0.880	1	$1.32 * 10^{-2}$	18.125	<0.001
C_{bg}^{a}				N_{wp}^{b}								
	df	Coefficient	χ^2		df	Coefficient	χ^2		df	Coefficient	χ^2	p
(Intercept)	-	$-1.70 * 10^{+0}$	-	-	-	$1.24 * 10^{-1}$	-	-	-	-	-	-
CO ₂	1	$9.21 * 10^{-1}$	84.134	<0.001	1	$-3.41 * 10^{-3}$	23.890	<0.001	-	-	-	-
Inoculation (I)	1	$1.18 * 10^{+0}$	41.030	<0.001	1	$1.68 * 10^{-1}$	134.460	<0.001	-	-	-	-
N fertilization (N)	1	$3.38 * 10^{-3}$	152.248	<0.001	1	$6.69 * 10^{-4}$	529.021	<0.001	-	-	-	-
CO ₂ *I	1	$-6.18 * 10^{-1}$	8.965	0.003	1	$3.68 * 10^{-2}$	1.190	0.275	-	-	-	-
CO ₂ *N	1	$-3.66 * 10^{-5}$	1.188	0.276	1	$1.58 * 10^{-4}$	5.915	0.015	-	-	-	-
I*N	1	$-2.22 * 10^{-3}$	22.648	<0.001	1	$-3.20 * 10^{-4}$	55.562	<0.001	-	-	-	-
CO ₂ *I*N	1	$8.09 * 10^{-4}$	1.109	0.292	1	$-7.54 * 10^{-5}$	0.620	0.431	-	-	-	-

*Significance determined using Type II Wald χ^2 tests ($\alpha=0.05$). P-values less than 0.05 are in bold. Superscripts included after trait labels indicate if models were fit with natural log (^a) or square root (^b) transformed response variables. Key: df=degrees of freedom; χ^2 =Wald Type II chi-square test statistic.

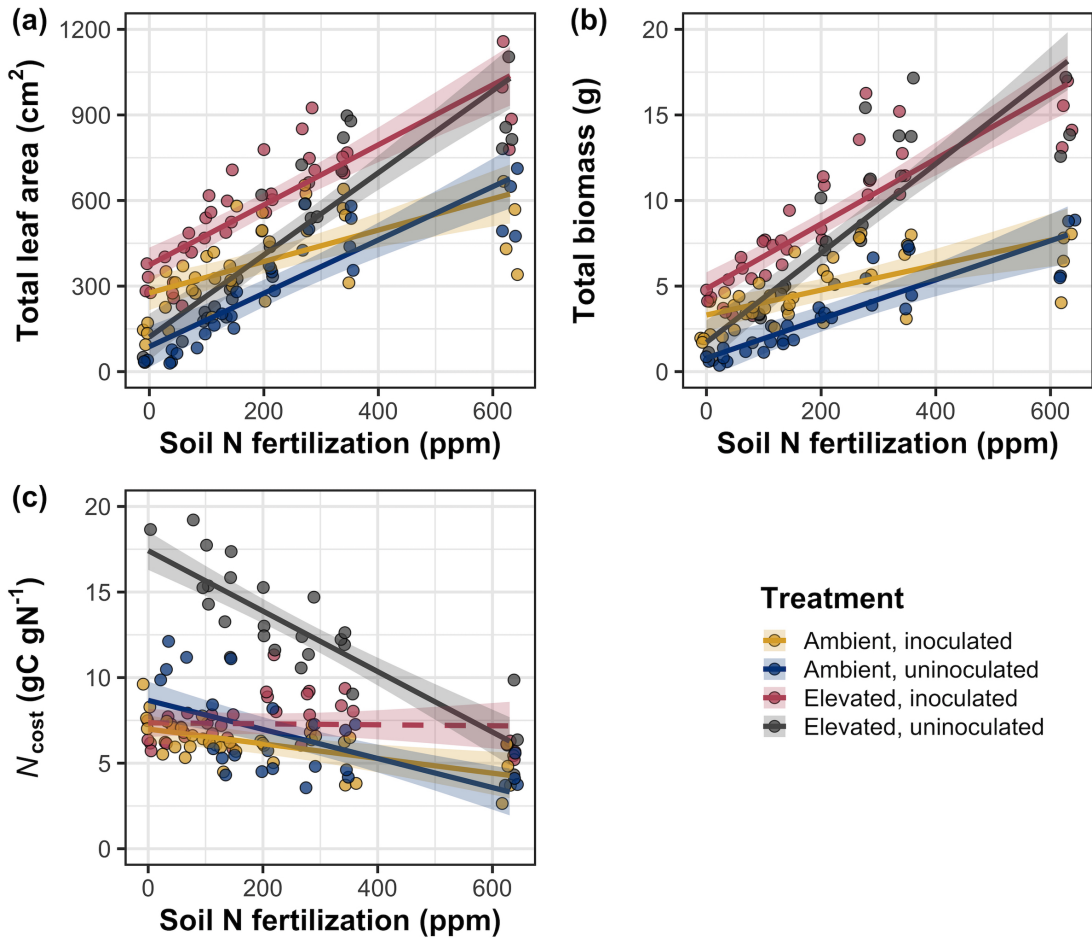


Figure 5.4. Effects of CO_2 , fertilization, and inoculation on total leaf area (a), total biomass (b), and structural carbon costs to acquire nitrogen (c). Soil nitrogen fertilization is represented on the x-axis in all panels. Colored points and trendlines are as explained in Figure 5.1.

5.3.5 Nitrogen fixation

Elevated CO₂ increased nodule biomass by 30% ($p<0.001$; Table 5.5), a pattern that was modified across the fertilization gradient (CO₂-by-fertilization interaction: $p=0.479$; Table 5.5), but not between inoculation treatments (CO₂-by-inoculation interaction: $p=0.404$; Table 5.5). Specifically, the negative effect of increasing fertilization on nodule biomass ($p<0.001$; Table 5.5) was stronger under elevated CO₂ (Tukey: $p<0.001$; Fig. 5.5a). An interaction between fertilization and inoculation (fertilization-by-inoculation interaction: $p<0.001$; Table 5.5) indicated a stronger negative effect of increasing fertilization in inoculated pots (Tukey: $p<0.001$; Fig. 5.5a).

There was no effect of CO₂ treatment on nodule: root biomass ($p=0.767$; Table 5.5), although an interaction between CO₂ and inoculation (CO₂-by-inoculation interaction: $p<0.001$; Table 5.5) indicated that the positive effect of inoculation on nodule: root biomass ($p<0.001$; Table 5.5) was stronger under ambient CO₂ (3129% increase; Tukey: $p<0.001$) than elevated CO₂ (379% increase; Tukey: $p<0.001$; Fig. 5.5b). The null effect of CO₂ on nodule: root biomass was consistently observed across the fertilization gradient (CO₂-by-fertilization interaction: $p=0.183$; Table 5.5; Fig. 5.5b). An interaction between fertilization and inoculation (fertilization-by-inoculation interaction: $p<0.001$; Table 5.5) indicated that the negative effect of increasing fertilization on nodule: root biomass ($p<0.001$; Table 5.5) was stronger in inoculated pots (Tukey: $p<0.001$; Fig. 5.5b).

There was no effect of CO₂ treatment on %N_{dfa} ($p=0.472$; Table 5.5), a pattern that was not modified by inoculation (CO₂-by-inoculation interaction: $p=0.156$; Table 5.5) or fertilization (CO₂-by-fertilization interaction: $p=0.099$;

Table 5.5). An interaction between fertilization and inoculation (fertilization-by-inoculation interaction: $p<0.001$; Table 5.5) indicated that the negative effect of increasing fertilization on $\%N_{dfa}$ ($p<0.001$; Table 5.5) was only observed in inoculated pots (Tukey: $p<0.001$; Fig. 5.5c).

Table 5.5. Effects of CO₂, fertilization, and inoculation on root nodule biomass (g), plant investments in symbiotic nitrogen fixation (unitless), and percent nitrogen fixed from the atmosphere (%N_{dfa}; unitless)*

	Root nodule biomass ^b			Root nodule: root biomass ^b			%N _{dfa} ^b			
	df	Coefficient	χ^2	p	Coefficient	χ^2	p	Coefficient	χ^2	p
(Intercept)	-	$9.41 * 10^{-3}$	-	-	$1.33 * 10^{-2}$	-	-	$7.48 * 10^{-1}$	-	-
CO ₂	1	$1.20 * 10^{-1}$	19.258	<0.001	$9.94 * 10^{-2}$	0.087	0.768	$-1.00 * 10^{-1}$	0.518	0.472
Inoculation (I)	1	$5.74 * 10^{-1}$	755.020	<0.001	$5.40 * 10^{-1}$	903.691	<0.001	$9.01 * 10^{+0}$	955.570	<0.001
Fertilization (N)	1	$7.71 * 10^{-6}$	84.376	<0.001	$-5.99 * 10^{-6}$	258.099	<0.001	$3.64 * 10^{-4}$	292.938	<0.001
CO ₂ *I	1	$-4.68 * 10^{-2}$	0.950	0.330	$-1.38 * 10^{-1}$	20.614	<0.001	$-1.44 * 10^{-1}$	2.010	0.156
CO ₂ *N	1	$-1.59 * 10^{-4}$	2.106	0.147	$-1.73 * 10^{-4}$	1.773	0.183	$-6.21 * 10^{-5}$	2.716	0.099
I*N	1	$-5.82 * 10^{-4}$	44.622	<0.001	$-7.45 * 10^{-4}$	133.918	<0.001	$-1.58 * 10^{-2}$	231.290	<0.001
CO ₂ *I*N	1	$7.26 * 10^{-5}$	0.196	0.658	$1.76 * 10^{-4}$	2.359	0.125	$2.77 * 10^{-3}$	2.119	0.145

*Significance determined using Type II Wald χ^2 tests ($\alpha=0.05$). P-values less than 0.05 are in bold, while p-values between 0.05 and 0.1 are italicized. Superscript letters indicate model coefficients fit to square-root (^b) transformed data. Key: df=degrees of freedom; χ^2 =Wald Type II chi-square test statistic.

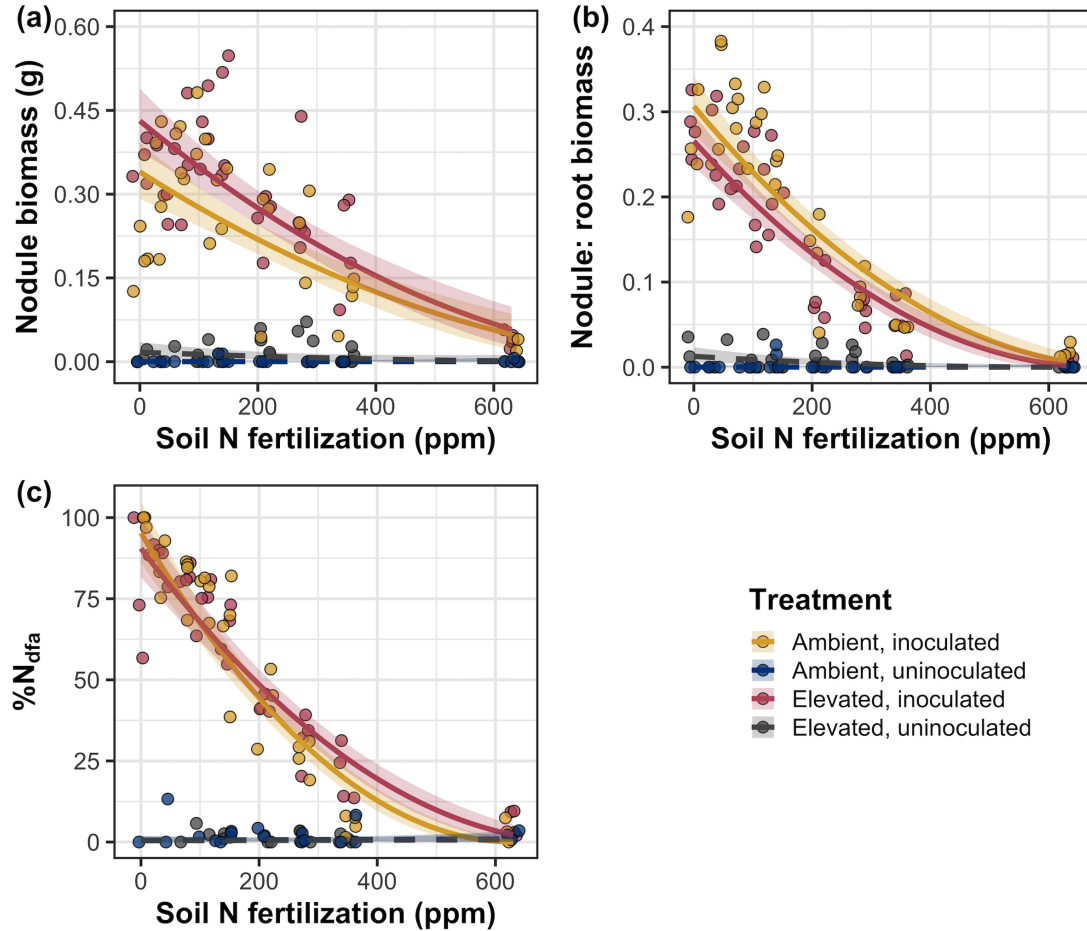


Figure 5.5. Effects of CO₂, fertilization, and inoculation on nodule biomass (a), nodule biomass: root biomass (b), and percent nitrogen fixed from the atmosphere (c). Soil nitrogen fertilization is represented on the x-axis. Colored points and trendlines are as explained in Figure 5.1. Curvilinear trendlines occur as a result of back-transforming models where response variables received either a natural log or square root transformation prior to fitting.

5.4 Discussion

In this study, I determined leaf and whole plant responses of 7-week *G. max* seedlings grown under two CO₂ concentrations, two inoculation treatments, and nine soil nitrogen fertilization treatments in a full-factorial growth chamber experiment. In support of hypotheses and patterns expected from optimal coordination theory, elevated CO₂ reduced N_{area} , V_{cmax25} , and J_{max25} . The relatively stronger reduction in V_{cmax25} than J_{max25} under elevated CO₂ resulted in an increase in $J_{\text{max25}}:V_{\text{cmax25}}$ under elevated CO₂. Reduced V_{cmax25} and J_{max25} under elevated CO₂ was similar across fertilization and inoculation treatments, indicating that leaf responses to CO₂ were not associated with nitrogen availability. Interestingly, results indicate that elevated CO₂ increased the fraction of leaf nitrogen allocated to photosynthesis and structure, leading to an increase in nitrogen use efficiency under elevated CO₂ despite the apparent reduction in N_{area} , V_{cmax25} , and J_{max25} .

Downregulated leaf biochemical process rates under elevated CO₂ corresponded with strong increases in total leaf area and total biomass. Increases in whole plant growth under elevated CO₂ were generally enhanced with increasing fertilization and were negatively related to structural carbon costs to acquire nitrogen. Inoculation generally did not modify whole plant responses to elevated CO₂ across the fertilization gradient, likely due to a strong reduction in root nodulation with increasing fertilization. However, strong positive effects of inoculation on whole plant growth were observed under low fertilization, consistent with hypotheses. Overall, observed leaf and whole plant responses to CO₂ support hypotheses and patterns expected from photosynthetic least-cost theory, showing that leaf responses to CO₂ were decoupled from soil nitrogen availability and abil-

ity to acquire nitrogen via symbiotic nitrogen fixation. Instead, leaf responses to CO₂ were driven by optimal resource investment to photosynthetic capacity, where optimal resource investment to photosynthetic capacity may have maximized nitrogen allocation to structures that support whole plant growth.

Elevated CO₂ reduced N_{area} , V_{cmax25} , J_{max25} , and stomatal conductance by 29%, 16%, 10%, and 20%, respectively. The larger reduction in V_{cmax25} than J_{max25} led to an 8% increase in $J_{\text{max25}}:V_{\text{cmax25}}$, while the larger reduction in N_{area} than V_{cmax25} resulted in a 21% increase in the fraction of leaf nitrogen allocated to photosynthesis under elevated CO₂. These acclimation responses are directionally consistent with previous studies that have investigated or reviewed leaf acclimation responses to CO₂ (Drake et al. 1997; Makino et al. 1997; Ainsworth et al. 2002; Ainsworth and Long 2005; Ainsworth and Rogers 2007; Smith and Dukes 2013; Smith and Keenan 2020; Poorter et al. 2022), and follow patterns expected from photosynthetic least-cost theory (Wright et al. 2003; Prentice et al. 2014; Smith et al. 2019; Smith and Keenan 2020). Together, increased $J_{\text{max25}}:V_{\text{cmax25}}$ and the fraction of leaf nitrogen allocated to photosynthesis under elevated CO₂ provide strong support for the idea that leaves reduced V_{cmax25} to allow net photosynthesis rates to become equally co-limited by Rubisco carboxylation and RuBP regeneration (Chen et al. 1993; Maire et al. 2012).

Increasing fertilization and inoculation induced strong positive effects on N_{area} , V_{cmax25} , J_{max25} . The positive effect of increasing fertilization on N_{area} was enhanced under ambient CO₂, which, paired with the reduction N_{area} under elevated CO₂, resulted in a stronger reduction in N_{area} under elevated CO₂ with increasing fertilization and in inoculated pots. These patterns suggest that N_{area}

responses to CO₂ were at least partially dependent on soil nitrogen fertilization and nitrogen acquisition strategy. However, increased fractions of leaf nitrogen allocated to Rubisco, bioenergetics, or photosynthesis under elevated CO₂ were not modified across the fertilization gradient and was only marginally enhanced in inoculated pots. These patterns suggest that increasing soil nitrogen fertilization and inoculation did not change relative nutrient investment in photosynthetic tissues, supporting the idea that photosynthetic responses to CO₂ were decoupled from soil nitrogen availability.

Leaf acclimation responses to elevated CO₂ corresponded with a 62% and 100% increase in total leaf area and total biomass, respectively. Increases in total leaf area and total biomass under elevated CO₂ corresponded with generally larger structural carbon costs to acquire nitrogen, a pattern driven by an increase in belowground carbon biomass and reduction in whole plant nitrogen biomass. This result suggests that elevated CO₂ reduces plant nitrogen uptake efficiency, which does not explain why plants grown under elevated CO₂ generally had higher biomass and total leaf area, unless growth stimulations under elevated CO₂ were driven by reductions in per-tissue nitrogen demand (Dong et al. 2022). Interestingly, strong negative effects of increasing fertilization on structural carbon costs to acquire nitrogen, which were generally similar between CO₂ concentrations, were driven by stronger increases in whole plant nitrogen biomass than belowground carbon biomass. This response allowed plants to increase nitrogen uptake efficiency with increasing fertilization, providing a possible mechanism that explains why increasing fertilization increased the positive effect of elevated CO₂ on whole plant growth.

Interestingly, results indicate that increased total leaf area and whole plant growth under elevated CO₂ was not modified by inoculation despite an apparent general negative effect of inoculation on N_{cost} . This response could have been due to the strong negative effect of increasing fertilization on nodulation, which may have masked any effect of inoculation treatments in high fertilization treatments. Reductions in nodulation with increasing fertilization are commonly observed patterns that allow species optimize nitrogen uptake efficiency as costs to acquire nitrogen via direct uptake become more similar (Gibson and Harper 1985; Rastetter et al. 2001). In this study, pairwise comparisons indicated strong positive effects of inoculation on total leaf area and total biomass (158% increase in total leaf area, 119% increase in total biomass) under elevated CO₂ at 0 ppm N ($p<0.05$ in both cases), but no observable inoculation effect on total leaf area or total biomass under elevated CO₂ at 350 ppm N or 630 ppm N ($p>0.05$ in both cases). While these responses did not generally differ from those observed under ambient CO₂, they do confirm the hypothesis that positive effects of inoculation on whole plant growth responses to elevated CO₂ would decrease with increasing fertilization. These results also support the paradigm that symbiotic nitrogen fixation is a nutrient acquisition strategy that may allow plants who sustain such symbioses to have competitive advantages for resources than species not capable of forming such symbioses (Menge et al. 2008; Rastetter et al. 2001).

Combined, results reported here suggest that soil nitrogen availability plays divergent roles in shaping leaf and whole plant acclimation responses to CO₂. Leaf acclimation responses were generally decoupled from fertilization, while whole plant acclimation responses relied heavily on an increase in nitrogen uptake ef-

ficiency and consequent reduction in costs of acquiring nitrogen associated with increasing fertilization. Whole plant responses to CO₂ indicated that fertilization may play a more important role in determining whole plant acclimation responses to CO₂ than nitrogen acquisition strategy, although any inoculation effect was likely masked by the strong reduction in root nodulation with increasing fertilization. These results suggest that plants acclimate to CO₂ in nitrogen-limited systems by minimizing the number of optimally coordinated leaves, and that reductions in leaf nitrogen content allocated to photosynthetic tissue under elevated CO₂ are not driven by changes in soil nitrogen availability as has been previously implied.

Many terrestrial biosphere models predict photosynthetic capacity through plant functional group-specific linear regressions between N_{area} and V_{cmax} (Rogers 2014; Rogers et al. 2017), which assumes that leaf nitrogen-photosynthesis relationships are constant across growing environments. These results build on previous work suggesting that leaf nitrogen-photosynthesis relationships dynamically change across growing environments (Luo et al. 2021; Dong et al. 2022), showing that CO₂ concentration increases the fraction of leaf nitrogen content allocated to photosynthesis independent of fertilization or acquisition strategy. Additionally, increasing fertilization strongly decreased the fraction of leaf nitrogen allocated to photosynthesis, a response that was largely determined by acquisition strategy. Specifically, reductions in the fraction of leaf nitrogen allocated to photosynthesis with increasing fertilization were only observed in inoculated pots that had less finite access to nitrogen, suggesting that constant leaf nitrogen-photosynthesis relationships may only be apparent in environments where nitrogen is limiting.

Terrestrial biosphere models that parameterize photosynthetic capacity through linear relationships between N_{area} and V_{cmax} (Rogers 2014; Rogers et al. 2017) may therefore be overestimating photosynthetic capacity in systems where nitrogen is not as limiting. Such models are also not capable of detecting changes in the fraction of leaf nitrogen allocated to photosynthesis with increasing CO_2 concentration. The inability of models to predict these responses likely contributes to the widespread divergence of model simulations under future environmental scenarios (Friedlingstein et al. 2014; Davies-Barnard et al. 2020), and should therefore be a target for resolving in future generations of terrestrial biosphere models.

These results demonstrate that optimal resource investment to photosynthetic capacity defines leaf acclimation responses to elevated CO_2 , and that these responses were independent of fertilization or inoculation treatment. Current model approaches for simulating photosynthetic responses to CO_2 generally invoke patterns expected from progressive nitrogen limitation, where reductions in N_{area} , and therefore photosynthetic capacity, due to elevated CO_2 are formulated as a function of progressive reductions in soil nitrogen availability. Results reported here contradict this formulation, suggesting that the leaf acclimation response is driven by optimal resource investment to photosynthetic capacity and is independent of soil resource supply. Optimality models that include principles from optimal coordination and photosynthetic least-cost theories (Wang et al. 2017; Stocker et al. 2020; Scott and Smith 2022) are capable of capturing such acclimation responses to CO_2 (Smith and Keenan 2020), suggesting that the implementation of these models may improve the simulation of photosynthetic processes in

terrestrial biosphere models under increasing CO₂ concentrations.

There are two study limitations that must be addressed to contextualize patterns observed in this study. First, restricting the volume of belowground substrate via a potted experiment does not adequately replicate belowground environments of natural systems, and therefore may modify effects of soil resource availability and inoculation on plant nitrogen uptake. This limitation may be particularly relevant if pot size limits whole plant growth (Poorter et al. 2012). I attempted to minimize the extent of pot size limitation experienced in the first experimental chapter while accounting for the expected increase in whole plant growth under elevated CO₂ by using 6-liter pots. Despite attempts to minimize growth limitation imposed by pot volume, fertilization and CO₂ treatments increased the biomass: pot volume ratio such that all treatment combinations to exceed 1 g L⁻¹ biomass: pot volume under high fertilization (Table D3; Fig. D2). The 1 g L⁻¹ biomass: pot volume recommendation from Poorter et al. (2012) was designated to avoid growth limitation imposed by pot volume. However, if pot size limitation indeed limited whole plant growth, then belowground carbon biomass, whole plant nitrogen biomass, and whole plant biomass should each exhibit strong saturation points with increasing fertilization, which was not observed here. Importantly, leaf acclimation responses to CO₂ observed in this study are consistent with findings reported in (Smith and Keenan 2020), who used data from field manipulation experiments that did not have any belowground space limitation.

Second, this study evaluated leaf and whole plant responses to CO₂ in 7-week seedlings. Given the long-term scale of the progressive nitrogen limitation

hypothesis, patterns observed here should be validated in longer-term nitrogen manipulation experiments. Previous work in free air CO₂ enrichment experiments show some support for patterns expected from the progressive nitrogen limitation hypothesis (Reich et al. 2006; Norby et al. 2010), although results are not consistent across experimental sites (Finzi et al. 2006; Moore et al. 2006; Liang et al. 2016) and little data from the field experiments exist that links photosynthetic and whole plant responses to CO₂ across soil nitrogen availability gradients. I found some support for patterns expected by the progressive nitrogen limitation hypothesis, namely the increase in plant nitrogen uptake under elevated CO₂ (Luo et al. 2004), though leaf acclimation responses to CO₂ were strongly indicative of optimal resource investment to photosynthetic capacity as expected from photosynthetic least-cost theory (Prentice et al. 2014; Smith et al. 2019; Smith and Keenan 2020).

This study provides strong evidence suggesting that leaf acclimation responses to elevated CO₂ were independent of soil nitrogen fertilization and ability to acquire nitrogen through symbiotic nitrogen fixation. However, whole plant acclimation responses to CO₂ were dependent on fertilization, where increasing fertilization increased the positive effect of whole plant growth under elevated CO₂. Results also indicate that fertilization played a relatively more important role in modifying whole plant responses to CO₂ than inoculation with symbiotic nitrogen-fixing bacteria, perhaps due to a reduction in nodulation across the fertilization gradient. These patterns support the hypothesis that leaf acclimation responses to CO₂ are driven by optimal resource investment to photosynthetic capacity. These results also build on previous work suggesting that constant leaf

nitrogen-photosynthesis relationships are dynamic and change across growing environments, calling the current formulation of photosynthetic processes used in many terrestrial biosphere models into question.

Chapter 6

Conclusions

The experiments included in this dissertation experimentally test mechanisms that drive patterns expected from photosynthetic least-cost theory across various edaphic and climatic gradients. These experiments provide important empirical data needed to test assumptions made in optimality models that use photosynthetic least-cost frameworks, and are among the first manipulative experiments to show support for patterns expected from theory. Below, I summarize main findings of each chapter, synthesize common patterns observed across experiments, and conclude with a few study ideas that will help refine our understanding of plant nutrient acquisition and allocation responses to environmental change.

In the first experimental chapter, I quantified carbon costs to acquire nitrogen in a species capable of forming associations with symbiotic nitrogen-fixing bacteria (*Glycine max*) and a species not capable of forming such associations (*Gossypium hirsutum*) grown under four soil nitrogen fertilization treatments and four light availability treatments in a full factorial greenhouse experiment. Supporting hypotheses, increasing light availability increased carbon costs to acquire nitrogen in both species due to a larger increase in belowground carbon biomass than whole plant nitrogen biomass. In further support of hypotheses, increasing fertilization decreased carbon costs to acquire nitrogen due to a larger increase in whole plant nitrogen biomass than belowground carbon biomass. Root nodulation data indicated that *G. max* shifted relative carbon allocation from nitrogen fixation to direct uptake with increasing fertilization, which may explain the reduced

responsiveness of *G. max* carbon costs to acquire nitrogen across the fertilization gradient.

Despite evidence that reductions in the response of *G. max* carbon costs to acquire nitrogen to increasing fertilization may have been driven by shifts away from nitrogen fixation with increasing fertilization, I urge caution in assigning causality to the differential response of carbon costs to acquire nitrogen between species. This is because *G. max* and *G. hirsutum* are not phylogenetically related and have different life histories. Differences in life history between the two species limit my ability to assess whether reductions in the negative effect of increasing fertilization on carbon costs to acquire nitrogen in *G. max* were driven by shifts to direct uptake with increasing fertilization. However, these patterns were later confirmed in the fourth experimental chapter, where similar weaker negative effects of increasing fertilization on carbon costs to acquire nitrogen were observed in *G. max* that were inoculated with symbiotic nitrogen-fixing bacteria compared to *G. max* that were left uninoculated across a similar soil nitrogen fertilization gradient.

In the second experimental chapter, I assessed whether changes in soil nitrogen availability or soil pH drove changes in nitrogen-water use tradeoffs. I measured leaf traits of mature upper canopy deciduous trees growing in a nine-year nitrogen-by-sulfur field manipulation experiment, where experimental sulfur additions were added with intent to acidify plots. Following patterns expected from photosynthetic least-cost theory, increasing soil nitrogen availability was associated with increased leaf nitrogen content, but not net photosynthesis, resulting in an increase in photosynthetic nitrogen use efficiency. In further support of theory,

increasing soil nitrogen availability exhibited slight, but insignificant, decreases in leaf $C_i:C_a$ and increases in measures of photosynthetic capacity. Perhaps the strongest evidence for the theory was a strong negative relationship between leaf nitrogen content and leaf $C_i:C_a$, of which increased with increasing soil nitrogen availability through a stronger increase in leaf nitrogen content than leaf $C_i:C_a$.

I found no effect of soil pH on nitrogen-water use tradeoffs aside from a marginal reduction in net photosynthesis rates that marginally reduced photosynthetic nitrogen use efficiency with increasing soil pH. Directionally, reductions in photosynthetic nitrogen use efficiency with increasing soil pH were expected per theory; however, this response was driven by no change in leaf nitrogen content and a reduction in net photosynthesis. Theory predicts that these tradeoffs should be driven by no change in net photosynthesis and an increase in leaf nitrogen content. The general null leaf response to changing soil pH may have been due to experimental treatments directly increased soil nitrogen availability and affected soil pH in opposite patterns, suggesting that soil nitrogen availability may be more important in dictating nitrogen-water use tradeoffs than soil pH per se.

In the third experimental chapter, I quantified variance in leaf nitrogen content across a precipitation and soil resource availability gradient in Texan grasslands. Specifically, I measured area-based leaf nitrogen content, components of area-based leaf nitrogen content (leaf mass per unit leaf area, leaf nitrogen per unit dry biomass), leaf $C_i:C_a$, and the unit cost of acquiring nitrogen relative to water in 504 individuals comprising 52 species. I found that area-based leaf nitrogen content was positively associated with increasing soil nitrogen availability, soil moisture, vapor pressure deficit, and was negatively related to increasing

leaf $C_i:C_a$. Following patterns expected from theory, a path analysis revealed that the positive soil nitrogen-leaf nitrogen relationship was driven by a positive relationship between soil nitrogen availability and the unit cost of acquiring and using nitrogen relative to water, a positive relationship between the unit cost of acquiring and using nitrogen relative to water, and negative relationship between leaf $C_i:C_a$ and leaf mass per unit leaf area. Interestingly, there was no effect of $C_i:C_a$ on leaf nitrogen content per unit dry biomass, indicating that variance in area-based leaf nitrogen content across the environmental gradient was driven by a change in leaf morphology and not leaf chemistry.

In the fourth experimental chapter, I quantified leaf and whole plant responses in *G. max* grown under two atmospheric CO₂ levels, with and without inoculation with *Bradyrhizobium japonicum*, and across nine nitrogen fertilization treatments in a full factorial growth chamber experiment. I found strong evidence that leaf nitrogen content, V_{cmax} , and J_{max} each decreased under elevated CO₂. A stronger reduction in V_{cmax} than J_{max} and stronger decrease in leaf nitrogen content than V_{cmax} or J_{max} suggested that leaves acclimated to elevated CO₂ by optimizing leaf photosynthetic resource use efficiency to achieve optimal coordination. In striking support of my hypotheses, I find that leaf acclimation responses to elevated CO₂ were decoupled from soil nitrogen fertilization and inoculation treatment, despite apparent strong increases in leaf nitrogen content, V_{cmax} , and J_{max} with increasing fertilization and in inoculated pots. These findings contrast the current formulation of photosynthetic processes in terrestrial biosphere models, where many models simulate reductions in leaf nitrogen content under elevated CO₂ as a function of progressive nitrogen limitation.

There are currently two iterations of optimality models that employ the use of patterns expected from photosynthetic least-cost theory, one for C₃ species (Wang et al. 2017; Smith et al. 2019; Stocker et al. 2020) and one more recently developed for C₄ species (Scott and Smith 2022). In both model variants, costs to acquire and use nitrogen relative to water are held constant using a global dataset of $\delta^{13}\text{C}$ (Cornwell et al. 2018). Throughout experiments, I show strong evidence suggesting that costs to acquire and use nitrogen are dynamic and vary predictably across environmental gradients, and that changes in these costs scale to alter leaf nitrogen-water use tradeoffs and acclimation responses to changing environments in ways predicted through photosynthetic least-cost theory. Thus, while optimality model simulations show good agreement with measured data (Smith et al. 2019; Stocker et al. 2020), such models may not be capturing an important source of variability in leaf nitrogen-water use tradeoffs by holding costs of resource use constant across environmental gradients.

First principles of photosynthetic least-cost theory suggest that, in a given environment, plants optimize photosynthesis rates by sacrificing inefficient use of a relatively more abundant (and less costly to acquire) resource for more efficient use of a relatively less abundant (and more costly to acquire) resource. Throughout experimental chapters, I show strong support for these patterns, where increasing soil nitrogen fertilization generally decreased the cost of acquiring nitrogen relative to water, a pattern that scaled to influence leaf nitrogen-water use tradeoffs. I did not find evidence to suggest that soil moisture influenced nitrogen-water use tradeoffs, though this was due to strong covariation between soil moisture and soil nitrogen availability. Overall, findings across experiments provide em-

pirical validation of photosynthetic least-cost theory needed to further develop optimality models and eventually implement such models in terrestrial biosphere model products. Many terrestrial biosphere model products do not include robust frameworks for simulating acclimation responses to changing environmental conditions (Smith and Dukes 2013), and empirical findings shown here provide some support that optimality models that use photosynthetic least-cost theory predictions may improve the ability of terrestrial biosphere models to accurately simulate photosynthetic processes.

Many terrestrial biosphere models predict photosynthetic capacity through plant functional group-specific linear regressions between area-based leaf nitrogen content and V_{cmax} (Rogers 2014; Rogers et al. 2017), which assumes that leaf nitrogen-photosynthesis relationships are constant across growing environments. I found constant leaf nitrogen-photosynthesis relationships with increasing soil nitrogen availability in the nitrogen-by-sulfur field manipulation experiment. However, results from the CO₂-by-nitrogen-by-inoculation manipulation experiment indicated that leaf nitrogen-photosynthesis responses to soil nitrogen availability were dependent on whether nitrogen was limiting. Further investigation regarding the effect of soil nitrogen availability in modifying leaf nitrogen-photosynthesis relationships is warranted to better understand the generality of leaf nitrogen photosynthesis relationships across environmental gradients. However, findings from these experiments suggest that representing photosynthetic processes through positive relationships between soil nitrogen availability, leaf nitrogen, and photosynthetic capacity may contribute to erroneous errors in model simulations and may explain the high degree of divergence in simulated processes across terrestrial bio-

sphere models (Friedlingstein et al. 2014; Davies-Barnard et al. 2020).

The experiments included in this dissertation have provided a strong foundation for me to continue growing as a plant physiological ecologist. I envision five primary avenues for future research that build on the work presented here, which are briefly summarized below:

1. Manipulative and environmental gradient experiments included here were designed to provide empirical data needed to test photosynthetic least-cost theory assumptions. While results included in this dissertation show similar directional responses as those predicted by photosynthetic least-cost theory, they do not address whether these patterns exhibit similar magnitudes as those predicted by optimality models that use photosynthetic least-cost principles. Thus, a clear future direction of these experiments would be to conduct model-data comparisons using data collected here (or similar experiments) to compare against optimality model simulations.
2. Experiments included here explicitly quantify effects of symbiotic nitrogen fixation on carbon costs to acquire nitrogen, nitrogen-water use tradeoffs, and leaf nitrogen-photosynthesis relationships. However, carbon costs to acquire nitrogen also vary in species that associate with different mycorrhizal types (Brzostek et al. 2014; Terrer et al. 2018), and dominant mycorrhizal type in an ecosystem has been shown to determine net biogeochemical cycle dynamics in deciduous forests of the northeastern United States (Phillips et al. 2013). Thus, future work should consider conducting similar experiments while manipulating mycorrhizal association to better understand how mycorrhizal symbioses modify leaf and whole plant acclimation responses to

changing environments.

3. Recent work indicates a high degree of variance in simulated symbiotic nitrogen fixation rates across terrestrial biosphere models (Meyerholt et al. 2016; Davies-Barnard et al. 2020), perhaps due to nitrogen fixation rates that are implemented across terrestrial biosphere models as a function of temperature (Houlton et al. 2008). While energetic costs of nitrogen fixation are dependent on temperature, I show that structural carbon costs to acquire nitrogen via symbiotic nitrogen fixation are driven by factors that influence demand to acquire nitrogen (i.e. CO₂, light) and are modified by soil nitrogen supply. The light-by-nitrogen greenhouse experiment was published in *Journal of Experimental Botany*, and a reviewer encouraged future work to include a model-data comparison comparing structural carbon costs to acquire nitrogen measured in the experiment to carbon costs to acquire nitrogen simulated by the FUN biogeochemical model (Fisher et al. 2010; Brzostek et al. 2014; Allen et al. 2020). Conveniently, FUN calculates carbon costs to acquire nitrogen following the same calculation used in the first and fourth experimental chapter. Conducting such a model-data comparison would be a useful step toward identifying biases in the FUN biogeochemical model, which is currently coupled to several terrestrial biosphere models (Clark et al. 2011; Shi et al. 2016; Lawrence et al. 2019; Davies-Barnard et al. 2020).
4. Carbon costs to acquire nitrogen relative to water were quantified at the leaf level as a function of δ¹³C and vapor pressure deficit, while structural carbon costs to acquire nitrogen were quantified at the whole plant level

as the ratio of belowground carbon allocation per unit whole plant nitrogen biomass. As increasing soil nitrogen availability decreases both leaf and whole plant estimates of costs to acquire and use nitrogen, one might expect leaf and whole plant carbon cost to acquire nitrogen estimates to covary. Future work should consider investigating if leaf and whole plant estimates of carbon costs to acquire nitrogen covary and evaluate whether environmental conditions (or species acquisition strategy) modifies any of this possible covariance. Strong covariance between leaf and whole plant costs of nitrogen acquisition could be a possible avenue to implement frameworks for allowing costs of nitrogen acquisition to vary in optimality models, as the FUN model calculates carbon costs of nitrogen acquisition at the whole plant level.

5. While experiments included here target effects of soil nitrogen availability on carbon costs to acquire nitrogen and associated leaf nitrogen-water use tradeoffs, photosynthetic least-cost theory predicts that plants acclimate their photosynthetic processes by minimizing the summed cost of nutrient (not just nitrogen) and water use. Therefore, the theory would predict similar leaf acclimation responses across soil phosphorus or other nutrient availability gradients. Recent iterations of the FUN biogeochemical cycle includes a framework for determining the carbon and nitrogen cost of acquiring and using phosphorus, which similarly varies in species with different nutrient acquisition strategies (Allen et al. 2020). The implementation of this model in a terrestrial biosphere model (E3SM) was also recently shown to improve model performance of ecosystem nutrient limitation (Braghieri et al. 2022). As nitrogen and phosphorus commonly co-limit leaf photo-

synthesis and primary productivity, extending experiments reported here to investigate carbon and nitrogen costs of phosphorus use, and whether these patterns scale to leaf nutrient-water use tradeoffs would be a useful next step in understanding extensions and limitations of photosynthetic least-cost theory.

The experiments included in this dissertation and the proposed experiments summarized above provide a snapshot view of the things that I have learned throughout my time as a graduate student. I am excited to continue learning and growing as a plant ecophysiological, ecologist, and scientist, and look forward to continuing along my journey of investigating nutrient acquisition and allocation responses to global change.

References

- Abrams, M. D. and S. A. Mostoller (1995). Gas exchange, leaf structure and nitrogen in contrasting successional tree species growing in open and under-story sites during a drought. *Tree Physiology* 15(6), 361–370.
- Adams, M. A., T. L. Turnbull, J. I. Sprent, and N. Buchmann (2016). Legumes are different: Leaf nitrogen, photosynthesis, and water use efficiency. *Proceedings of the National Academy of Sciences of the United States of America* 113(15), 4098–4103.
- Ainsworth, E. A., P. A. Davey, C. J. Bernacchi, O. C. Dermody, E. A. Heaton, D. J. Moore, P. B. Morgan, S. L. Naidu, H. S. Y. Ra, X. G. Zhu, P. S. Curtis, and S. P. Long (2002). A meta-analysis of elevated [CO₂] effects on soybean (*Glycine max*) physiology, growth and yield. *Global Change Biology* 8(8), 695–709.
- Ainsworth, E. A. and S. P. Long (2005). What have we learned from 15 years of free-air CO₂ enrichment (FACE)? A meta-analytic review of the responses of photosynthesis, canopy properties and plant production to rising CO₂. *New Phytologist* 165(2), 351–372.
- Ainsworth, E. A. and A. Rogers (2007). The response of photosynthesis and stomatal conductance to rising [CO₂]: mechanisms and environmental interactions. *Plant, Cell and Environment* 30(3), 258–270.
- Alam, S. M. (1999). Nutrient Uptake by Plants Under Stress Conditions. In *Handbook of Plant and Crop Stress* (Second ed.), Chapter 12, pp. 285–313. Marcel Dekker.
- Allen, K., J. B. Fisher, R. P. Phillips, J. S. Powers, and E. R. Brzostek (2020). Modeling the carbon cost of plant nitrogen and phosphorus uptake across temperate and tropical forests. *Frontiers in Forests and Global Change* 3, 1–12.
- Allison, S. D., C. I. Czimczik, and K. K. Treseder (2008). Microbial activity and soil respiration under nitrogen addition in Alaskan boreal forest. *Global Change Biology* 14(5), 1156–1168.

- Andersen, M. K., H. Hauggaard-Nielsen, P. Ambus, and E. S. Jensen (2005). Biomass production, symbiotic nitrogen fixation and inorganic N use in dual and tri-component annual intercrops. *Plant and Soil* 266(1-2), 273–287.
- Andrews, M., E. K. James, J. I. Sprent, R. M. Boddey, E. Gross, and F. B. dos Reis (2011). Nitrogen fixation in legumes and actinorhizal plants in natural ecosystems: Values obtained using ^{15}N natural abundance. *Plant Ecology and Diversity* 4(2-3), 117–130.
- Arndal, M. F., A. Tolver, K. S. Larsen, C. Beier, and I. K. Schmidt (2018). Fine root growth and vertical distribution in response to elevated CO₂, warming and drought in a mixed heathland–grassland. *Ecosystems* 21(1), 15–30.
- Arnone, J. A. (1997). Indices of plant N availability in an alpine grassland under elevated atmospheric CO₂. *Plant and Soil* 190(1), 61–66.
- Arora, V. K., A. Katavouta, R. G. Williams, C. D. Jones, V. Brovkin, P. Friedlingstein, J. Schwinger, L. Bopp, O. Boucher, P. Cadule, M. A. Chamberlain, J. R. Christian, C. Delire, R. A. Fisher, T. Hajima, T. Ilyina, E. Joetzjer, M. Kawamiya, C. D. Koven, J. P. Krasting, R. M. Law, D. M. Lawrence, A. Lenton, K. Lindsay, J. Pongratz, T. Raddatz, R. Séférian, K. Tachiiri, J. F. Tjiputra, A. Wiltshire, T. Wu, and T. Ziehn (2020). Carbon-concentration and carbon-climate feedbacks in CMIP6 models and their comparison to CMIP5 models. *Biogeosciences* 17(16), 4173–4222.
- Bae, K., T. J. Fahey, R. D. Yanai, and M. Fisk (2015). Soil nitrogen availability affects belowground carbon allocation and soil respiration in northern hardwood forests of New Hampshire. *Ecosystems* 18(7), 1179–1191.
- Barber, S. A. (1962). A diffusion and mass-flow concept of soil nutrient availability. *Soil Science* 93(1), 39–49.
- Barnes, J. D., L. Balaguer, E. Manrique, S. Elvira, and A. W. Davison (1992). A reappraisal of the use of DMSO for the extraction and determination of chlorophylls a and b in lichens and higher plants. *Environmental and Experimental Botany* 32(2), 85–100.
- Bates, D., M. Mächler, B. Bolker, and S. Walker (2015). Fitting linear mixed-effects models using lme4. *Journal of Statistical Software* 67(1), 1–48.

- Beaudette, D., J. Skovlin, S. Roeker, and A. Brown (2022). soilDB: Soil Database Interface. *R package version 2.7.7*.
- Bengtson, P., J. Barker, and S. J. Grayston (2012). Evidence of a strong coupling between root exudation, C and N availability, and stimulated SOM decomposition caused by rhizosphere priming effects. *Ecology and Evolution* 2(8), 1843–1852.
- Bernacchi, C. J., E. L. Singsaas, C. Pimentel, A. R. Portis, and S. P. Long (2001). Improved temperature response functions for models of Rubisco-limited photosynthesis. *Plant, Cell and Environment* 24(2), 253–259.
- Bialic-Murphy, L., N. G. Smith, P. Voothuluru, R. M. McElderry, M. D. Roche, S. T. Cassidy, S. N. Kivlin, and S. Kalisz (2021). Invasion-induced root-fungal disruptions alter plant water and nitrogen economies. *Ecology Letters* 24(6), 1145–1156.
- Bloom, A. J., F. S. Chapin, and H. A. Mooney (1985). Resource limitation in plants - an economic analogy. *Annual Review of Ecology and Systematics* 16(1), 363–392.
- Bloomfield, K. J., B. D. Stocker, T. F. Keenan, and I. C. Prentice (2023). Environmental controls on the light use efficiency of terrestrial gross primary production. *Global Change Biology* 29(4), 0–2.
- Bonan, G. B., M. D. Hartman, W. J. Parton, and W. R. Wieder (2013). Evaluating litter decomposition in earth system models with long-term litter bag experiments: an example using the Community Land Model version 4 (CLM4). *Global Change Biology* 19(3), 957–974.
- Bonan, G. B., P. J. Lawrence, K. W. Oleson, S. Levis, M. Jung, M. Reichstein, D. M. Lawrence, and S. C. Swenson (2011). Improving canopy processes in the Community Land Model version 4 (CLM4) using global flux fields empirically inferred from FLUXNET data. *Journal of Geophysical Research* 116(G2), G02014.
- Booth, B. B. B., C. D. Jones, M. Collins, I. J. Totterdell, P. M. Cox, S. Sitch, C. Huntingford, R. A. Betts, G. R. Harris, and J. Lloyd (2012). High sensitivity of future global warming to land carbon cycle processes. *Environmental Research Letters* 7(2), 024002.

- Borer, E. T., W. S. Harpole, P. B. Adler, E. M. Lind, J. L. Orrock, E. W. Seabloom, and M. D. Smith (2014). Finding generality in ecology: A model for globally distributed experiments. *Methods in Ecology and Evolution* 5(1), 65–73.
- Braghiere, R. K., J. B. Fisher, K. Allen, E. Brzostek, M. Shi, X. Yang, D. M. Ricciuto, R. A. Fisher, Q. Zhu, and R. P. Phillips (2022). Modeling global carbon costs of plant nitrogen and phosphorus acquisition. *Journal of Advances in Modeling Earth Systems* 14(8), 1–23.
- Brix, H. (1971). Effects of nitrogen fertilization on photosynthesis and respiration in Douglas-fir. *Forest Science* 17(4), 407–414.
- Brzostek, E. R., J. B. Fisher, and R. P. Phillips (2014). Modeling the carbon cost of plant nitrogen acquisition: Mycorrhizal trade-offs and multipath resistance uptake improve predictions of retranslocation. *Journal of Geophysical Research: Biogeosciences* 119, 1684–1697.
- Bubier, J. L., R. Smith, S. Juutinen, T. R. Moore, R. Minocha, S. Long, and S. Minocha (2011). Effects of nutrient addition on leaf chemistry, morphology, and photosynthetic capacity of three bog shrubs. *Oecologia* 167(2), 355–368.
- Cernusak, L. A., N. Ubierna, K. Winter, J. A. M. Holtum, J. D. Marshall, and G. D. Farquhar (2013). Environmental and physiological determinants of carbon isotope discrimination in terrestrial plants. *New Phytologist* 200(4), 950–965.
- Chen, J.-L., J. F. Reynolds, P. C. Harley, and J. D. Tenhunen (1993). Coordination theory of leaf nitrogen distribution in a canopy. *Oecologia* 93(1), 63–69.
- Clark, D. B., L. M. Mercado, S. Sitch, C. D. Jones, N. Gedney, M. J. Best, M. Pryor, G. G. Rooney, R. L. H. Essery, E. Blyth, O. Boucher, R. J. Harding, C. Huntingford, and P. M. Cox (2011). The Joint UK Land Environment Simulator (JULES), model description. Part 2: Carbon fluxes and vegetation dynamics. *Geoscientific Model Development* 4(3), 701–722.

- Cornwell, W. K., J. H. C. Cornelissen, K. Amatangelo, E. Dorrepael, V. T. Eviner, O. Godoy, S. E. Hobbie, B. Hoorens, H. Kurokawa, N. Pérez-Harguindeguy, H. M. Quested, L. S. Santiago, D. A. Wardle, I. J. Wright, R. Aerts, S. D. Allison, P. van Bodegom, V. Brovkin, A. Chatain, T. V. Callaghan, S. Díaz, E. Garnier, D. E. Gurvich, E. Kazakou, J. A. Klein, J. Read, P. B. Reich, N. A. Soudzilovskaia, M. V. Vaieretti, and M. Westoby (2008). Plant species traits are the predominant control on litter decomposition rates within biomes worldwide. *Ecology Letters* 11(10), 1065–1071.
- Cornwell, W. K., I. J. Wright, J. Turner, V. Maire, M. M. Barbour, L. A. Cernusak, T. E. Dawson, D. S. Ellsworth, G. D. Farquhar, H. Griffiths, C. Keitel, A. Knohl, P. B. Reich, D. G. Williams, R. Bhaskar, J. H. C. Cornelissen, A. Richards, S. Schmidt, F. Valladares, C. Körner, E.-D. Schulze, N. Buchmann, and L. S. Santiago (2018). Climate and soils together regulate photosynthetic carbon isotope discrimination within C₃ plants worldwide. *Global Ecology and Biogeography* 27(9), 1056–1067.
- Cramer, W. and I. C. Prentice (1988). Simulation of regional soil moisture deficits on a European scale. *Norsk Geografisk Tidsskrift - Norwegian Journal of Geography* 42(2-3), 149–151.
- Curtis, P. S. (1996). A meta-analysis of leaf gas exchange and nitrogen in trees grown under elevated carbon dioxide. *Plant, Cell and Environment* 19(2), 127–137.
- Daly, C., M. Halbleib, J. I. Smith, W. P. Gibson, M. K. Doggett, G. H. Taylor, J. Curtis, and P. P. Pasteris (2008). Physiographically sensitive mapping of climatological temperature and precipitation across the conterminous United States. *International Journal of Climatology* 28(15), 2031–2064.
- Davies-Barnard, T., J. Meyerholt, S. Zaehle, P. Friedlingstein, V. Brovkin, Y. Fan, R. A. Fisher, C. D. Jones, H. Lee, D. Peano, B. Smith, D. Wårldin, and A. J. Wiltshire (2020). Nitrogen cycling in CMIP6 land surface models: progress and limitations. *Biogeosciences* 17(20), 5129–5148.
- Davis, T. W., I. C. Prentice, B. D. Stocker, R. T. Thomas, R. J. Whitley, H. Wang, B. J. Evans, A. V. Gallego-Sala, M. T. Sykes, and W. Cramer (2017). Simple process-led algorithms for simulating habitats (SPLASH v.1.0): robust indices of radiation, evapotranspiration and plant-available moisture. *Geoscientific Model Development* 10, 689–708.

- Delaire, M., E. Frak, M. Sigogne, B. Adam, F. Beaujard, and X. Le Roux (2005). Sudden increase in atmospheric CO₂ concentration reveals strong coupling between shoot carbon uptake and root nutrient uptake in young walnut trees. *Tree Physiology* 25(2), 229–235.
- Dijkstra, F. A. and W. Cheng (2008). Increased soil moisture content increases plant N uptake and the abundance of ¹⁵N in plant biomass. *Plant and Soil* 302(1-2), 263–271.
- Doane, T. A. and W. R. Horwáth (2003). Spectrophotometric determination of nitrate with a single reagent. *Analytical Letters* 36(12), 2713–2722.
- Dong, N., I. C. Prentice, B. J. Evans, S. Caddy-Retalic, A. J. Lowe, and I. J. Wright (2017). Leaf nitrogen from first principles: field evidence for adaptive variation with climate. *Biogeosciences* 14(2), 481–495.
- Dong, N., I. C. Prentice, I. J. Wright, B. J. Evans, H. F. Togashi, S. Caddy-Retalic, F. A. McInerney, B. Sparrow, E. Leitch, and A. J. Lowe (2020). Components of leaf trait variation along environmental gradients. *New Phytologist* 228(1), 82–94.
- Dong, N., I. C. Prentice, I. J. Wright, H. Wang, O. K. Atkin, K. J. Bloomfield, T. F. Domingues, S. M. Gleason, V. Maire, Y. Onoda, H. Poorter, and N. G. Smith (2022). Leaf nitrogen from the perspective of optimal plant function. *Journal of Ecology* 110(11), 2585–2602.
- Dong, N., I. J. Wright, J. M. Chen, X. Luo, H. Wang, T. F. Keenan, N. G. Smith, and I. C. Prentice (2022). Rising CO₂ and warming reduce global canopy demand for nitrogen. *New Phytologist* 235(5), 1692–1700.
- Dovrat, G., H. Bakhshian, T. Masci, and E. Sheffer (2020). The nitrogen economic spectrum of legume stoichiometry and fixation strategy. *New Phytologist* 227(2), 365–375.
- Dovrat, G., T. Masci, H. Bakhshian, E. Mayzlish Gati, S. Golan, and E. Sheffer (2018). Drought-adapted plants dramatically downregulate dinitrogen fixation: Evidences from Mediterranean legume shrubs. *Journal of Ecology* 106(4), 1534–1544.

- Drake, B. G., M. A. Gonzàlez-Meler, and S. P. Long (1997). More efficient plants: a consequence of rising atmospheric CO₂? *Annual Review of Plant Biology* 48, 609–639.
- Duursma, R. A. (2015). Plantecophys - An R package for analyzing and modelling leaf gas exchange data. *PLOS ONE* 10(11), e0143346.
- Eamus, D., N. Boulain, J. Cleverly, and D. D. Breshears (2013). Global change-type drought-induced tree mortality: Vapor pressure deficit is more important than temperature per se in causing decline in tree health. *Ecology and Evolution* 3(8), 2711–2729.
- Eastman, B. A., M. B. Adams, E. R. Brzostek, M. B. Burnham, J. E. Carrara, C. Kelly, B. E. McNeil, C. A. Walter, and W. T. Peterjohn (2021). Altered plant carbon partitioning enhanced forest ecosystem carbon storage after 25 years of nitrogen additions. *New Phytologist* 230(4), 1435–1448.
- Ellsworth, D. S. and P. B. Reich (1996). Photosynthesis and leaf nitrogen in five Amazonian tree species during early secondary succession. *Ecology* 77(2), 581–594.
- Espelta, J. M., P. Cortés, M. Mangirón, and J. Retana (2005). Differences in biomass partitioning, leaf nitrogen content, and water use efficiency $\delta^{13}\text{C}$ result in similar performance of seedlings of two Mediterranean oaks with contrasting leaf habit. *Ecoscience* 12(4), 447–454.
- Evans, J. R. (1989). Photosynthesis and nitrogen relationships in leaves of C₃ plants. *Oecologia* 78(1), 9–19.
- Evans, J. R. and V. C. Clarke (2019). The nitrogen cost of photosynthesis. *Journal of Experimental Botany* 70(1), 7–15.
- Evans, J. R. and H. Poorter (2001). Photosynthetic acclimation of plants to growth irradiance: the relative importance of specific leaf area and nitrogen partitioning in maximizing carbon gain. *Plant, Cell and Environment* 24(8), 755–767.
- Evans, J. R. and J. R. Seemann (1989). The allocation of protein nitrogen in the photosynthetic apparatus: costs, consequences, and control. *Photosynthesis* 8, 183–205.

- Exbrayat, J.-F., A. A. Bloom, P. Falloon, A. Ito, T. L. Smallman, and M. Williams (2018). Reliability ensemble averaging of 21st century projections of terrestrial net primary productivity reduces global and regional uncertainties. *Earth System Dynamics* 9(1), 153–165.
- Farquhar, G. D., J. R. Ehleringer, and K. T. Hubick (1989). Carbon isotope discrimination and photosynthesis. *Annual Review of Plant Physiology and Plant Molecular Biology* 40(1), 503–537.
- Farquhar, G. D. and T. D. Sharkey (1982). Stomatal conductance and photosynthesis. *Annual Review of Plant Physiology* 33(1), 317–345.
- Farquhar, G. D., S. von Caemmerer, and J. A. Berry (1980). A biochemical model of photosynthetic CO₂ assimilation in leaves of C₃ species. *Planta* 149(1), 78–90.
- Fay, P. A., S. M. Prober, W. S. Harpole, J. M. H. Knops, J. D. Bakker, E. T. Borer, E. M. Lind, A. S. MacDougall, E. W. Seabloom, P. D. Wragg, P. B. Adler, D. M. Blumenthal, Y. M. Buckley, C. Chu, E. E. Cleland, S. L. Collins, K. F. Davies, G. Du, X. Feng, J. Firn, D. S. Gruner, N. Hagenah, Y. Hautier, R. W. Heckman, V. L. Jin, K. P. Kirkman, J. A. Klein, L. M. Ladwig, Q. Li, R. L. McCulley, B. A. Melbourne, C. E. Mitchell, J. L. Moore, J. W. Morgan, A. C. Risch, M. Schütz, C. J. Stevens, D. A. Wedin, and L. H. Yang (2015). Grassland productivity limited by multiple nutrients. *Nature Plants* 1(7), 15080.
- Field, C. B. and H. A. Mooney (1986). The photosynthesis-nitrogen relationship in wild plants. In T. J. Givnish (Ed.), *On the Economy of Plant Form and Function*, pp. 25–55. Cambridge: Cambridge University Press.
- Finzi, A. C., D. J. P. Moore, E. H. DeLucia, J. Lichter, K. S. Hofmockel, R. B. Jackson, H. S. Kim, R. Matamala, H. R. McCarthy, R. Oren, J. S. Pippen, and W. H. Schlesinger (2006). Progressive nitrogen limitation of ecosystem processes under elevated CO₂ in a warm-temperate forest. *Ecology* 87(1), 15–25.

- Firn, J., J. M. McGree, E. Harvey, H. Flores Moreno, M. Schutz, Y. M. Buckley, E. T. Borer, E. W. Seabloom, K. J. La Pierre, A. M. MacDougall, S. M. Prober, C. J. Stevens, L. L. Sullivan, E. Porter, E. Ladouceur, C. Allen, K. H. Moromizato, J. W. Morgan, W. S. Harpole, Y. Hautier, N. Eisenhauer, J. P. Wright, P. B. Adler, C. A. Arnillas, J. D. Bakker, L. Biederman, A. A. D. Broadbent, C. S. Brown, M. N. Bugalho, M. C. Caldeira, E. E. Cleland, A. Ebeling, P. A. Fay, N. Hagenah, A. R. Kleinhesselink, R. Mitchell, J. L. Moore, C. Nogueira, P. L. Peri, C. Roscher, M. D. Smith, P. D. Wragg, and A. C. Risch (2019). Leaf nutrients, not specific leaf area, are consistent indicators of elevated nutrient inputs. *Nature Ecology and Evolution* 3(3), 400–406.
- Fisher, J. B., S. Sitch, Y. Malhi, R. A. Fisher, C. Huntingford, and S.-Y. Tan (2010). Carbon cost of plant nitrogen acquisition: A mechanistic, globally applicable model of plant nitrogen uptake, retranslocation, and fixation. *Global Biogeochemical Cycles* 24(1), 1–17.
- Fox, J. and S. Weisberg (2019). *An R companion to applied regression* (Third ed.). Thousand Oaks, California: Sage.
- Franklin, O., R. E. McMurtrie, C. M. Iversen, K. Y. Crous, A. C. Finzi, D. Tissue, D. S. Ellsworth, R. Oren, and R. J. Norby (2009). Forest fine-root production and nitrogen use under elevated CO₂: contrasting responses in evergreen and deciduous trees explained by a common principle. *Global Change Biology* 15(1), 132–144.
- Friedlingstein, P., M. Meinshausen, V. K. Arora, C. D. Jones, A. Anav, S. K. Liddicoat, and R. Knutti (2014). Uncertainties in CMIP5 climate projections due to carbon cycle feedbacks. *Journal of Climate* 27(2), 511–526.
- Friel, C. A. and M. L. Friesen (2019). Legumes modulate allocation to rhizobial nitrogen fixation in response to factorial light and nitrogen manipulation. *Frontiers in Plant Science* 10, 1316.
- Fujikake, H., A. Yamazaki, N. Otake, K. Sueoshi, S. Matsuhashi, T. Ito, C. Mizuniwa, T. Kume, S. Hoshimoto, N.-S. Ishioka, S. Watanabe, A. Osa, T. Sekine, H. Uchida, A. Tsuji, and T. Ohyama (2003). Quick and reversible inhibition of soybean root nodule growth by nitrate involves a decrease in sucrose supply to nodules. *Journal of Experimental Botany* 54(386), 1379–1388.

- Ghannoum, O., J. R. Evans, and S. von Caemmerer (2011). Nitrogen and water use efficiency of C₄ plants. In A. S. Raghavendra and R. F. Sage (Eds.), *C₄ Photosynthesis and Related CO₂ Concentrating Mechanisms*, Chapter 8, pp. 129–146. Springer.
- Ghimire, B., W. J. Riley, C. D. Koven, J. Kattge, A. Rogers, P. B. Reich, and I. J. Wright (2017). A global trait-based approach to estimate leaf nitrogen functional allocation from observations:. *Ecological Applications* 27(5), 1421–1434.
- Giardina, C. P., M. D. Coleman, J. E. Hancock, J. S. King, E. A. Lilleskov, W. M. Loya, K. S. Pregitzer, M. G. Ryan, and C. C. Trettin (2005). The response of belowground carbon allocation in forests to global change. In D. Binkley and O. Manyailo (Eds.), *Tree Species Effects on Soils: Implications for Global Change*, Chapter 7 Volume 55, pp. 119–154. Berlin/Heidelberg: Springer-Verlag.
- Gibson, A. H. and J. E. Harper (1985). Nitrate effect on nodulation of soybean by *Bradyrhizobium japonicum*. *Crop Science* 25(3), 497–501.
- Gill, A. L. and A. C. Finzi (2016). Belowground carbon flux links biogeochemical cycles and resource-use efficiency at the global scale. *Ecology Letters* 19(12), 1419–1428.
- Goll, D. S., V. Brovkin, B. R. Parida, C. H. Reick, J. Kattge, P. B. Reich, P. M. van Bodegom, and Ü. Niinemets (2012). Nutrient limitation reduces land carbon uptake in simulations with a model of combined carbon, nitrogen and phosphorus cycling. *Biogeosciences* 9(3), 3173–3232.
- Gregory, L. M., A. M. McClain, D. M. Kramer, J. D. Pardo, K. E. Smith, O. L. Tessmer, B. J. Walker, L. G. Ziccardi, and T. D. Sharkey (2021, oct). The triose phosphate utilization limitation of photosynthetic rate: Out of global models but important for leaf models. *Plant, Cell and Environment* 44(10), 3223–3226.
- Grossiord, C., T. N. Buckley, L. A. Cernusak, K. A. Novick, B. Poulter, R. T. W. Siegwolf, J. S. Sperry, and N. G. McDowell (2020). Plant responses to rising vapor pressure deficit. *New Phytologist* 226(6), 1550–1566.

- Gulmon, S. L. and C. C. Chu (1981). The effects of light and nitrogen on photosynthesis, leaf characteristics, and dry matter allocation in the chaparral shrub, *Diplacus aurantiacus*. *Oecologia* 49(2), 207–212.
- Gutschick, V. P. (1981). Evolved strategies in nitrogen acquisition by plants. *The American Naturalist* 118(5), 607–637.
- Hallik, L., Ü. Niinemets, and I. J. Wright (2009). Are species shade and drought tolerance reflected in leaf-level structural and functional differentiation in Northern Hemisphere temperate woody flora? *New Phytologist* 184(1), 257–274.
- Harrison, S. P., W. Cramer, O. Franklin, I. C. Prentice, H. Wang, Å. Brännström, H. de Boer, U. Dieckmann, J. Joshi, T. F. Keenan, A. Lavergne, S. Manzoni, G. Mengoli, C. Morfopoulos, J. Peñuelas, S. Pietsch, K. T. Rebel, Y. Ryu, N. G. Smith, B. D. Stocker, and I. J. Wright (2021). Eco-evolutionary optimality as a means to improve vegetation and land-surface models. *New Phytologist* 231(6), 2125–2141.
- Henneron, L., P. Kardol, D. A. Wardle, C. Cros, and S. Fontaine (2020). Rhizosphere control of soil nitrogen cycling: a key component of plant economic strategies. *New Phytologist* 228(4), 1269–1282.
- Hijmans, R. J., R. Bivand, K. Forner, J. Ooms, E. Pebesma, and M. D. Sumner (2022). terra: Spatial data analysis. *R package version 1.7-18*.
- Hikosaka, K. and A. Shigeno (2009). The role of Rubisco and cell walls in the interspecific variation in photosynthetic capacity. *Oecologia* 160(3), 443–451.
- Hoagland, D. R. and D. I. Arnon (1950). The water culture method for growing plants without soil. *California Agricultural Experiment Station* 347(2), 1–32.
- Hobbie, E. A. (2006). Carbon allocation to ectomycorrhizal fungi correlates with belowground allocation in culture studies. *Ecology* 87(3), 563–569.
- Hobbie, E. A. and J. E. Hobbie (2008). Natural abundance of ^{15}N in nitrogen-limited forests and tundra can estimate nitrogen cycling through mycorrhizal fungi: a review. *Ecosystems* 11(5), 815–830.

- Hoek, T. A., K. Axelrod, T. Biancalani, E. A. Yurtsev, J. Liu, and J. Gore (2016). Resource availability modulates the cooperative and competitive nature of a microbial cross-feeding mutualism. *PLOS Biology* 14(8), e1002540.
- Högberg, M. N., M. J. I. Briones, S. G. Keel, D. B. Metcalfe, C. Campbell, A. J. Midwood, B. Thornton, V. Hurry, S. Linder, T. Näsholm, and P. Högberg (2010). Quantification of effects of season and nitrogen supply on tree below-ground carbon transfer to ectomycorrhizal fungi and other soil organisms in a boreal pine forest. *New Phytologist* 187(2), 485–493.
- Högberg, P., M. N. Högberg, S. G. Göttlicher, N. R. Betson, S. G. Keel, D. B. Metcalfe, C. Campbell, A. Schindlbacher, V. Hurry, T. Lundmark, S. Linder, and T. Näsholm (2008). High temporal resolution tracing of photosynthate carbon from the tree canopy to forest soil microorganisms. *New Phytologist* 177(1), 220–228.
- Houlton, B. Z., Y.-P. Wang, P. M. Vitousek, and C. B. Field (2008). A unifying framework for dinitrogen fixation in the terrestrial biosphere. *Nature* 454(7202), 327–330.
- Huber, M. L., R. A. Perkins, A. Laesecke, D. G. Friend, J. V. Sengers, M. J. Assael, I. N. Metaxa, E. Vogel, R. Mareš, and K. Miyagawa (2009). New international formulation for the viscosity of H₂O. *Journal of Physical and Chemical Reference Data* 38(2), 101–125.
- Hungate, B. A., J. S. Dukes, M. R. Shaw, Y. Luo, and C. B. Field (2003). Nitrogen and climate change. *Science* 302(5650), 1512–1513.
- IPCC (2021). *Climate Change 2021: The Physical Science Basis. Contribution of Working Group I to the Sixth Assessment Report of the Intergovernmental Panel on Climate Change*, Volume In Press. Cambridge, United Kingdom and New York, NY, USA: Cambridge University Press.
- Johnson, N. C., J. H. Graham, and F. A. Smith (1997). Functioning of mycorrhizal associations along the mutualism-parasitism continuum. *New Phytologist* 135(4), 575–585.
- Kachurina, O. M., H. Zhang, W. R. Raun, and E. G. Krenzer (2000). Simultaneous determination of soil aluminum, ammonium- and nitrate- nitrogen using 1 M potassium chloride. *Communications in Soil Science and Plant Analysis* 31(7-8), 893–903.

- Kaiser, C., M. R. Kilburn, P. L. Clode, L. Fuchslueger, M. Koranda, J. B. Cliff, Z. M. Solaiman, and D. V. Murphy (2015). Exploring the transfer of recent plant photosynthates to soil microbes: mycorrhizal pathway vs direct root exudation. *New Phytologist* 205(4), 1537–1551.
- Katabuchi, M. (2015). LeafArea: An R package for rapid digital analysis of leaf area. *Ecological Research* 30(6), 1073–1077.
- Kattge, J. and W. Knorr (2007). Temperature acclimation in a biochemical model of photosynthesis: a reanalysis of data from 36 species. *Plant, Cell and Environment* 30(9), 1176–1190.
- Kattge, J., W. Knorr, T. Raddatz, and C. Wirth (2009). Quantifying photosynthetic capacity and its relationship to leaf nitrogen content for global-scale terrestrial biosphere models. *Global Change Biology* 15(4), 976–991.
- Kayler, Z., A. Gessler, and N. Buchmann (2010). What is the speed of link between aboveground and belowground processes? *New Phytologist* 187(4), 885–888.
- Kayler, Z., C. Keitel, K. Jansen, and A. Gessler (2017). Experimental evidence of two mechanisms coupling leaf-level C assimilation to rhizosphere CO₂ release. *Environmental and Experimental Botany* 135, 21–26.
- Keeling, C. D., W. G. Mook, and P. P. Tans (1979, jan). Recent trends in the ¹³C:¹²C ratio of atmospheric carbon dioxide. *Nature* 277(5692), 121–123.
- Keeney, D. R. and D. W. Nelson (1983). Nitrogen—Inorganic Forms. In A. L. Page (Ed.), *Methods of Soil Analysis* (Second ed.), Chapter 33, pp. 643–698. Madison, WI, USA: ASA and SSSA.
- Kenward, M. G. and J. H. Roger (1997). Small sample inference for fixed effects from restricted maximum likelihood. *Biometrics* 53(3), 983.
- Knapp, A. K., M. L. Avolio, C. Beier, C. J. W. Carroll, S. L. Collins, J. S. Dukes, L. H. Fraser, R. J. Griffin-Nolan, D. L. Hoover, A. Jentsch, M. E. Loik, R. P. Phillips, A. K. Post, O. E. Sala, I. J. Slette, L. Yahdjian, and M. D. Smith (2017). Pushing precipitation to the extremes in distributed experiments: recommendations for simulating wet and dry years. *Global Change Biology* 23(5), 1774–1782.

- Knorr, W. (2000). Annual and interannual CO₂ exchanges of the terrestrial biosphere: process-based simulations and uncertainties. *Global Ecology and Biogeography* 9(3), 225–252.
- Knorr, W. and M. Heimann (2001). Uncertainties in global terrestrial biosphere modeling: 1. A comprehensive sensitivity analysis with a new photosynthesis and energy balance scheme. *Global Biogeochemical Cycles* 15(1), 207–225.
- Kulmatiski, A., P. B. Adler, J. M. Stark, and A. T. Tredennick (2017). Water and nitrogen uptake are better associated with resource availability than root biomass. *Ecosphere* 8(3), e01738.
- Lavergne, A., D. Sandoval, V. J. Hare, H. Graven, and I. C. Prentice (2020). Impacts of soil water stress on the acclimated stomatal limitation of photosynthesis: Insights from stable carbon isotope data. *Global Change Biology* 26(12), 7158–7172.
- Lawrence, D. M., R. A. Fisher, C. D. Koven, K. W. Oleson, S. C. Swenson, G. B. Bonan, N. Collier, B. Ghimire, L. Kampenhout, D. Kennedy, E. Kluzek, P. J. Lawrence, F. Li, H. Li, D. L. Lombardozzi, W. J. Riley, W. J. Sacks, M. Shi, M. Vertenstein, W. R. Wieder, C. Xu, A. A. Ali, A. M. Badger, G. Bisht, M. Broeke, M. A. Brunke, S. P. Burns, J. Buzan, M. Clark, A. Craig, K. M. Dahlin, B. Drewniak, J. B. Fisher, M. Flanner, A. M. Fox, P. Gentine, F. M. Hoffman, G. Keppel-Aleks, R. Knox, S. Kumar, J. Lenaerts, L. R. Leung, W. H. Lipscomb, Y. Lu, A. Pandey, J. D. Pelletier, J. Perket, J. T. Randerson, D. M. Ricciuto, B. M. Sanderson, A. Slater, Z. M. Subin, J. Tang, R. Q. Thomas, M. Val Martin, and X. Zeng (2019). The Community Land Model Version 5: description of new features, benchmarking, and impact of forcing uncertainty. *Journal of Advances in Modeling Earth Systems* 11(12), 4245–4287.
- LeBauer, D. S. and K. K. Treseder (2008). Nitrogen limitation of net primary productivity in terrestrial ecosystems is globally distributed. *Ecology* 89(2), 371–379.
- Lefcheck, J. S. (2016). piecewiseSEM: Piecewise structural equation modelling in R for ecology, evolution, and systematics. *Methods in Ecology and Evolution* 7(5), 573–579.

- Lenth, R., H. Singmann, J. Love, P. Buerkner, and M. Herve (2019). emmeans: Estimated marginal means, aka least-squares means. *R package version 1.8.5.*
- Li, W., H. Zhang, G. Huang, R. Liu, H. Wu, C. Zhao, and N. G. McDowell (2020). Effects of nitrogen enrichment on tree carbon allocation: A global synthesis. *Global Ecology and Biogeography* 29(3), 573–589.
- Liang, J., X. Qi, L. Souza, and Y. Luo (2016). Processes regulating progressive nitrogen limitation under elevated carbon dioxide: a meta-analysis. *Biogeosciences* 13(9), 2689–2699.
- Liang, X., T. Zhang, X. Lu, D. S. Ellsworth, H. BassiriRad, C. You, D. Wang, P. He, Q. Deng, H. Liu, J. Mo, and Q. Ye (2020). Global response patterns of plant photosynthesis to nitrogen addition: A meta-analysis. *Global Change Biology* 26(6), 3585–3600.
- López, J., D. A. Way, and W. Sadok (2021). Systemic effects of rising atmospheric vapor pressure deficit on plant physiology and productivity. *Global Change Biology* 27(9), 1704–1720.
- Lu, J., J. Yang, C. Keitel, L. Yin, P. Wang, W. Cheng, and F. A. Dijkstra (2022). Belowground carbon efficiency for nitrogen and phosphorus acquisition varies between *Lolium perenne* and *Trifolium repens* and depends on phosphorus fertilization. *Frontiers in Plant Science* 13, 1–9.
- Luo, X., T. F. Keenan, J. M. Chen, H. Croft, I. C. Prentice, N. G. Smith, A. P. Walker, H. Wang, R. Wang, C. Xu, and Y. Zhang (2021). Global variation in the fraction of leaf nitrogen allocated to photosynthesis. *Nature Communications* 12(1), 4866.
- Luo, Y., W. S. Currie, J. S. Dukes, A. C. Finzi, U. A. Hartwig, B. A. Hungate, R. E. McMurtrie, R. Oren, W. J. Parton, D. E. Pataki, R. M. Shaw, D. R. Zak, and C. B. Field (2004). Progressive nitrogen limitation of ecosystem responses to rising atmospheric carbon dioxide. *BioScience* 54(8), 731–739.
- Maire, V., P. Martre, J. Kattge, F. Gastal, G. Esser, S. Fontaine, and J.-F. Soussana (2012). The coordination of leaf photosynthesis links C and N fluxes in C₃ plant species. *PLoS ONE* 7(6), e38345.

- Makino, A. (2003). Rubisco and nitrogen relationships in rice: leaf photosynthesis and plant growth. *Soil Science and Plant Nutrition* 49(3), 319–327.
- Makino, A., M. Harada, T. Sato, H. Nakano, and T. Mae (1997). Growth and N Allocation in Rice Plants under CO₂ Enrichment. *Plant Physiology* 115(1), 199–203.
- Markham, J. H. and C. Zekveld (2007). Nitrogen fixation makes biomass allocation to roots independent of soil nitrogen supply. *Canadian Journal of Botany* (9), 787–793.
- Marschner, H. and B. Dell (1994). Nutrient uptake in mycorrhizal symbiosis. *Plant and Soil* 159(1), 89–102.
- Matamala, R. and W. H. Schlesinger (2000). Effects of elevated atmospheric CO₂ on fine root production and activity in an intact temperate forest ecosystem. *Global Change Biology* 6(8), 967–979.
- Medlyn, B. E., E. Dreyer, D. S. Ellsworth, M. Forstreuter, P. C. Harley, M. U. F. Kirschbaum, X. Le Roux, P. Montpied, J. Strassmeyer, A. Walcroft, K. Wang, and D. Loustau (2002). Temperature response of parameters of a biochemically based model of photosynthesis. II. A review of experimental data. *Plant, Cell and Environment* 25(9), 1167–1179.
- Menge, D. N. L., S. A. Levin, and L. O. Hedin (2008). Evolutionary tradeoffs can select against nitrogen fixation and thereby maintain nitrogen limitation. *Proceedings of the National Academy of Sciences* 105(5), 1573–1578.
- Menne, M. J., I. Durre, R. S. Vose, B. E. Gleason, and T. G. Houston (2012). An overview of the global historical climatology network-daily database. *Journal of Atmospheric and Oceanic Technology* 29(7), 897–910.
- Meyerholt, J., K. Sickel, and S. Zaehle (2020). Ensemble projections elucidate effects of uncertainty in terrestrial nitrogen limitation on future carbon uptake. *Global Change Biology* 26(7), 3978–3996.
- Meyerholt, J., S. Zaehle, and M. J. Smith (2016). Variability of projected terrestrial biosphere responses to elevated levels of atmospheric CO₂ due to uncertainty in biological nitrogen fixation. *Biogeosciences* 13(5), 1491–1518.

- Minocha, R., S. Long, A. H. Magill, J. D. Aber, and W. H. McDowell (2000). Foliar free polyamine and inorganic ion content in relation to soil and soil solution chemistry in two fertilized forest stands at the Harvard Forest, Massachusetts. *Plant and Soil* 222(1-2), 119–137.
- Moore, D. J., S. Aref, R. M. Ho, J. S. Pippen, J. G. Hamilton, and E. H. De Lucia (2006). Annual basal area increment and growth duration of *Pinus taeda* in response to eight years of free-air carbon dioxide enrichment. *Global Change Biology* 12(8), 1367–1377.
- Morgan, J. A., D. E. Pataki, C. Körner, H. Clark, S. J. Del Gross, J. M. Grünzweig, A. K. Knapp, A. R. Mosier, P. C. D. Newton, P. A. Niklaus, J. B. Nippert, R. S. Nowak, W. J. Parton, H. W. Polley, and M. R. Shaw (2004). Water relations in grassland and desert ecosystems exposed to elevated atmospheric CO₂. *Oecologia* 140(1), 11–25.
- Muñoz, N., X. Qi, M. W. Li, M. Xie, Y. Gao, M. Y. Cheung, F. L. Wong, and H.-M. Lam (2016). Improvement in nitrogen fixation capacity could be part of the domestication process in soybean. *Heredity* 117(2), 84–93.
- Nadelhoffer, K. J. and J. W. Raich (1992). Fine root production estimates and belowground carbon allocation in forest ecosystems. *Ecology* 73(4), 1139–1147.
- Niinemets, Ü. and J. D. Tenhunen (1997). A model separating leaf structural and physiological effects on carbon gain along light gradients for the shade-tolerant species *Acer saccharum*. *Plant, Cell and Environment* 20(7), 845–866.
- Norby, R. J., J. Ledford, C. D. Reilly, N. E. Miller, and E. G. O'Neill (2004). Fine-root production dominates response of a deciduous forest to atmospheric CO₂ enrichment. *Proceedings of the National Academy of Sciences* 101(26), 9689–9693.
- Norby, R. J., J. M. Warren, C. M. Iversen, B. E. Medlyn, and R. E. McMurtrie (2010). CO₂ enhancement of forest productivity constrained by limited nitrogen availability. *Proceedings of the National Academy of Sciences* 107(45), 19368–19373.

- Novick, K. A., D. L. Ficklin, P. C. Stoy, C. A. Williams, G. Bohrer, A. C. Oishi, S. A. Papuga, P. D. Blanken, A. Noormets, B. N. Sulman, R. L. Scott, L. Wang, and R. P. Phillips (2016). The increasing importance of atmospheric demand for ecosystem water and carbon fluxes. *Nature Climate Change* 6(11), 1023–1027.
- Noyce, G. L., M. L. Kirwan, R. L. Rich, and J. P. Megonigal (2019). Asynchronous nitrogen supply and demand produce nonlinear plant allocation responses to warming and elevated CO₂. *Proceedings of the National Academy of Sciences* 116(43), 21623–21628.
- Onoda, Y., K. Hikosaka, and T. Hirose (2004). Allocation of nitrogen to cell walls decreases photosynthetic nitrogen-use efficiency. *Functional Ecology* 18(3), 419–425.
- Onoda, Y., I. J. Wright, J. R. Evans, K. Hikosaka, K. Kitajima, Ü. Niinemets, H. Poorter, T. Tosens, and M. Westoby (2017). Physiological and structural trade-offs underlying the leaf economics spectrum. *New Phytologist* 214(4), 1447–1463.
- Oren, R., J. S. Sperry, G. G. Katul, D. E. Pataki, B. E. Ewers, N. Phillips, and K. V. R. Schäfer (1999). Survey and synthesis of intra- and interspecific variation in stomatal sensitivity to vapor pressure deficit. *Plant, Cell and Environment* 22(12), 1515–1526.
- Oreskes, N., K. Shrader-Frechette, and K. Belitz (1994). Verification, validation, and confirmation of numerical models in the Earth sciences. *Science* 263(5147), 641–646.
- Paillassa, J., I. J. Wright, I. C. Prentice, S. Pepin, N. G. Smith, G. Ethier, A. C. Westerband, L. J. Lamarque, H. Wang, W. K. Cornwell, and V. Maire (2020). When and where soil is important to modify the carbon and water economy of leaves. *New Phytologist* 228(1), 121–135.
- Parvin, S., S. Uddin, S. Tausz Posch, R. Armstrong, and M. Tausz (2020). Carbon sink strength of nodules but not other organs modulates photosynthesis of faba bean (*Vicia faba*) grown under elevated [CO₂] and different water supply. *New Phytologist* 227(1), 132–145.

- Paul, K. I., P. J. Polglase, A. M. O'Connell, J. C. Carlyle, P. J. Smethurst, and P. K. Khanna (2003). Defining the relation between soil water content and net nitrogen mineralization. *European Journal of Soil Science* 54(1), 39–48.
- Peng, Y., K. J. Bloomfield, L. A. Cernusak, T. F. Domingues, and I. C. Prentice (2021). Global climate and nutrient controls of photosynthetic capacity. *Communications Biology* 4(1), 462.
- Perkowski, E. A., E. F. Waring, and N. G. Smith (2021). Root mass carbon costs to acquire nitrogen are determined by nitrogen and light availability in two species with different nitrogen acquisition strategies. *Journal of Experimental Botany* 72(15), 5766–5776.
- Phillips, R. P., E. R. Brzostek, and M. G. Midgley (2013). The mycorrhizal-associated nutrient economy: a new framework for predicting carbon-nutrient couplings in temperate forests. *New Phytologist* 199(1), 41–51.
- Phillips, R. P., A. C. Finzi, and E. S. Bernhardt (2011). Enhanced root exudation induces microbial feedbacks to N cycling in a pine forest under long-term CO₂ fumigation. *Ecology Letters* 14(2), 187–194.
- Pinheiro, J., D. Bates, S. Debroy, and D. Sarkar (2022). nlme: linear and nonlinear mixed effects models. *R package version 3.1-162*.
- Poggio, L., L. M. De Sousa, N. H. Batjes, G. B. M. Heuvelink, B. Kempen, E. Ribeiro, and D. Rossiter (2021). SoilGrids 2.0: Producing soil information for the globe with quantified spatial uncertainty. *Soil* 7(1), 217–240.
- Pons, T. L. and R. W. Pearcy (1994). Nitrogen reallocation and photosynthetic acclimation in response to partial shading in soybean plants. *Physiologia Plantarum* 92(4), 636–644.
- Poorter, H., J. Bühler, D. Van Dusschoten, J. Climent, and J. A. Postma (2012). Pot size matters: A meta-analysis of the effects of rooting volume on plant growth. *Functional Plant Biology* 39(11), 839–850.
- Poorter, H., O. Knopf, I. J. Wright, A. A. Temme, S. W. Hogewoning, A. Graf, L. A. Cernusak, and T. L. Pons (2022). A meta-analysis of responses of C₃ plants to atmospheric CO₂: dose-response curves for 85 traits ranging from the molecular to the whole-plant level. *New Phytologist* 233(4), 1560–1596.

- Prentice, I. C., N. Dong, S. M. Gleason, V. Maire, and I. J. Wright (2014). Balancing the costs of carbon gain and water transport: testing a new theoretical framework for plant functional ecology. *Ecology Letters* 17(1), 82–91.
- Prentice, I. C., X. Liang, B. E. Medlyn, and Y.-P. Wang (2015). Reliable, robust and realistic: The three R's of next-generation land-surface modelling. *Atmospheric Chemistry and Physics* 15, 5987–6005.
- Priestley, C. H. B. and R. J. Taylor (1972). On the assessment of surface heat flux and evaporation Using large-scale parameters. *Monthly Weather Review* 100(2), 81–92.
- Querejeta, J. I., I. Prieto, C. Armas, F. Casanoves, J. S. Diémé, M. Diouf, H. Yossi, B. Kaya, F. I. Pugnaire, and G. M. Rusch (2022). Higher leaf nitrogen content is linked to tighter stomatal regulation of transpiration and more efficient water use across dryland trees. *New Phytologist* 235(4), 1351–1364.
- R Core Team (2021). R: A language and environment for statistical computing.
- Raich, J. W., D. A. Clark, L. Schwendenmann, and T. E. Wood (2014). Aboveground tree growth varies with belowground carbon allocation in a tropical rainforest environment. *PLoS ONE* 9(6), e100275.
- Rastetter, E. B., P. M. Vitousek, C. B. Field, G. R. Shaver, D. Herbert, and G. I. Ågren (2001). Resource optimization and symbiotic nitrogen fixation. *Ecosystems* 4(4), 369–388.
- Reich, P. B. (2014). The world-wide 'fast-slow' plant economics spectrum: a traits manifesto. *Journal of Ecology* 102(2), 275–301.
- Reich, P. B., S. E. Hobbie, T. Lee, D. S. Ellsworth, J. B. West, D. Tilman, J. M. H. Knops, S. Naeem, and J. Trost (2006). Nitrogen limitation constrains sustainability of ecosystem response to CO₂. *Nature* 440(7086), 922–925.
- Reichman, G. A., D. L. Grunes, and F. G. Viets (1966). Effect of soil moisture on ammonification and nitrification in two Northern Plains soils. *Soil Science Society of America Journal* 30(3), 363–366.

- Rhine, E. D., R. L. Mulvaney, E. J. Pratt, and G. K. Sims (1998). Improving the Berthelot reaction for determining ammonium in soil extracts and water. *Soil Science Society of America Journal* 62(2), 473.
- Rogers, A. (2014). The use and misuse of V_{cmax} in Earth System Models. *Photosynthesis Research* 119(1-2), 15–29.
- Rogers, A., B. E. Medlyn, J. S. Dukes, G. B. Bonan, S. Caemmerer, M. C. Dietze, J. Kattge, A. D. B. Leakey, L. M. Mercado, Ü. Niinemets, I. C. Prentice, S. P. Serbin, S. Sitch, D. A. Way, and S. Zaehle (2017). A roadmap for improving the representation of photosynthesis in Earth system models. *New Phytologist* 213(1), 22–42.
- Saathoff, A. J. and J. Welles (2021). Gas exchange measurements in the unsteady state. *Plant Cell and Environment* 44(11), 3509–3523.
- Sage, R. F. and R. W. Pearcy (1987). The nitrogen use efficiency of C₃ and C₄ plants: I. Leaf nitrogen, growth, and biomass partitioning in *Chenopodium album* (L.) and *Amaranthus retroflexus* (L.). *Plant Physiology* 84(3), 954–958.
- Saleh, A. M., M. Abdel-Mawgoud, A. R. Hassan, T. H. Habeeb, R. S. Yehia, and H. AbdElgawad (2020). Global metabolic changes induced by arbuscular mycorrhizal fungi in oregano plants grown under ambient and elevated levels of atmospheric CO₂. *Plant Physiology and Biochemistry* 151, 255–263.
- Saxton, K. E. and W. J. Rawls (2006). Soil water characteristic estimates by texture and organic matter for hydrologic solutions. *Soil Science Society of America Journal* 70(5), 1569–1578.

- Schaefer, K., C. R. Schwalm, C. Williams, M. A. Arain, A. Barr, J. M. Chen, K. J. Davis, D. Dimitrov, T. W. Hilton, D. Y. Hollinger, E. Humphreys, B. Poulter, B. M. Racza, A. D. Richardson, A. Sahoo, P. Thornton, R. Vargas, H. Verbeeck, R. Anderson, I. Baker, T. A. Black, P. Bolstad, J. Chen, P. S. Curtis, A. R. Desai, M. C. Dietze, D. Dragoni, C. M. Gough, R. F. Grant, L. Gu, A. K. Jain, C. Kucharik, B. E. Law, S. Liu, E. Lokipitiya, H. A. Margolis, R. Matamala, J. H. McCaughey, R. Monson, J. W. Munger, W. Oechel, C. Peng, D. T. Price, D. Ricciuto, W. J. Riley, N. Roulet, H. Tian, C. Tonitto, M. Torn, E. Weng, and X. Zhou (2012). A model-data comparison of gross primary productivity: Results from the North American Carbon Program site synthesis. *Journal of Geophysical Research: Biogeosciences* 117(G3), G03010.
- Schmitt, M. R. and G. E. Edwards (1981). Photosynthetic capacity and nitrogen use efficiency of maize, wheat, and rice: A comparison between C₃ and C₄ photosynthesis. *Journal of Experimental Botany* 32(3), 459–466.
- Schneider, C. A., W. S. Rasband, and K. W. Eliceiri (2012). NIH Image to ImageJ: 25 years of image analysis. *Nature Methods* 9(7), 671–675.
- Scott, H. G. and N. G. Smith (2022). A Model of C₄ photosynthetic acclimation based on least-cost optimality theory suitable for Earth system model incorporation. *Journal of Advances in Modeling Earth Systems* 14(3), 1–16.
- Shi, M., J. B. Fisher, E. R. Brzostek, and R. P. Phillips (2016). Carbon cost of plant nitrogen acquisition: Global carbon cycle impact from an improved plant nitrogen cycle in the Community Land Model. *Global Change Biology* 22(3), 1299–1314.
- Shi, M., J. B. Fisher, R. P. Phillips, and E. R. Brzostek (2019). Neglecting plant-microbe symbioses leads to underestimation of modeled climate impacts. *Biogeosciences* 16(2), 457–465.
- Smith, B., D. Wärldin, A. Arneth, T. Hickler, P. Leadley, J. Siltberg, and S. Zaehle (2014). Implications of incorporating N cycling and N limitations on primary production in an individual-based dynamic vegetation model. *Biogeosciences* 11(7), 2027–2054.
- Smith, N. G. and J. S. Dukes (2013). Plant respiration and photosynthesis in global-scale models: incorporating acclimation to temperature and CO₂. *Global Change Biology* 19(1), 45–63.

- Smith, N. G. and J. S. Dukes (2018). Drivers of leaf carbon exchange capacity across biomes at the continental scale. *Ecology* 99(7), 1610–1620.
- Smith, N. G. and T. F. Keenan (2020). Mechanisms underlying leaf photosynthetic acclimation to warming and elevated CO₂ as inferred from least-cost optimality theory. *Global Change Biology* 26(9), 5202–5216.
- Smith, N. G., T. F. Keenan, I. C. Prentice, H. Wang, I. J. Wright, Ü. Niinemets, K. Y. Crous, T. F. Domingues, R. Guerrieri, F. Y. Ishida, J. Kattge, E. L. Kruger, V. Maire, A. Rogers, S. P. Serbin, L. Tarvainen, H. F. Togashi, P. A. Townsend, M. Wang, L. K. Weerasinghe, and S.-X. Zhou (2019). Global photosynthetic capacity is optimized to the environment. *Ecology Letters* 22(3), 506–517.
- Smith, N. G., D. L. Lombardozzi, A. Tawfik, G. B. Bonan, and J. S. Dukes (2017). Biophysical consequences of photosynthetic temperature acclimation for climate. *Journal of Advances in Modeling Earth Systems* 9(1), 536–547.
- Smith, N. G., S. L. Malyshev, E. Shevliakova, J. Kattge, and J. S. Dukes (2016). Foliar temperature acclimation reduces simulated carbon sensitivity to climate. *Nature Climate Change* 6(4), 407–411.
- Smith, S. E. and D. J. Read (2008). *Mycorrhizal Symbiosis*. Academic Press.
- Soil Survey Staff (2022). Web Soil Survey. *Natural Resources Conservation Service, United States Department of Agriculture, Available online at the following link: <http://websoilsurvey.sc.egov.usda.gov/>.* Accessed 11/18/2022.
- Soudzilovskaia, N. A., J. C. Douma, A. A. Akhmetzhanova, P. M. van Bodegom, W. K. Cornwell, E. J. Moens, K. K. Treseder, and J. H. C. Cornelissen (2015). Global patterns of plant root colonization intensity by mycorrhizal fungi explained by climate and soil chemistry. *Global Ecology and Biogeography* 24(3), 371–382.
- Stark, J. M. and M. K. Firestone (1995). Mechanisms for soil moisture effects on activity of nitrifying bacteria. *Applied and Environmental Microbiology* 61(1), 218–221.

- Stocker, B. D., H. Wang, N. G. Smith, S. P. Harrison, T. F. Keenan, D. Sandoval, T. Davis, and I. C. Prentice (2020). P-model v1.0: An optimality-based light use efficiency model for simulating ecosystem gross primary production. *Geoscientific Model Development* 13(3), 1545–1581.
- Stocker, B. D., J. Zscheischler, T. F. Keenan, I. C. Prentice, J. Peñuelas, and S. I. Seneviratne (2018). Quantifying soil moisture impacts on light use efficiency across biomes. *New Phytologist* 218(4), 1430–1449.
- Sulman, B. N., D. T. Roman, K. Yi, L. Wang, R. P. Phillips, and K. A. Novick (2016). High atmospheric demand for water can limit forest carbon uptake and transpiration as severely as dry soil. *Geophysical Research Letters* 43(18), 9686–9695.
- Sulman, B. N., E. Shevliakova, E. R. Brzostek, S. N. Kivlin, S. L. Malyshev, D. N. L. Menge, and X. Zhang (2019). Diverse mycorrhizal associations enhance terrestrial C storage in a global model. *Global Biogeochemical Cycles* 33(4), 501–523.
- Sweet, S. K., D. W. Wolfe, A. DeGaetano, and R. Benner (2017). Anatomy of the 2016 drought in the northeastern United States: Implications for agriculture and water resources in humid climates. *Agricultural and Forest Meteorology* 247, 571–581.
- Taylor, B. N. and D. N. L. Menge (2018). Light regulates tropical symbiotic nitrogen fixation more strongly than soil nitrogen. *Nature Plants* 4(9), 655–661.
- Terrer, C., S. Vicca, B. A. Hungate, R. P. Phillips, and I. C. Prentice (2016). Mycorrhizal association as a primary control of the CO₂ fertilization effect. *Science* 353(6294), 72–74.
- Terrer, C., S. Vicca, B. D. Stocker, B. A. Hungate, R. P. Phillips, P. B. Reich, A. C. Finzi, and I. C. Prentice (2018). Ecosystem responses to elevated CO₂ governed by plant–soil interactions and the cost of nitrogen acquisition. *New Phytologist* 217(2), 507–522.
- Thieurmel, B. and A. Elmarhraoui (2019). suncalc: Compute sun position, sunlight phases, moon position, and lunar phase. *R package version 0.5.1*.

- Thomas, R. Q., E. N. J. Brookshire, and S. Gerber (2015). Nitrogen limitation on land: how can it occur in Earth system models? *Global Change Biology* 21(5), 1777–1793.
- Thomas, R. Q., S. Zaehle, P. H. Templer, and C. L. Goodale (2013). Global patterns of nitrogen limitation: confronting two global biogeochemical models with observations. *Global Change Biology* 19(10), 2986–2998.
- Thornton, P. E., J.-F. Lamarque, N. A. Rosenbloom, and N. M. Mahowald (2007). Influence of carbon-nitrogen cycle coupling on land model response to CO₂ fertilization and climate variability. *Global Biogeochemical Cycles* 21(4), GB4018.
- Tingey, D. T., D. L. Phillips, and M. G. Johnson (2000). Elevated CO₂ and conifer roots: effects on growth, life span and turnover. *New Phytologist* 147(1), 87–103.
- Udvardi, M. and P. S. Poole (2013). Transport and metabolism in legume-rhizobia symbioses. *Annual Review of Plant Biology* 64, 781–805.
- USDA NRCS (2022). The PLANTS Database.
- Uselman, S. M., R. G. Qualls, and R. B. Thomas (2000). Effects of increased atmospheric CO₂, temperature, and soil N availability on root exudation of dissolved organic carbon by an N-fixing tree (*Robinia pseudoacacia* L.). *Plant and Soil* 222, 191–202.
- van Diepen, L. T. A., E. A. Lilleskov, K. S. Pregitzer, and R. M. Miller (2007). Decline of arbuscular mycorrhizal fungi in northern hardwood forests exposed to chronic nitrogen additions. *New Phytologist* 176(1), 175–183.
- Vance, C. P. and G. H. Heichel (1991). Carbon in N₂ fixation: Limitation or exquisite adaptation. *Annual Review of Plant Physiology and Plant Molecular Biology* 42(1), 373–392.
- Viet, H. D., J.-H. Kwak, K.-S. Lee, S.-S. Lim, M. Matsushima, S. X. Chang, K.-H. Lee, and W.-J. Choi (2013). Foliar chemistry and tree ring δ¹³C of *Pinus densiflora* in relation to tree growth along a soil pH gradient. *Plant and Soil* 363(1-2), 101–112.

- Vitousek, P. M., K. Cassman, C. C. Cleveland, T. Crews, C. B. Field, N. B. Grimm, R. W. Howarth, R. Marino, L. Martinelli, E. B. Rastetter, and J. I. Sprent (2002). Towards an ecological understanding of biological nitrogen fixation. In *The Nitrogen Cycle at Regional to Global Scales*, pp. 1–45. Springer Netherlands.
- Vitousek, P. M. and R. W. Howarth (1991). Nitrogen limitation on land and in the sea: How can it occur? *Biogeochemistry* 13(2), 87–115.
- Vitousek, P. M., S. Porder, B. Z. Houlton, and O. A. Chadwick (2010). Terrestrial phosphorus limitation: mechanisms, implications, and nitrogen-phosphorus interactions. *Ecological Applications* 20(1), 5–15.
- Walker, A. P., A. P. Beckerman, L. Gu, J. Kattge, L. A. Cernusak, T. F. Domingues, J. C. Scales, G. Wohlfahrt, S. D. Wullschleger, and F. I. Woodward (2014). The relationship of leaf photosynthetic traits - V_{cmax} and J_{max} - to leaf nitrogen, leaf phosphorus, and specific leaf area: a meta-analysis and modeling study. *Ecology and Evolution* 4(16), 3218–3235.
- Walker, A. P., A. L. Johnson, A. Rogers, J. Anderson, R. A. Bridges, R. A. Fisher, D. Lu, D. M. Ricciuto, S. P. Serbin, and M. Ye (2021). Multi-hypothesis comparison of Farquhar and Collatz photosynthesis models reveals the unexpected influence of empirical assumptions at leaf and global scales. *Global Change Biology* 27(4), 804–822.
- Wang, H., I. C. Prentice, T. F. Keenan, T. W. Davis, I. J. Wright, W. K. Cornwell, B. J. Evans, and C. Peng (2017). Towards a universal model for carbon dioxide uptake by plants. *Nature Plants* 3(9), 734–741.
- Wang, H., I. C. Prentice, I. J. Wright, D. I. Warton, S. Qiao, X. Xu, J. Zhou, K. Kikuzawa, and N. C. Stenseth (2023). Leaf economics fundamentals explained by optimality principles. *Science Advances* 9(3), eadd566.
- Wang, J., J. M. Knops, C. E. Brassil, and C. Mu (2017). Increased productivity in wet years drives a decline in ecosystem stability with nitrogen additions in arid grasslands. *Ecology* 98(7), 1779–1786.
- Wang, W., Y. Wang, G. Hoch, Z. Wang, and J. Gu (2018). Linkage of root morphology to anatomy with increasing nitrogen availability in six temperate tree species. *Plant and Soil* 425(1-2), 189–200.

- Weatherburn, M. W. (1967). Phenol-hypochlorite reaction for determination of ammonia. *Analytical Chemistry* 39(8), 971–974.
- Wellburn, A. R. (1994). The spectral determination of chlorophylls a and b, as well as total carotenoids, using various solvents with spectrophotometers of different resolution. *Journal of Plant Physiology* 144(3), 307–313.
- Wen, Z., P. J. White, J. Shen, and H. Lambers (2022). Linking root exudation to belowground economic traits for resource acquisition. *New Phytologist* 233(4), 1620–1635.
- Westerband, A. C., I. J. Wright, V. Maire, J. Paillassa, I. C. Prentice, O. K. Atkin, K. J. Bloomfield, L. A. Cernusak, N. Dong, S. M. Gleason, C. Guilherme Pereira, H. Lambers, M. R. Leishman, Y. Malhi, and R. H. Nolan (2023). Coordination of photosynthetic traits across soil and climate gradients. *Global Change Biology* 29(3), 1–29.
- Wieder, W. R., C. C. Cleveland, W. K. Smith, and K. Todd-Brown (2015). Future productivity and carbon storage limited by terrestrial nutrient availability. *Nature Geoscience* 8(6), 441–444.
- Wieder, W. R., D. M. Lawrence, R. A. Fisher, G. B. Bonan, S. J. Cheng, C. L. Goodale, A. S. Grandy, C. D. Koven, D. L. Lombardozzi, K. W. Oleson, and R. Q. Thomas (2019). Beyond static benchmarking: using experimental manipulations to evaluate land model assumptions. *Global Biogeochemical Cycles* 33(10), 1289–1309.
- Wright, I. J., P. B. Reich, and M. Westoby (2003). Least-cost input mixtures of water and nitrogen for photosynthesis. *The American Naturalist* 161(1), 98–111.
- Wright, I. J., P. B. Reich, M. Westoby, D. D. Ackerly, Z. Baruch, F. Bongers, J. Cavender-Bares, T. Chapin, J. H. C. Cornelissen, M. Diemer, J. Flexas, E. Garnier, P. K. Groom, J. Gulias, K. Hikosaka, B. B. Lamont, T. Lee, W. Lee, C. Lusk, J. J. Midgley, M.-L. Navas, Ü. Niinemets, J. Oleksyn, N. Osada, H. Poorter, P. Poot, L. Prior, V. I. Pyankov, C. Roumet, S. C. Thomas, M. G. Tjoelker, E. J. Veneklaas, and R. Villar (2004). The worldwide leaf economics spectrum. *Nature* 428(6985), 821–827.
- Xu-Ri and I. C. Prentice (2017). Modelling the demand for new nitrogen fixation by terrestrial ecosystems. *Biogeosciences* 14(7), 2003–2017.

- Yahdjian, L., L. A. Gherardi, and O. E. Sala (2011). Nitrogen limitation in arid-subhumid ecosystems: A meta-analysis of fertilization studies. *Journal of Arid Environments* 75(8), 675–680.
- Yuan, W., Y. Zheng, S. Piao, P. Ciais, D. Lombardozzi, Y. Wang, Y. Ryu, G. Chen, W. Dong, Z. Hu, A. K. Jain, C. Jiang, E. Kato, S. Li, S. Lienert, S. Liu, J. E. Nabel, Z. Qin, T. Quine, S. Sitch, W. K. Smith, F. Wang, C. Wu, Z. Xiao, and S. Yang (2019). Increased atmospheric vapor pressure deficit reduces global vegetation growth. *Science Advances* 5(8), 1–12.
- Zaehle, S., B. E. Medlyn, M. G. De Kauwe, A. P. Walker, M. C. Dietze, T. Hickler, Y. Luo, Y. P. Wang, B. El-Masri, P. Thornton, A. Jain, S. Wang, D. Warlind, E. Weng, W. Parton, C. M. Iversen, A. Gallet-Budynek, H. McCarthy, A. C. Finzi, P. J. Hanson, I. C. Prentice, R. Oren, and R. J. Norby (2014). Evaluation of 11 terrestrial carbon-nitrogen cycle models against observations from two temperate Free-Air CO₂ Enrichment studies. *New Phytologist* 202(3), 803–822.
- Zaehle, S., S. Sitch, B. Smith, and F. Hatterman (2005). Effects of parameter uncertainties on the modeling of terrestrial biosphere dynamics. *Global Biogeochemical Cycles* 19(3), GB3020.
- Zhu, Q., W. J. Riley, J. Tang, N. Collier, F. M. Hoffman, X. Yang, and G. Bisht (2019). Representing nitrogen, phosphorus, and carbon interactions in the E3SM land model: development and global benchmarking. *Journal of Advances in Modeling Earth Systems* 11(7), 2238–2258.
- Ziegler, C., M. E. Dusenge, B. Nyirambangutse, E. Zibera, G. Wallin, and J. Uddling (2020). Contrasting dependencies of photosynthetic capacity on leaf nitrogen in early- and late-successional tropical montane tree species. *Frontiers in Plant Science* 11, 1–12.
- Ziehn, T., J. Kattge, W. Knorr, and M. Scholze (2011). Improving the predictability of global CO₂ assimilation rates under climate change. *Geophysical Research Letters* 38(10), L10404.

Appendices

Appendix A

Supplemental material for “Structural carbon costs to acquire nitrogen are determined by nitrogen and light availability in two species with different nitrogen acquisition strategies”

Table A1. Summary table containing volumes of compounds used to create modified Hoagland’s solutions for each soil nitrogen fertilization treatment. All volumes are expressed as milliliters per liter (mL L^{-1})

Compound	0 ppm N	70 ppm N	210 ppm N	630 ppm N
1 M $\text{NH}_4\text{H}_2\text{PO}_4$	0	0.33	1	1
2 M KNO_3	0	0.67	2	2
2 M $\text{Ca}(\text{NO}_3)_2$	0	0.67	2	2
1 M NH_4NO_3	0	0.33	1	0
8 M NH_4NO_3	0	0	0	2
1 M KH_2PO_4	1	0.67	0	0
1 M KCl	4	1.33	0	0
1 M CaCO_3	4	3	0	0
2 M MgSO_4	1	1	1	1
10% Fe-EDTA	1	1	1	1
Trace Elements	1	1	1	1

Table A2. Analysis of variance results exploring species-specific effects of light availability, nitrogen fertilization, and their interactions on the ratio of whole plant biomass to pot volume (g L⁻¹)*

	df	Coefficient	χ^2	p
<i>G. hirsutum</i>				
Intercept		0.740	-	-
Light (L)	1	$-4.23 * 10^{-3}$	189.581	<0.001
Nitrogen (N)	1	$7.86 * 10^{-4}$	17.927	<0.001
L*N	1	$-6.61 * 10^{-6}$	4.709	0.030
<i>G. max</i>				
Intercept		-0.233	-	-
Light (L)	1	$-1.12 * 10^{-2}$	69.500	<0.001
Nitrogen (N)	1	$8.29 * 10^{-4}$	40.297	<0.001
L*N	1	$-8.51 * 10^{-6}$	5.548	0.019

*Significance determined using Wald's χ^2 tests ($p=0.05$). P-values less than 0.05 are in bold and p-values between 0.05 and 0.1 are italicized. Negative coefficients for light treatments indicate a positive effect of increasing light availability on all response variables, as light availability is treated as percent shade cover in all linear mixed-effects models.

Table A3. Slopes of the regression line describing the relationship between each dependent variable and nitrogen fertilization at each light level*

Shade cover	Slope
<i>G. hirsutum</i>	
0%	$8.29 * 10^{-4a}$
30%	$5.74 * 10^{-4a}$
50%	$4.03 * 10^{-4a}$
80%	$1.48 * 10^{-4a}$
<i>G. max</i>	
0%	$7.86 * 10^{-4}$
30%	$5.87 * 10^{-4}$
50%	$4.55 * 10^{-4}$
80%	$2.57 * 10^{-5}$

*Slopes represent estimated marginal mean slopes from linear mixed-effects models described in the Methods. Slopes were calculated using the ‘emmeans’ R package (Lenth et al. 2019). Superscripts indicate slopes fit to natural-log (^a) or square root (^b) transformed data. Slopes statistically different from zero (Tukey: $p < 0.05$) are indicated in bold. Marginally significant slopes (Tukey: $0.05 < p < 0.1$) are italicized.

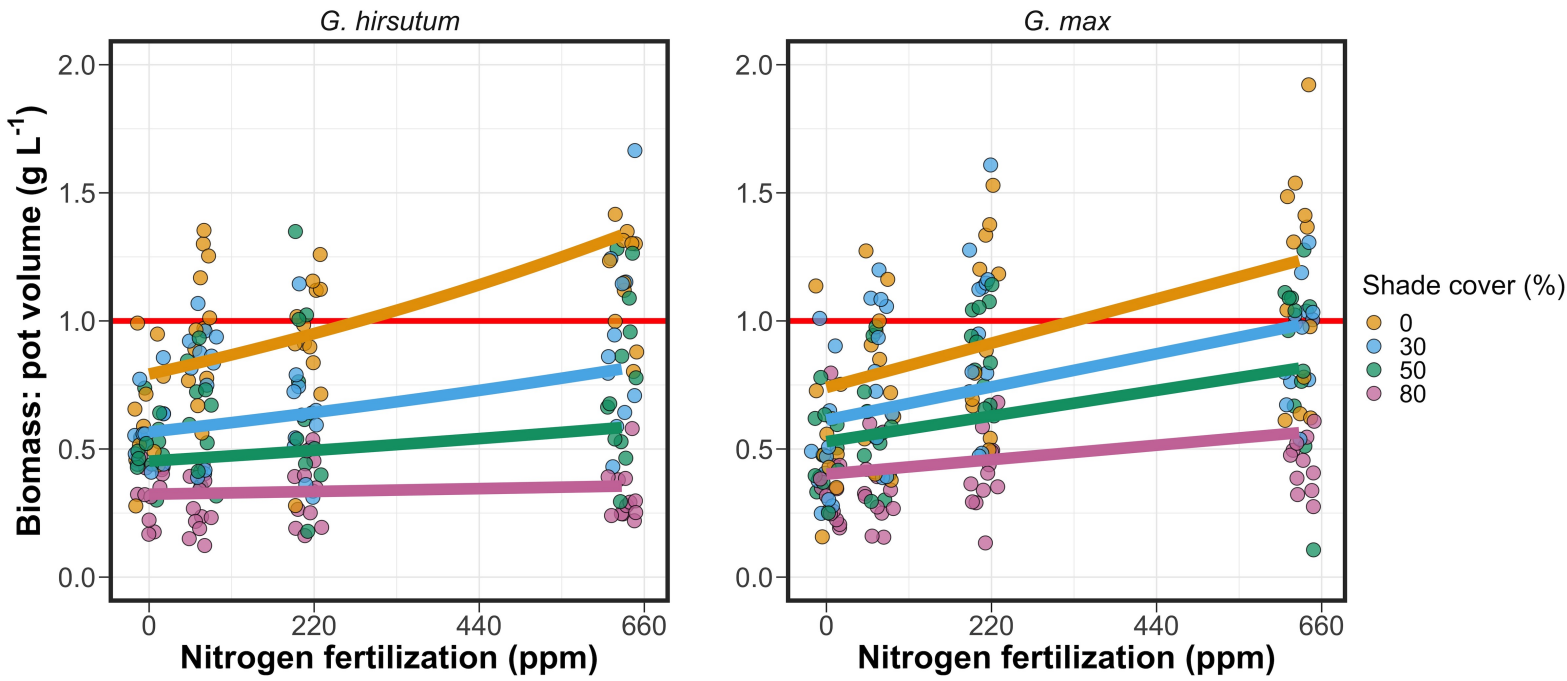


Figure A1. Effects of shade cover and nitrogen fertilization on the ratio of plant biomass to rooting volume in *G. hirsutum* (left panel) and *G. max* (right panel). The red horizontal line indicates the recommended 1 g L^{-1} threshold for biomass:pot volume recommended by Poorter et al. (2012) to avoid pot size-induced growth limitation. Nitrogen fertilization treatments are represented on the x-axis. Shade cover treatments are represented through colored points and trendlines. Points are jittered for visibility. Yellow points and trendlines represent the 0% shade cover treatment, blue points and trendlines represent the 30% shade cover treatment, green points and trendlines represent the 50% shade cover treatment, and purple points and trendlines represent the 80% shade cover treatment. Solid trendlines indicate slopes that are significantly different from zero (Tukey: $p < 0.05$), while dashed trendlines indicate slopes that are not statistically different from zero.

Appendix B

Supplemental material for “Soil nitrogen availability modifies leaf nitrogen economies in mature temperate deciduous forests: a direct test of photosynthetic least-cost theory”

Table B1. Sample sizes of each species, abbreviated by their USDA NRCS PLANTS database code, within each plot at each site*

	ACRU	ACSA	FAGR	FRAM	QURU	N_{plot}
Bald Hill						
+N; +S	0	6	1	0	1	8
+N; -S	1	2	2	0	1	6
-N; +S	2	2	0	0	2	6
-N; -S	2	3	3	0	2	10
Carter Creek						
+N; +S	0	6	1	2	0	9
+N; -S	0	4	0	2	0	6
-N; +S	0	5	1	4	0	10
-N; -S	0	7	0	0	0	7
Mount Pleasant						
+N; +S	3	2	1	0	3	9
+N; -S	0	5	4	1	0	10
-N; +S	1	2	4	0	0	7
-N; -S	3	3	1	2	1	10
N_{spp}	12	47	18	11	10	98

*Plots within each site are represented based on nitrogen and sulfur addition status. The final column on the right depicts total sample size per plot in each site (N_{plot}) and the final row on the bottom represents cumulative species sample size across all plots and all sites (N_{spp}). Key: ACRU=*A. rubrum*; ACSA=*A. saccharum*; FAGR=*F. grandifolia*; FRAM=*F. americana*; QURU=*Q. rubra*

Table B2. Analysis of variance results exploring the linear effect of leaf temperature on net photosynthesis rate (A_{net} ; $\mu\text{mol m}^{-2} \text{s}^{-1}$) and stomatal conductance (g_{sw} ; $\mu\text{mol m}^{-2} \text{s}^{-1}$) measured at $400 \mu\text{mol mol}^{-1} \text{CO}_2$

	df	A_{net}		g_{sw}	
		χ^2	p	χ^2	p
Leaf temperature	1	1.287	0.257	1.716	0.190

*Results detail linear mixed effects model where temperature was regressed against net photosynthesis or stomatal conductance, with site and species designated as random intercept terms. Significance was determined using Type II Wald χ^2 tests ($\alpha=0.05$).

Table B3. Second order log-polynomial regression coefficients that described the effect of leaf temperature on net photosynthesis (A_{net} ; $\mu\text{mol m}^{-2} \text{s}^{-1}$) and stomatal conductance (g_s ; $\mu\text{mol m}^{-2} \text{s}^{-1}$) measured at 400 $\mu\text{mol mol}^{-1} \text{CO}_2$ ^{*}

	a	b	c
A_{net}	9.422	-0.573	0.010
g_s	-0.170	-0.186	0.003

*Net photosynthesis and stomatal conductance values were fit to the log polynomial equation $\log(y) = a + bx + cx^2$, where x is leaf temperature in °C.

Table B4. Mean, standard error, and 95% confidence interval ranges of soil nitrogen availability estimates across all measured plots. All units are expressed as $\mu\text{g N g}^{-1}$ resin d^{-1}

Site	Treatment	Mean	SE	Lower 95% CI	Upper 95% CI
Bald Hill	Ammonium sulfate	27.11	6.14	15.08	39.13
Bald Hill	Control	14.41	5.02	4.56	24.26
Bald Hill	Sodium nitrate	20.65	3.15	14.46	26.83
Bald Hill	Sulfur	6.33	2.19	2.04	10.62
Carter Creek	Ammonium sulfate	26.94	5.36	16.43	37.44
Carter Creek	Control	19.87	1.92	16.10	23.64
Carter Creek	Sodium nitrate	15.51	4.16	7.36	23.65
Carter Creek	Sulfur	5.50	1.40	2.75	8.25
Mount Pleasant	Ammonium sulfate	8.02	2.31	3.49	12.56
Mount Pleasant	Control	2.00	0.57	0.89	3.11
Mount Pleasant	Sodium nitrate	2.52	0.68	1.19	3.85
Mount Pleasant	Sulfur	2.42	0.39	1.66	3.17

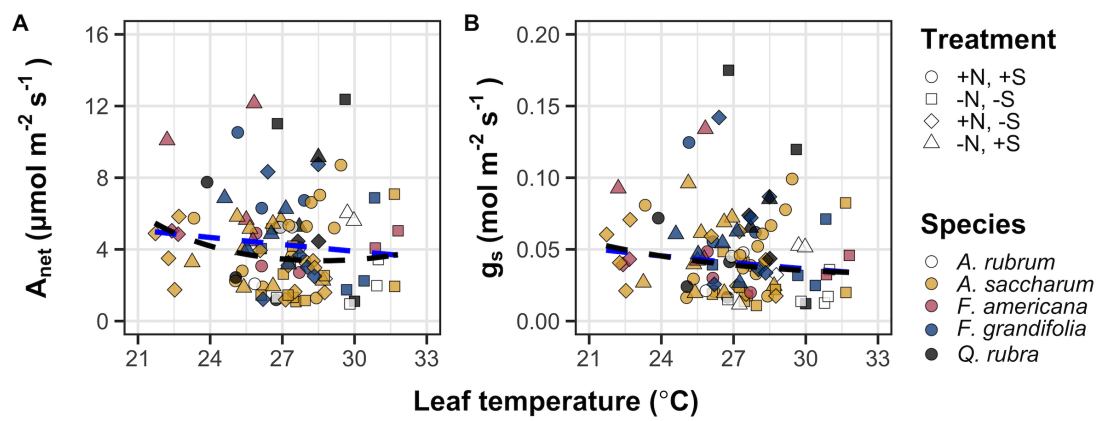


Figure B1. Effects of leaf temperature on net photosynthesis rate (A) and stomatal conductance (B) values when measured at $400 \mu\text{mol mol}^{-1} \text{CO}_2$. Leaf temperature is represented on the x-axis, while species are represented as colored points. Colored points and shapes are as explained in Figure 3.1. The dashed blue trendline describes the linear relationship between leaf temperature and each response variable, while the dashed black trendline describes the same relationship with a log-polynomial regression equation.

Appendix C

Supplemental material for “Supplemental material for "The relative cost of resource use for photosynthesis drives variance in leaf nitrogen content across a climate and soil resource availability gradient”

C.1 Calculations for soil water holding capacity

Water holding capacity (θ_{WHC} ; mm) was calculated as a function of the volumetric soil water storage at field capacity (W_{FC} ; $m^3 m^{-3}$), and the volumetric soil water storage at wilting point (W_{PWP} ; $m^3 m^{-3}$):

$$\theta_{WHC} = (W_{FC} - W_{PWP})(1 - f_{gravel}) * \min(z_{bedrock}, z_{max}) \quad (C4.1)$$

where f_{gravel} (%) is the fraction of gravel content in soil, $z_{bedrock}$ (mm) is the distance to bedrock, and z_{max} (mm) is the maximum allowable distance to bedrock, set to 2000 mm. W_{FC} is calculated as:

$$\theta_{FC} = k_{fc} + (1.283 * (k_{fc})^2 - 0.374 * k_{fc} - 0.015) \quad (C4.2)$$

where

$$\begin{aligned} k_{fc} = & -0.251 * f_{sand} + 0.195 * f_{clay} + 0.011 * f_{OM} \\ & + 0.006 * (f_{sand} * f_{OM}) - 0.027 * (f_{clay} \\ & * f_{OM}) + 0.452 * (f_{sand} * f_{clay}) + 0.299 \end{aligned} \quad (C4.3)$$

W_{PWP} is calculated as:

$$W_{PWP} = k_{pwp} + (0.14 * k_{pwp} - 0.02) \quad (C4.4)$$

where

$$\begin{aligned}
 k_{pwp} = & -0.024 * f_{sand} + 0.487 * f_{clay} + 0.006 * f_{OM} \\
 & + 0.005 * (f_{sand} * f_{OM}) - 0.013 * (f_{clay} \\
 & * f_{OM}) + 0.068 * (f_{sand} * f_{clay}) + 0.031
 \end{aligned} \tag{C4.5}$$

In Equations C4.4 and C4.5, f_{sand} (%) is the fraction of sand content in soil (%), f_{clay} (%) is the fraction of clay content in soil (%), and f_{OM} is the fraction of organic matter in soil (%). Organic matter in the soil was calculated by converting soil organic carbon data extracted from SoilGrids 2.0 to soil organic matter using the van Bemmelen factor (1.724 conversion factor).

Table C1. List of sampled species and their plant functional group assignment

Symbol	Species	Photo. pathway	Growth duration	Growth habit	N-fixer?	Plant functional group	Number sampled
ACAN11	<i>Acaciella angustissima</i>	C ₃	perennial	forb	yes	C ₃ N-fixer	3
AMAR2	<i>Ambrosia artemisiifolia</i>	C ₃	annual	forb	no	C ₃ non-fixer	25
AMPS	<i>Ambrosia psilostachya</i>	C ₃	perennial	forb	no	C ₃ non-fixer	32
ARAL3	<i>Argemone albiflora</i>	C ₃	annual	forb	no	C ₃ non-fixer	3
ARPU9	<i>Aristida purpurea</i>	C ₄	perennial	graminoid	no	C ₄ non-fixer	2
ASAS	<i>Asclepias asperula</i>	C ₃	perennial	forb	no	C ₃ non-fixer	3
ASLA4	<i>Asclepias latifolia</i>	C ₃	perennial	forb	no	C ₃ non-fixer	3
ASSY	<i>Asclepias syriaca</i>	C ₃	perennial	forb	no	C ₃ non-fixer	18
BOIS	<i>Bothriochloa ischaemum</i>	C ₄	perennial	graminoid	no	C ₄ non-fixer	6
BOSA	<i>Bothriochloa saccharoides</i>	C ₄	perennial	graminoid	no	C ₄ non-fixer	6
CAPL3	<i>Carex planostachys</i>	C ₄	perennial	graminoid	no	C ₄ non-fixer	3
CAREX	<i>Carex</i> spp.	C ₄	perennial	graminoid	no	C ₄ non-fixer	16
CHFE3	<i>Chamaesyce fendleri</i>	C ₃	perennial	forb	no	C ₃ non-fixer	2
CHPI8	<i>Chrysopsis pilosa</i>	C ₃	annual	forb	no	C ₃ non-fixer	3
COCO13	<i>Conoclinium coelestinum</i>	C ₃	perennial	forb	no	C ₃ non-fixer	3
COER	<i>Commelina erecta</i>	C ₃	perennial	forb	no	C ₃ non-fixer	3
CRGLL	<i>Croton glandulosus</i>	C ₃	annual	forb	no	C ₃ non-fixer	22
CYDA	<i>Cynodon dactylon</i>	C ₄	perennial	graminoid	no	C ₄ non-fixer	15
DIAN	<i>Dichanthium annulatum</i>	C ₄	perennial	graminoid	no	C ₄ non-fixer	8
ENPE4	<i>Engelmannia peristenia</i>	C ₃	perennial	forb	no	C ₃ non-fixer	6
EUMA8	<i>Euphorbia marginata</i>	C ₃	annual	forb	no	C ₃ non-fixer	6
GAPU	<i>Gaillardia pulchella</i>	C ₃	annual	forb	no	C ₃ non-fixer	16
GLGO	<i>Glandularia gooddingii</i>	C ₃	perennial	forb	no	C ₃ non-fixer	2
HEAN3	<i>Helianthus annuus</i>	C ₃	annual	forb	no	C ₃ non-fixer	6

Table C1. List of sampled species and their plant functional group assignment (cont.)

Symbol	Species	Photo. pathway	Growth duration	Growth habit	N-fixer?	Plant functional group	Number sampled
HECA8	<i>Heterotheca canescens</i>	C ₃	perennial	forb	no	C ₃ non-fixer	2
HETE3	<i>Heliotropium tenellum</i>	C ₃	annual	forb	no	C ₃ non-fixer	3
IVAX	<i>Iva axillaris</i>	C ₃	perennial	forb	no	C ₃ non-fixer	4
LIAT	<i>Lilaeopsis attenuata</i>	C ₃	perennial	forb	no	C ₃ non-fixer	3
LIPU	<i>Liatris punctata</i>	C ₃	perennial	forb	no	C ₃ non-fixer	3
LOPE	<i>Lolium perenne</i>	C ₃	perennial	graminoid	no	C ₃ non-fixer	9
MIQU2	<i>Mimosa quadrivalvis</i>	C ₃	perennial	forb	yes	C ₃ N-fixer	15
NALE3	<i>Nassella leucotricha</i>	C ₃	perennial	graminoid	no	C ₃ non-fixer	19
OECU2	<i>Oenothera curtiflora</i>	C ₃	annual	forb	no	C ₃ non-fixer	3
OENOT	<i>Oenothera</i> spp.	C ₃	annual	forb	no	C ₃ non-fixer	1
PAVI2	<i>Panicum virgatum</i>	C ₄	perennial	graminoid	no	C ₄ non-fixer	12
RACO3	<i>Ratibida columnifera</i>	C ₃	perennial	forb	no	C ₃ non-fixer	40
RHSET	<i>Rhynchosia senna</i>	C ₃	perennial	forb	yes	C ₃ N-fixer	1
RUHI2	<i>Rudbeckia hirta</i>	C ₃	perennial	forb	no	C ₃ non-fixer	3
RUNU	<i>Ruellia nudiflora</i>	C ₃	perennial	forb	no	C ₃ non-fixer	15
RUTR	<i>Rubus trivialis</i>	C ₃	perennial	vine	no	C ₃ non-fixer	3
SAFA2	<i>Salvia farinacea</i>	C ₃	perennial	forb	no	C ₃ non-fixer	7
SCHIZ4	<i>Schizachyrium</i> spp.	C ₄	perennial	graminoid	no	C ₄ non-fixer	8
SCSC	<i>Schizachyrium scoparium</i>	C ₄	perennial	graminoid	no	C ₄ non-fixer	3
SODI	<i>Solanum dimidiatum</i>	C ₃	perennial	forb	no	C ₃ non-fixer	1
SOEL	<i>Solanum elaeagnifolium</i>	C ₃	perennial	forb	no	C ₃ non-fixer	53
SOHA	<i>Sorghum halapense</i>	C ₄	perennial	graminoid	no	C ₄ non-fixer	38
STTE3	<i>Stillingia texana</i>	C ₃	perennial	forb	no	C ₃ non-fixer	3
VEOC	<i>Verbesina occidentalis</i>	C ₃	perennial	forb	no	C ₃ non-fixer	3
VEST	<i>Verbena stricta</i>	C ₃	perennial	forb	no	C ₃ non-fixer	3

Table C2. Model selection results for soil moisture and vapor pressure deficit. Soil moisture was used in a bivariate regression against log-transformed β , while vapor pressure deficit was used in bivariate regressions against leaf $C_l:C_a$

Day	Soil moisture		VPD	
	AICc	RMSE	AICc	RMSE
1	1870.80	1.4147	-848.01	0.0738
2	1870.12	1.4136	-847.68	0.0738
3	1870.10	1.4135	-847.48	0.0738
4	1870.37	1.4141	-867.19	0.0725
5	1870.76	1.4148	-847.10	0.0738
6	1870.99	1.4153	-847.00	0.0738
7	1871.26	1.4158	-846.90	0.0738
8	1871.54	1.4164	-846.83	0.0738
9	1871.93	1.4172	-846.88	0.0738
10	1872.43	1.4181	-846.90	0.0738
15	1874.20	1.4221	-847.64	0.0738
20	1876.69	1.4272	-847.40	0.0738
30	1878.14	1.4301	-848.10	0.0738
60	1877.83	1.4307	-849.99	0.0737
90	1877.69	1.4298	-849.35	0.0738

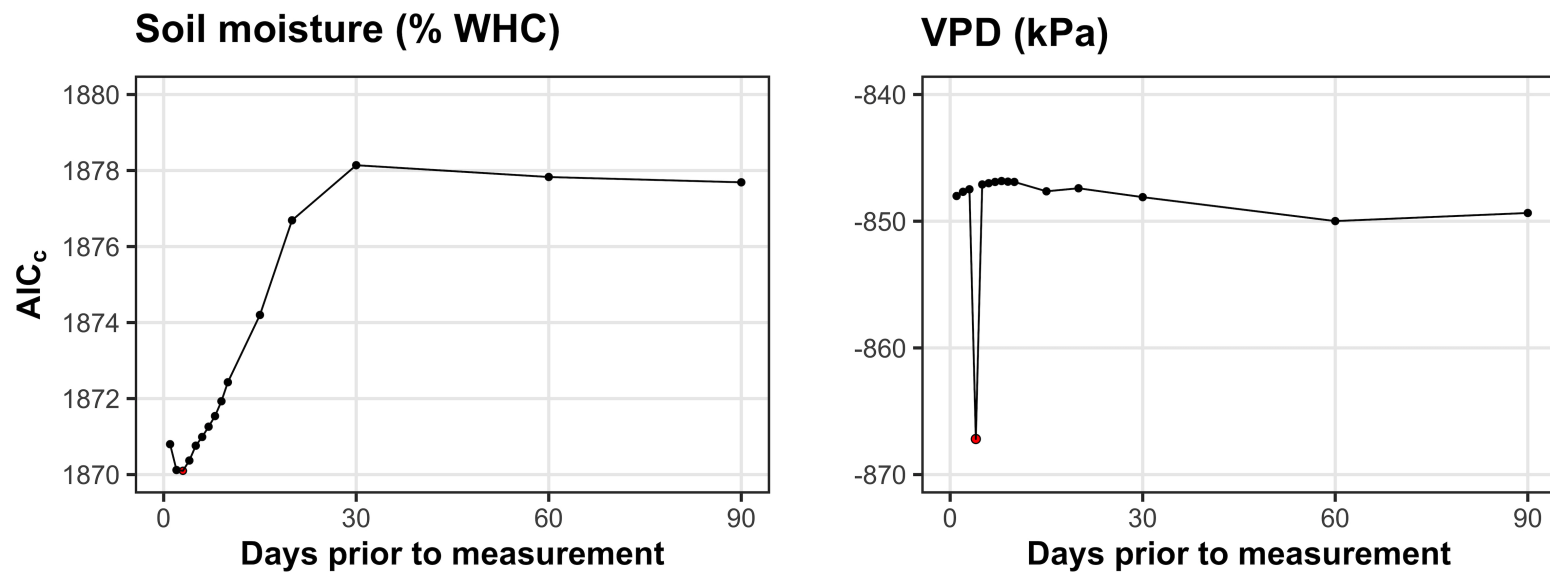


Figure C1. Model selection results exploring relevant timescales for soil moisture (left panel) and vapor pressure deficit (right panel). The x-axis indicates the number of days before each site visit and the y-axis notes the corrected Akaike Information Criterion value. The timescale with the lowest AIC_c value, and therefore most relevant timescale to include in statistical models, is noted as a red point.

Appendix D

Supplemental material for “Optimal resource investment to photosynthetic capacity maximizes nutrient allocation to whole plant growth under elevated CO₂”

Table D1. Summary table containing volumes of compounds used to create modified Hoagland’s solutions for each soil nitrogen fertilization treatment. All volumes are expressed as milliliters per liter (mL L⁻¹)

Compound	0 ppm N	35 ppm N	70 ppm N	105 ppm N	140 ppm N
1 M NH ₄ H ₂ PO ₄	0	0.165	0.33	0.5	0.67
2 M KNO ₃	0	0.335	0.67	1	1.33
2 M Ca(NO ₃) ₂	0	0.335	0.67	1	1.33
1 M NH ₄ NO ₃	0	0.165	0.33	0.5	0.67
8 M NH ₄ NO ₃	0	0	0	0	0
1 M KH ₂ PO ₄	1	0.85	0.67	0.5	0.33
1 M KCl	3	2.45	2	1.5	1
1 M CaCO ₃	4	3.33	2.67	2	1.33
2 M MgSO ₄	1	1	1	1	1
10% Fe-EDTA	1	1	1	1	1
Trace elements	1	1	1	1	1

Compound	210 ppm N	280 ppm N	350 ppm N	630 ppm N
1 M NH ₄ H ₂ PO ₄	1	1	1	1
2 M KNO ₃	2	2	2	2
2 M Ca(NO ₃) ₂	2	2	2	2
1 M NH ₄ NO ₃	1	3.5	0	0
8 M NH ₄ NO ₃	0	0	0.75	2
1 M KH ₂ PO ₄	0	0	0	0
1 M KCl	0	0	0	0
1 M CaCO ₃	0	0	0	0
2 M MgSO ₄	1	1	1	1
10% Fe-EDTA	1	1	1	1
Trace elements	1	1	1	1

Table D2. Summary of the daily growth chamber program, including all time steps where air temperature (T_{set} ; °C) and photosynthetically active radiation (PAR; $\mu\text{mol m}^{-2} \text{ s}^{-1}$) setpoints are ramped up or ramped down

Time	T_{set}	PAR (\pm SD)
09:00	21	278 \pm 2
09:45	21	557 \pm 4
10:30	25	797 \pm 4
11:15	25	1230 \pm 12
22:45	21	797 \pm 4
23:30	21	557 \pm 4
00:15	17	278 \pm 2
01:00	17	0 \pm 0

Table D3. Effects of CO₂, fertilization, and inoculation on whole plant biomass: pot volume (BVR; g L⁻¹)*

	df	Coefficient	χ^2	p
(Intercept)	-	$1.33 * 10^{-1}$	-	-
CO ₂	1	$1.53 * 10^{-1}$	146.004	<0.001
Inoculation (I)	1	$4.19 * 10^{-1}$	19.320	<0.001
Fertilization (N)	1	$1.90 * 10^{-3}$	279.387	<0.001
CO ₂ *I	1	$1.03 * 10^{-1}$	0.007	0.934
CO ₂ *N	1	$2.44 * 10^{-3}$	49.725	<0.001
I*N	1	$-6.90 * 10^{-4}$	9.006	0.003
CO ₂ *I*N	1	$-4.95 * 10^{-4}$	0.640	0.424

*Significance determined using Type II Wald χ^2 tests ($\alpha=0.05$). P-values less than 0.05 are in bold. Key: df=degrees of freedom; χ^2 =Wald Type II chi-square test statistic.

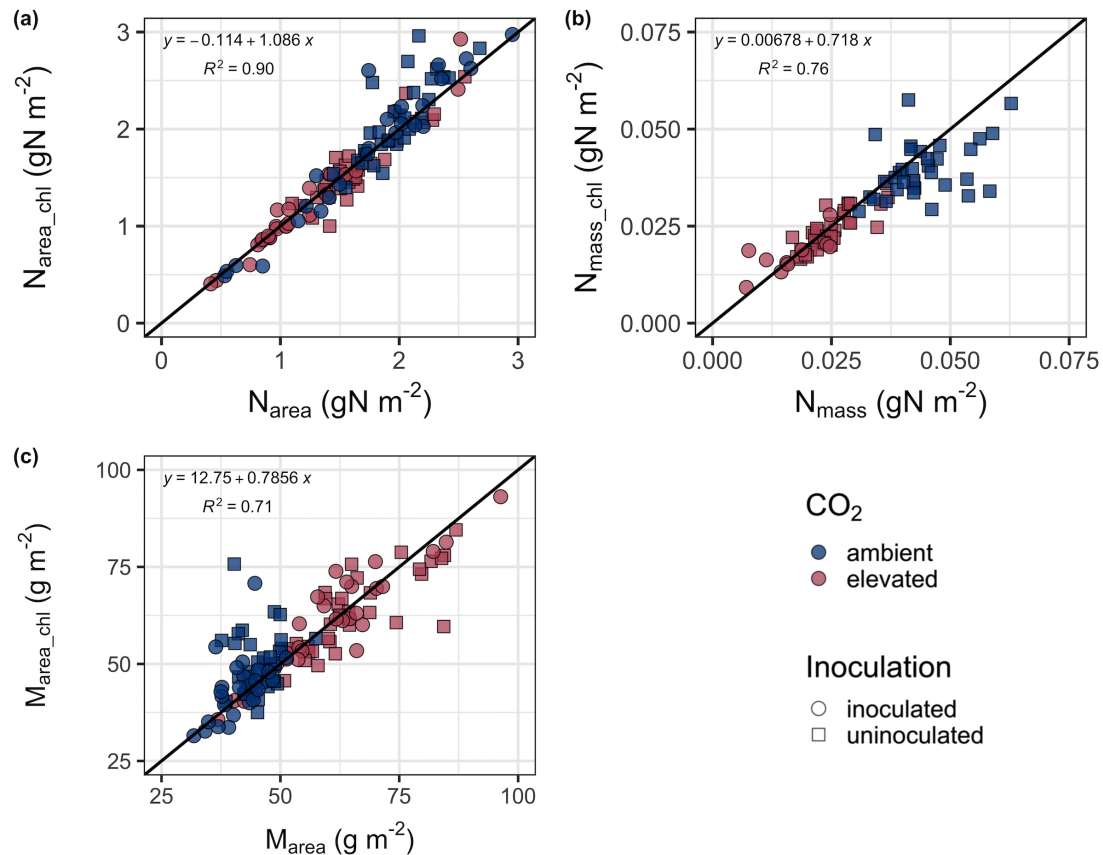


Figure D1. Relationships between area-based leaf nitrogen content (a), mass-based leaf nitrogen content (b), and leaf mass per unit leaf area (c) measured on the focal leaf used to generate CO₂ response curves (x-axis) and leaf nitrogen content measured on the leaf used for chlorophyll extractions (y-axis). Blue points refer to leaves grown under ambient CO₂ and red points refer leaves grown under elevated CO₂. Square points indicate uninoculated pots and circular points indicate inoculated pots. Pearson's correlation coefficient, associated *p*-values, and the line of the regression line that described each bivariate are included in the top left corner of each plot. The solid black line visualizes the trend given a 1:1 bivariate relationship.

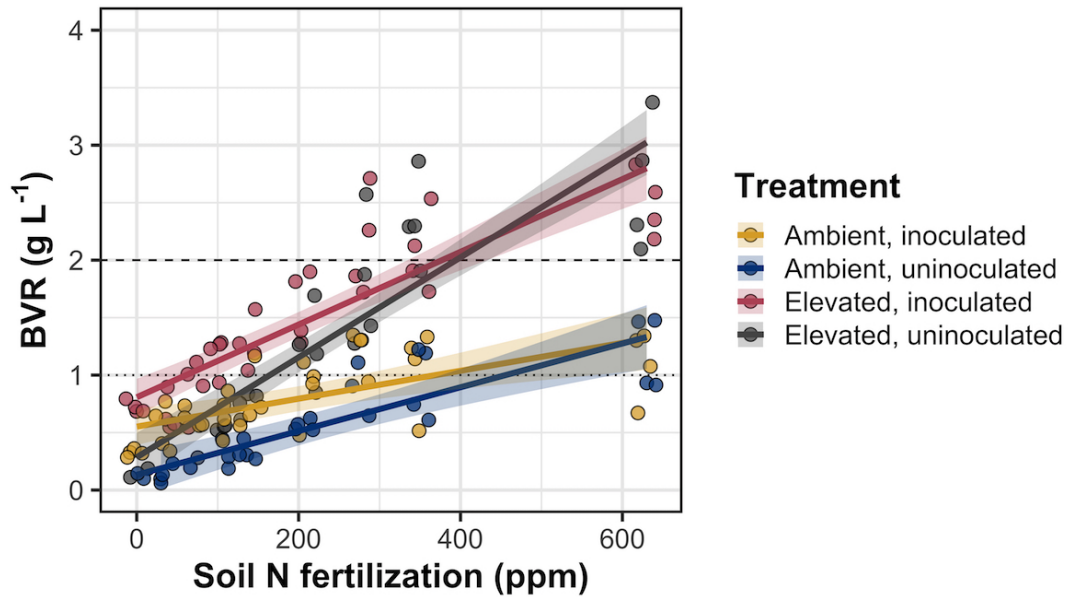


Figure D2. Effects of CO₂, fertilization, and inoculation on the ratio of whole plant biomass to pot volume. Soil nitrogen fertilization is represented on the x-axis in all panels. Yellow points and trendlines indicate inoculated individuals grown under ambient CO₂, blue points and trendlines indicate uninoculated individuals grown under ambient CO₂, red points and trendlines indicate inoculated individuals grown under elevated CO₂, and gray points indicate uninoculated individuals grown under elevated CO₂. Solid trendlines indicate regression slopes that are different from zero ($p<0.05$). The dotted horizontal line indicates the point where biomass:pot volume exceeds 1 g L⁻¹, and the dashed line indicates the point where biomass:pot volume exceeds 2 g L⁻¹.